Coordination Cages as a Scaffold for Permanently Porous Liquids

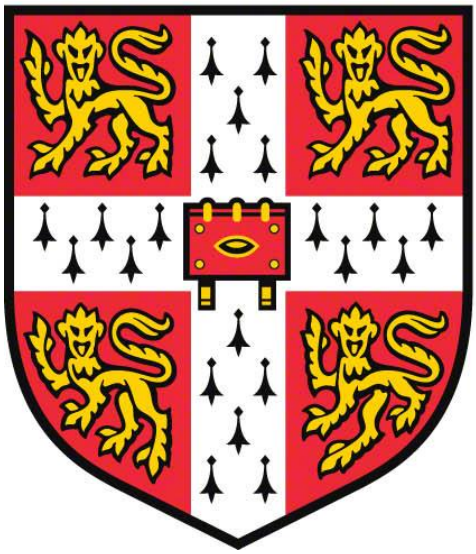

Lillian Ma

Wolfson College

July 2019

A dissertation submitted to the University of Cambridge as part of the Doctor of Philosophy.

Declaration

I hereby declare that this dissertation, entitled *Coordination Cages as a Scaffold for Permanently Porous Liquids*, is the result of work that I have undertaken in the University Chemical Laboratory at the University of Cambridge between October 2015 and July 2019. Except where stated to the contrary, this dissertation is my own work; credit for results obtained from collaboration with other parties is referenced to directly in the text. Figures that have been reproduced or adapted from other sources are indicated as such in their corresponding caption references and have been used with permission. This dissertation has not been, nor is currently being, submitted for any other degree, diploma or other academic qualification at this or any other university. It does not exceed 60,000 words in length.

Lillian Ma

July 2019

Abstract

Name: Lillian Ma

Title: Coordination Cages as a Scaffold for Permanently Porous Liquids

Porosity is a property that is conventionally associated with solids. While liquids can have transient pores, these cavities exist as temporary voids between the molecules of the liquid. The idea of permanently porous liquids combines the porosity of solids with the fluid properties of liquids by engineering intrinsic porosity into the liquid state. This class of materials shows potential in applications such as extractions and gas separations.

We present the first adaptation of coordination cages into porous liquids by functionalizing a series coordination cages of different sizes and structures with alkylimidazolium and PEG-imidazolium moieties. The alkylimidazolium-functionalized cages showed increased solubility in similarly structured ionic liquids, yielding a Type II porous liquid. The PEG-imidazolium-functionalized cages were liquid at room temperature and acted as Type I porous liquids. Of these cages, a liquid $Zn^{II}_4L_4$ tetrahedral capsule was chosen for additional characterization and applications. Rheological and thermal analysis of this liquid cage confirmed its fluidity. Positron annihilation lifetime spectroscopy indicated that the host pores remained empty under solvent-free conditions. This liquid cage was then used for host-guest experiments both in solution and in the neat state. The porous liquid was shown to encapsulate small alcohols shape-selectively, with a preference for alcohols with more branching. The liquid cage also dissolved and encapsulated three different chlorofluorocarbons.

Additionally, we also present the first hetero-cage, which we define to be a coordination cage that is charge-balanced by a second, different cage of opposite charge. A hetero-cage was synthesized by charge-balancing a liquid coordination cage with +20 charge with 5 equivalents of a solid anionic cage with -4 charge. The resulting material was characterized by NMR, which confirmed that the cages were charge-balancing each other in the absence of additional counterions. Thermal analysis of hetero-cages indicated that the material was comprised of a solid suspension of the anionic cage in the liquid cationic cage, and that the phase change behaviors of the parent cages are preserved in the hetero-cage.

Acknowledgments

First, I would like to thank my supervisor Professor Jonathan Nitschke for his guidance and support during my PhD; thank you for giving this anglophile an opportunity to pursue a degree in the country of her dreams with the some of the brightest scientists in the world.

Next, I would like to acknowledge my collaborators, without whom none of this could have happened theoretically or experimentally. I would to thank Dr. Cally Haynes for showing me by example what it means to be a good scientist, collaborator and person. Thank you for always being my steady compass when I got lost wading through a sea of British mannerisms. I would like to acknowledge Dr. Angela Grommet as the original trailblazer for this project – thank you for paving the road and convincing me to take this journey with you. To Hugh Ryan, thank you for always being patient with me while we fumbled our way through scientific areas beyond the borders of our comfort zones together. I could not ask for a better successor.

A special thank you to Dr. Tom Bennett for helping me and the liquid cage squad venture into the realm of materials chemistry – your expertise and advice was always unfailingly reliable. To Chris Parkins and Louis Longley, thank you for conducting rheology and thermal analysis on these weird and wonderful materials. An especially warm acknowledgment goes to Anna Walçzak and Matthew Price for being delightful students who were undaunted in the face of running five consecutive columns on the same synthetic step.

Among my friends, I want to thank Dr. Larissa von Krbek for being the perfect desk-mate who always had a snack, hug and ear ready to soothe my frazzled nerves – you are the epitome of German efficiency and kindness. I would also like to add a special mention to Dr. Marion Kieffer, my sister-in-arms, who always filled our bay with laughter and Disney songs in French. To Alexandra Gablier, thank you for turning what should have been a stressful writing ordeal into an experience filled with memories of K-pop and the taste of Knoppers.

Finally, thank you to my family – my mother and two grandmothers. The three of you proved to me that, in this world, a tiny Asian woman can stand just as tall as a man.

Abbreviations

AsF_6^-	Hexafluoroarsenate
BF_4^-	Tetrafluoroborate
Boc	*Tert*-Butyloxycarbonyl
$CDCl_3$	Deuterated chloroform
CD_3CN	Deuterated acetonitrile
C_6F_6	Hexafluorobenzene
CFC	Chlorofluorocarbon
CF_3Cl	Chlorotrifluoromethane, CFC-11
CF_2Cl_2	Dichlorodifluoromethane, CFC-12
$CFCl_3$	Trichlorofluoromethane, CFC-13
$CHCl_3$	Chloroform
CH_3CN	Acetonitrile
CH_4	Methane
CO_2	Carbon dioxide
D_2O	Deuterated water
DCA^-	Dichloroacetate
DMF	*N*,*N*-dimethylformamide
DS^-	Dodecyl sulfate
DSC	Differential Scanning Calorimetry
EA	Elemental analysis
equiv.	Equivalents
G'	Storage modulus
G''	Loss modulus
h	Hour
[hmim]	1-hexyl-3-methylimidazolium
HR-ESI-MS	High-resolution electrospray mass spectrometry
LR-ESI-MS	Low-resolution electrospray mass spectrometry
min	Minute
MS	Mass spectrometry
N_2	Nitrogen
NMR	Nuclear magnetic resonance

NPf_2^-	Pentaflimide, bis(pentafluoroethanesulfonyl)imide
NTf_2^-	Triflimide, bis(trifluoromethanesulfonyl)imide
OAc^-	Acetate
OTf	Triflate
PF_6^-	Hexafluorophosphate
rad	Radian
RT	Room temperature
s	Second
SO_4^-	Sulfate
T_{decomp}	Decomposition temperature
T_g	Glass transition temperature
TGA	Thermal gravimetric analysis
T_m	Melting temperature
TMA^+	Tetramethylammonium
VT	Variable temperature
wt%	Weight percent

Table of Contents

CHAPTER 1

Introduction

1.1 An Overview of Discrete Microporous Hosts

While porous materials are divided into numerous categories by the International Union of Pure and Applied Chemistry based on their pore sizes,[1] this work focuses on materials in the microporous region (0.2-2.0 nm). Microporous materials can be further subdivided into two major categories: porous extended networks and discrete porous hosts.[2] Metal-organic frameworks (MOFs),[3] covalent-organic frameworks (COFs),[4] zeolites,[5] porous carbons[6] and porous polymers[7] all fall under the former category. These porous networks are renowned for their applications in gas adsorption,[8,9] catalysis,[10–12] and molecular separations.[13–15] However, microporous materials also include discrete porous hosts such as metal-organic cages,[16] porous organic cages,[17] calix[n]arenes[18] and cucurbiturils.[19] In contrast to porous extended networks, which are often investigated as solids under solvent-free conditions, many of these cages and macrocycles have demonstrated host-guest behavior in the solution-state.[20–22] This introduction to porosity will focus mainly on the discussion and investigation of discrete microporous hosts.

1.1.1 Discrete Organic Porous Hosts

Although porosity is often associated with porous extended networks, discrete supramolecular structures such as macrocycles can also act as porous hosts. Kim *et al.* demonstrated that cucurbit[6]uril (CB[6]) showed the highest selectivity for CO_2 over CO among all known porous organic materials.[23] The authors recrystallized CB[6] from HCl and found that these crystals showed high CO_2 selectivity through gas sorption studies and FT-IR analysis. The enthalpy of CO_2 adsorption in the cucurbituril was estimated to be 33.0 kJ/mol – a value comparable with MOFs that exhibit strong CO_2 binding. This large enthalpy value was explained by the crystal structure of $CO_2 \subset$ [CB6], which showed that the cucurbituril had three different binding sites for the gas (Figure 1.1). CO_2 was bound in these different cavities through hydrogen bonding and/or dipole-quadrople interactions. This study illustrated how macrocycles can display a degree of gas selectivity previously only associated with porous extended networks such as MOFs.

Discrete porous hosts are not limited to macrocycles. In 2009, Cooper *et al.* designed and synthesized a covalently bonded organic cage that could assemble into microporous crystals.[24] The porosity of this material was attributed to a combination of the host cavities and the inefficient packing of the cages in the solid state. The authors demonstrated that the porosity in the crystals of an unfunctionalized octahedral cage was mainly comprised of the cage cavities, with limited porosity observed between cages (Figure 1.2a). However, appending

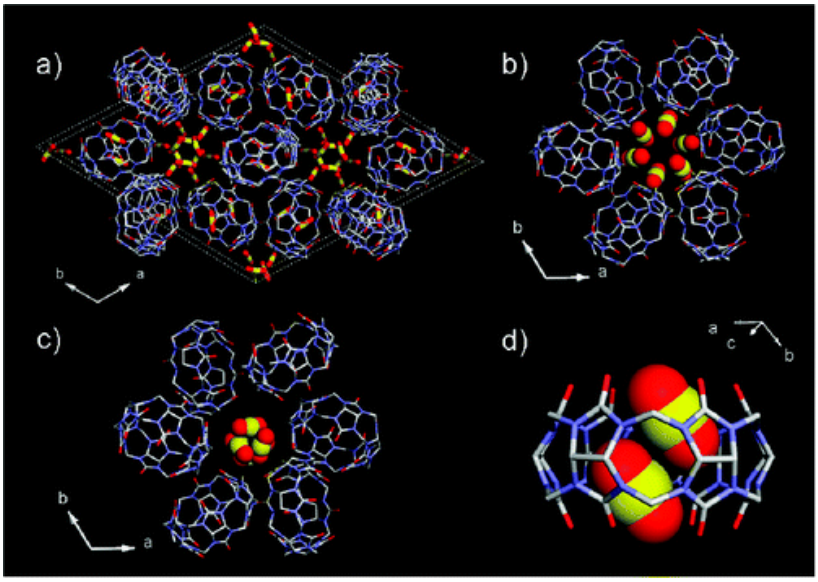

Figure 1.1: a) X-ray crystal structure of CO_2 adsorbed in cucrbit[6]uril. b), c) and d) show the three different binding sites for the gas. Figure adapted from reference 23.

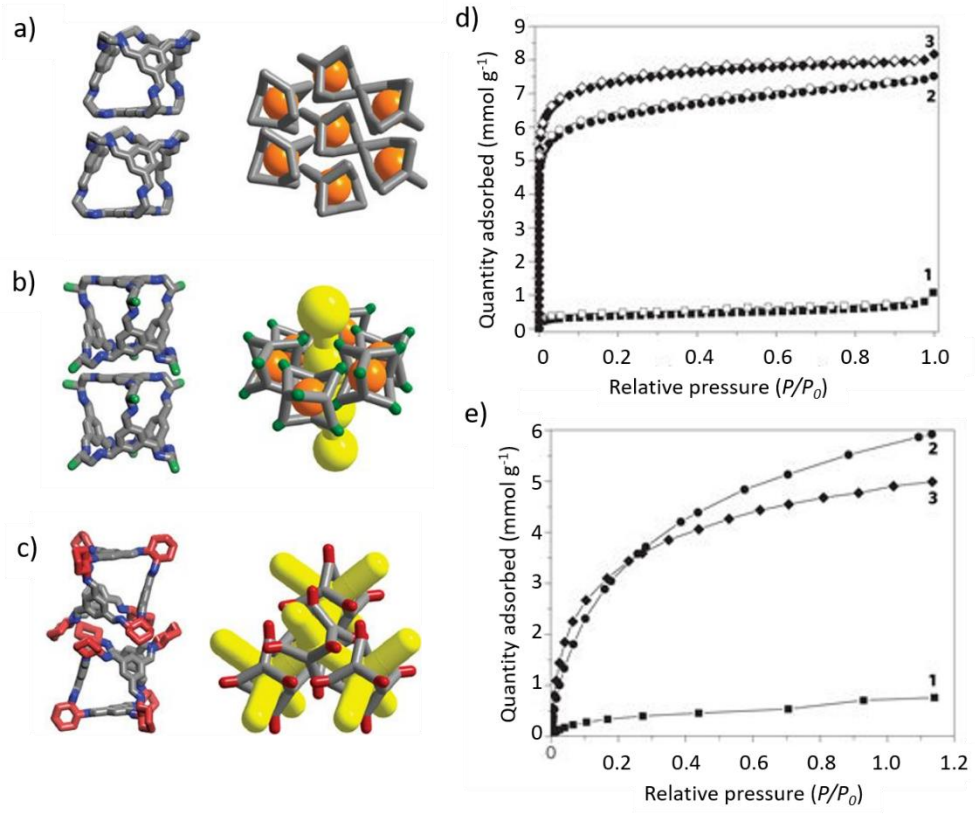

Figure 1.2: a) Crystal structure of the unfunctionalized cage (**1**). b) and c) are crystal structures of the cyclohexyl (**2**) and methyl-functionalized cages (**3**), respectively. d) and e) show the H_2 and CH_4 adsorption isotherms of cages **1**, **2**, and **3**, respectively. Figure adapted from reference 24.

methyl groups onto the vertices of this cage resulted in a crystal with increased porosity because the methyl groups hindered efficient packing between cages (Figure 1.2b). Furthermore, functionalizing the cage with sterically hindered cyclohexane moieties yielded crystals that contained 3D pore networks in between the individual hosts (Figure 1.2c). Therefore, the porosity calculations conducted on the crystal structures of these three cages demonstrated that cages functionalized with sterically hindered functional groups packed less efficiently, resulting in an overall increase in porosity. Gas adsorption isotherms of the three cages showed that the cyclohexyl and methyl-functionalized cages both adsorbed significantly more H_2, CH_4 and CO_2 than their unfunctionalized counterpart (Figure 1.2d,e). Therefore, this work demonstrated that porosity can not only be engineered in crystalline organic cages, but also can be controlled by varying the functional groups appended onto the cage vertices.

1.1.2 Metal-organic cages

While metal-organic cages (MOCs) generally have cavities within the microporous range, this category of discrete hosts is often overlooked when discussing porous materials.[2] However, these cages can be used for applications one generally associates with conventional porous materials. For example, Yaghi *et al.* reported the design and synthesis of a library of cages capable of adsorbing different gases in their solid state.[25] Using metal carboxylate clusters as the vertices of the cages, the authors showed that connecting these clusters with linear or triangular linkers produced truncated tetrahedra and heterocuboids of different sizes (Figure 1.3a). Three of these metal-organic polyhedra (MOPs) were then used in gas adsorption experiments, which showed that the cages were capable of adsorbing N_2, CO_2, Ar, CH_4, H_2 and benzene (Figure 1.3b). The authors demonstrated that MOP-51 in adsorbed a comparable amount of CH_4 to MOF-5. Contrary to many solution-state host-guest experiments for MOPs, this study demonstrated that MOPs can also be used for applications in the solid state.

Unlike many porous extended networks, the applications of MOCs are not limited to the solid-state, and many studies have been conducted on the host-guest behaviors of these capsules in solution.[26–28] One drawback of MOFs is their instability in the presence of water.[29,30] Although more water-stable MOFs have been developed, MOCs have been shown to not only be stable when dissolved in water, but also to encapsulate guests and catalyze reactions in aqueous conditions.[31] One of the most famous examples of a MOC acting as a homogenous catalyst in water was reported by Fujita *et al.* The authors presented an Pd_6L_4 octahedral cage capable of catalyzing Diels-Alder reactions with unusual regioselectivity.[32]

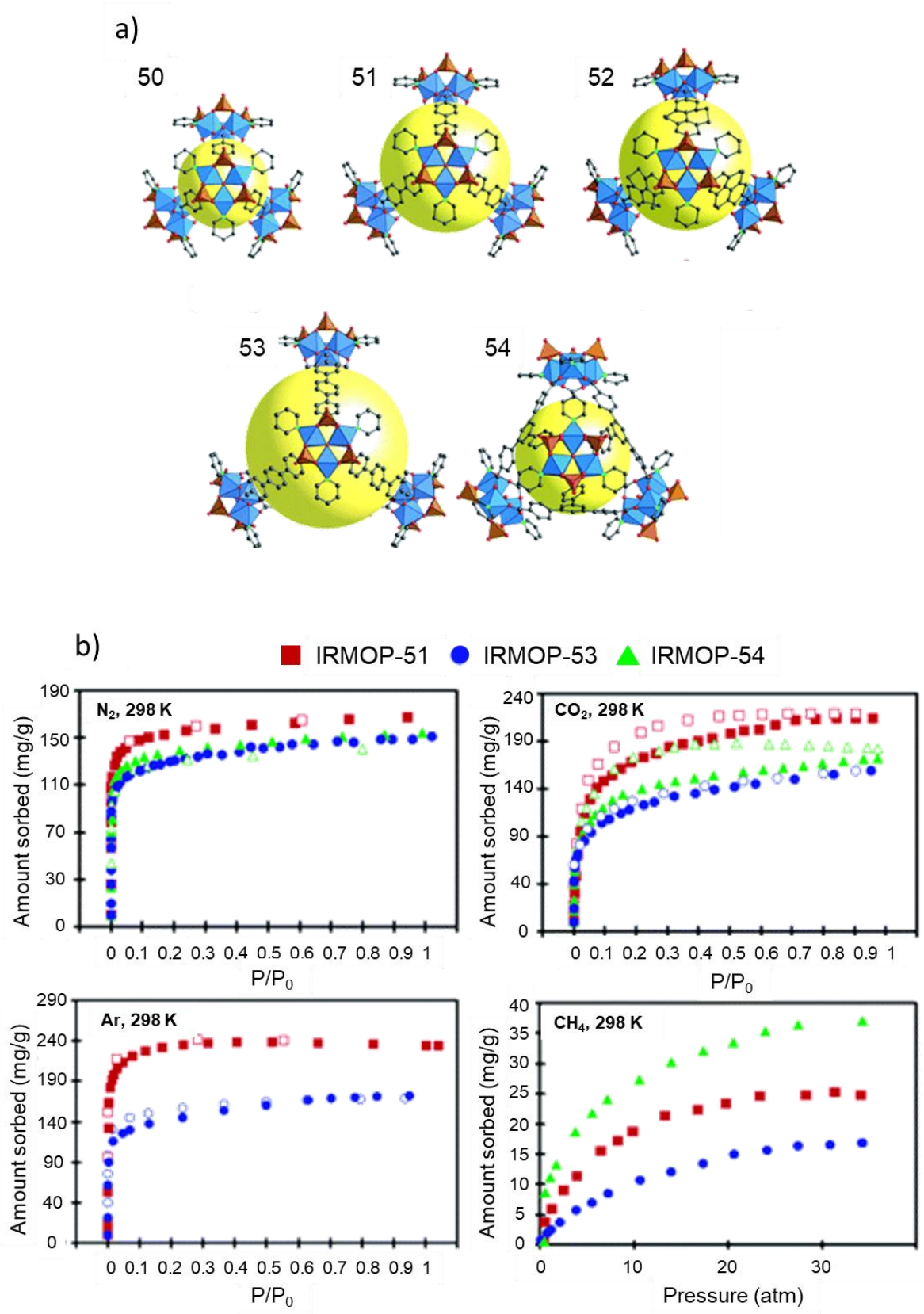

Figure 1.3: a) MOPs 50-54 assembled from iron carboxylate corners and different linear and triangular linkers. b) gas sorption isotherms of MOP-51, MOP-53 and MOP-54 with N_2, CO_2, Ar and CH_4. Filled shapes = sorption, open shapes = desorption. Figure adapted from reference 25.

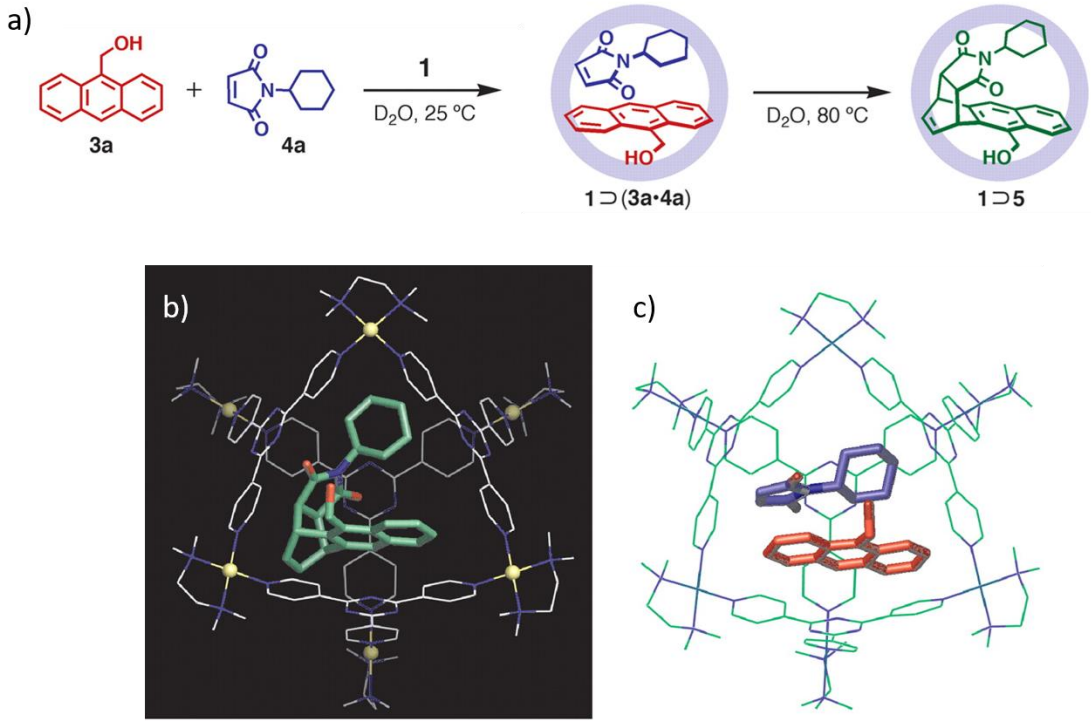

Figure 1.4: a) Diels-Alder reaction between 9-hydroxymethylanthrancene and N-cyclohexyl-phthalimide in the Pd_6L_4 cage to selectively yield the 1,4-adduct. b) Crystal structure of the 1,4-adduct encapsulated in the Pd_6L_4 cage and c) Force field calculations show the optimized position of both substrates in cage **1**. Figure adapted from reference 32.

While the Diels-Alder coupling of anthracenes and phthalimides generally results in the adduct bridging the central ring (9,10-position), the cage can alter this selectivity to favor the 1,4-adduct at the terminal ring (Figure 1.4a). When 9-hydroxymethylanthrancene and N-cyclohexylphthalimide were added to a solution of the Pd_6L_4 cage in water, the host-guest complex formed in 5 minutes; upon subsequent heating at 80 °C, the substrates reacted to yield solely the Diels-Alder adduct at the 1,4-position. No other isomers were observed in the product (Figure 1.4b). The authors attributed this change in selectivity to the fixed orientation of the guests when encapsulated by the cage; force-field calculations showed that the limited space in the cavity positions the guests in favor of the 1,4-position (Figure 1.4c). Therefore, MOCs can not only be employed as homogenous catalysts in aqueous phases, but also can promote specific product selectivity due to their rigid cavities.

1.1.3 Coordination cages based on subcomponent self-assembly

While most metal-organic cages are formed *via* the coordination between a metal ion and ligand, subcomponent self-assembly is a synthetic method that allows for the formation of a ligand from multiple subcomponents in tandem with metal-ligand coordination.[33] This

process is achieved by conducting dynamic covalent imine condensations in the presence of metal salts. If the formation of the imine produces a chelating site for the metal ion, the templation effect from the metal-ligand complexation can drive the equilibrium towards the condensation product.[34] This self-assembly strategy has been employed to form a number of supramolecular structures, including many metal-organic cages.[35–37]

Like other MOCs, subcomponent self-assembly based coordination cages are often excluded from the category of porous materials despite having microporous cavities. However, Nitschke *et al.* have shown that these cages can be used in applications similar to those associated with conventional porous materials. An $Fe^{II}_4L_6$ tetrahedral coordination cage was formed *via* subcomponent self-assembly and was shown to encapsulate and release sulfur-hexafluoride (SF_6) in a controlled manner (Figure 1.5a).[38] SF_6 was bubbled through a solution of cage in D_2O and the formation of the host-guest complex was observed by ^1H and ^{19}F NMR. The aromatic protons of $SF_6 \subset Fe^{II}_4L_6$ shifted downfield when compared to the free host and an extra signal appeared in the ^{19}F NMR, which the authors attributed to being SF_6 bound in slow-exchange on the NMR timescale. The successful gas encapsulation was further confirmed by the crystal structure of $SF_6 \subset Fe^{II}_4L_6$, which showed how the bound guest was stabilized by van der Waals interactions (Figure 1.5b). Subsequent addition of acid to the cage opened the capsule and released the guest. While there are many studies conducted on the adsorption of gasses in microporous solids, this work is an example of how MOCs can sequester gasses in the solution-state.

One of the advantages of subcomponent self-assembly is that the resulting structures are dynamic in nature. An example of this dynamicity employed in a creative manner is demonstrated by Nitschke *et al*. through the formation of a library of cages *via* anion templation (Figure 1.6).[39] A dialdehyde subcomponent was combined with *p*-toluidine and $Cd(NTf_2)_2$ to form a $Cd^{II}_2L_4$ helicate. The addition of ClO_4^- and AsF_6^- to this assembly resulted in a structural transformation yielding a $Cd^{II}_8L_{12}$ cuboid cage and $Cd^{II}_{12}L_{18}$ hexagonal prism, respectively. The subsequent addition of a halide anion (F^-, Br^-, Cl^-) to the cuboid cage resulted in a secondary transformation into a $Cd^{II}_{10}L_{15}$ pentagonal prism. Similarly, the addition of chloride to the hexagonal prism resulted in a structural rearrangement forming a second pentagonal prism. Therefore, the authors demonstrated that the dynamic nature of these self-assemblies could be harnessed to form a library of new architectures *via* anion triggered structural reconfigurations.

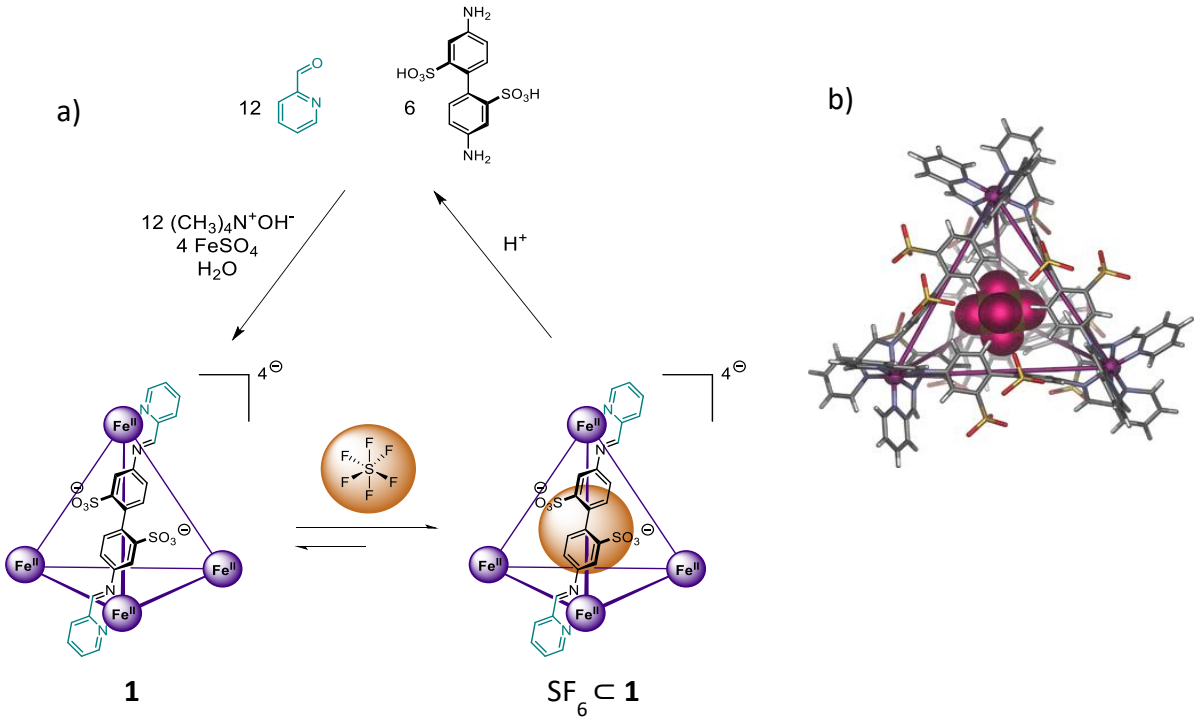

Figure 1.5: a) Synthesis of cage **1** (left) and formation of the $SF_6 \subset$ **1** host-guest complex. b) Crystal structure of $SF_6 \subset$ **1**. Figure adapted from reference 38.

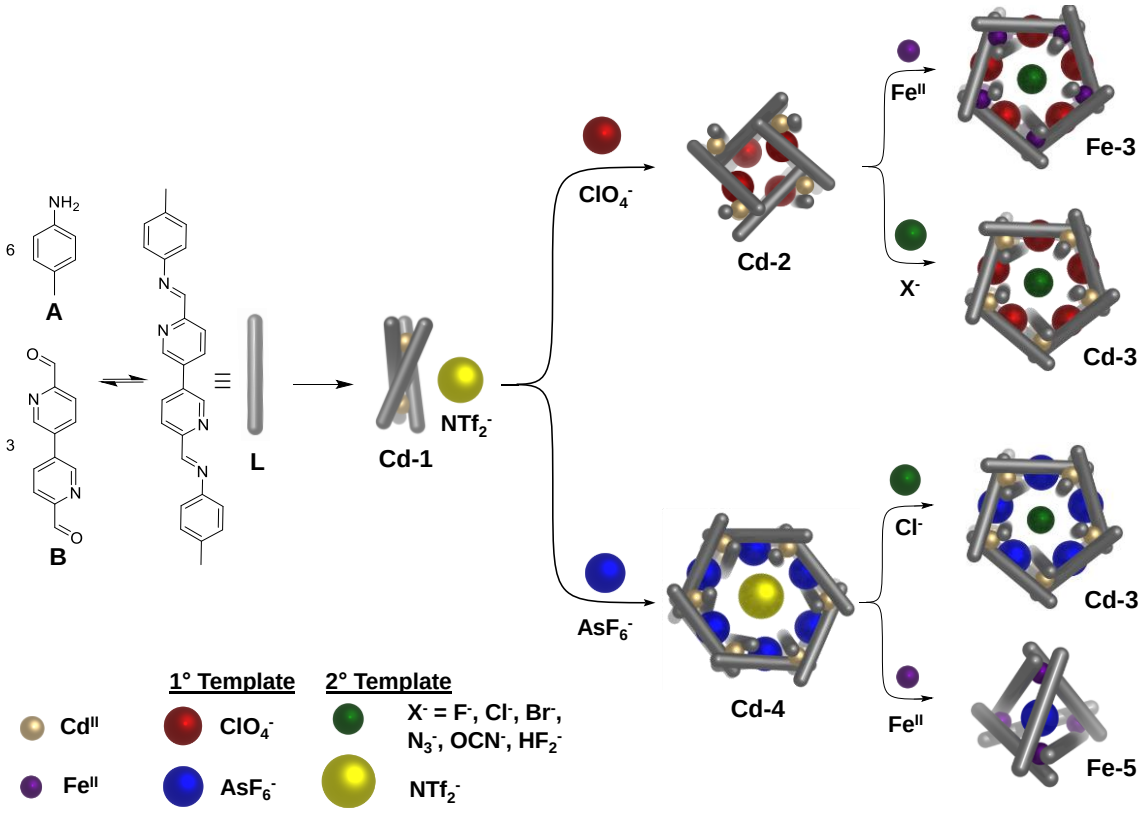

Figure 1.6: Schematic representation of the structural reconfiguration pathways resulting from the self-assembly of subcomponents **A** and **B** with different metal salts. Figure adapted from reference 39.

While the dynamic nature of coordination cages formed from subcomponent self-assembly may suggest that these supramolecular structures are less stable than other MOCs, coordination cages have been found to be soluble and stable in a variety of solvents. Most notably, Nitshcke *et al.* have demonstrated that coordination cages can be solubilized in ionic liquids (Figure 1.7).[40] A $Fe^{II}_4L_4$ tetrahedral capsule was dissolved in 1-ethyl-3-methylimidazolium ethylsulfate ([emim][$EtOSO_3$]) at a concentration of 3.3 mM. After the addition of 1,3,5-trifluorobenzene, a known guest for this cage, ^{19}F NMR analysis of the sample showed the successful formation of the 1,3,5-trifluorobenzene host-guest complex. The authors also demonstrated that 1,3,5-trifluorobenzene could be displaced from the cage cavity by the addition of 1-fluoroadamantane – a result consistent with the behavior of the cage in H_2O solution. Lastly, the authors dissolved an $Fe^{II}_4L_6$ tetrahedral cage in water, an $Fe^{II}_8L_{12}$ cubic cage in trihexyltetradecylphosphonium triflimide ([$P_{6,6,6,14}$][NTf_2]) and demonstrated that when these two solutions of cages are combined with the previous solution of $Fe^{II}_4L_4$ cage in [emim][$EtOSO_3$], the resulting mixture forms an immiscible triphasic system. All three cages were also capable of selectively encapsulating guests in their respective phases (Figure 1.7).

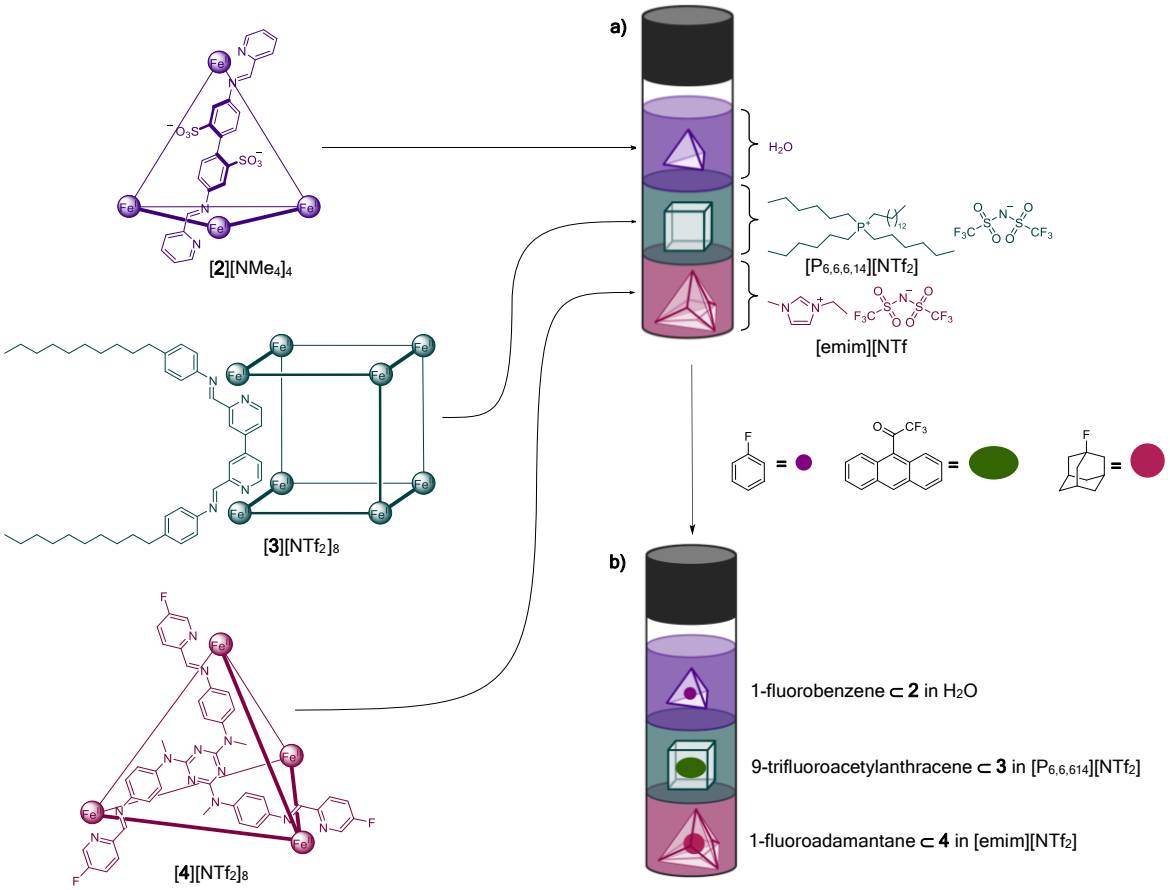

Figure 1.7 Cages **2, 3,** and **4** were observed to partition selectively into H_2O, [$P_{6,6,6,14}$][NTf2], and [emim][NTf_2] to form a triphasic system; the cages also selectively bound 1-fluorobenzene, 9-trifluoroacety-lanthracene, and 1-fluoroadamantane, respectively. Figure adapted from reference 40.

1.2 Ionic Liquids

Ionic liquids (ILs) are broadly defined as salts with melting temperatures below 100 °C.[41] The first example of a liquid salt at room temperature was reported by Walden in 1914, where he stated that the melting temperature of ethylammonium nitrate ($[EtNH_3][NO_3]$) was 12 °C.[42] However, it was not until 1992, when Wilkes and Zawortko designed a 1-ethyl-3-methylimidazolium tetrafluoroborate ionic liquid, that our conventional concept of ionic liquids was born (Figure 1.8).[43] The low melting temperatures of ionic liquids are attributed to the inefficient packing of flexible cations and asymmetric anions in the solid state, thus resulting in lower lattice enthalpies.[44] Today ionic liquids are used for a variety of applications including catalysis,[45] solvent for reactions,[41,46] gas adsorption[47] and extractions.[48] The tunability and low vapor-pressure of these materials have led to them being hailed as the "green solvents for the future".[49] The properties and applications of ionic liquids will be discussed in more depth below.

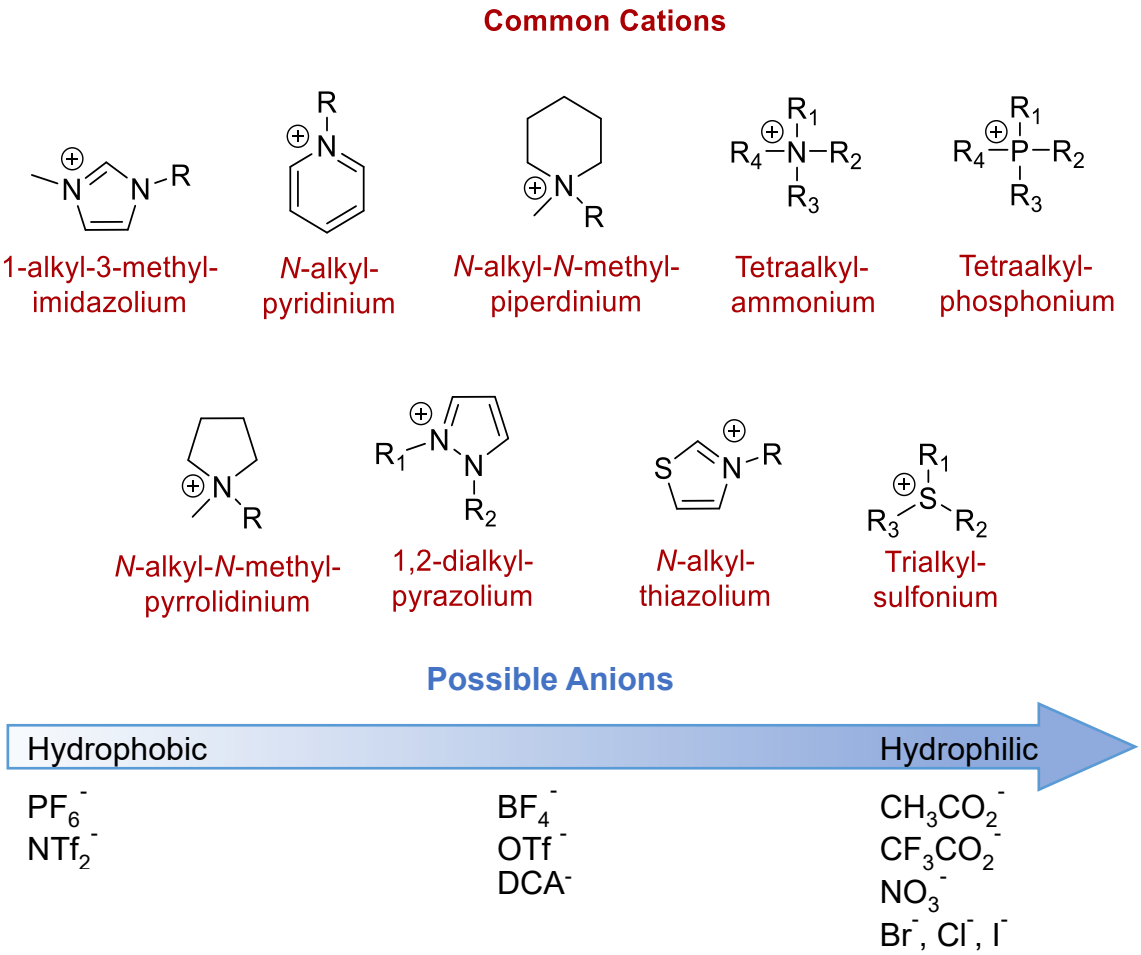

Figure 1.8: Common cations and anions of ionic liquids. Anions are listed in increasing hydrophilicity.

1.2.1 Properties of ionic liquids

While ionic liquids can be comprised of a seemingly infinite number of cation and anion combinations, this class of materials generally has similar physical properties, which includes low vapor pressure and high thermal stability. For example, Kabo *et al*. reported the vapor pressure of 1-butyl-3-methylimidazolium hexafluorophosphate ([C_4mim][PF_6]) as 1.2 Pa at 120 °C.[50] In contrast, the vapor pressure for glycerol at the same temperature is 315 Pa.[51] The low vapor pressures of ionic liquids make them good candidates for green solvents because, unlike conventional organic solvents, they do not release toxic and flammable fumes. Ionic liquids also exhibit high thermal stability with decomposition temperatures ranging from 220-470 °C (Table 1.1).[52] The thermal stability of ionic liquids is dependent on the nature of their cations and anions. For example, pyrrolidinium ionic liquids are generally exceptionally stable, and increasing the alkyl-chains on alkylimidazolium ionic liquids decreases the material's thermal stability.[52] Furthermore, the general trend of anion stability in ionic liquids follows the trend of NTf_2^- > BF_4^- > AsF_6^- > I^- > Br^- > Cl^-.[52] The nucleophilicity and basicity of halide anions decrease the thermal stabilities of ionic liquids in which they are present.[53] Conversely, fluorinating anions decreases the nucleophilicity of the anion and results in more thermally stable ionic liquids.[54] Consequently, the thermal stability of ionic liquids can be tuned by varying the cation and anion components.

The tunability of ionic liquids is not restricted to their thermal stability and can be used to control their viscosity. Most ionic liquids are 2-3 orders of magnitude more viscous than conventional organic solvents. For example, the viscosity of toluene and 1-hexyl-3-methylimidazolium triflimide ([C_6mim][NTf_2]) are 0.6 cP and 70 cP at room temperature,

Table 1.1: Onset of decomposition temperature of some [C_2mim][X].[52]

Ionic Liquid	Decomposition; T_{onset} (°C)
[C_2mim][Cl]	285
[C_2mim][Br]	311
[C_2mim][I]	303
[C_2mim][AsF_6]	416
[C_2mim][BF_4]	445
[C_2mim][NTf_2]	455

respectively.[55] However, other ionic liquids such as bis(hydroxyethyl)-ammonium acetate can have a viscosity of 5647 cP.[56] While the viscosity of ionic liquids may result in chemical processing difficulties such as decantation and filtration, highly viscous ionic liquids are favored as stationary phases for gas-liquid chromatography.[57] Systematic studies of alkylimidazolium ionic liquids show that an increase of temperature usually results in a decrease in viscosity, with this trend being particularly pronounced in ionic liquids with viscosities higher than ~10^3 cP at room temperature.[58–61] Conversely, an increase in the length of alkyl chains on the cations of an alkylimidazolium ionic liquid results in an increase of viscosity because longer alkyl chains result in more van der Waals interactions.[58] Changing the anions of an ionic liquid can also affect its viscosity; the viscosity of ionic liquids sharing a cation generally increases in the order of $DCA^- < NTf_2^- < OTf^- < BF_4^- < PF_6^- < OAc^-$.[58] The lower viscosities of ionic liquids with DCA^- and NTf_2^- anions are attributed to the delocalized charge distribution of the anion which results in weaker coulombic attractions between the anion and cations of the ionic liquid.[58,62–64] Conversely, ionic liquids with smaller, rigid and more symmetric anions such as PF_6^- and BF_4^- generally have higher viscosities due to the lack of conformational degrees of freedom.[65,66] Therefore, even though ionic liquids generally have high viscosities, this physical property can be tuned by varying the cations and anions of these materials.

1.2.2 Applications of ionic liquids

The tunability of ionic liquids results in a range of diverse applications for these versatile materials. The low vapor pressure of ionic liquids makes them environmentally friendly alternatives to traditional organic solvents. In 1986, Pflug and Wilkes *et al.* conducted Friedel-Crafts alkylations and acylations in an imidazolium chloroaluminate ionic liquid.[46] The authors discovered that the reaction was not only successful in the ionic liquid, but also the anion of the solvent played a catalytic role. By 1999, ionic liquids were shown to be good solvents for Diels-Alder reactions, hydrogenations, hydroformylations, olefin dimerizations and Heck reactions.[67]

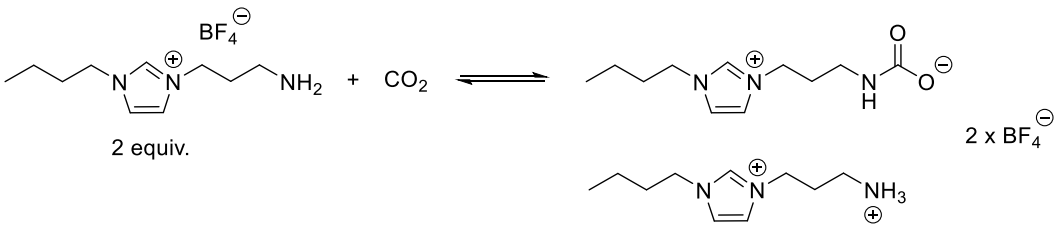

Figure 1.9: Proposed reaction between the amine-functionalized ionic liquid and CO_2.

Additionally, ionic liquids have been used for CO_2 capture and separation. In 2002, Davis *et al*. reported a new amine-functionalized alkylimidazolium ionic liquid that was shown to reversibly sequester CO_2 as a carbamate salt (Figure 1.9).[47] CO_2 can be repeatedly introduced and removed from the ionic liquid without decomposition of the material. While other commercially available ionic liquids have also been shown to dissolve CO_2,[68] this "task-specific" ionic liquid was designed especially for CO_2 capture. The amine functional groups mimic the conventional aqueous solutions of alkylamines used to sweeten natural gas.[69] Over 95% of natural gas sweetening operations in the U.S.A still use aqueous amine processes[70] – ionic liquids provide a safer and less toxic alternative. In contrast to conventional amine sequestering reagents, this ionic liquid is comparable in its efficiency but is also nonvolatile, providing a safer, and more environmentally conscious method of gas scrubbing.

In addition to catalysis and gas capture, ionic liquids have been shown to dissolve cellulose, which was previously only soluble in strong acids such as phosphoric acid.[71] On the other hand, ionic liquids have also been used as electrolytes in lithium batteries in place of conventional aprotic organic solvents, many of which are volatile and flammable.[72]

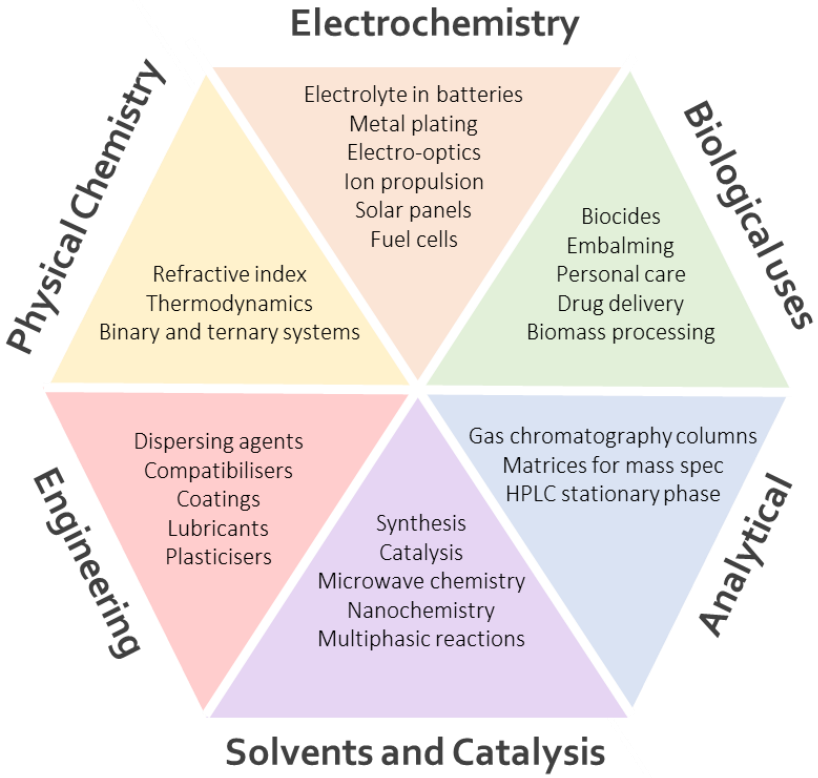

Figure 1.10: Different areas of science and technology where ionic liquids have been applied. Figure adapted from reference 73.

Furthermore, the ability to tune the solubility of ionic liquids makes them good candidates for liquid-liquid extractions in immiscible phases.[67] Ionic liquids have also been used as lubricants under high temperatures, high vacuum or corrosive environments – conditions under which conventional hydrocarbon lubricants would fail.[74] In general, ionic liquids are a class of materials that could be engineered for a diverse range of specific industrial applications (Figure 1.10).

1.3 Permanently Porous Liquids

1.3.1 The definition of a porous liquid

The concept of porous liquids was developed by Stuart James in 2007.[75] James proposed that intrinsic porosity could be engineered into the liquid state, creating a new material that combines the porosity of conventional solids and fluid mechanics of liquids. While extrinsic porosity can exist in liquids, these transient cavities are limited to temporary voids between the molecules of the fluid.[76] While there may be many methods to introduce permanent porosity into liquids, James proposed that porous liquids could be categorized into three main types (Figure 1.11).

Type I porous liquids are comprised of rigid hosts that are empty and liquid in the neat state (Figure 1.11). The main challenge in designing Type I porous liquids is to ensure that the structure of the host does not allow for inter- or intramolecular penetration. While the idea of porous liquids was proposed in 2007, Type I porous liquids have arguably existed since the 1990s. A paper published on the conformational analysis of alkylated cyclodextrins presented a perpentyl-β-CD that was a liquid at room temperature.[77] While the tubular shapes of these macrocycles appear to make interpenetration of hosts difficult, the crystal structure of

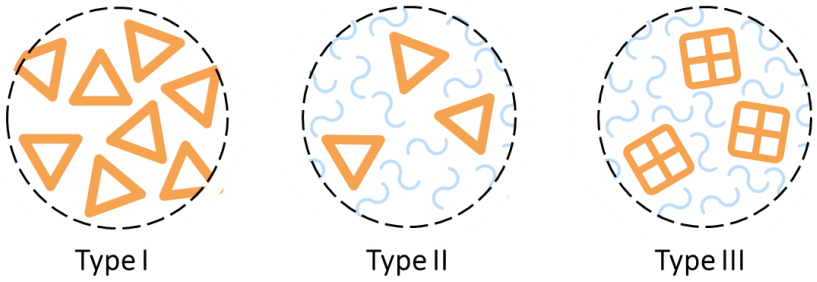

Figure 1.11: Diagram to illustrate the three types of porous liquids. Type I: neat liquid hosts with empty cavities. Type II: rigid hosts dissolved in a solvent too sterically hindered to penetrate the cavities. Type III: microporous frameworks dispersed in a solvent too sterically hindered to occupy the pores.

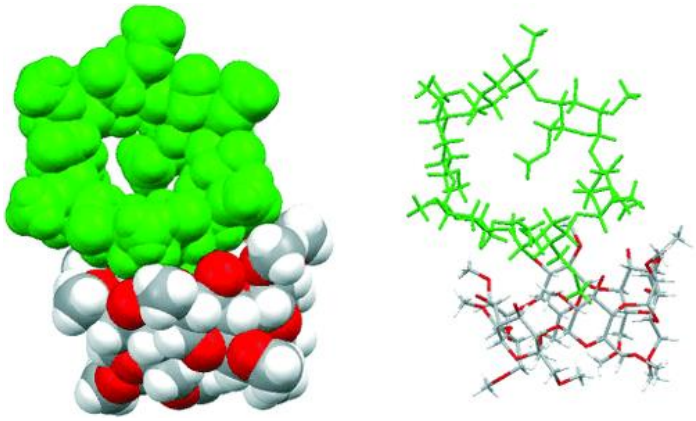

Figure 1.12: Crystal structure of permethyl-β-CD. One cyclodextrin (green) occupies the cavity of a second cyclodextrin. Twisting of the sugar residues also results in the cavity of the CD filling intramolecularly. Figure adapted from reference 75.

permethyl-β-CD showed that these macrocycles are both intramolecularly and intermolecularly filled when crystallized in the absence of a guest (Figure 1.12).[78] The flexibility of the macrocycle allows the structure to adopt a conformation in which one of the methyl groups points towards the cavity. The crystal structure also shows one cyclodextrin being partially filled by the methoxy group of a second cyclodextrin. Furthermore, the alkyl groups on perpentyl-β-CD increases the probability that the cyclodextrin will be occupied by these long chains either in an intermolecular or intramolecular fashion. Nevertheless, these cyclodextrins are the first example of a discrete porous host behaving as a liquid at room temperature.

In contrast to Type I porous liquids, Type II and Type III porous liquids are technically porous solutions (Figure 1.11). Type II porous liquids consist of rigid empty hosts dissolved in a solvent too sterically hindered to penetrate the host's pores. Cram *et al.* published the first Type II porous liquid in 1993, though the authors did not identify their material as such. This paper features a hemicarcerand dissolved in diphenyl ether.[79] The solvent was too large to be encapsulated so the host remained empty in solution – a result confirmed by ^{1}H NMR. However, no direct pieces of evidence such as PALS experiments or molecular simulations were presented to indicate that the hosts remained intact and empty. Positron annihilation lifetime spectroscopy (PALS) is a technique used to approximate the void sizes in a variety of materials such as MOFs and polymers. Positrons are introduced to a sample from a source such as Na^{22}. These positrons will either rapidly annihilate upon impact with an electron or they will thermalize into positroniums, which will reside in the voids of the materials until eventual annihilation. Therefore, the average sizes of the pores in the system can be estimated by the

lifetime of the *ortho*-positroniums (*o*-Ps). This analytical technique is often used to evaluate the porosity of permanently porous liquids.

Another example of a Type II porous liquid was published in 2007 by Rauchfus *et al.*[80] A small $\{CpCo(CN)_3\}_4(Cp^*Ru)_4]$ (Co_4Ru_4) metallocube was shown to be stable under solvent-free conditions due to the rigidity of its linear connectors. The limited size of the cube apertures prevented common solvents such as CH_3CN from entering the pores of the cage. The crystal structure of Co_4Ru_4 confirmed that CH_3CN only resided on the outside of the cage even though the capsule was crystallized in this solvent. Therefore, a solution of this cage in a solvent that is equal or greater in size to CH_3CN would technically yield a Type II porous liquid. However, the authors did not intentionally design this cage to be a good candidate for porous liquids and therefore did not investigate its porous properties.

Like Type II porous liquids, Type III porous liquids are comprised of solid porous extended networks dispersed in a sterically hindered solvent. Multiple examples of Type III porous liquids have been published and will be discussed in Section 1.3.4.

1.3.2 Type I porous liquid

The first rationally designed porous liquid was published by Cooper *et al.* in 2012, featuring an iminospherand porous organic cage functionalized with alkyl chains of different lengths.[81] Each cage was functionalized with 12 equivalents of a linear alkyl group ranging between 6 and 8 carbons, with the octyl-functionalized cage having a melting point of 50 °C. In 2014, Cooper *et al*. furthered this work by functionalizing the same cage scaffold with alkyl

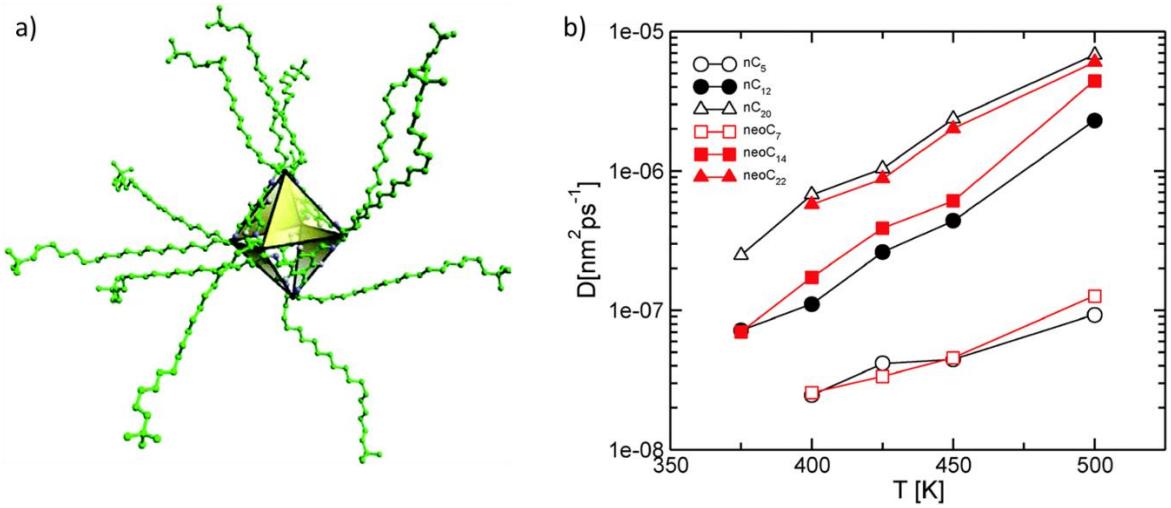

Figure 1.13: a) Computational model of an empty alkyl-functionalized organic cage. b) Computationally modelled translational diffusion coefficients as a function of temperature for cages functionalized by alkyl groups of varying lengths. Figure adapted from reference 82.

chains that were either linear or contained a terminal branched group and ranged between 5 to 22 carbons (Figure 1.13a).[82] They hypothesized that the branched motifs at the ends of the alkyl groups would slow the rate at which the chains occupied the cage cavity. DSC analysis of these cages showed that increasing alkyl lengths were correlated to lower melting temperatures, with the cage functionalized by a linear alkyl chain of 12 carbons melting at only 40 °C. Computational modelling was used to calculate the diffusion coefficients of the alkylated cages to approximate the viscosity of these porous liquids. Cages functionalized with longer alkyl groups were shown to be less viscous than their shorter-chained counterparts (Figure 1.13b). Conversely, computational modelling also showed that long linear alkyl chains rapidly entered the cage while terminal branching slowed the rate of encapsulation.[81] Cooper *et al.* concluded that the pentyl-functionalized cage, which melted at 156 °C and remained 30% empty in the liquid state, was the first example of a liquid material that contains intrinsic porosity. Computer simulations also demonstrated that the cages were able to solubilize CH_4, and that the gas preferred to occupy the cage cavities rather than temporary extrinsic pores formed by the alkyl tails.

The remaining Type I porous liquids that have been published to date were designed and synthesized by Dai *et al.* The first Type I porous liquid from the Dai group was published in 2015, and features the surface engineering of a hollow silica sphere with a cationic organosilane-based corona charge-balanced by a polyethylene glycol-tailed sulfonate anion

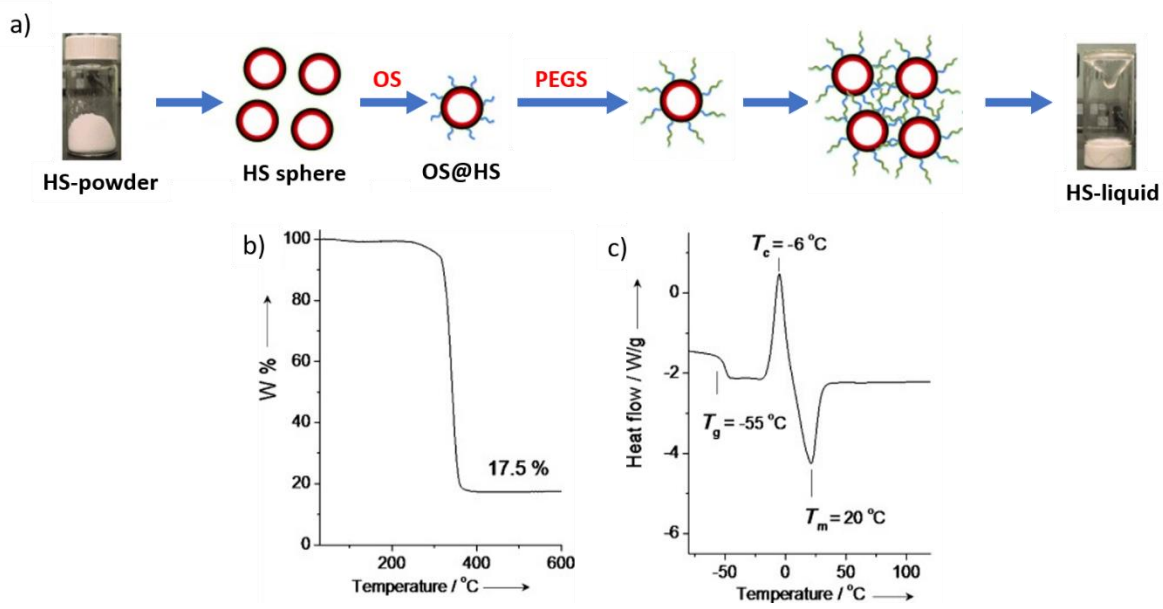

Figure 1.14: a) Synthetic strategy for adapting hollow silica spheres (HS) into a Type I porous liquid by functionalizing it with an organosilane (OS) corona charge balanced by PEG-sulfonate anions (PEG). b) TGA trace and c) DSC curve of the porous liquid. Figure adapted from reference 83.

(Figure 1.14a).[83] The microporous shells of the silica spheres prevented penetration of the cavity by any species larger than 1.9 nm. Therefore, the 2 nm organosilane moieties were too sterically hindered to occupy any pores of the host. TGA analysis of the liquid showed no mass loss below 260 °C, demonstrating that the material was solvent-free (Figure 1.14b). A glass-transition (-55 °C) and crystallization point (-6 °C) for the porous liquid were observed by DSC (Figure 1.14c). However, upon further heating, the material was found to melt at 20 °C, further confirming its liquid nature at room temperature. The viscosity of the material was determined to be 6.8 Pa·S at 40 °C – approximately the same viscosity as honey. The porous liquid mounted on a polymeric membrane was shown to have accelerated gas transport of CO_2 when compared to PEG, but no difference in selectivity between N_2 and CO_2. The authors proposed that the enhanced diffusivity of CO_2 through the porous liquid rendered it a good material for gas separation.

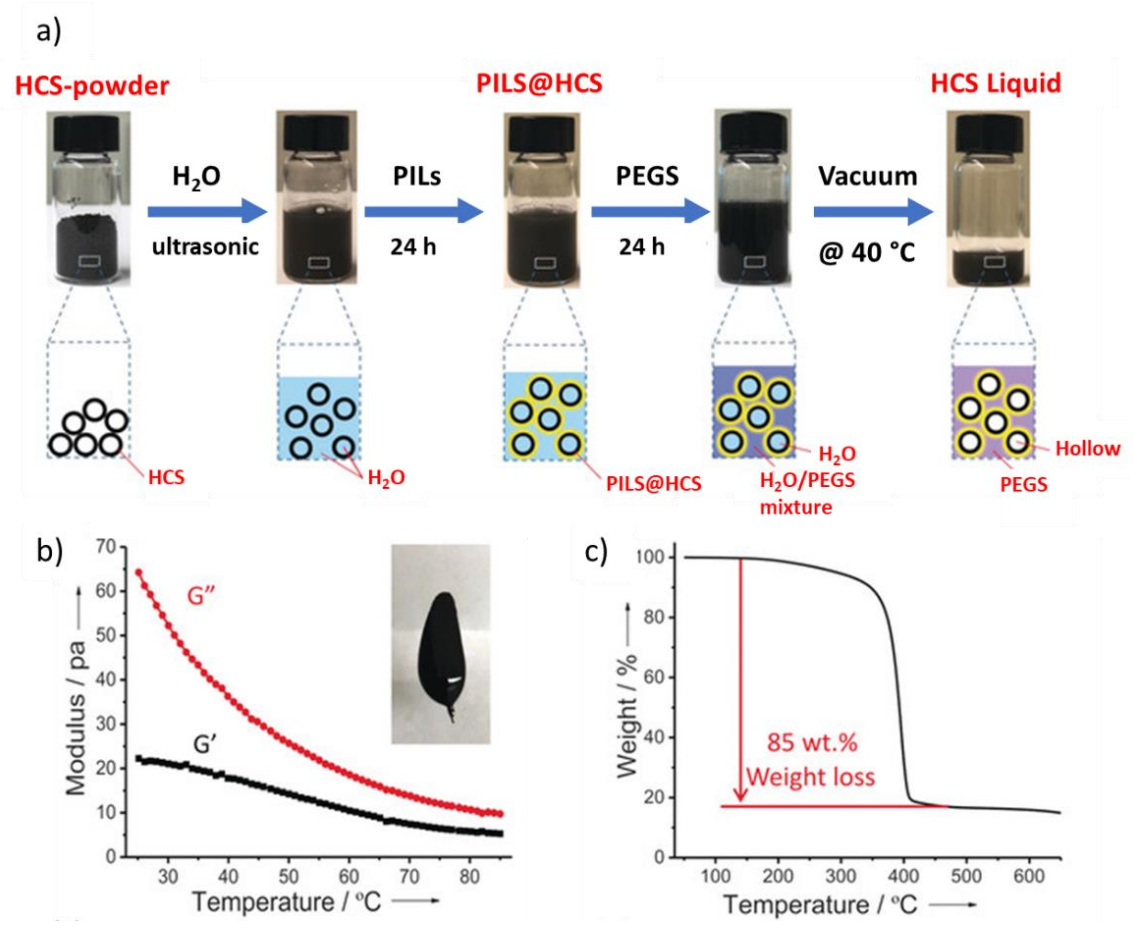

Figure 1.15: a) Synthesis of a hollow carbon sphere liquid (HCS-liquid). b) Rheology analysis of HCS-liquid with a temperature sweep past 80 °C; storage modulus = G' and loss modulus = G". c) TGA trace of HCS-liquid under N_2; no mass loss was observed until onset of decomposition. Figure adapted from reference 84.

Dai *et al.* then extended this strategy to create a second Type I porous liquid by electrostatically attaching a polymerized ionic liquid (PIL) to the surface of a porous nanocarbon (Figure 1.15a).[84] The positively charged ionic liquid was then charge-balanced with the same PEG-tailed sulfonate anion featured in the previously published silica-based porous liquid. The microporous shell of the hollow carbon sphere (HCS) blocked the PILs from occupying the sphere cavity. Rheological analysis of the porous liquid showed that the loss modulus (G") was always higher than the storage modulus (G') – a behavior that is characteristic of fluids (Figure 1.15b). Furthermore, TGA analysis of the material showed no mass loss until the decomposition of the sample, demonstrating that no solvent remained in the sphere cavities (Figure 1.15c). The porous liquid was also analyzed by positron annihilation lifetime spectroscopy (PALS), and the *o*-Ps lifetime of the porous liquid sample was found to be 2.54 ns – a value larger than those of the PEG (1.86 ns) and a composite of polymerized ionic liquid and PEG (1.87 ns). The authors concluded that the longer *o*-Ps lifetimes observed for the porous liquid indicated that the hosts in the material remained empty in the neat state. The liquid porous carbon was shown to have enhanced CO_2 adsorption when compared to PEG and the PIL, and the authors claimed this material showed potential for gas storage applications.

1.3.3 Type II porous liquid

There is only one example of a preconceived Type II porous liquid in the literature to date. In 2015, Cooper *et al.* functionalized an organic cage with 6 crown ether groups and discovered that the resulting capsule showed high solubility in 15-crown-5 ether – a solvent too sterically hindered to bind in the cavity of the cage (Figure 4.16a).[85] This concentrated solution was comprised of 44 wt% cage, which is equivalent to 12 solvent molecules per cage molecule. The viscosity of the porous liquid was dependent on both concentration and temperature. At higher temperatures, the material was less viscous. However, the viscosity of the solution increased at higher cage concentrations (Figure 4.16b). At room temperature, a sample containing a 1:36 molar ratio of cage to solvent resulted in a solution with a viscosity of ~140 cP, while a sample with a cage to solvent ratio of 1:72 had a viscosity of ~20 cP.

The porosity of the cages was determined through molecular dynamic simulations and PALS. Simulations showed that all of the cages remained consistently empty at both 350 K and 400 K. The distribution of cavity sizes in the system was also calculated, and the results showed that the cavities of the cages added up to 0.7% of the total volume. This value is small when compared to those of porous solids, but it demonstrates that intrinsic porosity can be

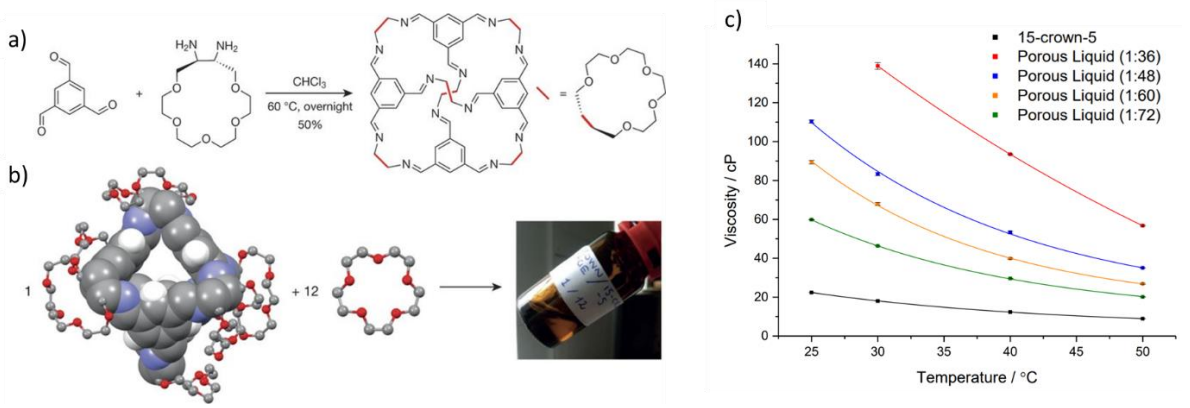

Figure 4.16: a) Synthesis of crown-ether-functionalized organic cage. b) Solvation of the crown-ether cage in 15-crown-5 solvent to create a Type II porous liquid. c) Rheological analysis of the porous liquid showing a temperature sweep experiment conducted on samples of different concentrations. Figure adapted from reference 85.

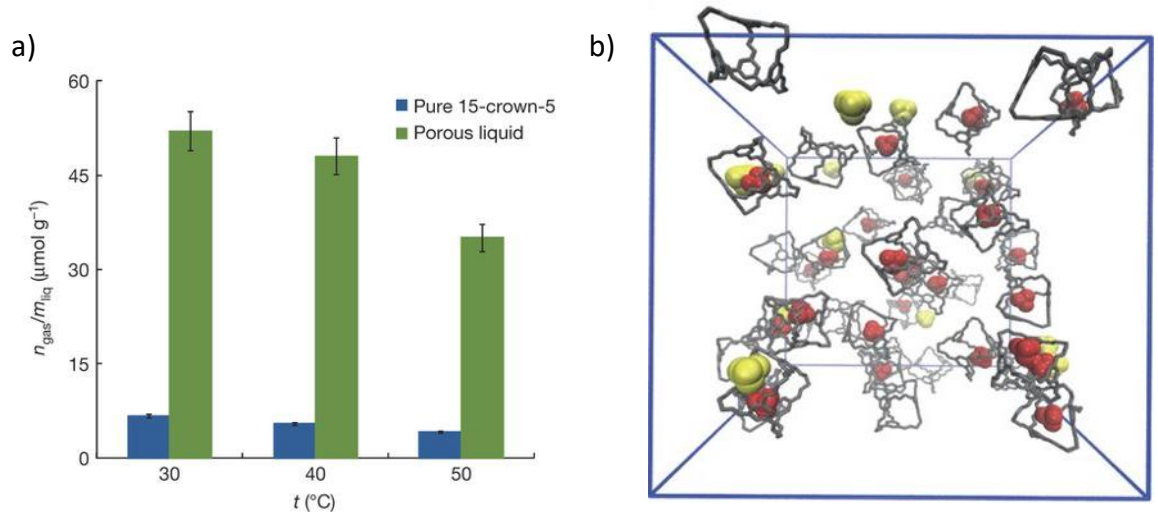

Figure 4.17: a) Results from molecular simulations showed that CH_4 is 8 times more soluble per mass of the porous liquid than per mass of the pure solvent. b) Molecular simulation of the porous liquid dissolving CH_4. Encapsulated CH_4 molecules within the cage are colored red and CH_4 molecules dissolved in extrinsic cavities are colored yellow. Figure adapted from reference 85.

engineered into liquids. In addition to simulations, PALS results showed the porous liquid had an *o*-Ps lifetime of 2.34 ± 0.1 ns – a value between the *o*-Ps lifetimes of the pure solid cage (2.05 ± 0.1 ns) and the 15-crown-5 solvent (3.00 ± 0.1 ns). The authors concluded that this pore diameter was reasonable for their material because it was approximately the average of the pore diameters of its components. The porous liquid was then used to adsorb CH_4, and results showed that the cage solution solubilized approximately 8 times more CH_4 than the pure 15-crown-5 solvent (Figure 4.17a). Molecular simulations also showed that the majority of gas molecules were encapsulated in the cage cavities, rather than trapped in extrinsic solvent pores

(Figure 4.17b). The authors acknowledged that this material currently cannot compete with porous solids with regards to gas storage, but proposed that this porous liquid could be used for gas separation instead.

One of the main drawbacks of the crown-ether based porous liquid was that the cage synthesis required six steps. To address this problem, the authors designed a second Type II porous liquid by using a mixture of diamines to make "scrambled cages"[86] with the same iminospherand scaffold as the aforementioned crown-ether-functionalized cage (Figure 1.18a). These scrambled cages were dissolved in hexachloropropene (PCP), a sterically hindered solvent, to yield a 10 wt% Type II porous liquid. The material had a viscosity of 11.7 cP at 298 K, and was at least 10 times less viscous than the crown-ether based porous liquid. The authors then demonstrated *via* gas saturation experiments that these cage solutions could solubilize CO_2, N_2 and Xe, in addition to CH_4. The subsequent addition of a smaller, stronger binding guest such as $CHCl_3$ triggered the cage to release the bound gas (Figure 1.18b).

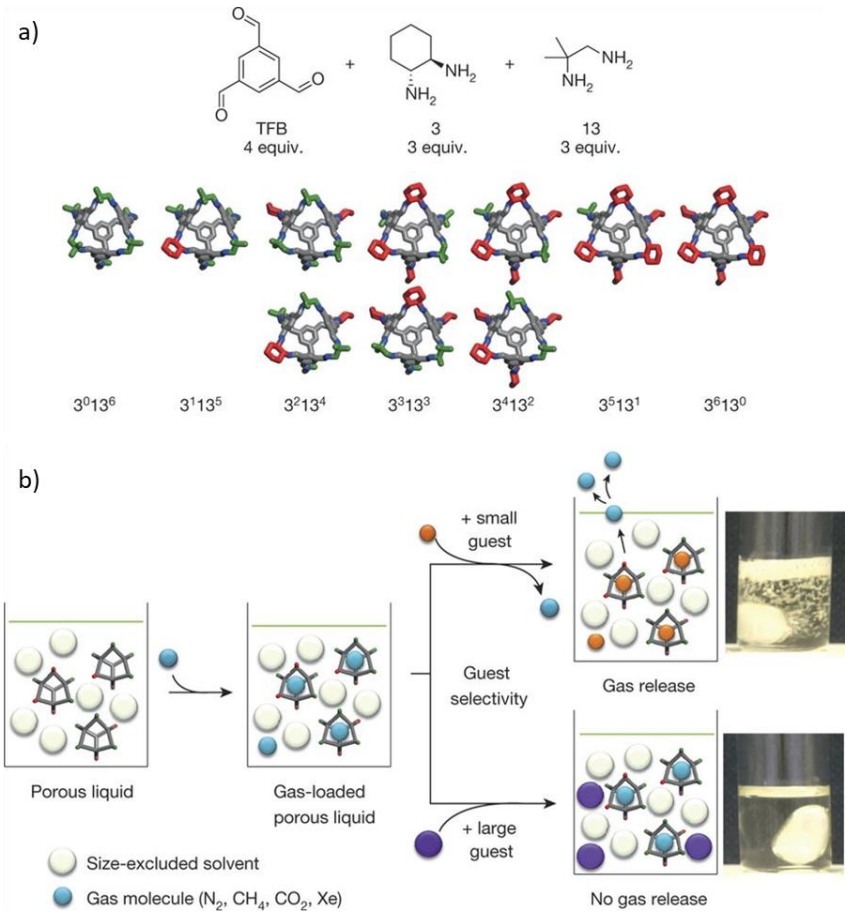

Figure 1.18: a) Reaction of TFB with a mixture of anilines yielded a statistical mixture of scrambled cages. b) Scrambled cages dissolved in PCP were found to encapsulate N_2, CH_4, CO_2 and Xe. The gaseous guest could then be displaced *via* the addition of a small guest such as $CHCl_3$. The addition of a second sterically hindered guest did not trigger guest release. Figure adapted from reference 85.

1.3.4 Type III porous liquid

While examples of Type III porous liquids existed before this class of materials was defined by Stuart James,[87,88] none of these materials were synthesized with the goal of being a porous liquid and thus their liquid properties and porosity were not analyzed in depth. However, in 2018, three different research groups each published a Type III porous liquid based on dissolving ZIF-8 in an ionic liquid. The first of these papers was by Dai *et al*. and the authors showed that ZIF-8, ZSM-5 and Silicalite-1 could be dispersed in a newly designed ionic liquid too sterically hindered to penetrate the hosts (Figure 1.19).[89] Of these three different types of porous hosts, ZIF-8 showed the highest solubility in the porous liquid, yielding a solution that consisted of 30 wt% host. PALS analysis of the ZIF-8 porous liquid confirmed the presence of empty pores. The porous liquid was then shown to adsorb CO_2 and the authors demonstrated that increasing the concentration of ZIF-8 resulted in more efficient gas adsorption.

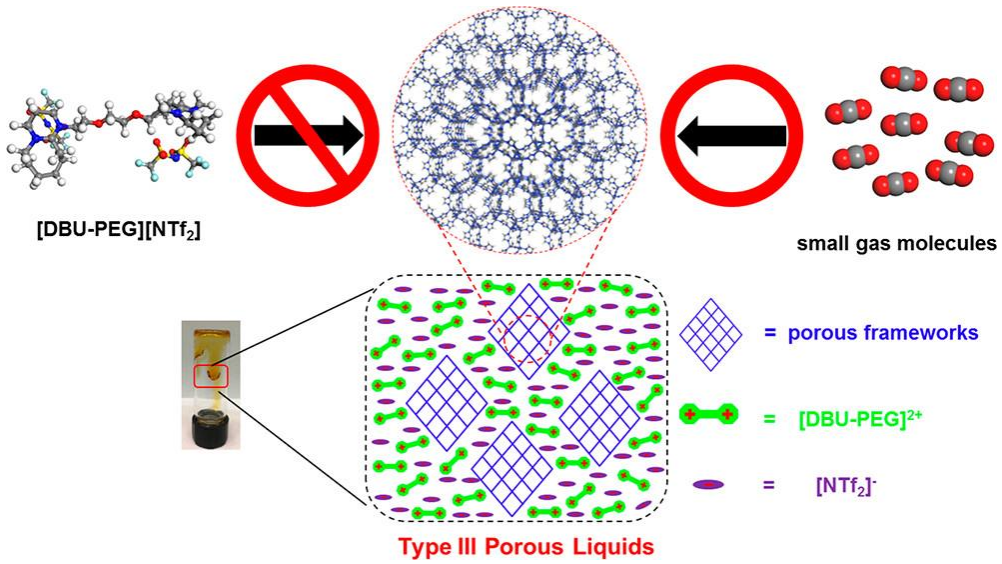

Figure 1.19: Graphical abstract of a novel Type III porous liquid based on the solvation of ZIF-8 in [DBU-PEG][NTf_2], a new ionic liquid too sterically hindered to occupy the pores of the host. The porous liquid is shown to adsorb CO_2. Figure adapted from reference 89.

The second Type III porous liquid was published three months later by Liu *et al.* The authors showed that ZIF-8 was also soluble and stable in *N*-butyl pyridinium-based ionic liquid [Bpy][NTf_2].[90] The direct mixture of dry ZIF-8 and the ionic liquid resulted in aggregation of the solid. Therefore, ZIF-8 and [Bpy][NTf_2] were combined in methanol solution, after which the solvent was removed at 100 °C under vacuum (Figure 1.20a) to yield a homogenous porous solution with a host concentration of 1.4 wt%. PALS analysis of the sample confirmed the presence of empty pores, which were then used to adsorb N_2 and I_2 gas. After iodine was

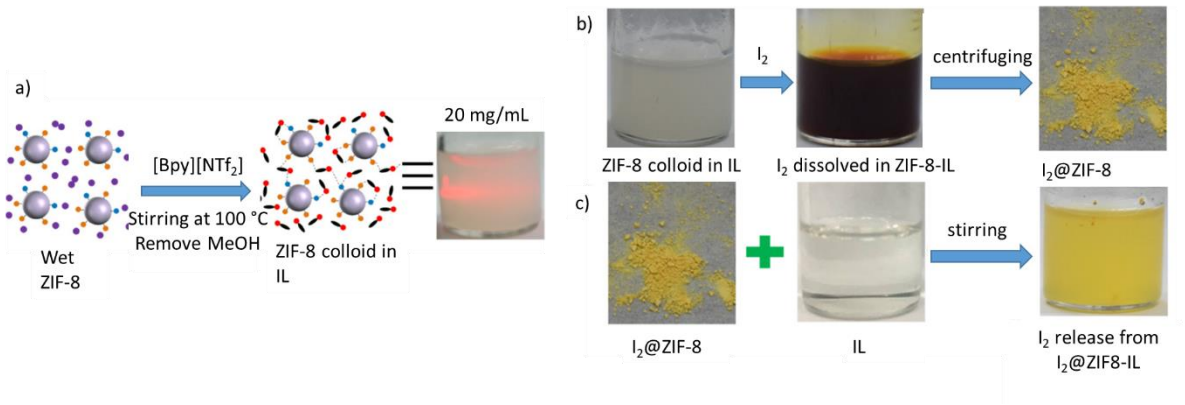

Figure 1.20: a) Homogenous dispersion of ZIF-8 in [Bpy][NTf_2]. b) Adsorption of I_2 in ZIF-8 porous liquid; the host-guest complex can be isolated *via* centrifugation. c) Solvation of $I_2 \subset$ ZIF-8 in pure ionic liquid resulted in guest-release into solution. Figure adapted from reference 90.

solubilized in the porous liquid, the $I_2 \subset$ ZIF-8 host-guest complex could be collected *via* centrifugation (Figure 1.20b). Dissolving the isolated host-guest complex in a new sample of [Bpy][NTf_2] resulted in the subsequent release of the guest (Figure 1.20c).

The final ZIF-8-based porous liquid was presented by Gomes *et al.* in the same year.[91] The authors demonstrated that a Type III porous liquid could be synthesized by suspending ZIF-8 (up to 5 wt%) in ionic liquid [$P_{6,6,6,14}$][NTf_2]. Density measurements of the porous liquid show that the product is less dense than the pure ionic liquid, indicating that intrinsic porosity was present in the liquid material. Molecular simulations of the porous liquid confirmed this observation. The authors also showed that not all MOFs are good candidates for Type III porous liquids by demonstrating how the density of Mg-MOF-74 suspended in [$P_{6,6,6,14}$][NTf_2] was higher than that of the pure ionic liquid. This density increase was attributed to the ionic liquid ions occupying the MOF pores. Both the MOF and ZIF-based porous liquids were analyzed by gravimetric gas solubility measurements and results indicated that the 5 wt% ZIF-8 porous liquid was capable of adsorbing 100% more N_2 and CH_4 than the pure ionic liquid (Figure 4.21a), although pure ZIF-8 still significantly outperformed the porous liquid samples. Conversely, the MOF-74-based porous liquid did not show increased performance, thus confirming the authors' hypothesis that the material did not have accessible porosity (Figure 4.21b).

These three examples of Type III porous liquids are all based on ZIF-8 dissolved in an ionic liquid. However, the permutations of extended networks and sterically hindered solvents to combine are seemingly endless. Interestingly, while Dai *et al.* designed an ionic liquid specifically as a solvent for ZIF-8,[89] no examples of porous extended networks tailor-made for Type III porous liquids have been published to date.

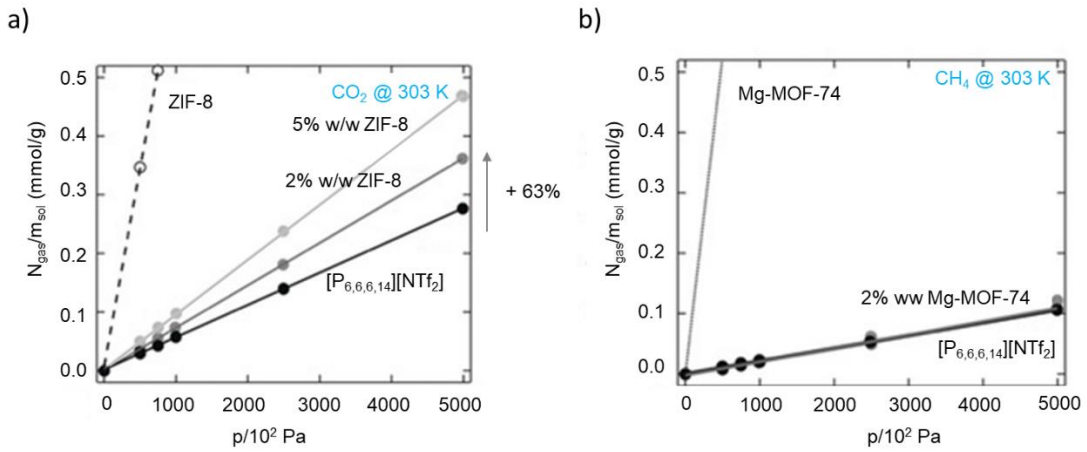

Figure 4.21: a) Solubility of CO_2 in ZIF-8 suspensions at 303 K from atmospheric pressure to 5 bar and b) solubility of CH_4 in a 2 wt% suspension of Mg-MOF-74 in $[P_{6,6,6,14}][NTf_2]$ and the pure ionic liquid. Figure adapted from reference 91.

1.3.5 Other porous liquids

In addition to the aforementioned examples of porous liquids, Bennett *et al.* demonstrated that ZIF-4, which is formed of Zn(imidazolate)$_4$ tetrahedra linked by Zn-N dative bonds, is intact and stable beyond its melting point of 865 K, making it the first liquid MOF.[92] ZIF-4 was heated to 865 K and cooled naturally to room temperature, resulting in a glass-like solid. Both neutron and X-ray structure factors of the glass ZIF showed that the network topology remained unchanged when compared to the crystalline ZIF. Therefore, heating the sample past its melting point did not affect the structure of the framework.

The distribution of Zn cation coordination numbers was calculated as a function of temperature and the authors discovered that while four-fold coordination was maintained at low temperatures, the proportion of undercoordinated Zn increased at higher temperatures. The authors hypothesized that the melting mechanics of the system involved the fast rearrangement

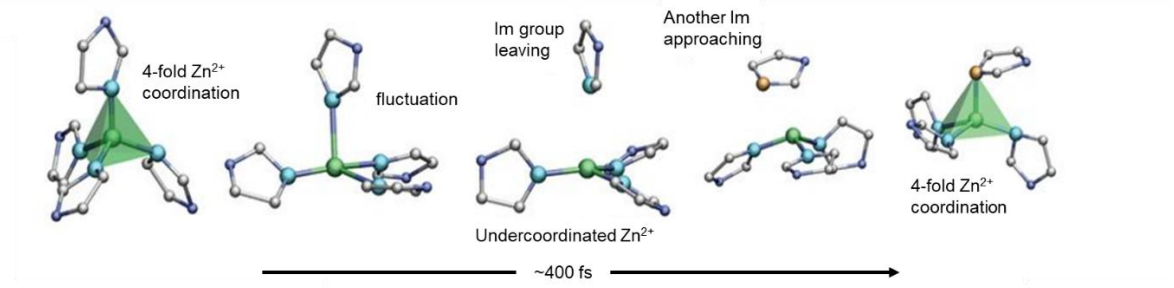

Figure 1.22: Proposed mechanism for the intact melting of ZIF-4 involving the fast rearrangement of the imidazolate ligands. Figure adapted from reference 92.

of ZIF-4, where one imidazolate moiety of the tetrahedron leaves and is quickly replaced by a neighboring imidazolate (Figure 1.22). Molecular simulations of the system also demonstrated that the liquid MOF was more porous than its solid glass analogue. While the MOF in its liquid state at above 1,200 K would be considered a Type I porous liquid, all other examples of porous liquids in this work refer to materials with permanent porosity that are liquid at 298 K. Therefore, this liquid MOF has not be categorized into any of the three types of porous liquids.

1.4 Aims and Objectives

Porous liquids make up a novel class of materials, which combines the conventional porosity associated with solids and the fluid mechanics of liquids. These liquids with intrinsic porosity have been used for the adsorption and separation of a variety of gasses, but have not been demonstrated to encapsulate any solid or liquid guests. As of today, porous liquids have been based on several different rigid hosts ranging from MOFs and zeolites to silica nanospheres and porous organic cages. However, to the best of our knowledge, coordination cages have not yet been employed in this field. Therefore, we propose to use coordination cages as a scaffold for a new library of permanently porous liquids. One method of incorporating metal-organic cages into porous liquids is to synthesize a coordination cage that is a room temperature ionic liquid. The rigidity of the cage scaffold and the empty cavities of the liquid capsule would render this material a Type I porous liquid. An alternate, and potentially less synthetically complex, route would be to solvate coordination cages in bulky solvents, such as ionic liquids, to generate Type II porous liquids. In this thesis, we investigate both of these methods.

Additionally, we propose that subcomponent self-assembled cages are especially good candidates for being hosts in porous liquids. One of the main drawbacks of porous liquids is the synthetic complexity of many of these materials. However, subcomponent self-assembly is a versatile and modular method that could allow for the facile synthesis of liquid cages with different sizes and architectures. Furthermore, these capsules have also been shown to encapsulate a diverse range of guests. Therefore, a porous liquid based on these hosts could potentially be used under solvent-free conditions to encapsulate non-gaseous guests. We hypothesize that the employment of coordination cages based on subcomponent self-assembly as hosts in porous liquids would result in a novel class of materials capable of furthering the nascent field of liquids with intrinsic porosity.

1.5 References

(1) Rouquerol, J.; Avnir, D.; Fairbridge, C. W.; Everett, D. H.; Haynes, J. M.; Pernicone, N.; Ramsay, J. D. F.; Sing, K. S. W.; Unger, K. K. *Pure Appl. Chem.* **1994**, *66* (8), 1739–1758.

(2) Slater, A. G.; Cooper, A. I. *Science (80-.).* **2015**, *348* (6238), 8075.

(3) Zhou, H.-C.; Long, J. R.; Yaghi, O. M. *Chem. Rev.* **2012**, *112* (2), 673–674.

(4) Ding, S. Y.; Wang, W. *Chem. Soc. Rev*. **2013**, *42*, (2), 548–568.

(5) Mohau Moshoeshoe; Misael Silas Nadiye-Tabbiruka; Veronica Obuseng. *Am. J. Mater. Sci.* **2017**, *7* (5), 196–221.

(6) Stein, A.; Wang, Z.; Fierke, M. A. *Adv. Mater*. **2009**, *21* (3), 265–293.

(7) Wu, D.; Xu, F.; Sun, B.; Fu, R.; He, H.; Matyjaszewski, K. *Chem. Rev.* **2012**, *112* (7), 3959–4015.

(8) Chen, T. H.; Popov, I.; Kaveevivitchai, W.; Chuang, Y. C.; Chen, Y. S.; Jacobson, A. J.; Miljanic, O. *Angew. Chemie - Int. Ed.* **2015**, *54* (47), 13902–13906.

(9) Li, J. R.; Kuppler, R. J.; Zhou, H. C. *Chem. Soc. Rev.* **2009**, *38* (5), 1477–1504.

(10) Lee, J.; Farha, O. K.; Roberts, J.; Scheidt, K. A.; Nguyen, S. T.; Hupp, J. T. *Chem. Soc. Rev.* **2009**, *38* (5), 1450–1459.

(11) Wang, J. L.; Wang, C.; Lin, W. *ACS Catalysis*. **2012**, *2* (12), 2630–2640.

(12) Ding, S. Y.; Gao, J.; Wang, Q.; Zhang, Y.; Song, W. G.; Su, C. Y.; Wang, W. *J. Am. Chem. Soc.* **2011**, *133* (49), 19816–19822.

(13) Chen, B.; Liang, C.; Yang, J.; Contreras, D. S.; Clancy, Y. L.; Lobkovsky, E. B.; Yaghi, O. M.; Dai, S. *Angew. Chemie - Int. Ed.* **2006**, *45* (9), 1390–1393.

(14) Fan, H.; Mundstock, A.; Feldhoff, A.; Knebel, A.; Gu, J.; Meng, H.; Caro, J. *J. Am. Chem. Soc.* **2018**, *140* (32), 10094–10098.

(15) Qiu, S.; Xue, M.; Zhu, G. *Chem. Soc. Rev.* **2014**, *43* (16), 6116–6140.

(16) Chakrabarty, R.; Mukherjee, P. S.; Stang, P. J. *Chem. Rev.* **2011**, *111* (11), 6810–6918.

(17) Hasell, T.; Cooper, A. I. *Nat. Rev. Mater*. **2016**, *1* (9), 1-14.

(18) Ananchenko, G. S.; Moudrakovski, I. L.; Coleman, A. W.; Ripmeester, J. A. *Angew. Chemie - Int. Ed.* **2008**, *47* (30), 5616–5618.

(19) Masson, E.; Ling, X.; Joseph, R.; Kyeremeh-Mensah, L.; Lu, X. *RSC Adv*. **2012**, *2* (4), 1213–1247.

(20) Kusaba, S.; Yamashina, M.; Akita, M.; Kikuchi, T.; Yoshizawa, M. *Angew. Chemie - Int. Ed.* **2018**, *57* (14), 3706–3710.

(21) Heinz, T.; Rudkevich, D. M.; Rebek, J. *Nature* **1998**, *394* (6695), 764–766.

(22) Rizzuto, F. J.; Carpenter, J. P.; Nitschke, J. R. *J. Am. Chem. Soc.* **2019**, *141* (22), 9087-9095.

(23) Kim, H.; Kim, Y.; Yoon, M.; Lim, S.; Park, S. M.; Seo, G.; Kim, K. *J. Am. Chem. Soc.* **2010**, *132* (35), 12200–12202.

(24) Tozawa, T.; Jones, J. T. A.; Swamy, S. I.; Jiang, S.; Adams, D. J.; Shakespeare, S.; Clowes, R.; Bradshaw, D.; Hasell, T.; Chong, S. Y. *Nat. Mater.* **2009**, *8* (12), 973.

(25) Sudik, A. C.; Millward, A. R.; Ockwig, N. W.; Côté, A. P.; Kim, J.; Yaghi, O. M. *J. Am. Chem. Soc.* **2005**, *127* (19), 7110–7118.

(26) Handke, M.; Adachi, T.; Hu, C.; Ward, M. D. *Angew. Chemie - Int. Ed.* **2017**, *56* (45), 14003–14006.

(27) Fujita, D.; Suzuki, K.; Sato, S.; Yagi-Utsumi, M.; Yamaguchi, Y.; Mizuno, N.; Kumasaka, T.; Takata, M.; Noda, M.; Uchiyama, S.; et al. *Nat. Commun.* **2012**, *3*.

(28) Zheng, Y. R.; Suntharalingam, K.; Johnstone, T. C.; Lippard, S. J. *Chem. Sci.* **2015**, *6* (2), 1189–1193.

(29) Greathouse, J. A.; Allendorf, M. D. *J. Am. Chem. Soc.* **2006**, *128* (33), 10678–10679.

(30) Huang, L.; Wang, H.; Chen, J.; Wang, Z.; Sun, J.; Zhao, D.; Yan, Y. *Microporous Mesoporous Mater.* **2003**, *58* (2), 105–114.

(31) Bolliger, J. L.; Belenguer, A. M.; Nitschke, J. R. *Angew. Chemie - Int. Ed.* **2013**, *52* (31), 7958–7962.

(32) Yoshizawa, M.; Tamura, M.; Fujita, M. *Science (80-.).* **2006**, *312* (5771), 251–254.

(33) Ronson, T. K.; Zarra, S.; Black, S. P.; Nitschke, J. R. *Chem. Commun.* **2013**, *49* (25), 2476–2490.

(34) Nitschke, J. R. *Angew. Chemie - Int. Ed.* **2004**, *43* (23), 3073–3075.

(35) Ronson, T. K.; Zarra, S.; Black, S. P.; Nitschke, J. R. *Chem. Commun.* **2013**, *49* (25), 2476–2490.

(36) Bunzen, H.; Nonappa; Kalenius, E.; Hietala, S.; Kolehmainen, E. *Chem. - A Eur. J.* **2013**, *19* (39), 12978–12981.

(37) Wu, X.; Xu, N.; Zhu, Z.; Cai, Y.; Zhao, Y.; Wang, D. *Polym. Chem.* **2014**, *5* (4), 1202–1209.

(38) Riddell, I. A.; Smulders, M. M. J.; Clegg, J. K.; Nitschke, J. R. *Chem. Commun.* **2011**, *47* (1), 457–459.

(39) Riddell, I. A.; Ronson, T. K.; Clegg, J. K.; Wood, C. S.; Bilbeisi, R. A.; Nitschke, J. R. *J. Am. Chem. Soc.* **2014**, *136* (26), 9491–9498.

(40) Grommet, A. B.; Bolliger, J. L.; Browne, C.; Nitschke, J. R. *Angew. Chemie - Int. Ed.* **2015**, *54* (50), 15100–15104.

(41) Welton, T. *Chem. Rev.* **1999**, *99* (8), 2071–2084.

(42) Walden, P. *Bull Acad Imper Sci* **1914**, *8*, 405–422.

(43) Wilkes, J. S.; Zaworotko, M. J. *J. Chem. Soc. Chem. Commun.* **1992**, No. 13, 965–967.

(44) Krossing, I.; Slattery, J. M.; Daguenet, C.; Dyson, P. J.; Oleinikova, A.; Weingärtner, H. *J. Am. Chem. Soc.* **2006**, *128* (41), 13427–13434.

(45) Olivier-Bourbigou, H.; Magna, L.; Morvan, D. *Appl. Catal., A: General*. **2010**, 1–56.

(46) Boon, J. A.; Levisky, J. A.; Pflug, J. L.; Wilkes, J. S. *J. Org. Chem.* **1986**, *51* (4), 480–483.

(47) Bates, E. D.; Mayton, R. D.; Ntai, I.; Davis, J. H. *J. Am. Chem. Soc.* **2002**, *124* (6), 926–927.

(48) Ventura, S. P. M.; E Silva, F. A.; Quental, M. V.; Mondal, D.; Freire, M. G.; Coutinho, J. A. P. *Chem. Rev*. **2017**, *117* (10), 6984–7052.

(49) Earle, M. J.; Seddon, K. R. *Pure Appl. Chem.* **2007**, *72* (7), 1391–1398.

(50) Aschenbrenner, O.; Supasitmongkol, S.; Taylor, M.; Styring, P. *Green Chem.* **2009**, *11* (8), 1217–1221.

(51) Mokbel, I.; Sawaya, T.; Zanota, M. L.; Naccoul, R. A.; Jose, J.; De Bellefon, C. *J. Chem. Eng. Data* **2012**, *57* (2), 284–289.

(52) Maton, C.; De Vos, N.; Stevens, C. V. *Chem. Soc. Rev.* **2013**, *42* (13), 5963–5977.

(53) Lancaster, N. L.; Welton, T.; Young, G. B. *J. Chem. Soc. Perkin Trans. 2* **2001**, (12), 2267–2270.

(54) Blake, D. M.; Moens, L.; Rudnicki, D.; Pilath, H. *J. Sol. Energy Eng.* **2006**, *128* (1), 54.

(55) Widegren, J. A.; Magee, J. W. *J. Chem. Eng. Data* **2007**, *52* (6), 2331–2338.

(56) Burrell, G. L.; Burgar, I. M.; Separovic, F.; Dunlop, N. F. *Phys. Chem. Chem. Phys.* **2010**, *12* (7), 1571–1577.

(57) Anderson, J. L.; Armstrong, D. W. *Anal. Chem.* **2003**, *75* (18), 4851–4858.

(58) Yu, G.; Zhao, D.; Wen, L.; Yang, S.; Chen, X. *AIChE J.* **2012**, *58* (9), 2885–2899.

(59) Kanakubo, M.; Harris, K. R.; Tsuchihashi, N.; Ibuki, K.; Ueno, M. *Fluid Phase Equilib.* **2007**, *261* (1–2), 414–420.

(60) Harris, K. R.; Woolf, L. A.; Kanakubo, M. *J. Chem. Eng. Data*. **2005**, *50* (5), 1777–1782.

(61) Schreiner, C.; Zugmann, S.; Hartl, R.; Gores, H. J. *J. Chem. Eng. Data* **2010**, *55* (10), 4372–4377.

(62) Hagiwara, R.; Ito, Y. *J. Fluorine Chem.* **2000**, *105* (2), 221–227.

(63) Kulkarni, P. S.; Branco, L. C.; Crespo, J. G.; Nunes, M. C.; Raymundo, A.; Afonso, C. A. M. *Chem. - A Eur. J.* **2007**, *13* (30), 8478–8488.

(64) Zhou, Z. Bin; Matsumoto, H.; Tatsumi, K. *Chem. - A Eur. J.* **2004**, *10* (24), 6581–6591.

(65) Zhou, Z. Bin; Matsumoto, H.; Tatsumi, K. *Chem. - A Eur. J.* **2006**, *12* (8), 2196–2212.

(66) Zhou, Z. Bin; Matsumoto, H.; Tatsumi, K. *Chem. - A Eur. J.* **2005**, *11* (2), 752–766.

(67) Huddleston, J. G.; Willauer, H. D.; Swatloski, R. P.; Visser, A. E.; Rogers, R. D. *Chem. Commun.* **1998**, (16), 1765–1766.

(68) Quinn, R.; Appleby, J. B.; Pez, G. P. *J. Am. Chem. Soc.* **1995**, *117* (1), 329–335.

(69) Polasek, J.; Bullin, J. *Energy Progress.* **1984**, 1–9.

(70) Baker, R. W.; Lokhandwala, K. *Ind. Eng. Chem. Res.* **2008**, *47* (7), 2109–2121.

(71) Swatloski, R. P.; Spear, S. K.; Holbrey, J. D.; Rogers, R. D. *J. Am. Chem. Soc.* **2002**, *124* (18), 4974–4975.

(72) Garcia, B.; Lavallée, S.; Perron, G.; Michot, C.; Armand, M. *Electrochim. Acta* **2004**, *49* (26), 4583–4588.

(73) Plechkova, N. V.; Seddon, K. R. *Chem. Soc. Rev.* **2008**, *37* (1), 123–150.

(74) Bermúdez, M. D.; Jiménez, A. E.; Sanes, J.; Carrión, F. J. *Molecules.* **2009**, *14* (8), 2888–2908.

(75) O'Reilly, N.; Giri, N.; James, S. L. *Chem. - A Eur. J.* **2007**, *13* (11), 3020–3025.

(76) Pohorille, A.; Pratt, L. R. *J. Am. Chem. Soc.* **1990**, *112* (13), 5066–5074.

(77) Meier-Augenstein, W.; Burger, B. V.; Burger, W. J. G.; Spies, H. S. C. *Zeitschrift fur Naturforsch. - Sect. B J. Chem. Sci.* **1992**, *47* (6), 877–886.

(78) Caira, M. R.; Bourne, S. A.; Mhlongo, W. T.; Dean, P. M. *Chem. Commun.* **2004**, *10* (19), 2216–2217.

(79) Robbins, T. A.; Knobler, C. B.; Bellew, D. R.; Cram, D. J. *J. Am. Chem. Soc.* **1994**, *116* (1), 111–122.

(80) Hsu, S. C. N.; Ramesh, M.; Espenson, J. H.; Rauchfus, T. B. *Angew. Chemie - Int. Ed.* **2003**, *42* (23), 2663–2666.

(81) Giri, N.; Davidson, C. E.; Melaugh, G.; Del Pópolo, M. G.; Jones, J. T. A.; Hasell, T.; Cooper, A. I.; Horton, P. N.; Hursthouse, M. B.; James, S. L. *Chem. Sci.* **2012**, *3* (6), 2153–2157.

(82) Melaugh, G.; Giri, N.; Davidson, C. E.; James, S. L.; Del Pópolo, M. G. *Phys. Chem. Chem. Phys.* **2014**, *16* (20), 9422–9431.

(83) Zhang, J.; Chai, S. H.; Qiao, Z. A.; Mahurin, S. M.; Chen, J.; Fang, Y.; Wan, S.; Nelson,

K.; Zhang, P.; Dai, S. *Angew. Chemie - Int. Ed.* **2015**, *54* (3), 932–936.

(84) Li, P.; Schott, J. A.; Zhang, J.; Mahurin, S. M.; Sheng, Y.; Qiao, Z. A.; Hu, X.; Cui, G.; Yao, D.; Brown, S.; et al. *Angew. Chemie - Int. Ed.* **2017**, *56* (47), 14958–14962.

(85) Giri, N.; Del Pópolo, M. G.; Melaugh, G.; Greenaway, R. L.; Rätzke, K.; Koschine, T.; Pison, L.; Gomes, M. F. C.; Cooper, A. I.; James, S. L. *Nature* **2015**, *527* (7577), 216–220.

(86) Jiang, S.; Jones, J. T. A.; Hasell, T.; Blythe, C. E.; Adams, D. J.; Trewin, A.; Cooper, A. I. *Nat. Commun.* **2011**, *2* (1).

(87) Yamada, M.; Arai, M.; Kurihara, M.; Sakamoto, M.; Miyake, M. *J. Am. Chem. Soc.* **2004**, *126* (31), 9482–9483.

(88) Devaux, A.; Popović, Z.; Bossart, O.; De Cola, L.; Kunzmann, A.; Calzaferri, G. *Microporous Mesoporous Mater.* **2006**, *90* (1-3 SPEC. ISS.), 69–72.

(89) Shan, W.; Fulvio, P. F.; Kong, L.; Schott, J. A.; Do-Thanh, C. L.; Tian, T.; Hu, X.; Mahurin, S. M.; Xing, H.; Dai, S. *ACS Appl. Mater. Interfaces* **2018**, *10* (1), 32–36.

(90) Liu, S.; Liu, J.; Hou, X.; Xu, T.; Tong, J.; Zhang, J.; Ye, B.; Liu, B. *Langmuir* **2018**, *34* (12), 3654–3660.

(91) Costa Gomes, M.; Pison, L.; Červinka, C.; Padua, A. *Angew. Chemie - Int. Ed.* **2018**, *57* (37), 11909–11912.

(92) Gaillac, R.; Pullumbi, P.; Beyer, K. A.; Chapman, K.; Keen, D. A.; Bennett, T. D.; Coudert, F. X. *Nat. Mater.* **2017**, *16* (11), 1149–1155.

CHAPTER 2

Materials and Methods

2.1 General Methods

All reagents and solvents were used as supplied from commercial sources unless otherwise specified. The purity of deuterated solvents can be critical with cage systems. Notably, CD_3CN supplied by Sigma-Aldrich contained an unknown impurity that interfered with host-guest experiments. However, CD_3CN supplied by Fluorochem (produced by Eurisotop) proved to be of sufficient quality for our experiments, and was therefore exclusively used. Fe^{II} dodecyl sulfate and [hmim][BF_4] were synthesized by Dr. Angela Grommet. The synthesis of aldehydes **3F-3N** was optimized by this author but the compounds were subsequently synthesized by Zhichen Wu. Cages **3.1-3.20** were synthesized by Zhichen Wu under the supervision of Dr. Angela Grommet. Characterization for these structures can be obtained by contacting Professor Jonathan Nitschke. Rheology measurements and data processing was conducted by Christopher Parkins. Positron annihilation lifetime spectroscopy and data processing was conducted by Dr. Cara Doherty. DSC and TGA analysis was performed in conjunction with Dr. Thomas Bennett and Louis Longley. Flash column chromatography purifications were conducted with a Biotage Isolera Four Advanced Automated Flash Purification System on silica prepacked cartridges.

2.2 Nuclear Magnetic Resonance Spectroscopy (NMR)

NMR spectra were recorded using a 400 MHz Avance III HD Smart Probe or a 500 MHz DCH Cryoprobe. All experiments were run at 298 K unless otherwise indicated. Chemical shifts for ^{1}H, ^{13}C and ^{19}F are reported in ppm on the δ scale. ^{1}H and ^{13}C were referenced to the chemical shift of the residual solvent peak while a reference capillary of C_6F_6 (-164.6 ppm) or 1,3,5-tris(trifluoromethyl)benzene (-63.63 ppm) was used as an external standard for ^{19}F NMR. Coupling constants (*J*) are reported in hertz (Hz). The abbreviations used to denote the NMR spectra are as follows: b, broad; s, singlet; d, doublet; dd, doublet of doublets; t, triplet; q, quartet; m, multiplet.

DOSY NMR experiments were performed on a 400 MHz Avance III HD Smart Probe at 298 K. Maximum gradient strength was 6.57 G/cm A. The standard Bruker pulse program, ledbpgp2s, employing a stimulated echo and longitudinal eddy-current delay (LED) using bipolar gradient pulses for diffusion using 2 spoil gradients was utilised. Rectangular gradients

were used with a total duration of 1.5 ms. Gradient recovery delays were 875 –1400 μs. Individual rows of the S4 quasi-2D diffusion databases were phased and baseline corrected.

2.3 Mass Spectrometry (MS)

Low resolution electrospray ionization mass spectrometry (LR-ESI-MS) was performed on a Micromass Quattro LC mass spectrometer (cone voltage 10-30 eV; desolvation temperature 313 K; ionisation temperature 313 K) infused from a Harvard syringe pump at a rate of 10 μL min−1. High resolution electrospray ionization mass spectrometry (HR-ESI-MS) was performed on either a Waters LCT Premier Mass Spectrometer featuring a Z spray source with electrospray ionisation and modular LockSpray interface at the Department of Chemistry, University of Chemistry or a Themofisher LTQ Orbitrap XL at the National Mass Spectrometry Facility, Swansea University.

2.4 Rheology

Rheological characterization was performed using a TA Instruments DHR-2 controlled stress rheometer fitted with a Peltier stage set to 25 °C. The plate and geometry were both pre-treated with 100 °C heat for 30 minutes to remove surface moisture. Sample loading was performed at 50 °C. Samples underwent sample conditioning for 120 s at 0.1 rad/s before 300 s of equilibrium. Dynamic oscillatory strain amplitude sweep measurements were conducted at a frequency of 10 rad/s. Dynamic oscillatory frequency sweep measurements were conducted between 0.1 and 100 rad/s at a 1% strain amplitude. Flow sweep measurements were carried out between 0.1 and 100 1/s. Flow ramp measurements were carried out linearly between 1 and 100 s^{-1} with a sampling rate of 1 s/pt. Oscillatory temperature ramp measurements were carried out at 1% strain and 10 rad/s with a ramp speed of 5 °C/min. All measurements were performed using a 20 mm 1° cone geometry with a gap size of 26 μm and analyzed using TA Instruments TRIOS software.

2.5 Differential Scanning Calorimetry (DSC) and Thermal Gravimetric Analysis (TGA)

Thermal stability was determined with a TA Instruments Q2000 DSC, a Netzsch 214 Polyma DSC and a TA Instruments Q600 SDT in the Department of Materials Science and Metallurgy at the University of Cambridge or a TA TGA Q50 V20.13 Build 39 at the Cambridge Graphene Centre at the University of Cambridge. All experiments were conducted under argon and heated or cooled at 10 °C/min.

2.6 Positron Annihilation Lifetime Spectroscopy (PALS)

A 1.5 MBq ^{22}NaCl source sealed in Mylar was immersed in cage **5.2** and placed between the EG&G Ortec Spectrometers. Lifetimes were collected at 298 K where a minimum of 5 files of 1 x 10^6 integrated counts was collected over 24 hours. The spectra were analysed using the LT v9 software.[1] The data were fitted to 3 lifetimes and a source correction (1.640 ns, 2.48%). The first lifetime, τ1 was attributed to *para*-positronium (*p*-Ps) annihilation (bound state of the positron with an electron of the opposite spin) and fixed to 0.125 ns. The second lifetime τ2 was associated with free annihilation of the positron with free electrons within the sample (~0.4 ns). The final lifetime, τ3 (*ortho*-positronium, *o*-Ps, bound state of a positron with an electron of same spin) was attributed to the free volume within the porous liquid.

The long lifetime τ3 and the associated Intensity (I3) were used to determine the average size and the relative number of free-volume elements respectively. The *o*-Ps can live up to 142 ns in vacuum, however it annihilates when it interacts with electrons from the sample; therefore, in general, the larger the free space, the longer the lifetime. The average free volume diameter was calculated using τ3 (ns) with the Tao-Eldrup equation (Equation 5.1).[2,3]

$$\tau_3 = \frac{1}{2}\left[1 - \frac{R}{R_0} + \frac{1}{2\pi}\sin\left(\frac{2\pi R}{R_0}\right)\right] \qquad \textbf{Equation 2.1}$$

where R is the free-volume of radius (Å) and R_0=ΔR+R. ΔR was determined empirically to be 1.66 Å and is the thickness of an electron layer in an infinite potential well of radius R_0, within the sample in which a single *o*-Ps is confined.

2.7 Molecular Modelling

Molecular model simulations (MM2 and MM3 force fields) of supramolecular complexes were performed using SCIGRESS version FJ 2.6 (EU 3.1.9) Build 5996.8255.20141202. PM6-optimized models of the guests were also created in SCIGRESS.[4] Guest volumes were calculated using PLATON software with the following parameters:[5]

Probe radius = 1.2 Å, Grid step = 0.1 Å, Atomic radii: C = 1.70 Å, H = 1.20 Å, Cl = 1.75 Å, F = 1.47 Å, O = 1.52 Å.

2.8 References

(1) Kansy, J. *Nucl. Instruments Methods Phys. Res. Sect. A Accel. Spectrometers, Detect. Assoc. Equip.* **1996**, *374* (2), 235–244.

(2) Tao, S. J. *J. Chem. Phys.* **1972**, *56* (11), 5499–5510.

(3) Eldrup, M.; Lightbody, D.; Sherwood, J. N. *Chem. Phys.* **1981**, *63, (1-2)*, 51-58.

(4) Stewart, J. J. P. *J. Mol. Model.* **2007**, *13* (12), 1173–1213.

(5) Spek, A. L. *Acta Crystallogr. Sect. D Biol. Crystallogr.* **2009**, *65* (2), 148–155.

CHAPTER 3

Preliminary Results

3.1 Introduction

While permanently porous liquids have been adapted from a variety of hosts such as porous carbon,[1] silica nanospheres[2] and porous organic cages,[3] no research has been conducted on using coordination cages as a scaffold for liquids with intrinsic porosity. Although MOFs have been used to produce Type III porous liquids,[4,5] other coordination chemistry-based architectures have not been implemented in this novel field. We are predominantly interested in synthesizing liquid coordination cages that would function as Type I porous liquids, and secondarily in methods to develop Type II porous liquids based on metal-organic cages. The two main questions to consider when designing porous liquids based on coordination cages is how to lower the melting point of a coordination cage and how to ensure that the functional groups used to depress the melting point do not penetrate and occupy the cavities of the host.

Research has shown that attaching alkyl and PEG chains to various molecular structures often depresses the melting point of the material.[6–9] Cooper *et al.* demonstrated that porous organic cages functionalized with long alkyl chains exhibited significantly lower melting temperatures than their unfunctionalized counterparts. This temperature difference is attributed to the flexibility of these alkyl moieties, which can reduce the efficiency of packing within the system, thus lowering the energy needed to melt the structure. In contrast to neutrally charged porous organic cages, there are other variables beyond the cage scaffold to consider for metal-organic cages. Counterions have been shown to play a significant role in controlling different properties of cages. For example, anion exchange can be used to tune the solubility of a cage, allowing these structures to be dissolved in acetonitrile, ethyl acetate and water.[10–12] Anions can also template the formation of different structures from the same base ligand.[13] Therefore, we are interested in understanding how different anions, and mixtures of anions, influence the phase change behavior of cages.

Furthermore, previous research shows that imidazolium groups can lower the melting thresholds of larger macrocyclic structures such as calixarenes.[14] Therefore, we hypothesized that covalently attaching imidazolium moieties onto a cage could lower the melting point of the capsule. Another reason to use imidazoliums in these systems is that the covalent attachment of an imidazolium to the end of an alkyl or PEG group could prevent the chains from penetrating and occupying the cavity of cationic cages *via* coulombic repulsion. Since porous liquids are comprised of hosts with empty cavities, it is important to ensure that the alkyl and PEG chains functionalizing the cage do not occupy the pores of the material.

Due to the fact that no published research on the adaptation of coordination cages into porous liquids is present in the scientific literature, we have included this chapter of preliminary results to contextualize the research presented in this thesis. The bulk of the work featured below was conducted by Dr. Angela Grommet and Zhichen Wu, though this author made contributions in the early stages of the project. The ligands and cages presented in this chapter were designed by Dr. Grommet, while the initial results and experimental optimizations were conducted by this author. Ligand synthesis was repeated by Zhichen Wu under partial supervision of this author; Wu also conducted the cage syntheses and characterizations under the predominant supervision of Dr. Grommet. Dr. Grommet proposed that functionalizing an $Fe^{II}_4L_4$ tetrahedral cage with alkyl chains terminating in imidazolium groups would simultaneously lower the melting point of the capsule and prevent the alkyl tails from occupying the host cavity. Therefore, in this chapter, we present the first example of an alkylimidazolium-functionalized cage and examine how alkyl chain length, anion structure and imidazolium groups may affect the melting temperature of the assembly. We hypothesized that longer alkyl chains would depress the melting point of the cage more effectively than their shorter counterparts, and that flexible anions with lower symmetry would further hinder effective stacking in the neat state. Furthermore, we postulated that cages functionalized with linear alkyl groups would encapsulate the hydrophobic chains, but that adding a terminal imidazolium unit would hinder intra- and/or intermolecular penetration. Therefore, we proposed that a combination of these three structural motifs could result in a liquid coordination cage with empty cavities.

3.2 Synthesis of Alkylimidazolium-Functionalized Aldehydes

To achieve the goal of attaining a liquid coordination cage, we designed alkyl bromide and alkylimidazolium-functionalized aldehydes with chain lengths varying from 4 to 8 carbons. The goal of this design was twofold: to determine how the length of alkyl chains can affect the melting temperature of cages and whether the addition of an imidazolium group would prevent alkyl chain penetration of the cage cavities while simultaneously lowering the melting point of the assembly. These new aldehyde subcomponents were based on 5-hydroxypicolinaldehyde, which was synthesized from a known procedure.[15] The starting material was functionalized with different alkyl bromide groups to yield aldehydes **3F-3H** (Scheme 3.1). An imidazolium

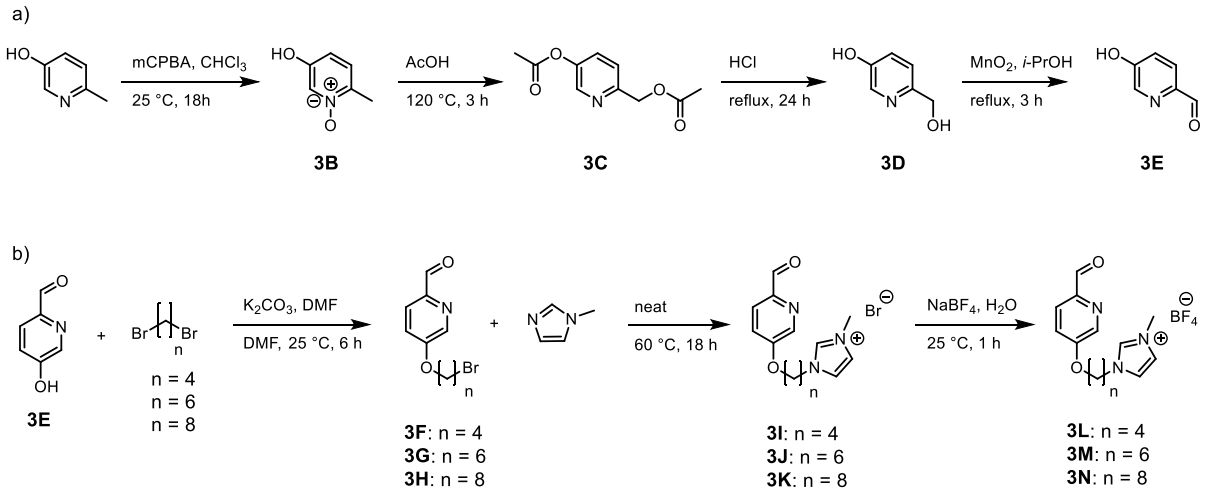

Scheme 3.1: Synthesis of aldehyde **3E**, different length alkyl bromo aldehydes (**3F-3H**) and alkylimidazolium aldehydes with BF_4^- counterions (**3L-3N**).

group was then added to the terminal end of the alkyl tail to generate alkylimidazolium aldehydes **3I-3K**, which were subsequently converted to aldehydes **3L-M** *via* anion exchange from bromide (Br^-) to tetrafluoroborate (BF_4^-) (Scheme 3.1). However, **3L** was not synthesized successfully because the hydrophilic product was lost during the reaction workup.

3.3 Self-assembly of Alkylimidazolium-Functionalized Cages 3.1-3.8

While the alkylimidazolium-functionalized pyridinecarboxaldehydes could be assembled with a myriad of aniline-based subcomponents, trianiline **3A** was chosen for preliminary testing because this subcomponent is known to assemble into a discrete $Fe^{II}_4L_4$ tetrahedral cage when assembled with the respective stoichiometric amounts of subcomponents, and is not known to form any other structures.[16] Trianiline **3A** has also been assembled with various anions such as bis(trifluoromethanesulfonylimide) (NTf_2^-), tetrafluoroborate (BF_4^-), sulfate (SO_4^-) and dodecyl sulfate (DS^-); this versatility facilitates our investigation into the relationship between the melting point of a cage and its counterions. While the cage is known to bind anions such as NTf_2^- and hexafluorophosphate (PF_6^-) in slow exchange on the NMR chemical shift timescale,[16] DS^- is too sterically hindered to occupy the host cavity, and BF_4^- is too small to remain bound. Therefore, the assemblies were conducted with iron (II) dodecyl sulfate ($Fe(DS)_2$) and iron (II) tetrafluoroborate ($Fe(BF_4)_2$). We acknowledge that BF_4^- anions

could temporarily enter the cage cavities due to its small size, but in this thesis, we are defining a host as "empty" if no guest is encapsulated in slow exchange on the NMR timescale.

Cage assemblies were prepared by Zhichen Wu from **3A** (1 equiv.), Fe(II) salt (1.1 equiv.) and either **3F-H** of **3M-N** (3 equiv.) in acetonitrile (CH_3CN).[17] The assemblies were heated at 60 °C for 48 h under N_2 before being purified by precipitation with diethyl ether and collected *via* centrifugation. By contrasting the melting temperatures of these assemblies, one can determine the degree to which imidazolium units, anion mixtures and alkyl lengths influence the melting temperature of the cage. **3A** was assembled with alkyl bromide-functionalized aldehydes **3F-3H** in the presence of $Fe(BF_4)_2$ to give cages **3.1-3.3**, respectively (Scheme 3.2). These self-assemblies were then repeated with $Fe(DS)_2$, resulting in cages **3.4-3.6** (Scheme 3.2). The juxtaposition of the melting points of cages **3.1-3.3** and **3.4-3.6** could be used to determine how different anions affect the phase behavior of these cages.

3A was also assembled with alkylimidazolium aldehydes **3M** and **3N** with $Fe(BF_4)_2$ (cages **3.7-3.8**) and $Fe(DS)_2$ (cages **3.9-3.10**) *via* the experimental conditions used to synthesize cages **3.1-3.6** (Scheme 3.2). According to this synthetic scheme, cages **3.7-3.8** should contained only BF_4^- anions while cages **3.9-3.10** should be comprised of an 8:12 ratio of DS^- and BF_4^-. This ratio is consistent with 8 equiv. of $Fe(DS)_2$ to 12 equiv. of the BF_4^- charge-balanced aldehyde subcomponent. These mixed anion assemblies could be used to demonstrate whether a mixture of BF_4^- and DS^- anions would result in assemblies with lower melting temperatures than cages assembled with solely BF_4^-. Unfortunately, cages **3.9-3.10** could not be isolated

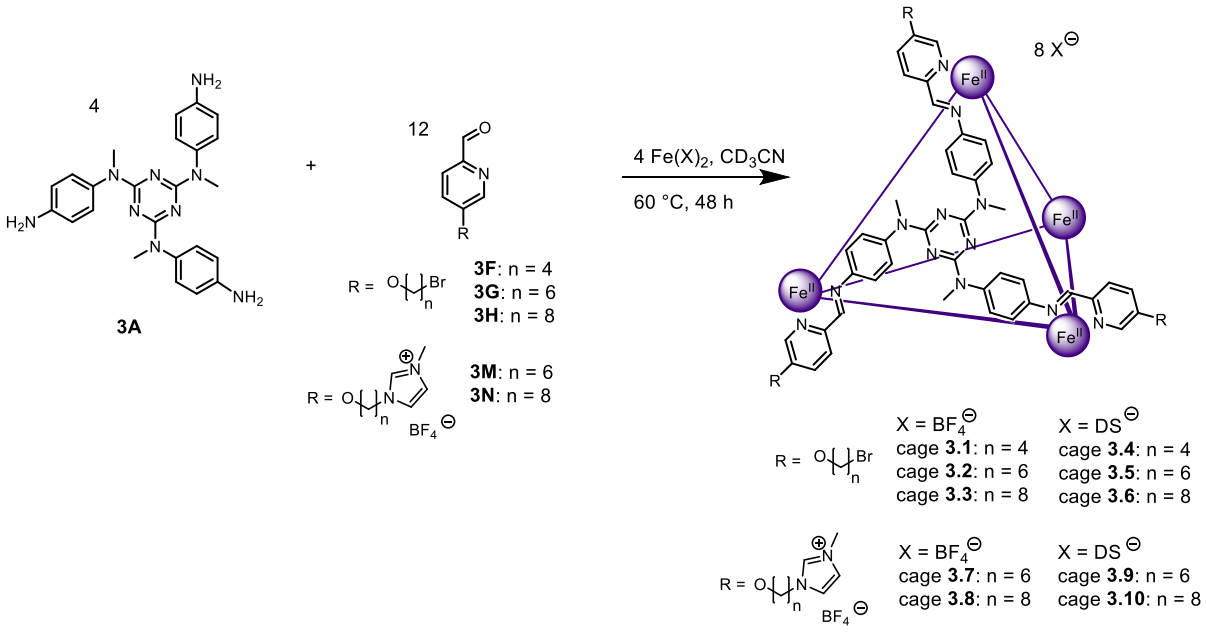

Scheme 3.2: Synthesis of cages **3.1-3.8**.

from their subcomponents, and therefore were not used in subsequent melting point analyses. Nevertheless, the comparison of cages **3.7** and **3.8** could still demonstrate whether different alkyl chain lengths in alkylimidazolium-functionalized cages affected the melting temperatures of their respective assemblies.

Dr. Grommet and Zhichen Wu analyzed cages **3.1-3.8** *via* ^{1}H and ^{19}F NMR spectroscopy.[17] The spectra obtained from these NMR experiments will not be presented in this thesis because these investigations were not conducted by this author. However, these results can be obtained from Professor Jonathan Nitschke and will be discussed below. Only one set of aromatic signals were present in the ^{1}H NMR spectra, which was consistent with the published data of the empty unfunctionalized cage.[16] This result indicated that the formation of these cages was successful and that none of the cage cavities were occupied. This observation was further confirmed by the lack of an encapsulated BF_4^- peak in the ^{19}F NMR spectra. The absence of encapsulated guest peaks was consistent with our hypothesis that BF_4^- and DS^- would be suitable anions for this system because of their size incompatibility with these cage scaffolds.

It is important to note that while we hypothesized that no alkyl chain binding would be observed in the case of alkylimidazolium-functionalized cages due to the coulombic repulsion of the imidazolium units and the cationic scaffold of the cage, the alkyl bromide-functionalized cages also appeared empty by NMR analysis. We attributed this lack of alkyl chain binding in the alkyl bromide-functionalized cages to the face-capped nature of the cage scaffold. While many face-capped cages have been demonstrated to fully encapsulate guests of varying shapes and sizes,[16,18,19] we hypothesized that the apertures of these cages were too sterically hindered to allow for the partial encapsulation of an alkyl chain. However, due to the fact that neither the alkyl bromide nor alkylimidazolium-functionalized cages exhibited binding of their alkyl chains, there is insufficient information to deduce whether terminal imidazolium groups can actually prevent linear alkyl chains from being bound within the cage cavities. Nevertheless, Grommet *et al.* concluded that cages **3.1-3.8** were assembled successfully, and the samples were subsequently dried under vacuum for 18 h to yield glass-like solids for Mel-Temp analysis.

3.4 Melting Temperatures of Cages 3.1-3.8

The phase change behavior of cages **3.1-3.8** were determined using a Mel-Temp apparatus by Dr. Angela Grommet and Zhichen Wu.[17] The melting points reported below are approximate values because the samples changed phase very gradually, thus rendering a visual assessment of the melting onset difficult. Samples used for melting were prepared by depositing a small amount of cage into a capillary under oxygen-free conditions. The capillary was then sealed, and the melting process was conducted under N_2 by heating the sample to 200 °C. The melting temperatures of the cages are reported in Table 1.

No phase changes were observed for cages **3.1-3.3** below 200 °C. In contrast, cages **3.5** and **3.6** appeared to undergo a solid to liquid phase transition at 168 °C and 169 °C, respectively. In contrast, no phase transitions were observed in the unfunctionalized cage below 300 °C.[17] The lower melting temperatures of the cages containing DS^- anions was consistent with our hypothesis that a more flexible anion with lower symmetry would hinder efficient packing in the neat state when compared to a rigid anion with higher symmetry such as BF_4^-. While cages **3.5** and **3.6** melted below 200 °C, no phase change was observed for butyl bromide-functionalized cage **3.4**. This discrepancy could be due to the fact that cage **3.4** was functionalized with a shorter alkyl chain than cage **3.5** and **3.6**. However, since no similar difference in phase behavior was observed for hexyl-functionalized cage **3.5** and octyl-functionalized cage **3.6**, we concluded that these results were inconclusive with regards to how different alkyl lengths affected the melting temperatures of these assemblies. Nevertheless, we acknowledge the possibility that different alkyl tails may influence the phase behavior of the assemblies above 200 °C.

Table 3.1: Melting temperatures of cages **3.1-3.8**. Assemblies conducted with alkyl bromide aldehydes **3F-3H** are highlighted in yellow and assemblies conduced with alkylimidazolium aldehydes **3M-3N** are highlighted in green. "> 200 °C" was used to indicate that the sample was heated past 200 °C but no phase change was observed.

Aldehyde	**Metal Salt**	
	$Fe(BF_4)_2$	**$Fe(DS)_2$**
3F, n = 4	Cage **3.1** = >200 °C	Cage **3.4** = >200 °C
3G, n = 6	Cage **3.2** = >200 °C	Cage **3.5** = 168 °C
3H, n = 8	Cage **3.3** = >200 °C	Cage **3.6** = 169 °C
3M, n = 6	Cage **3.7** = >200 °C	N/A
3N, n = 8	Cage **3.8** = >200 °C	N/A

Similar to cages **3.1-3.3**, cages **3.7-3.8** were not observed to undergo any phase transitions below 200 °C. This comparison indicated that the addition of an imidazolium group did not depress the melting point of the cages to a temperature below 200 °C.

3.5 Conclusions and Future Work

In this chapter, we presented the design and synthesis of alkyl bromide and alkylimidazolium-functionalized subcomponents, which were then used to assemble a new library of $Fe^{II}_4L_4$ cages. We hypothesized that a combination of long alkyl chains, imidazolium moieties and large flexible anions would depress the melting point of these assemblies to the extent that the resulting cages would be liquid at room temperature.

While the cages in this chapter were not liquid, these experimental results provided a valuable foundation on which future porous liquids can be built. The successful synthesis of alkylimidazolium-functionalized cages demonstrated that the positively charged imidazolium units did not interfere with subcomponent self-assembly. While there was insufficient data to determine whether terminal imidazolium groups are necessary to prevent the encapsulation of linear alkyl chains in cages based on central aldehyde subcomponent **3A**, we postulate that imidazolium moieties could potentially hinder intra- and intermolecular penetration in future cages that may contain wider apertures. Thermal analysis also indicated that the assemblies containing large flexible anions with lower symmetry such as DS^- exhibited lower melting temperatures than their counterparts that contained rigid highly symmetrical anions such as BF_4^-.

Although this preliminary system furthered our understanding of cages and their phase behaviors, Dr. Grommet's design contained a few flaws that should be addressed and amended in subsequent attempts to generate these materials. For example, Grommet *et al.* did not address the structural integrity of the cage samples after melting. Also, there is insufficient data to conclude that the materials were melting instead of undergoing a glass transition or decomposing. Differential scanning calorimetry (DSC) and thermal gravimetry analysis (TGA) could be used to determine the decomposition temperatures of these cages as well as to distinguish whether the visually observed phase changes were melting, glass transition or decomposition features. Most importantly, while the melting temperatures for some of the alkylimidazolium-functionalized cages were lower than the melting temperature of the

unfunctionalized cage, additional amendments to the design of these materials need to be made to generate a liquid coordination cage. A variable that was not considered in this chapter was the cage scaffold. Therefore, we hypothesize that using different central ligands could result in new cages with lower phase transition temperatures.

3.6 Experimental Methods

General procedure of the synthesis of 5-((ω'-bromoalkyl)oxy)picolinaldehyde **3F-3H***:*

A solution of 5-hydroxypicolinaldehyde (98 mg, 0.8 mmol) in 2 mL DMF was added dropwise to a stirred mixture of K_2CO_3 (166 mg, 1.2 mmol) and the corresponding 1,ω-dibromoalkane (1.6 mmol) in 8 mL of DMF. The mixture was stirred at 298 K for 6 hours. Water (30 mL) was added to the mixture and the solution was then extracted with toluene (2 x 100 mL). The extract was washed with water (2 x 50 mL), and dried over anhydrous $MgSO_4$. After filtration, the solvent was removed and the residue was chromatographed on a silica gel column (230-400 mesh) using a mixture of hexane and ethyl acetate as the mobile phase to give product as a yellow solid.

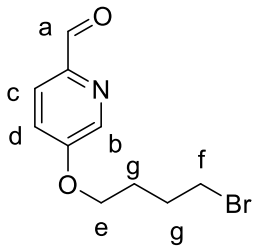

3F

*5-((4'-bromobutyl)oxy)picolinaldehyde **3F**:*

3F (94 mg, yield 46%): ^{1}H NMR (400 MHz, 298 K, $CDCl_3$): δ = 9.98 (s, 1H, H_a), 8.41 (d, J = 2.8 Hz, 1H, H_b), 7.95 (d, J = 8.8 Hz, 1H, H_c), 7.28 (dd, J = 8.8 Hz, 2.8Hz, 1H, H_d), 4.14 (t, J = 6.0 Hz, 2H, H_e), 3.49 (t, J = 6.4 Hz, 2H, H_f), 2.05 (m, 4H, H_g). ^{13}C NMR (125 MHz, 298 K, $CDCl_3$): δ = 192.1, 158.4, 146.5, 138.8, 123.5, 120.6, 67.9, 33.1, 29.3, 27.8. GC-MS(EI): *m/z*: Calcd: $M^{+\bullet}$ = 257.259, Found: $M^{+\bullet}$ = 257.259.

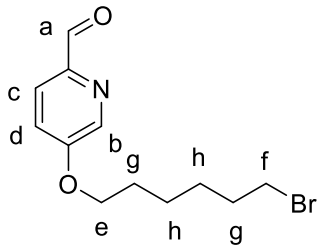

3G

*5-((6'-bromohexyl)oxy)picolinaldehyde **3G**:*

3G (113 mg, yield 49%): ^{1}H NMR (400 MHz, 298 K $CDCl_3$): δ = 9.98 (d, J = 0.4 Hz, 1H, H_a), 8.42 (d, J = 2.8 Hz, 1H, H_b), 7.95 (d, J = 8.4 Hz, 1H, H_c), 7.28 (overlaps with $CHCl_3$, dd, J = 8.4 Hz, 2.8Hz, 1H, H_d), 4.10 (t, J = 6.4 Hz, 2H, H_e), 3.43 (t, J = 6.8 Hz, 2H, H_f), 1.89 (m, 4H, H_g), 1.53 (m, 4H, H_h). ^{13}C NMR (125 MHz, 298 K, $CDCl_3$): δ = 192.2, 158.7, 146.3, 138.9, 123.5, 120.6, 68.8, 33.8, 32.7, 28.9, 27.9, 25.3. GC-MS(EI): *m/z*: Calcd: $M^{+\bullet}$ = 285.287, Found: $M^{+\bullet}$ = 285.287.

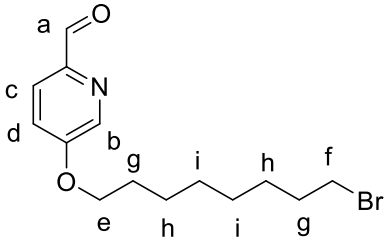

3H

*5-((8'-bromooctyl)oxy)picolinaldehyde **3H**:*

3H (106 mg, yield 42%): ^{1}H NMR (400 MHz, 298 K, $CDCl_3$): δ = 9.97 (d, J = 0.4 Hz, 1H, H_a), 8.41 (d, J = 2.8 Hz, 1H, H_b), 7.94 (d, J = 8.8 Hz, 1H, H_c), 7.27 (overlaps with $CHCl_3$, dd, J = 8.4 Hz, 2.8Hz, 1H, H_d), 4.08 (t, J = 6.4 Hz, 2H, H_e), 3.40 (t, J = 6.8 Hz, 2H, H_f), 1.84 (m, 4H, H_g), 1.46 (m, 4H, H_h), 1.37 (m, 4H, H_i). ^{13}C NMR (125 MHz, 298 K, $CDCl_3$): δ = 192.2, 158.7, 146.2, 138.9, 123.5, 120.5, 68.9, 34.1, 32.8, 29.2, 29.0, 28.8, 27.2, 25.9. GC-MS(EI): *m/z*: Calcd: $M^{+\bullet}$ = 313.315, Found: $M^{+\bullet}$ = 313.315.

General procedure of the synthesis of 3-(ω'-((6''-formylpyridin-3''-yl)oxy)alkyl)-1-methylimidazolium bromide **3I-3K**:

1-methylimidazolium (1 equiv.) and corresponding 5-((ω'-bromoalkyl)oxy) picolinaldehyde **3F-3H** (1.1 equiv.) were mixed and stirred neat at 333 K for 18 hours. The mixture was dissolved in a minimal amount of water and washed with toluene (5 x 5 mL). The solvent was removed to give product as a yellow oil or solid.

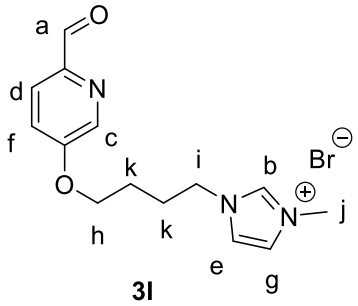

3I

*3-(4'-((6''-formylpyridin-3''-yl)oxy)butyl)-1-methylimidazolium bromide **3I***:

3I (51 mg, 54%): ^{1}H NMR (400 MHz, 298 K, CD_3CN,): δ = 9.90 (s, 1H, H_a), 9.12 (s, 1H, H_b), 8.44 (d, J = 2.8 Hz, 1H, H_c), 7.92 (d, J = 8.8 Hz, 1H, H_d), 7.50 (unresolved dd, J = 1.6 Hz, 1H, H_e), 7.45 (dd, J = 2.8 Hz, 8.8 Hz, 1H, H_f), 7.44 (unresolved dd, J = 1.6 Hz, 1H, H_g), 4.30 (t, J = 7.2 Hz, 2H, H_h), 4.20 (t, J = 6.0 Hz, 2H, H_i), 3.87(s, 3H, H_j), 2.05 (m, 2H, H_k), 1.83 (m, 2H, H_k). ^{13}C NMR (125 MHz, 298 K, CD_3CN): δ = 193.0, 159.4, 147.2, 139.9, 137.5, 124.6, 124.3, 123.2, 121.8, 69.1, 49.9, 36.9, 27.3, 26.1. ESI-MS: *m/z*: Calcd: M^+ = 260.14, $[2M + Br]^+$ = 599.20, 601.20, Found: M^+ = 260.09, $[2M + Br]^+$ = 599.19, 601.18.

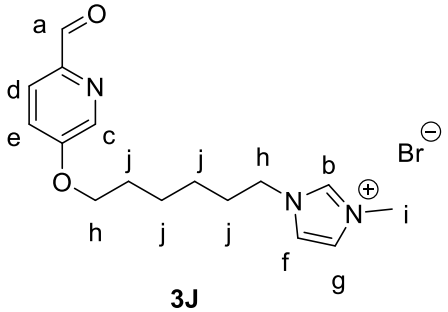

3J

*3-(6'-((6''-formylpyridin-3''-yl)oxy)hexyl)-1-methylimidazolium bromide **3J***:

3J (297 mg, 86%): ^{1}H NMR (400 MHz, 298 K, CD_3CN): δ = 9.90 (s, 1H, H_a), 9.00 (br, 1H, H_b), 8.42 (d, J = 2.8 Hz, 1H, H_c), 7.91 (d, J = 8.4 Hz, 1H, H_d), 7.43 (m, 2H, H_e and H_f), 7.38 (unresolved dd, J = 1.6 Hz, 1H, H_g), 4.17 (m, 4H, H_h), 3.86(s, 3H, H_i), 1.84 (m, 4H, H_j), 1.51 (m, 2H, H_j), 1.38 (m, 2H, H_j). ^{13}C NMR (125 MHz, 298 K, CD_3CN): δ = 193.0, 159.6, 147.1, 139.9, 137.4, 124.5, 124.3, 123.2, 121.7,

69.7, 50.3, 36.8, 30.5, 29.3, 26.3, 25.8. ESI-MS: *m/z*: Calcd: M^+ = 288.17, $[2M + Br]^+$ = 655.26, 657.26, Found: M^+ = 288.11, $[2M + Br]^+$ = 655.27, 657.27.

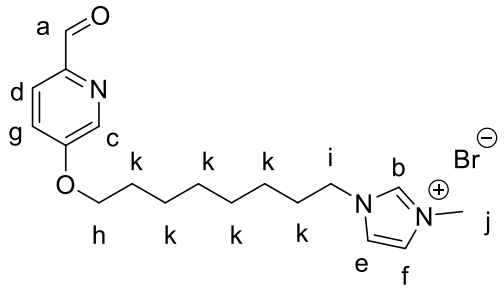

3K

*3-(8'-((6''-formylpyridin-3''-yl)oxy)octyl)-1-methylimidazolium bromide **3K***:

3K (46 mg, 81%): ^{1}H NMR (400 MHz, 298 K, CD_3CN): δ = 9.88 (d, *J* = 0.5 Hz, 1H, H_a), 9.18 (s, 1H, H_b), 8.39 (d, *J* = 2.5 Hz, 1H, H_c), 7.79 (d, *J* = 9.0 Hz, 1H, H_d), 7.50 (unresolved dd, *J* = 1.5 Hz, 1H, H_e), 7.44 (unresolved dd, *J* = 1.5 Hz, 1H, H_f), 7.42 (dd, *J* = 9.0 Hz, 2.5Hz, 1H, H_g), 4.19 (t, *J* = 7.5 Hz, 2H, H_h), 4.12 (t, *J* = 6.5 Hz, 2H, H_i), 3.88(s, 3H, H_j), 1.83 (m, 2H, H_k), 1.77 (m, 2H, H_k), 1.43 (m, 2H, H_k), 1.33 (m, 6H, H_k). ^{13}C NMR (125 MHz, 298 K, CD_3CN): δ = 193.0, 159.6, 147.0, 139.8, 137.4, 124.5, 124.3, 123.1, 121.6, 69.8, 50.3, 36.8, 30.5, 29.6, 29.43, 29.37, 26.5, 26.2. ESI-MS: *m/z*: Calcd: M^+ = 316.20, $[2M + Br]^+$ = 711.32, 713.32, Found: M^+ = 316.13, $[2M + Br]^+$ = 711.36, 713.36.

General procedure of the synthesis of 3-(ω'-((6''-formylpyridin-3''-yl)oxy)alkyl) -1-methylimidazolium tetrafluoroborate **3M-3N**:

$NaBF_4$ (1.2 equiv.) and corresponding 3-(ω'-((6''-formylpyridin-3''-yl)oxy) alkyl)-1-methylimidazolium bromide **3J-K** (1 equiv.) were dissolved in a minimal amount of water and extracted with DCM (5 x 5 mL). The organic layer was concentrated to a volume of 5 mL and washed with a solution of saturated $NaBF_4$ in water (5 x 2 mL) until the washes did not produce any precipitate when tested with $AgNO_3$. The organic layer was then washed with water (3 x 2 mL) to remove the extra salt. The solvent was removed to give the product as a yellow oil.

3L was could not be isolated from the reaction mixture. Its synthesis is not featured below.

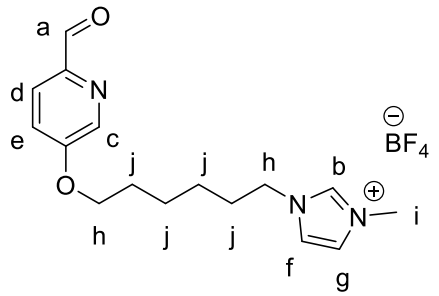

3M

*3-(6'-((6''-formylpyridin-3''-yl)oxy)hexyl)-1-methylimidazolium tetrafluoroborate **3M***:

3M (87 mg, 48%): ^{1}H NMR (500 MHz, 298 K, CD_3CN): δ = 9.89 (s, 1H, H_a), 8.48 (s, 1H, H_b), 8.39 (d, J = 3.0 Hz, 1H, H_c), 7.90 (d, J = 9.0 Hz, 1H, H_d), 7.40 (m, 2H, H_e and H_f), 7.35 (s, 1H, H_g), 4.13 (m, 4H, H_h), 3.83(s, 3H, H_i), 1.85 (m, 2H, H_j), 1.79 (m, 2H, H_j), 1.49 (m, 2H, H_j), 1.37 (m, 2H, H_j). ^{13}C NMR (125 MHz, 298 K, CD_3CN): δ = 193.1, 159.7, 147.1, 139.9, 137.0, 124.7, 124.4, 123.3, 121.7, 69.7, 50.4, 36.8, 30.5, 29.3, 26.3, 25.8. ^{19}F NMR (377 MHz, CD_3CN, referenced to trifluoroacetic acid): δ = -150.5, -150.6. ESI-MS: *m/z*: Calcd: M^+ = 288.17, $[2M + BF_4]^+$ = 663.34, Found: M^+ = 288.06, $[2M + BF_4]^+$ = 663.33.

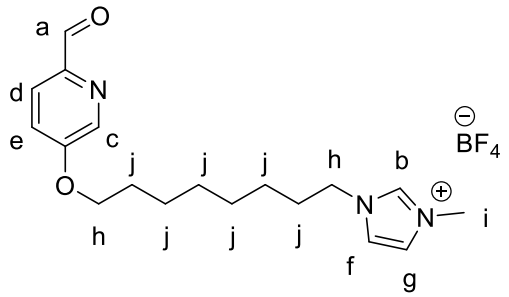

3N

*3-(8'-((6''-formylpyridin-3''-yl)oxy)octyl)-1-methylimidazolium tetrafluoroborate **3N***:

3N (130 mg, 71%): ^{1}H NMR (400 MHz, 298 K, CD_3CN): δ = 9.90 (d, J = 0.4 Hz, 1H, H_a), 8.41 (m, 2H, $H_{b,c}$), 7.91 (dd, J = 8.8 Hz, 0.4 Hz, 1H, H_d), 7.41 (dd, J = 8.8 Hz, 2.8 Hz, 0.4 Hz, 1H, H_e), 7.36 (unresolved dd, J = 2.0 Hz, 1H, H_f), 7.33 (unresolved dd, J = 2.0 Hz, 1H, H_g), 4.13 (m, 4H, H_h), 3.82 (s, 3H, H_i), 1.81 (m, 4H, H_j), 1.46 (m, 2H, H_j), 1.34 (m, 6H, H_j). ^{13}C NMR (125 MHz, 298 K, CD_3CN): δ = 193.0, 159.7, 147.1, 139.9, 137.0, 124.7, 124.4, 123.3, 121.7, 69.9, 50.5, 36.8, 30.6, 29.7, 29.54, 29.46, 26.6, 26.4. ^{19}F NMR (377 MHz, CD_3CN, referenced to trifluoroacetic acid): δ = -150.7, -150.8. ESI-MS: *m/z*: Calcd: M^+ = 316.02, $[2M + BF_4]^+$ = 719.41, Found: M^+ = 316.07, $[2M + BF_4]^+$ = 719.40.

3.7 References

(1) Li, P.; Schott, J. A.; Zhang, J.; Mahurin, S. M.; Sheng, Y.; Qiao, Z. A.; Hu, X.; Cui, G.; Yao, D.; Brown, S.; et al. *Angew. Chemie - Int. Ed.* **2017**, *56* (47), 14958–14962.

(2) Zhang, J.; Chai, S. H.; Qiao, Z. A.; Mahurin, S. M.; Chen, J.; Fang, Y.; Wan, S.; Nelson, K.; Zhang, P.; Dai, S. *Angew. Chemie - Int. Ed.* **2015**, *54* (3), 932–936.

(3) Giri, N.; Del Pópolo, M. G.; Melaugh, G.; Greenaway, R. L.; Rätzke, K.; Koschine, T.; Pison, L.; Gomes, M. F. C.; Cooper, A. I.; James, S. L. *Nature* **2015**, *527* (7577), 216–220.

(4) Shan, W.; Fulvio, P. F.; Kong, L.; Schott, J. A.; Do-Thanh, C. L.; Tian, T.; Hu, X.; Mahurin, S. M.; Xing, H.; Dai, S. *ACS Appl. Mater. Interfaces* **2018**, *10* (1), 32–36.

(5) Costa Gomes, M.; Pison, L.; Červinka, C.; Padua, A. *Angew. Chemie - Int. Ed.* **2018**, *57* (37), 11909–11912.

(6) Pantusa, M.; Bartucci, R.; Marsh, D.; Sportelli, L. *Biochim. Biophys. Acta - Biomembr.* **2003**, *1614* (2), 165–170.

(7) Li, C. Y.; Birnkrant, M. J.; Natarajan, L. V.; Tondiglia, V. P.; Lloyd, P. F.; Sutherland, R. L.; Bunning, T. J. *Soft Matter* **2005**, *1* (3), 238–242.

(8) Giri, N.; Davidson, C. E.; Melaugh, G.; Del Pópolo, M. G.; Jones, J. T. A.; Hasell, T.; Cooper, A. I.; Horton, P. N.; Hursthouse, M. B.; James, S. L. *Chem. Sci.* **2012**, *3* (6), 2153–2157.

(9) Jordan, E. F.; Feldeisen, D. W.; Wrigley, A. N. *J. Polym. Sci. Part A-1 Polym. Chem.* **1971**, *9* (7), 1835–1851.

(10) Percástegui, E. G.; Mosquera, J.; Ronson, T. K.; Plajer, A. J.; Kieffer, M.; Nitschke, J. R. *Chem. Sci.* **2019**, *10* (7), 2006–2018.

(11) Grommet, A. B.; Nitschke, J. R. *J. Am. Chem. Soc.* **2017**, *139* (6), 2176–2179.

(12) Grommet, A. B.; Hoffman, J. B.; Percástegui, E. G.; Mosquera, J.; Howe, D. J.; Bolliger, J. L.; Nitschke, J. R. *J. Am. Chem. Soc.* **2018**, *140* (44), 14770–14776.

(13) Riddell, I. A.; Smulders, M. M. J.; Clegg, J. K.; Hristova, Y. R.; Breiner, B.; Thoburn, J. D.; Nitschke, J. R. *Nat. Chem.* **2012**, *4* (9), 751–756.

(14) Dinarès, I.; Garcia De Miguel, C.; Mesquida, N.; Alcalde, E. *J. Org. Chem.* **2009**, *74* (1), 482–485.

(15) Seredyuk, M.; Gaspar, A. B.; Ksenofontov, V.; Galyametdinov, Y.; Kusz, J.; Gütlich, P. *J. Am. Chem. Soc.* **2008**, *130* (4), 1431–1439.

(16) Bolliger, J. L.; Ronson, T. K.; Ogawa, M.; Nitschke, J. R. *J. Am. Chem. Soc.* **2014**, *136* (41), 14545–14553.

(17) Grommet, A.B.; Wu, Z. *Unpublished*.

(18) Bolliger, J. L.; Belenguer, A. M.; Nitschke, J. R. *Angew. Chemie - Int. Ed.* **2013**, *52* (31), 7958–7962.

(19) Castilla, A. M.; Ronson, T. K.; Nitschke, J. R. *J. Am. Chem. Soc.* **2016**, *138* (7), 2342–2351.

CHAPTER 4

Alkylimidazolium-Functionalized Cages as Type II Porous Liquids

4.1 Introduction

The results of Chapter 3 demonstrate that the covalent addition of imidazolium groups to coordination cages can lower the melting point of these supramolecular structures. Though the cages presented in Chapter 3 had lower melting points than their unfunctionalized counterpart, none of the cages were liquid at room temperature. Chapter 3 presented self-assemblies in which the aldehyde subcomponent was modified while the central C_3 symmetric trianiline ligand **3A** remained the same for all assemblies. However, no studies have been conducted on varying the central ligand and there is little information on how changing the scaffold of the cage affects the melting point of the structure. Previous research shows that varying the central ligand of a cage produces hosts of different sizes and porosity; as a result, these cages also exhibit diverse host-guest behavior.[1] Therefore, it is likely that the central ligand of a cage could also impact the melting point and other physical properties of the structure. Hence, we chose to deviate from using trianiline central ligands and investigated how the physical properties of a cage assembled from a C_3 symmetric trialdehyde central subcomponent and an alkylimidazolium-functionalized aniline differ from the cages presented in Chapter 3. An increased understanding of how subcomponents influence the melting point of the cages will allow for the potential rational design of future Type I permanently porous liquids based on coordination cages.

In addition to furthering our understanding of liquid coordination cages, we also acknowledge that our structures have the potential of being adapted into Type II permanently porous liquids. Andrew Cooper and coworkers have incorporated porous organic cages into Type II porous liquids by creating a solution of crown ether-functionalized cages dissolved in 15-crown-5 ether.[2] Cooper discovered that functionalizing the organic cages with crown ether moieties greatly increased the solubility of the capsule in 15-crown-5 ether. Previous research also showed that coordination cages are soluble in ionic liquids at 2 mM concentration.[3] Therefore, we hypothesized that alkylimidazolium-functionalized cages may also display increased solubility in ionic liquids of similar molecular structures to these cages. While there is a diverse array of ionic liquids, imidazolium ionic liquids with short alkyl chains would be the most suitable for our system because of the structural similarities between the alkylimidazolium moieties of our cages and the cation of the ionic liquid. Hence, in this chapter, we also investigate the solvation of alkylimidazolium-functionalized cages in ionic liquids to generate Type II porous liquids.

4.2 Synthesis of Alkylimidazolium-Functionalized Anilines

Trialdehyde **4A** was chosen as the new central subcomponent because we were interested in whether changing the scaffold ligand could lower the melting point of the resulting cage. In contrast to central subcomponent **3A**, **4A** was an aldehyde-based subcomponent, and the ether bridges in its structure also added a degree of flexibility that was not present in trianiline **3A**. Trialdehyde **4A** was synthesized by refluxing 5-picolinaldehyde with cyanuric chloride and sodium carbonate in benzene (Scheme 4.1). After purification, trialdehyde **4A** was obtained with good yield (85%).

An additional reason to move away from using aniline-based central ligands is because the synthesis of alkylimidazolium-functionalized pyridine carboxaldehydes (**3P-3T**) was complex and expensive. We chose not to purchase 5-hydroxypicolinaldehyde because it was a costly starting material, and large quantities of this molecule were needed for the synthesis of **3P-3T**. However, there were many drawbacks to synthesizing 5-hydropicolinaldehyde. For example, this synthesis four steps to the overall synthetic procedure, resulting in a total of seven steps to synthesize a single subcomponent. The synthesis of 5-hydroxypicolinaldehyde was also hazardous and required the refluxing of concentrated hydrochloric acid. Consequently, eliminating the need for 5-hydroxypicolinaldehyde would result in a shorter, safer and less expensive synthetic procedure. Conversely, the starting material we chose for synthesizing an alkylimidazolium-functionalized aniline was *N*-Boc-4-aminophenol (Scheme 4.2) – an economical and commercially available compound. The alkylimidazolium-functionalized aniline **4E** could then be self-assembled with a diverse range of aldehyde ligands to yield a new collection of alkylimidazolium-functionalized coordination cages.

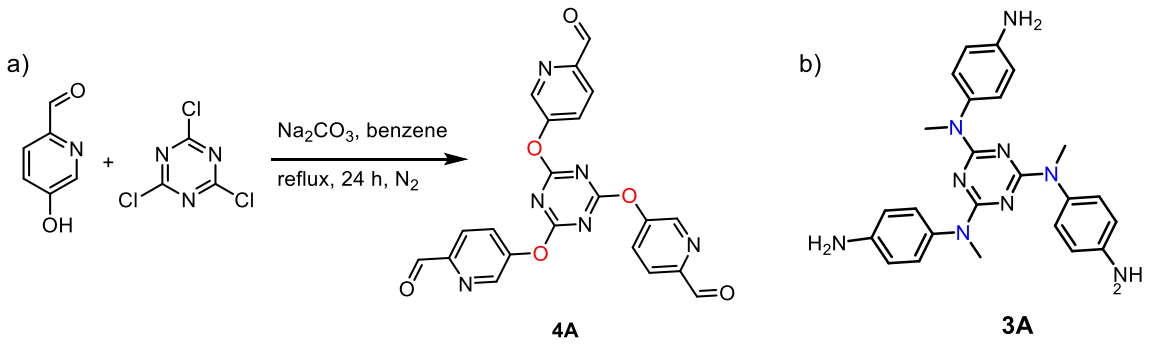

Scheme 4.1: a) Synthesis of trialdehyde **4A**. Ether bridges highlighted in red to contrast against the b) tertiary amine bridges in subcomponent **3A.**

Therefore, alkylimidazolium aniline **4E** was designed and synthesized *via* a procedure adapted from ligand **3L-M** (Scheme 4.2). The imidazolium moiety was also added to aniline **4E** because the results of Chapter 3 demonstrated that imidazolium groups were compatible with the cage synthesis and we hypothesized that these cationic moieties could hinder potential inter- and intramolecular cage penetration. Due to the fact that the secondary oxygen bridges off the central triazine ring of **4A** (highlighted in red, Scheme 4.1a) do not contain the methyl group appended on to the tertiary amine bridges of ligand **3A** (Scheme 4.1b), we postulated that the apertures of cages assembled from **4A** could be less sterically hindered thus increasing the risk of alkyl groups occupying the cage cavities. The four-step synthesis of the alkylimidazolium-functionalized aniline yielded ionic liquid **4E** as a brown liquid.

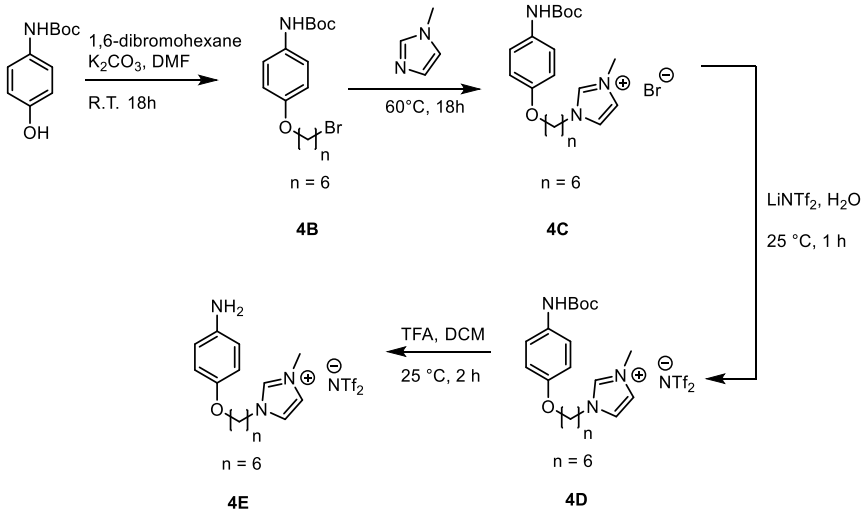

Scheme 4.2: Synthesis of alkylimidazolium-functionalized aniline **4E**.

4.3 Self-assembly of Alkylimidazolium-Functionalized Cages

4.3.1 Self-assemblies with iron salts

Trialdehyde **4A** was originally designed by Dr. Ana Castilla, and her results indicated that this trialdehyde could be successfully assembled with *p*-toluidine in the presence of $Fe(NTf_2)_2$ to yield a discrete tetrahedron with an encapsulated triflimide anion.[4] While our goal was to synthesize an empty liquid cage, we chose to use $Fe(NTf_2)_2$ in initial self-assemblies with aniline **4E** because trialdehyde **4A** was known to assemble with this metal salt. Therefore,

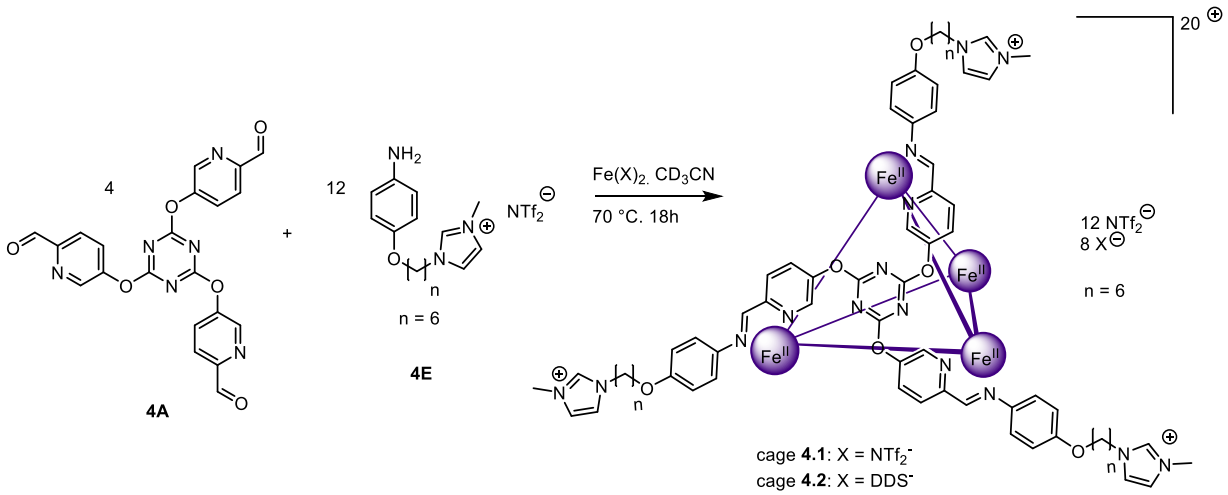

Scheme 4.3: Synthesis of cages **4.1** and **4.2**. Cage **4.1** formed successfully with 20 NTf_2^- anions. The presence of DS^- in self-assembly of cage **4.2** did not result in a discrete species.

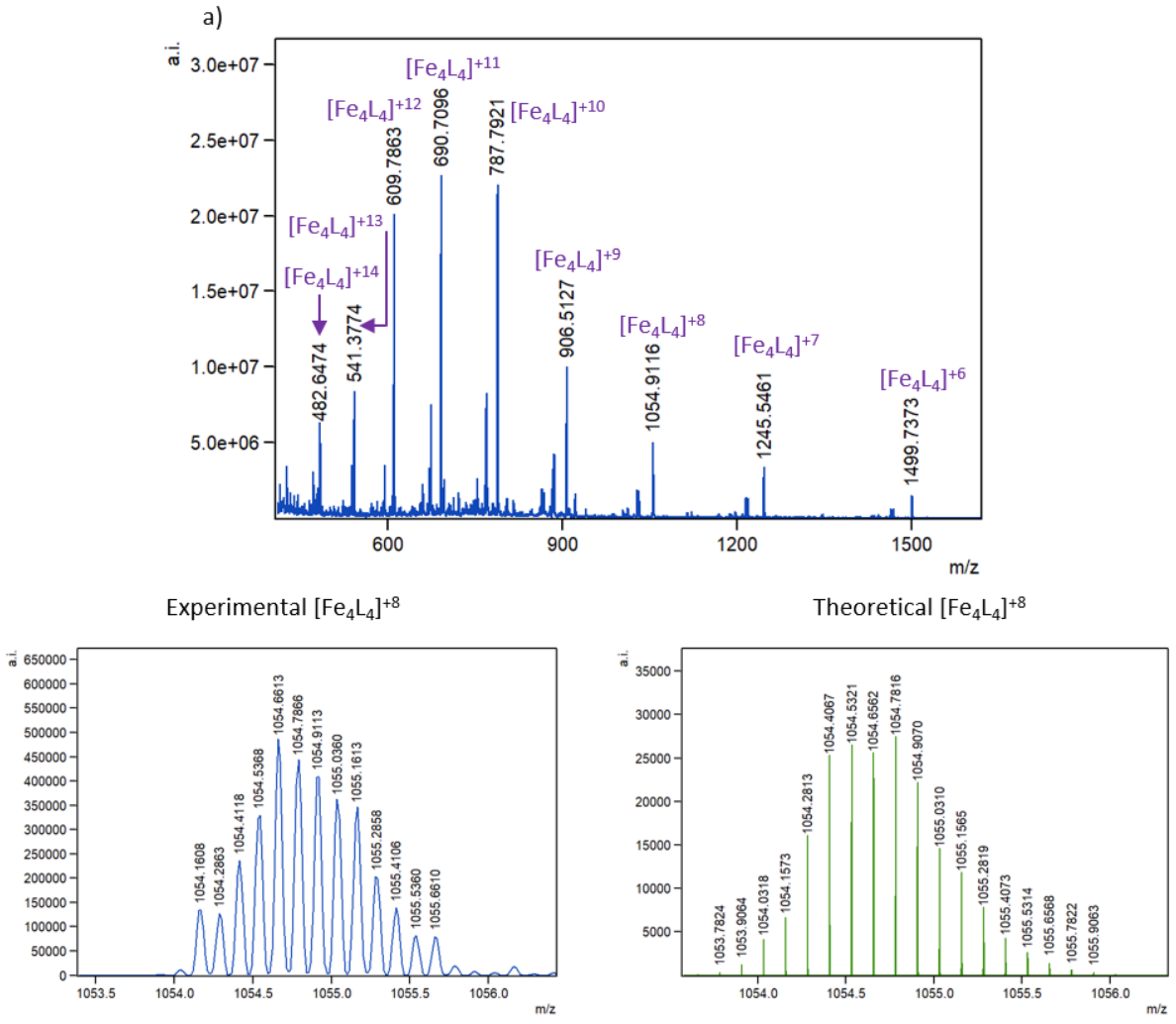

Figure 4.1: a) LR-ESI-MS spectrum of cage **4.1**.; the observed distribution of charge states was consistent with the proposed structure. b) HR-ESI-MS spectrum of cage **4.1**; the isotope pattern was consistent with theoretical calculations.

trialdehyde **4A**, aniline **4E** and $Fe(NTf_2)_2$ were assembled in CH_3CN overnight at 70 °C yielding glass-like cage **4.1** (Scheme 4.3).

^1H NMR of cage **4.1** in CD_3CN showed two sets of signals in the aromatic region which were indicative of successful formation of free cage and the NTf_2^- host-guest complex. The ^{19}F NMR spectrum of cage **4.1** showed both a free and encapsulated NTf_2^- peak, further confirming the results from ^1H NMR. Both ^1H and ^{19}F NMR spectra were consistent with Dr. Castilla's previous analysis of the unfunctionalized tetrahedron.[4] Both low and high resolution electrospray mass spectrometry (LR-ESI-MS, HR-ESI-MS) was used to analyze the cage; the fragmentation and isotope patterns observed in HR-ESI-MS and LR-ESI-MS were consistent with calculated values (Figure 4.1).

While NMR and MS indicated that cage **4.1** assembled successfully, these results also confirmed that NTf_2^- anions occupied the cage cavities. The neat cage was also solid at 298 K. Therefore, these qualities of the cage rendered **4.1** a poor candidate as a Type I permanently porous liquid. However, results from Chapter 3 indicated that the presence of DS^- anions significantly lowered the melting points of their respective cages. Consequently, we hypothesized that introducing DS^- anions into this system would depress the melting point of cage **4.1** further. We chose to assemble trialdehyde **4A** and aniline **4E** with $Fe(DS)_2$ as a preliminary experiment and we acknowledge that the usage of **4E** will introduce NTf_2^- anions into the system that could then be encapsulated in the resulting cage. The cage resulting from this assembly would not be charge-balanced solely by DS^- but a mixture of DS^- (8 equiv.) and NTf_2^- (12 equiv.). Ultimately, this experiment would demonstrate whether $Fe(DS)_2$ was a suitable metal salt for self-assemblies with ligand **4A**.

Therefore, trialdehyde **4A**, aniline **4E** and $Fe(DS)_2$ were combined in CH_3CN and heated at 70 °C for 18 h to yield cage **4.2**. The ^1H NMR spectrum of **4.2** exhibited many signals, indicating that the assembly did not form a single species. Also, no encapsulated NTf_2^- was observed in the ^{19}F NMR, indicating that the M_4L_4 tetrahedral cage capable of binding NTf_2^- was not present in the mixture of structures. LR-ESI-MS did not show any charge distributions consistent with cage formation. From these characterization techniques, we concluded that the presence of DS^- anions interfered with the assembly of a tetrahedron from this central ligand. Due to the fact that this assembly did not form a discrete species, a melting temperature was not taken for this sample.

4.3.2 Self-assemblies with zinc salts

Referring to Dr. Castilla's previous work, ligand **4A** assembled with *p*-toluidine and $Zn(BF_4)_2$ resulted in a cage with an empty cavity because the tetrafluoroborate (BF_4^-) anion was too small to be encapsulated.[4] Therefore, we deviated away from using iron in the metal corners and moved towards assembling the trialdehyde ligand with zinc salts. To ensure that BF_4^- was the only anion present in the assembly, an analogue of aniline **4E** charge-balanced by BF_4^- was designed (Scheme 4.4).

The synthesis of alkylimidazolium-functionalized aniline **4G** was the same as **4E** with the exception that sodium tetrafluoroborate was used to exchange the anion of the aniline ionic liquid to BF_4^-. However, while Boc protected aniline **4F** was successfully isolated in good yield, removal of the protecting group resulted in aniline **4G** becoming more hydrophilic. The increase in water solubility was likely due to the inadvertent anion exchange from BF_4^- to trifluoroacetate (TFA^-) and the appearance of the amine functional group. The workup of the deprotection reaction required the product to be washed with water. However, water-soluble **4G** was dissolved in the washes and could not be extracted with organic solvents.

Nevertheless, the same deprotection conditions were previously used on **4D** and no anion exchange from NTf_2^- to TFA^- was observed. This behavior was attributed to the difference in solubility between NTf_2^- and BF_4^-, with the latter being a more water-soluble anion. The combination of the amine group in **4G** as well as the hydrophilicity of BF_4^- resulted

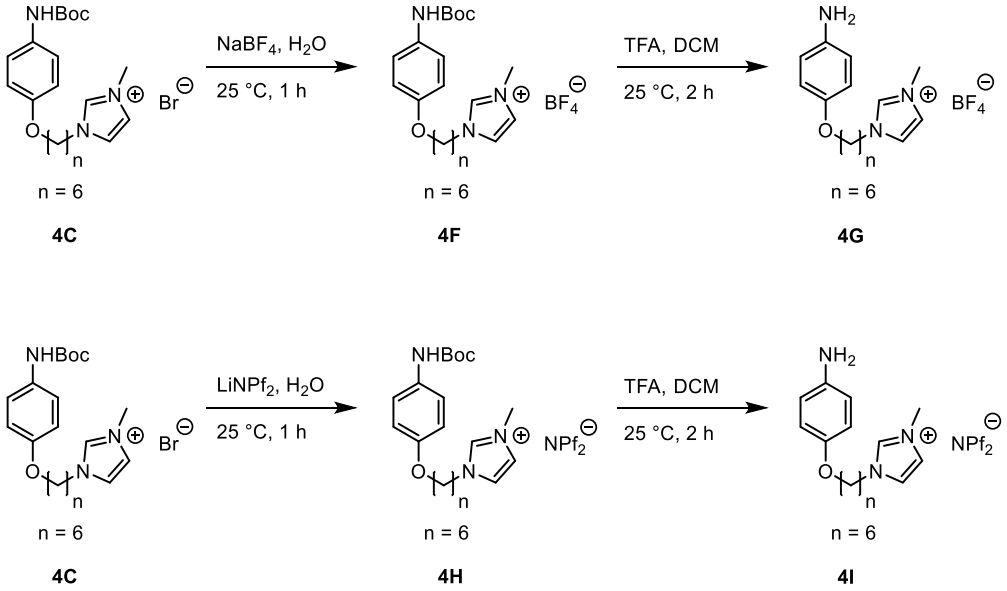

Scheme 4.4: Anion exchange on **4C** to synthesize aniline variants with BF_4^- and NPf_2^- as counterions.

in the compound being water-soluble. The TFA^- anions present in the aqueous layer could then easily undergo anion exchange with the BF_4^- anions in aniline **4G**. Therefore, the hydrophobic nature of NTf_2^- hindered anion exchange. While other deprotection methods were explored, none were found to be feasible because an acid was always needed to remove the Boc group. However, the anion of the dissociated acid could still undergo anion exchange with the product. One way to potentially circumvent the use of a Boc protecting group could be to use 4-nitrophenol instead of *N*-Boc-4-aminophenol as the starting material of the synthesis. The NO_2 group could then be reduced to an amine *via* hydrogenation in the last synthetic step.

Tetrafluoroborate was initially chosen as the anion to alkylimidazolium-functionalized aniline **4G** because previous research indicated that the Zn_4L_4 cage assembled from ligand **4A** was empty in the presence of BF_4^-. Nevertheless, the difficulties encountered in synthesizing **4G** meant that an alternate route to yield empty cage was necessary. While the zinc cages assembled from ligand **4A** encapsulated NTf_2^-, we hypothesized that a larger analogue of NTf_2^- would be too sterically hindered to occupy the cage cavity. Therefore, alkylimidazolium-functionalized aniline **4I** was designed with bis(pentafluoroethylsulfonyl) imide (NPf_2^-) as the counteranion. **4I** was hypothesized to be less synthetically complex than aniline **4G** because the NPf_2^- anions should result in the compound exhibiting solubility behavior similar to **4E**. Therefore, an anion exchange was performed on **4C** with $LiNPf_2$ to give analogue **4H** in good yield. The subsequent deprotection step was also successful, as was consistent with aniline **4E**, and resulted in pure ionic liquid **4I**. The ^{19}F NMR spectrum of **4I** showed that no NPf_2^- was displaced by TFA^- during the deprotection step.

Aniline **4I** was combined with trialdehyde **4A** and $Zn(BF_4^-)_2$ in CH_3CN and heated at 70 °C for 18h to form tetrahedral cage **4.3** (Scheme 4.5). This self-assembly was hypothesized to yield an empty capsule because the NPf_2^- anions were too sterically hindered to penetrate the cage cavity while BF_4^- anions were too small to remain encapsulated. The obtained cage was a glass-like solid at room temperature and the formation of the cage was confirmed by ^1H NMR spectroscopy. The peaks of **4.3** in the aromatic region of the spectrum were consistent with the ^1H NMR spectrum of the unfunctionalized cage previously recorded by Dr. Castilla. Additionally, the ^{19}F NMR spectrum of the cage contained three fluorine signals that were consistent with the signals from NPf_2^- and BF_4^-. However, no encapsulated fluorine peaks were observed, indicating that the cage remained empty.

The cage was further characterized with LR-ESI-MS (Figure 4.2a). Due to the mixture of anions, each charge state of the cage showed a distribution of the BF_4^- and NPf_2^- anions

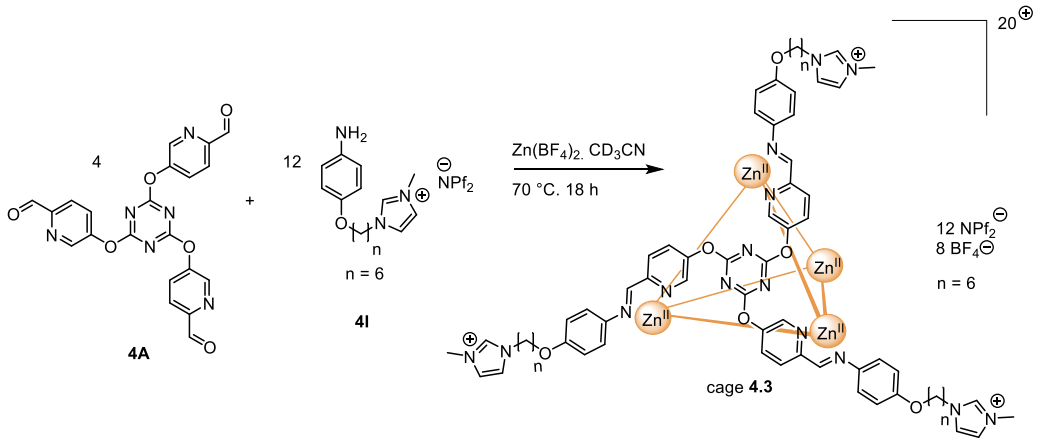

Scheme 4.5: Synthesis of cage **4.3**. The mixture of anions resulted in the cage having an empty cavity. BF_4^- anions were too small to remain in the cavity and NPf_2^- anions were too large to enter the cage.

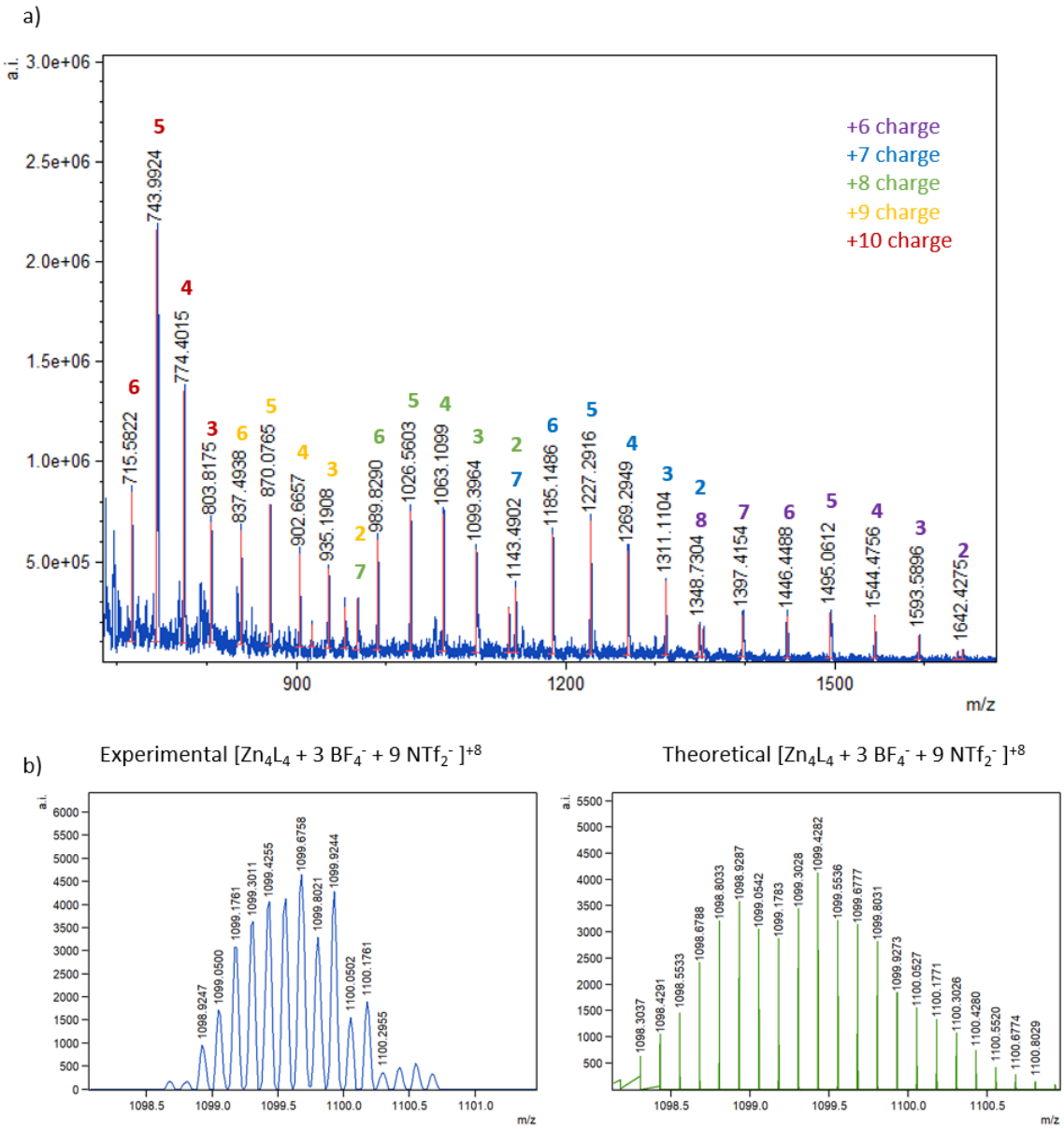

Figure 4.2: a) LR-ESI-MS of cage 4.3. Different charge states of the cage are assigned to various colors. Numbers within in each color correspond to the number of BF_4^- anions present. b) HR-ESI-MS of cage 4.3. The experimental result was consistent with the calculated isotope pattern.

present in that charge state. All observed experimental peaks were consistent with calculated values indicating that the stoichiometry of the assembly was $Zn^{II}_4L_4$ – a result that was confirmed when cage **4.3** was analyzed by HR-ESI-MS (Figure 4.2b) in which the experimental results were consistent with predicted isotope pattern. Therefore, using the results of NMR and MS, we concluded that we successfully synthesized an empty $Zn^{II}_4L_4$ tetrahedral cage.

4.4 Thermal Analysis of Cage 4.3

As a preliminary means of characterization, cage **4.3** was investigated by a Mel-Temp apparatus under N_2, and a solid to fluid phase change was observed at approximately 120 °C. However, to better characterize the phase behavior of cage **4.3**, DSC and TGA were used to analyze the material. Since cage **4.3** appeared to be a glassy solid, we hypothesized that it would exhibit a glass transition temperature. The neat material was heated from 25 °C to 400 °C at 10 °C/min under argon, and the resulting DSC curve did not contain a clearly resolved T_g, but a very broad feature spanning 100-200 °C potentially indicative of a T_g was observed (Figure 4.3). This temperature range was consistent with the phase transition onset observed visually. However, the resolution of this feature was too low to assign its identity.

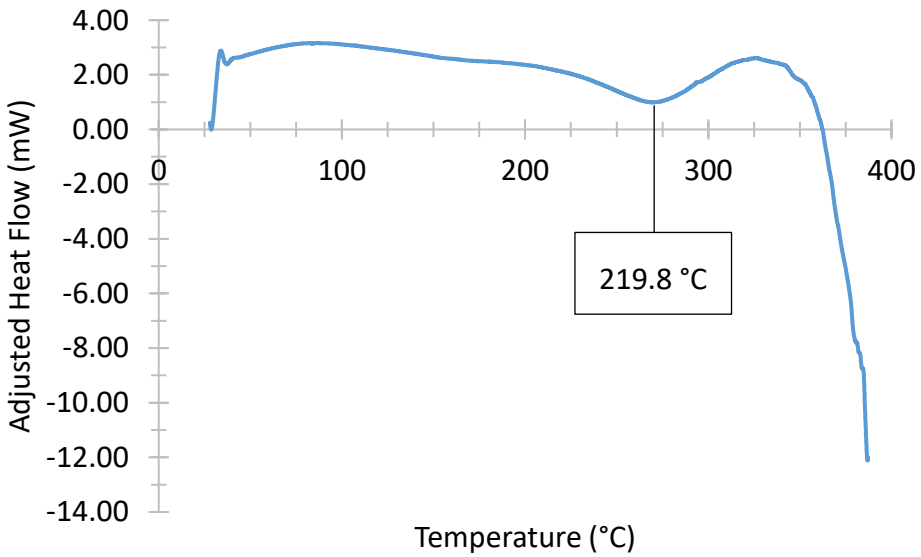

Figure 4.3: DSC scan of cage **4.3** (11.0 mg) from 25 °C to 400 °C heated at 10 °C/min. One broad exothermic feature with onset of 219.8 °C.

The lack of a clear T_g in the DSC trace does not conclusively indicate that the material does not undergo a glass transition but demonstrates that a T_g was unobservable under these experimental conditions. Literature shows that while a slow heating rate improves resolution between multiple peaks, a faster heating rate can improve the sensitivity of the instrument as well as the detection of glass transitions. Therefore, this experiment should be conducted again with a faster heat ramp to determine whether a glass-transition is present in the expected range. The DSC curve for cage **4.3** exhibited a broad exothermic feature at 219.8 °C consistent with either crystallization or a crosslinking of polymers. We hypothesized that the high temperature resulted in the dative bonds of the cage dissociating, allowing for the amine and aldehyde subcomponents to crosslink and form a polyimine thermoset.

In addition to DSC, we also used TGA to determine the thermal stability of **4.3**. TGA was performed on a neat sample of cage **4.3** by heating the material from 25 °C to 480 °C at 10 °C/min under argon (Figure 4.4). The cage began gradually decomposing at 226.7 °C, a temperature close to the onset of the crosslinking feature in the DSC trace of the cage. At 345.6 °C, the cage began to decompose rapidly; no observation of mass loss before the decomposition temperature demonstrates the high thermal stability of the material. The lack of other features below 150 °C suggested that no solvent remained inside the cage pores.

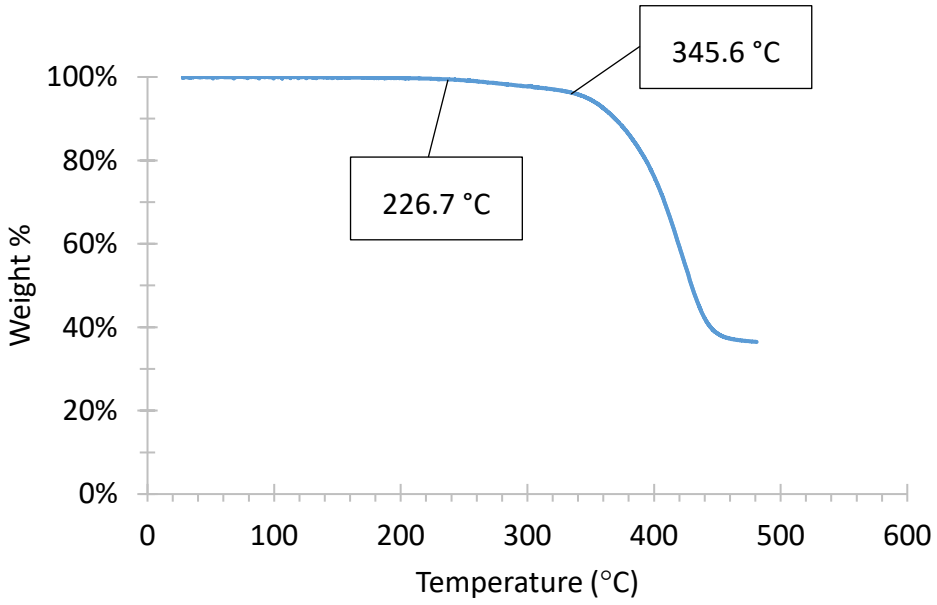

Figure 4.4: TGA trace of cage **4.3** (30.5 mg) from 25 °C to 480 °C at 10 °C/min. Cage showed signs of decomposition at 226.7 °C and rapidly decomposed at 345.6 °C.

4.5 Cage 4.3 as a Type II Porous Liquid

4.5.1 Hot-plate microscopy images of PL4.3

While cage **4.3** was an empty cage, the material was not liquid at room temperature and therefore did not qualify as a Type I permanently porous liquid. Nevertheless, we hypothesized that this cage could be adapted into a Type II permanently porous liquid by dissolving **4.3** in an ionic liquid. While coordination cages have been dissolved in ionic liquids in the past,[3] the concentration of cages in solution was low (2 mM) which meant that the overall porosity of those systems was also limited. However, we hypothesized that the alkyl imidazolium moieties of cage **4.3** would greatly increase its solubility in an ionic liquid of a similar nature. Therefore,

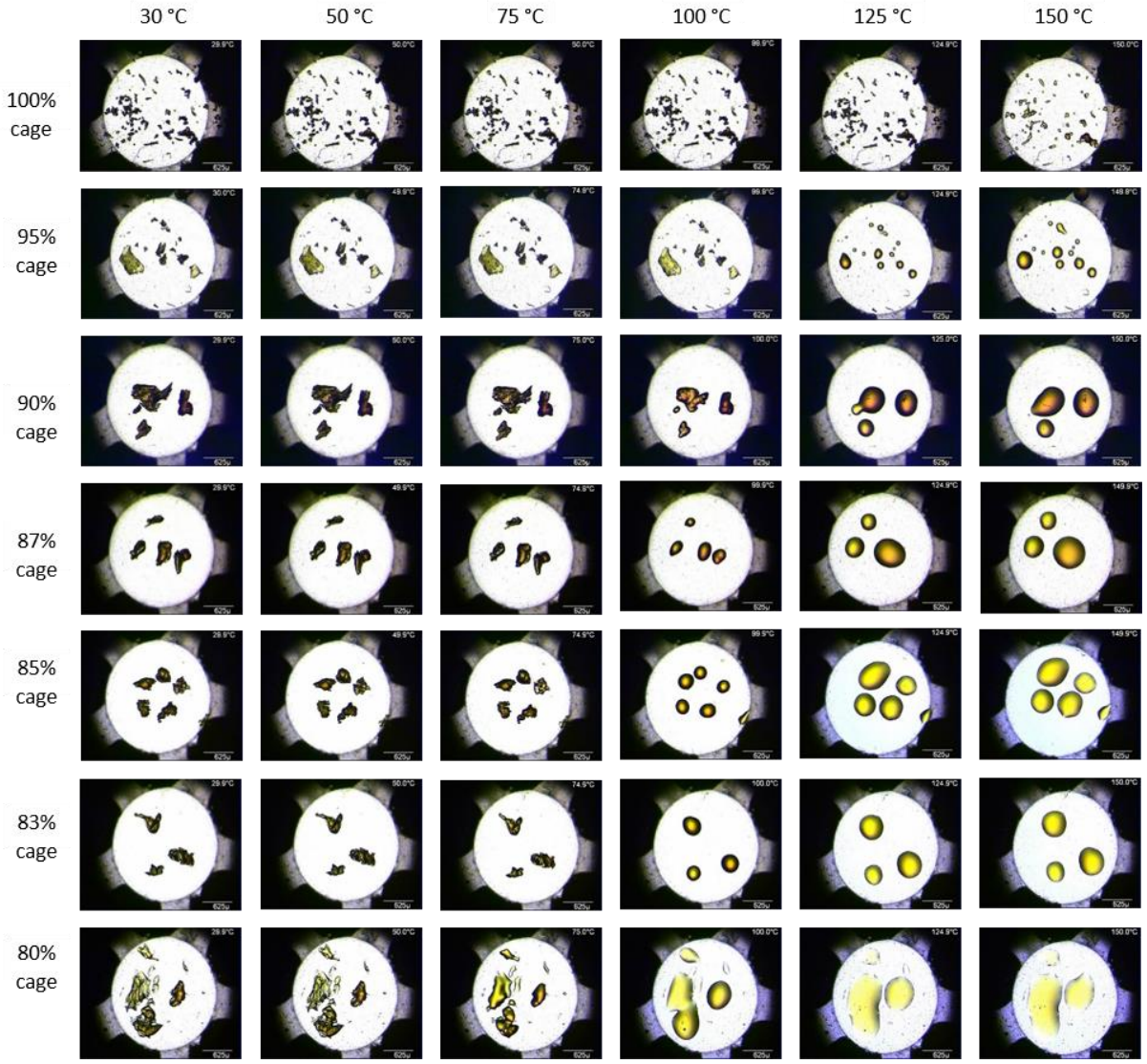

Figure 4.5: Hot-plate microscopy images of cage **4.3** with increasing wt% of [hmim][NTf_2]. When the sample is 80 wt% cage and 20 wt% ionic liquid, the microscopy images show the cage being spreadable and exhibiting fluid-like behavior.

1-hexyl-3-methylimidazolium tetrafluoroborate ([hmim][BF_4]) was chosen as the solvent for cage **4.3** because its cation shares a similar structure to the alkyl imidazolium groups in **4.3**, and its counteranion was BF_4^- – an anion previously shown too small to be encapsulated in cage **4.3**.

Cage **4.3** was adapted into a Type II porous liquid by adding a solution of [hmim][BF_4] in CH_3CN to neat cage **4.3**. The mixture was then stirred for 30 minutes after which the solvent was removed under vacuum to give porous liquid **4.3** (**PL4.3**) – a homogenous mixture of cage **4.3** in [himim][BF_4]. To determine how much [hmim][BF_4] was needed to completely solubilize cage **4.3**, samples of **PL4.3** with increasing weight percentages of ionic liquid were prepared. This method was used to prepare samples of **PL4.3** containing 100 wt%, 95 wt%, 90 wt%, 87 wt%, 85 wt%, 83 wt% and 80 wt% of cage **4.3**. Due to the inconclusive DSC results of cage **4.3**, DSC was not used to characterize the shift in phase transition temperature between

Table 4.1: Samples of **PL4.3** with varying weight percentages of cage **4.3** and their respective approximate phase transition temperatures.

Cage 4.3 (wt%)	*[hmim][BF_4] (wt%)*	*Phase transition temperature (°C)*
100	0	117
95	5	91
90	10	71
87	13	62
85	15	51
83	17	44
80	20	25

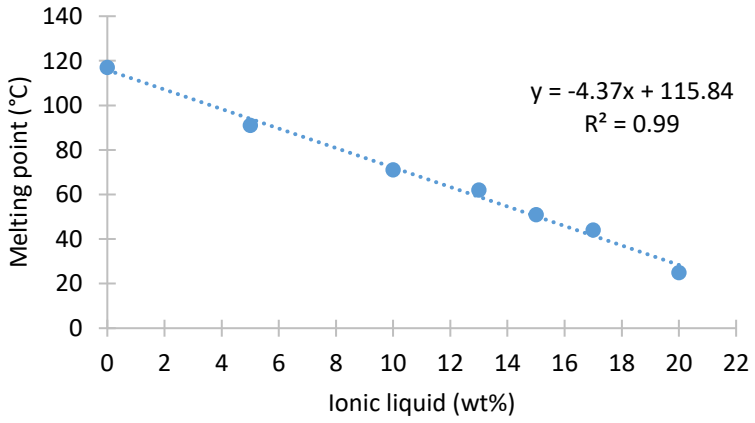

Figure 4.6: Plot of percent ionic liquid added to cage **4.3** against the approximate phase transition temperature of the sample.

the samples containing different amounts of cage at this time. Although, if experimental conditions in which the glass transition of cage **4.3** becomes observable by DSC are found, these samples could be reanalyzed *via* this technique in the future. Instead, each sample was observed *via* hot-plate microscopy as the sample was heated from 30 to 150 °C and the phase transition temperatures were determined visually (Figure 4.5, Table 4.1). However, the onset of the phase transition was difficult to determine by eye and therefore these preliminary results are approximate phase transition temperatures.

The approximate phase transition temperatures of each sample was then plotted against the weight percent of [hmim][BF_4] in the sample (Figure 4.6). The plot was fitted to a linear function and had an R^2 value of 0.99. The linear function of the graph was used to determine that adding 21 wt% of ionic liquid would yield a liquid mixture at 298 K. Therefore, a sample of **PL4.3** that exhibits fluid-like behavior at room temperature should be comprised of 79 wt% cage **4.3** dissolved in 21 wt% [hmim][BF_4]. Therefore, all future references to **PL4.3** refer to a solution of 80 wt% cage **4.3** dissolved in 20 wt% [hmim][BF_4].

4.5.2 Synthesis and characterization of PL4.3

In addition to hot-plate microscopy, **PL4.3** was also characterized in solution by ^{1}H NMR and ^{19}F NMR. The ^{1}H NMR showed both peaks corresponding to the ionic liquid and cage **4.3** (Figure 4.7) as was expected of a mixture of the two materials. The ^{19}F NMR spectrum of **PL4.3** contained three fluorine signals consistent with NPf_2^- and BF_4^-.

PL4.3 was also characterized in the neat state. Solvent-free samples were prepared by dissolving **PL4.3** in CH_3CN and adding the solution to a 5 mm NMR tube (Figure 4.8). A long needle was then inserted into the tube and the solvent was removed with a steady flow of air until the sample coated the inside of the NMR tube. A CD_3CN capillary was then added to introduce a deuterium signal for locking. The main drawback of this sample preparation method was the lack of uniformity in the porous liquid coating. A steady pressure of air would result in the porous liquid slow drying and accumulating on the bottom of the NMR tube. Therefore, as more CH_3CN was removed, air pressure was increased to push the residual sample up the sides of the tube. However, this process was difficult to control and did not always result in evenly coated samples consistently. This method also offered no means to determine if all the solvent was removed from the material.

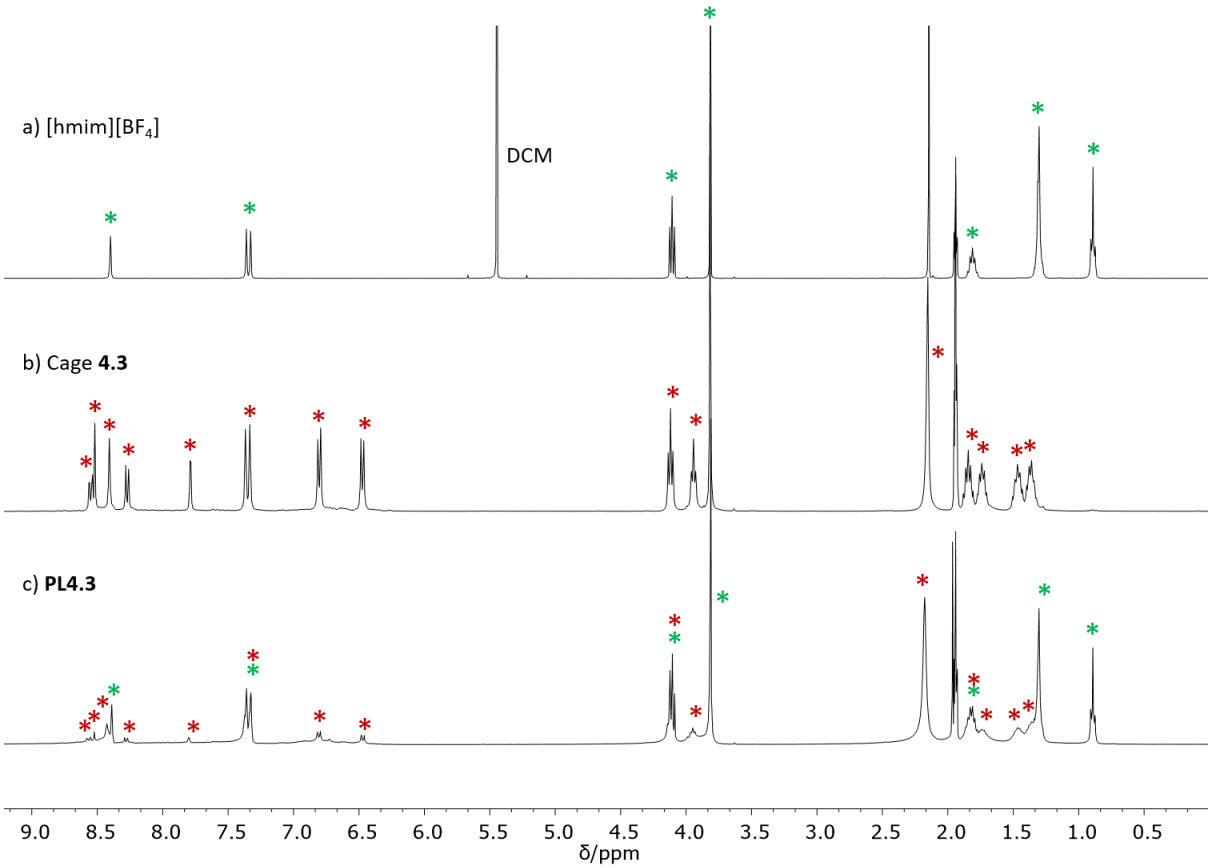

Figure 4.7: ^{1}H NMR (400 MHz, 298 K, CD_3CN) spectra of a) [hmim][BF_4] - with all peaks of the ionic liquid marked with green asterisks (*) b) cage **4.3** - with all peaks of the cage marked with red asterisks (*)and c) **PL4.3** - with [hmim][BF_4] peaks marked with a green asterisks and cage **4.3** peaks with red asterisks.

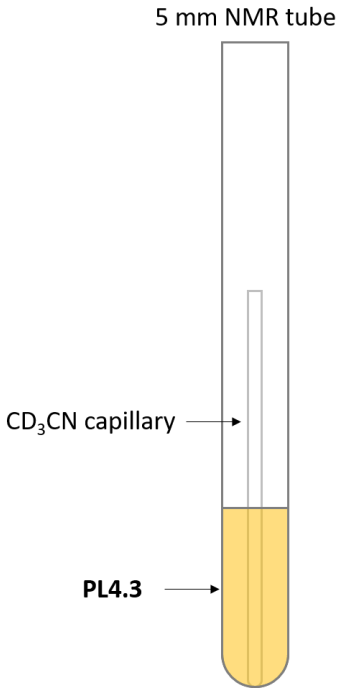

Figure 4.8: NMR apparatus used to analyse **PL4.3** in the neat state.

PL4.3 was characterized by variable temperature ^{1}H and ^{19}F NMR at 70 °C. Increasing the temperature reduced the viscosity of the sample and improved shimming. Nevertheless, ^{1}H NMR spectrum of **PL4.3** was very broad and the observed peaks were consistent with [hmim][BF_4]; no cage peaks were observed due to the broadness of the spectrum. However, three broad fluorine peaks consistent with BF_4^- and NPf_2^- could be observed in the VT-^{19}F NMR spectrum (Figure 4.9). In addition to the three anion peaks, there were also three small fluorine peaks that were attributed to being an artefact of poor shimming. Nevertheless, in the absence of a neat ^{1}H NMR spectrum in which the peaks for cage **4.3** are visible, NMR data is inconclusive with regards to the intactness of cage **4.3** in **PL4.3** under solvent-free conditions.

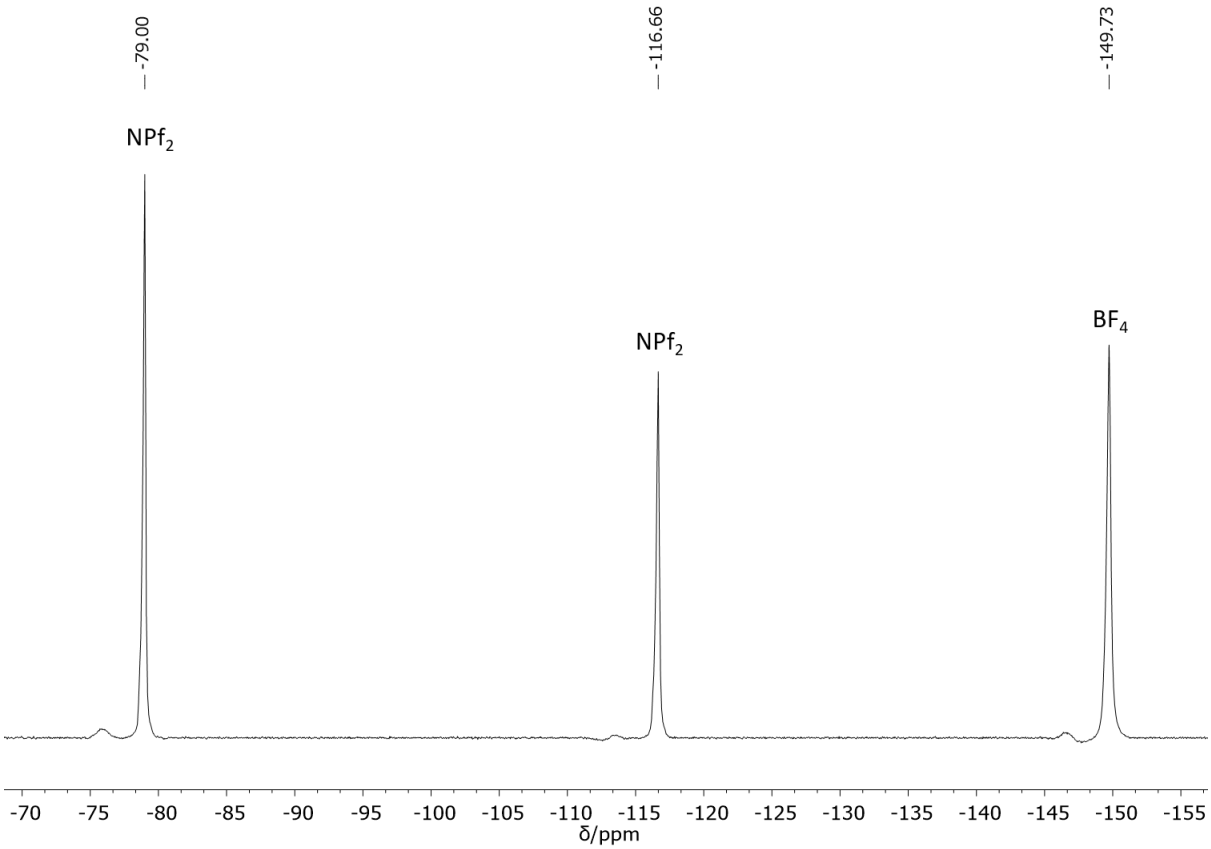

Figure 4.9: ^{19}F NMR (377 MHz, 343 K) spectrum of **PL4.3**.

4.6 Host-Guest Chemistry of PL4.3

Having successfully adapted cage **4.3** into a Type II permanently porous liquid, we investigated whether the pores of **PL4.3** could be utilized for guest encapsulation. Dr. Castilla

previously obtained a crystal structure of the unfunctionalized iron analogue of cage **4.3** (Figure 4.10).[4] Using VOIDOO,[5] Castilla calculated the pores size of the unfunctionalized cage with a probe radius of 1.6 Å and determined that the volume of the empty iron cage was 271 $Å^3$. While cage **4.3** was comprised of zinc and not iron corners, we assumed that the cavity of **4.3** would be similar to that of the unfunctionalized iron cage because the two capsules share the same central ligand **4A**.

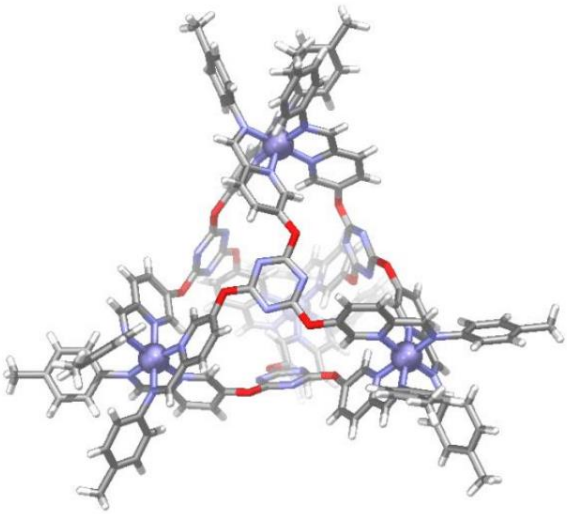

Figure 4.10: Crystal structure of the unfunctionalized $Fe^{II}_4L_4$ tetrahedral cage assembled from ligand **4A**, $Fe(NTf_2)_2$ and *p*-toluidine. Figure adapted from reference 5.

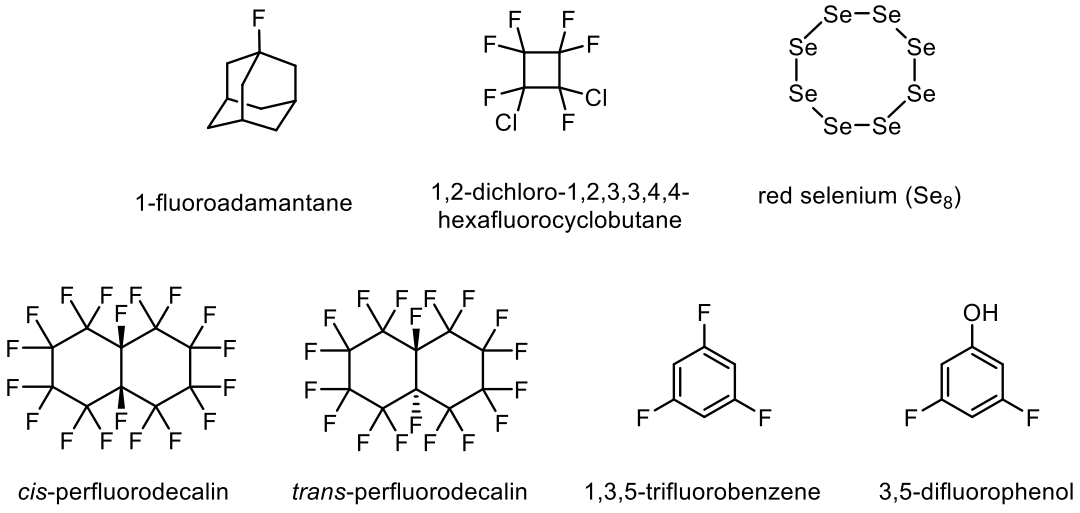

Figure 4.11: Guests chosen for cage **4.3**. All guests have a non-proton NMR active nuclei that can be used to track encapsulation.

The following molecules were chosen as potential guests: *cis*-perfluorodecalin, *trans*-perfluorodecalin, 1,3,5-trifluorobenzene, 3,5-difluorophenol, red selenium (Se_8), 1-fluoroadamantane and 1,2-dichloro-1,2,3,3,4,4-hexafluorocyclobutane (R-C316) (Figure 4.11).These molecules were chosen for this system because they contained other NMR active nuclei such as fluorine and selenium, thus allowing encapsulation to be determined by methods beyond just ^{1}H NMR.

The host-guest experiments for each of these guests were conducted in CH_3CN solution as well as in neat **PL4.3**. For experiments performed in solution, 10 wt% of the guest was added to a a 2 mM solution of cage **4.3** in CD_3CN (0.5 mL). Neat porous liquid experiments were conducted by adding 10 wt% of guest to a neat sample of cage **4.3** dissolved in 20 wt% [hmim][BF_4]. Both host-guest experiments in solution and in the neat state were stirred for 18 h at 298 K before being dissolved in CD_3CN and analyzed by NMR. All host-guest complexes were characterized by ^{1}H and ^{19}F NMR, with the exception of red selenium, which was analyzed by ^{77}Se NMR in addition to ^{1}H NMR. No evidence of encapsulation was observed by NMR for any guest other than 1,3,5-trifluorobenzene and 3,5-trifluorophenol. The ^{1}H, ^{19}F and ^{77}Se NMR peaks of all failed host-guest experiments aligned with peaks observed in the NMR spectra of the free cage, indicating no guest encapsulation in either fast or slow exchange. We hypothesized that the secondary ether bridges on the central ligand introduced flexibility into the overall structure, thus allowing the cage to deform more easily than cages formed from ligand **3A**. The lack of rigidity in cage **4.3** prevented many guests from being encapsulated and staying in the cavity of the cage.

On the other hand, an encapsulated guest peak was observed by ^{19}F NMR for the host-guest experiments containing 1,3,5-trifluorobenzene and 3,5-difluorophenol. However, there was insufficient data to conclude whether the guests were being encapsulated within the cage cavity or interacting with an external component of **4.3**. Therefore, we hypothesized that if the guests resided in the pores of **PL4.3**, the destruction of cage **4.3** would result in the elimination of the encapsulated guest peak observed by ^{19}F NMR. However, if the guest was interacting externally, destruction of the host should change the encapsulated guest peak. To test this hypothesis, acid was added to the host-guest complexes in order to disassemble cage **4.3**. *P*-toluenesulfonic acid (100 eq.) was added to an CD_3CN solution of **PL4.3** $\subset$ 1,3,5-trifluorobenzene and the reaction was stirred for 18 h at 298 K. This process was repeated on **PL4.3** $\subset$ 3,5-difluorophenol. Both these experiments were then analyzed by ^{1}H and ^{19}F NMR in CD_3CN.

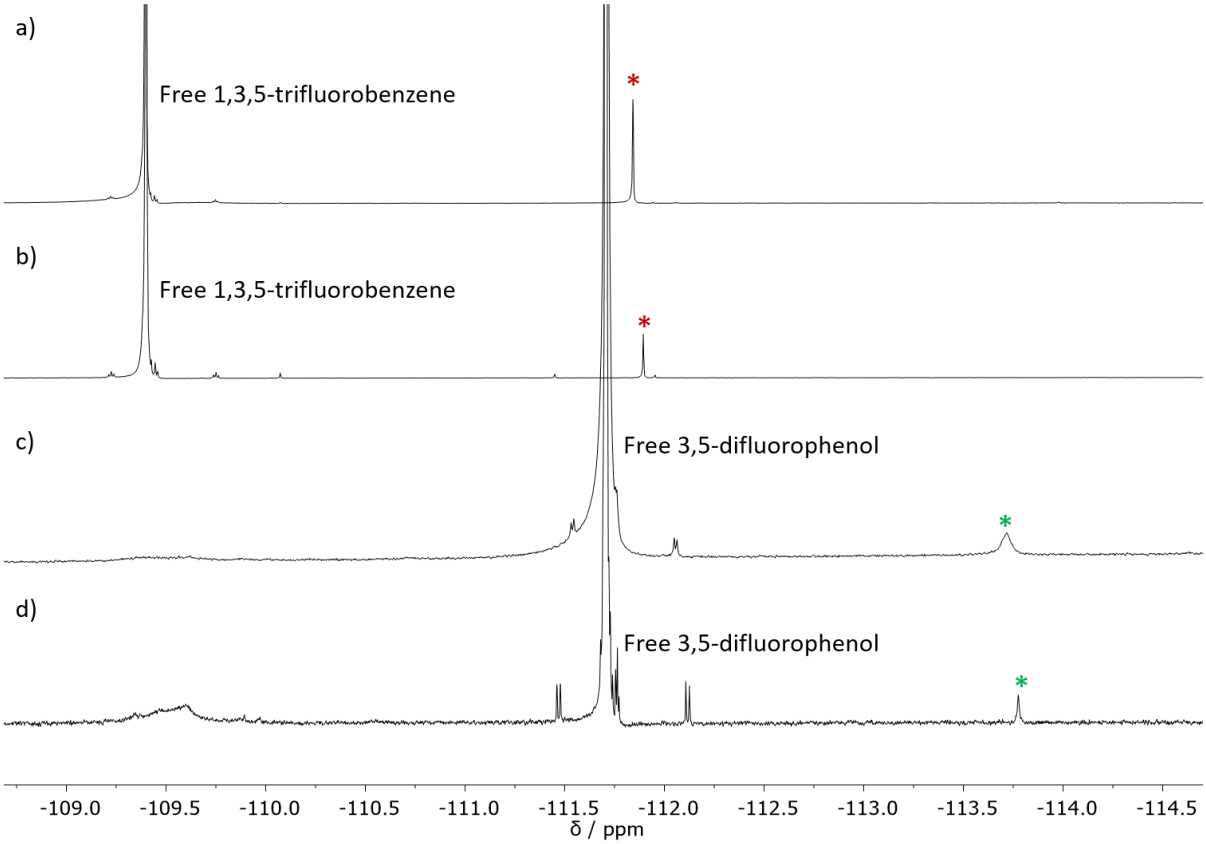

Figure 4.12: Partial ^{19}F NMR (377 MHz, 298 K, CD_3CN) spectra of a) **PL4.3** with 1,3,5-trifluorobenzene, b) **PL4.3** with 1,3,5-trifluorobenzene after the addition of *p*-TsOH, c) **PL4.3** with 3,5-difluorophenol, and d) **PL4.3** with 3,5-difluorophenol after the addition of *p*-TsOH. Peaks resutling from π-π stacking are marked with red asterisks (*) for 1,3,5-trifluorobenzene and green asterisks (*) for 3,5-difluorphenol.

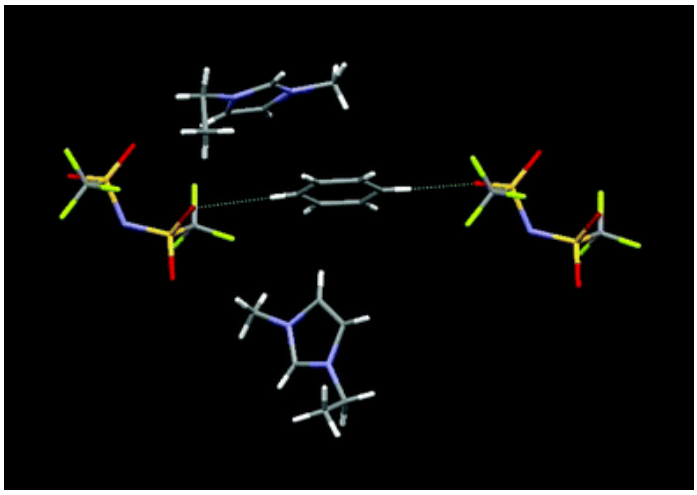

Figure 4.13: Representation of a benzene molecule interacting with imidazolium *via* π-π and cation-π interactions. Figure adapted from reference 5.

^{1}H NMR analysis of the destroyed host-guest complexes showed a peak at 9.89 ppm – indicative of the aldehyde subcomponent resulting from the disassembly of cage **4.3**. The other peaks in the aromatic region were no longer consistent with the spectrum of cage **4.3**, indicating successful destruction of the host. However, when the destroyed host-guest complexes were analyzed by ^{19}F NMR, the "encapsulated" guest peak was still present (Figure 4.12). While this result may initially seem paradoxical, the data suggest that neither guest was binding within the cage cavity because the "encapsulated" peak persisted after the destruction of the cage **4.3**. Literature shows precedence of imidazolium-based ionic liquids exhibiting strong π-π and cation-π interactions with aromatic molecules (Figure 4.13).[6] Therefore, we hypothesized that the 1,3,5-trifluorobenzene and 3,5-difluorophenol molecules were interacting with the imidazolium units in the porous liquid, and were not bound within the cage cavity.

Two control experiments were designed to test this hypothesis. We hypothesized that cage **4.3** stirred with an aromatic guest would still exhibit an "encapsulated" guest peak in the absence of [hmim][BF_4], because the guest could interact with the imidazolium moieties that functionalize the cage. Similarly, we also hypothesized that [hmim][BF_4] stirred with an

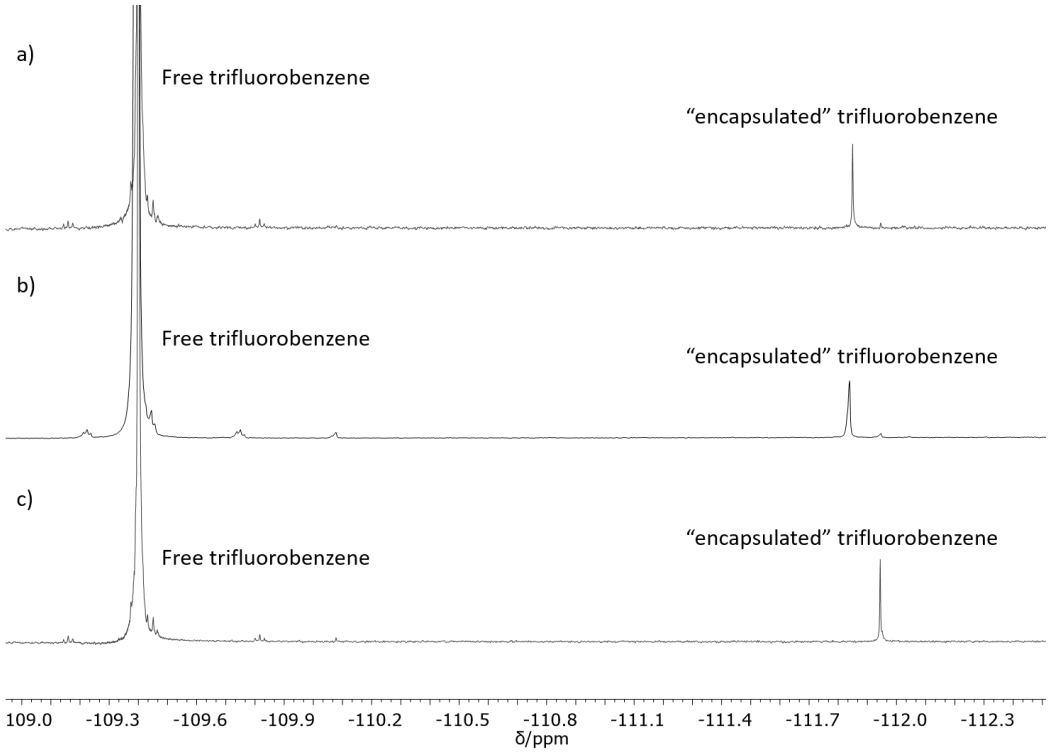

Figure 4.14: Partial ^{19}F NMR (377 HMz, 298 K, CD_3CN) spectra of a) **PL4.3** with 1,3,5-trifluorobenzene, b) cage **4.3** with 1,3,5-trifluorobenzene and c) [hmim][BF_4] with 1,3,5-trifluorobenzene. The "encapsulated" guest peak was present in all three spectra.

aromatic guest would show the same "encapsulated" peak because the guest could interact with the imidazolium cations of the ionic liquid. 1,3,5-trifluorobenzene was chosen as the guest for these control experiments. 1,3,5-trifluorobenzene (10 wt%) was added to a 0.5 mL sample of cage **4.3** in CD_3CN solution and equilibrated at 298 K for 18 h. 1,3,5-trifluorobenzene (10 wt%) was also added to a sample of [hmim][BF_4] and stirred at 298 K for 18 h before being dissolved in CD_3CN. The control experiments were then analyzed by ^{19}F NMR in CD_3CN and the results corroborated our hypothesis that the guest was not bound in the cage but was externally interacting with the imidazolium units of the ionic liquid and the cage (Figure 4.14). ^{19}F NMR spectra showed an "encapsulated" guest peak for each sample – even for the experiment with only [hmim][BF_4] and no cage **4.3**, suggesting that the presence of the "encapsulated" peak was not dependent on the cage. Assuming that the "encapsulated" peak was a result of π-π and cation-π interactions between the benzene scaffold of the 1,3,5-trifluorobenzene and the aromatic imidazolium groups, we hypothesized that 3,5-difluorophenol also interacted with imidazolium molecules in a similar way.

4.7 Conclusions and Future Work

This chapter presents the first Type II permanently porous liquid based on a coordination cage. Cage **4.3** was synthesized by assembling aniline **4I** with trialdehyde **4A** in the presence of $Zn(BF_4)_2$. The usage of a mixture of BF_4^- and NPf_2^- anions to charge-balance the cationic cage resulted in the assembly of an empty capsule because NPf_2^- was too sterically hindered to be encapsulated and BF_4^- was too small to occupy the cavities. ^{19}F NMR showed three peaks consistent with these two free anions. Thermal analysis of the material indicated that cage had a high thermal stability and contained no residual solvent in the neat state. Cage **4.3** was then adapted into a Type II permanently porous liquid by dissolving cage **4.3** in 20 wt% [hmim][BF_4]. Host-guest experiments were performed with this porous liquid but none of the selected guests were encapsulated.

Further characterization of **PL4.3** could include rheology, DSC/TGA and PALS. Rheology could be used to analyze the viscosity and fluid behavior of the material. DSC and TGA of **PL4.3** could determine the phase change behavior as well as thermal stability of the material. These results could then be compared against the DSC/TGA traces of cage **4.3** and [hmim][BF_4] to contrast the stability of this porous liquid against its individual components. A

faster heat ramp may be needed in the DSC experiments to better resolve any glass transition temperatures that may too broad to be detected at a slower, more conventional, rate. Although the porous liquid did not encapsulate any of the guests featured in this chapter, it may still bind other guests that we did not investigate; further research is required in this area.

In this work, cage **4.3** was not observed to bind any neutral guests in CH_3CN; however, the host in **PL4.3** experiences a different external chemical environment when compared to cage **4.3** dissolved in CH_3CN, and we hypothesize that guest uptake may be different between neat **PL4.3** and a solution of **4.3** in CH_3CN. One potential way to screen for guests, while conserving the amount of cage **4.3** needed for host-guest experiments, could be to synthesize the unfunctionalized counterpart to cage **4.3** and dissolve it in [hmim][BF_4] at low concentrations; this porous liquid could then be used to perform preliminary host-guest experiments. The unfunctionalized cage can be easily assembled by combining trialdehyde **4A** with *p*-toluidine and $Zn(NTf_2)_2$.[4] The solution of unfunctionalized cage in [hmim][BF_4] would have a similar chemical composition to **PL4.3**, and host-guest behavior in the two systems should be comparable. Guests that are discovered to bind in the solution of unfunctionalized cage and [hmim][BF_4] can then be tested with **PL4.3**.

While this chapter focuses on cage **4.3**, the alkylimidazolium anilines featured above could be self-assembled with a variety of other aldehyde subcomponents and metal salts. Subcomponent self-assembly is an especially useful technique for making new porous liquids because these materials are notoriously difficult to synthesize. Therefore, a modular technique that could yield a library of cages with different sizes and architectures could be extremely valuable for this nascent field. These liquid cages can then be used for future applications such as liquid extractions, gas encapsulation, and molecular separations.

4.8 Experimental Methods

4.8.1 Synthesis of alkylimidazolium-functionalized anilines

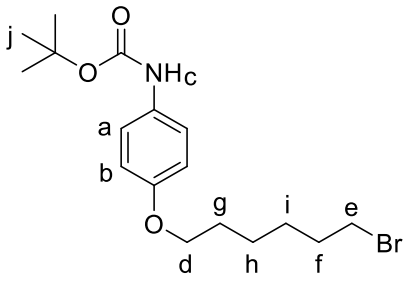

4B

*tert-butyl (4-((6-bromohexyl)oxy)phenyl)carbamate **4B***:

1,6-dibromohexane (62.16 mL, 0.43 mol, 6 eq.) was added dropwise to a stirring suspension of tert-butyl (4-hydroxyphenyl)carbamate (15.00 g, 71.68 mmol) and K_2CO_3 (14.86 g, 107.53 mmol, 1.50 eq.) in DMF (1.20 L). The reaction was stirred for 18 h at 298 K after which the solvent was removed via rotary evaporation. The product was extracted with DCM (250 mL) and the organic extract was washed with water (3 x 200 mL). The organic layer was then dried with anhydrous $MgSO_4$, filtered, and concentrated on the rotary evaporator. The crude product was purified via flash column chromatography on silica with DCM/hexane 1:1 as the eluent. The pure product was obtained as white crystals (18.20 g, 68% yield). ^{1}H NMR (400 MHz, 298 K, $CDCl_3$): δ = 7.23 (d, 2H, J = 8.9 Hz, H_a), δ = 6.82 (d, 2H, J = 9.0 Hz, H_b), δ = 6.32 (s, 1H, H_c), δ = 3.92 (t, 2H, J = 6.4 Hz, H_d), δ = 3.42 (t, 2H, J = 6.8 Hz, H_e), δ = 1.89 (m, 2H, H_f), δ = 1.77 (m, 2H, H_g), δ = 1.51 (m, 16H, $H_{h,i,j}$). ^{13}C NMR (100 MHz, $CDCl_3$): δ 155.3, 152.9, 131.5, 120.4, 115.0, 80.4, 68.2, 34.0, 32.8, 29.3, 28.5, 28.1, 25.4 ppm. HR-MS (ESI) found: 372.1181[M]$^+$; $C_{17}H_{27}NO_3Br$ requires: 372.1169. Elemental analysis (%) calculated for $C_{17}H_{26}BrNO_3$: C, 54.84; H, 7.04; Br, 21.46; N, 3.76. Found: C, 55.26; H, 7.05; Br, 21.26; N, 3.82.

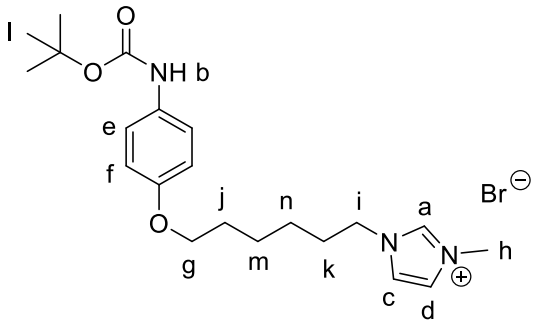

4C

1-(6-(4-((tert-butoxycarbonyl)amino)phenoxy)hexyl)-3-methyl-1H-imidazol-3-ium bromide ***4C****:*

1-methylimidazole (4.29 g, 53.77 mmol, 1.1 eq) was added to tert-butyl (4-((6-bromohexyl)oxy)phenyl)carbamate **4B**. The reaction was stirred at 298 K for 18 h after which the product was extracted with water (200 mL) and filtered. The extract was washed with DCM (5 x 100 mL) and concentrated via rotary evaporation, yielding a yellow oil as the pure product (16.0 g, 72% yield). ^{1}H NMR (400 MHz, 298 K, D_2O): δ = 8.71 (s, 1H, H_a), δ = 7.47 (s, 1H, H_b), δ = 7.42 (s, 1H, J = 1.7 Hz, H_c), δ = 7.38 (s, 1H, J = 1.8 Hz, H_d), δ = 7.23 (d, 2H, J = 8.8 Hz, H_e), δ = 6.71 (d, 2H, J = 9.0 Hz, H_f), δ = 4.06 (t, 2H, J = 7.3 Hz, H_g), δ = 3.86 (s, 3H, H_h), δ = 3.72 (t, 2H, J = 6.4 Hz, H_i), δ = 1.72 (m, 2H, H_j), δ = 1.57 (m, 2H, H_k), δ = 1.37 (s, 18H, H_l), δ = 1.30 (m, 2H, H_m), δ = 1.21 (m, 2H, H_n). ^{13}C NMR (100 MHz, D_2O): δ 154.4, 154.1, 135.6, 131.6, 123.5, 122.0, 120.7, 114.7, 79.9, 68.3, 49.3, 35.8, 29.3, 28.5, 28.0, 25.5, 25.0 ppm. HR-MS (ESI) found: 374.2445 $[M\text{-}Br]^+$; $C_{21}H_{32}N_3O_3$ requires: 374.2438. Elemental analysis (%) calculated for $C_{21}H_{32}BrN_3O_3$: C, 55.51; H, 7.10; Br, 17.58; N, 9.25. Found: C, 55.15; H, 7.17; Br, 18.41; N, 9.22.

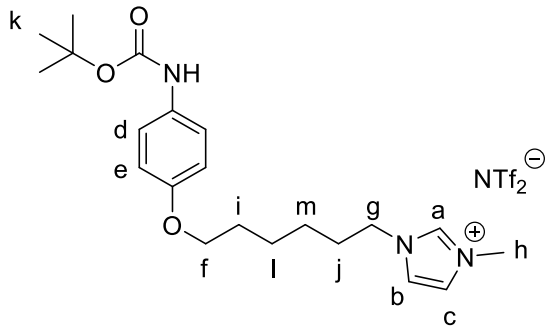

4D

*1-(6-(4-((tert-butoxycarbonyl)amino)phenoxy)hexyl)-3-methyl-1H-imidazol-3-ium bis(trifluoromethane)sulfonimide **4D**:*

Lithium bis(trifluoromethane)sulfonimide (31.6 mg, 0.11 mmol, 1.10 eq.) was added to a solution of 1-(6-(4-((tert-butoxycarbonyl)amino)phenoxy)hexyl)-3-methyl-1H-imidazol-3-ium bromide **4C** (102.1 mg, 0.22 mmol) in water (3 mL) and stirred for 15 minutes. The product was then extracted into DCM (3 mL) and washed with water (3 mL) until the addition of aqueous silver nitrate solution to the wash no longer resulted in the precipitation of silver bromide. This workup resulted in the pure product as a yellow oil (89.1 mg, 0.20 mmol, 87% yield). ^{1}H NMR (400 MHz, 298 K, CD_3CN): δ = 8.37 (s, 1H, H_a), δ = 7.35 (t, 1H, J = 1.86 Hz, H_b), δ = 7.31 (t, 1H, J = 1.86 Hz, H_c), δ = 7.27 (d, 2H, J = 9.01 Hz, H_d), δ = 6.82 (d, 2H, J = 9.03 Hz, H_e), δ = 4.11 (t, 2H, J = 7.22 Hz, H_f), δ = 3.92 (t, 2H, J = 6.46 Hz, H_g), δ = 3.80 (s, 3H, H_h), δ = 1.84 (m, 2H, H_i), δ = 1.73 (m, 2H, H_j), δ = 1.47 (m, 11H, $H_{k,l}$), δ = 1.35 (m, 2H, H_m). ^{13}C NMR (100 MHz, CD_3CN): δ 155.8, 154.3, 136.7, 133.1, 125.6, 124.6, 123.2, 122.4, 121.4, 119.3, 116.1, 115.5, 80.1, 68.7, 55.3, 50.4, 36.8, 30.5, 29.6, 28.5, 26.3, 26.0 ppm. ^{19}F NMR (377 MHz, $CDCl_3$, referenced to hexafluorobenzene in a C_6F_6 capillary): δ = -80.12 (NTf_2^-). HR-MS (ESI) found: 374.2445 $[M\text{-}NTf_2]^+$; $C_{21}H_{32}N_3O_3$ requires: 374.2438.

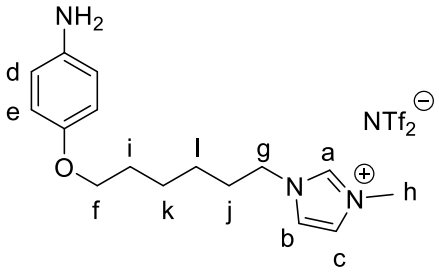

4E

1-(6-(4-aminophenoxy)hexyl)-3-methyl-1H-imidazol-3-ium bis(trifluoromethane)sulfonimide ***4E****:*

Trifluoroacetic acid (2.8 mL, 36.57 mmol, 25.00 eq) was added to a stirring solution of **4D** (963.0 mg, 1.47 mmol) in DCM (28 mL). The reaction was stirred at 298 K for 1 h then quenched with 30 mL of saturated $NaHCO_3$. The organic layer was removed, washed with water (3 x 30 mL), and concentrated via rotary evaporation. This synthesis afforded the pure product as a yellow oil (198.20 mg, 0.30 mmol, 76%). ^{1}H NMR (400 MHz, 298 K, CD_3CN): δ = 8.36 (s, 1H, H_a), δ = 7.35 (t, 1H, J = 1.6 MHz, H_b), δ = 7.31 (t, 1H, J = 1.6 MHz, H_c), δ = 6.67 (d, 2H, J = 8.8 MHz, H_d), δ = 6.57 (d, 2H, , J = 8.8 MHz, H_e), δ = 4.11 (t, 2H, , J = 7.2 MHz, H_f), δ = 3.85 (t, 2H, , J = 6.4 MHz, H_g), δ = 3.80 (s, 3H, H_h), δ = 1.84 (m, 2H, H_i), δ = 1.69 (m, 2H, H_j), δ = 1.46 (m, 2H, H_k), δ = 1.36 (m, 2H, H_l). ^{13}C NMR (100 MHz, CD_3CN): δ 152.3, 142.5, 140.1, 136.8, 136.8, 124.6, 123.3, 122.5, 119.3, 116.6, 116.5, 69.1, 50.5, 36.8, 30.5, 29.8, 26.38, 26.1 ppm. ^{19}F NMR (377 MHz, $CDCl_3$, referenced to hexafluorobenzene in a C_6F_6 capillary): δ = -80.12 (NTf_2^-). HR-MS (ESI) found: 274.1923 $[M\text{-}NTf_2]^+$; $C_{16}H_{24}N_3O$ requires: 274.1914.

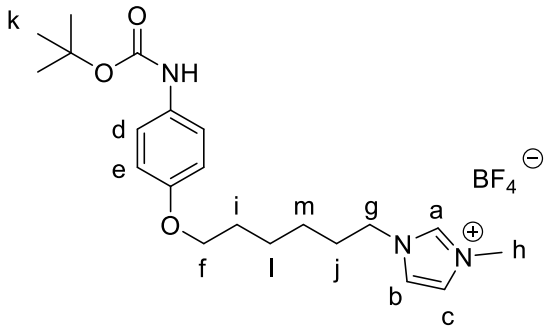

4F

*1-(6-(4-((tert-butoxycarbonyl)amino)phenoxy)hexyl)-3-methyl-1H-imidazol-3-ium tetrafluoroborate **4F**:*

Sodium tetrafluoroborate (12.1 mg, 0.11 mmol, 1.10 eq.) was added to a solution of 1-(6-(4-((tert-butoxycarbonyl)amino)phenoxy)hexyl)-3-methyl-1H-imidazol-3-ium bromide **4C** (101.1 mg, 0.22 mmol) in water (3 mL) and stirred for 15 minutes. The product was then extracted into DCM (3 mL) and washed with water (3 mL) until the addition of aqueous silver nitrate solution to the wash no longer resulted in the precipitation of silver bromide. This workup resulted in the pure product as a yellow oil (101.3 mg, 0.15 mmol, 70% yield). ^{1}H NMR (400 MHz, 298 K, CD_3CN): δ = 8.37 (s, 1H, H_a), δ = 7.35 (t, 1H, J = 1.7 Hz, H_b), δ = 7.31 (t, 1H, J = 1.6 Hz, H_c), δ = 7.27 (d, 2H, J = 9.0 Hz, H_d), δ = 6.82 (d, 2H, J = 8.9 Hz, H_e), δ = 4.11 (t, 2H, J = 7.3 Hz, H_f), δ = 3.92 (t, 2H, J = 6.4 Hz, H_g), δ = 3.80 (s, 3H, H_h), δ = 1.84 (m, 2H, H_i), δ = 1.73 (m, 2H, H_j), δ = 1.47 (m, 11H, $H_{k,l}$), δ = 1.35 (m, 2H, H_m). ^{13}C NMR (100 MHz, CD_3CN): δ 155.8, 154.3, 136.7, 133.1, 125.7, 124.6, 123.2, 122.5, 121.4, 119.3, 116.1, 115.5, 80.1, 68.7, 55.3, 50.4, 36.8, 30.5, 29.6, 28.5, 26.3, 26.0 ppm. ^{19}F NMR (377 MHz, $CDCl_3$, referenced to hexafluorobenzene in a C_6F_6 capillary): δ = -151.60 (BF_4^-), -151.66 (BF_4^-). HR-MS (ESI) found: 374.2445 $[M\text{-}BF_4]^+$; $C_{21}H_{32}N_3O_3$ requires: 374.2438.

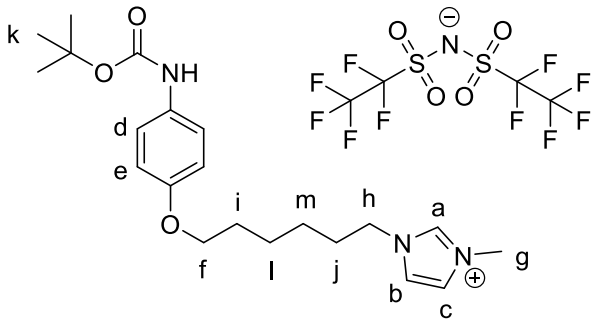

4H

1-(6-(4-((tert-butoxycarbonyl)amino)phenoxy)hexyl)-3-methyl-1H-imidazol-3-ium bis(pentafluoroethylsulfonylimide **4H**:

Lithium bis(pentafluoroethanesulfonyl)imide (659.9mg, 1.70 mmol, 1.10 eq.) was added to a solution of 1-(6-(4-((tert-butoxycarbonyl)amino)phenoxy)hexyl)-3-methyl-1H-imidazol-3-ium bromide **4C** (704.2 mg, 1.55 mmol) in water (3 mL) and stirred for 15 minutes. The product was then extracted into DCM (3 mL) and washed with water (3 mL portions) until the addition of aqueous silver nitrate solution to the wash no longer resulted in the precipitation of silver bromide. This workup resulted in the pure product as a yellow oil (1.0 g, 1.32 mmol, 86% yield). ^{1}H NMR (400 MHz, 298 K, CD_3CN): δ = 8.37 (s, 1H, H_a), δ = 7.35 (s, 1H, H_b), δ = 7.31 (s, 1H, H_c), δ = 7.27 (d, 2H, J = 8.7 Hz, H_d), δ = 6.82 (d, 2H, J = 8.9 Hz, H_e), δ = 4.11 (t, 2H, J = 7.2 Hz, H_f), δ = 3.92 (t, 2H, J = 6.3 Hz, H_g), δ = 3.80 (s, 3H, H_h), δ = 1.84 (m, 2H, H_i), δ = 1.73 (m, 2H, H_j), δ = 1.47 (m, 11H, $H_{k,l}$), δ = 1.35 (m, 2H, H_m). ^{13}C NMR (100 MHz, CD_3CN): δ 155.8, 154.3, 136.8, 133.1, 124.6, 123.2, 121.4, 115.5, 80.2, 68.7, 50.4, 36.8, 30.5, 29.6, 28.5, 26.3, 26.0 ppm. ^{19}F NMR (377 MHz, $CDCl_3$, referenced to hexafluorobenzene in a C_6F_6 capillary): δ = -79.84 (NPf_2^-), -118.12 (NPf_2^-). HR-MS (ESI) found: 374.25 $[M\text{-}NPf_2]^+$; $C_{21}H_{32}N_3O_3$ requires: 374.50. Elemental analysis (%) calculated for $C_{25}H_{32}F_{10}N_4O_7S_2$: C, 39.79; H, 4.27; F, 25.17; N, 7.42; S, 9.50. Found: C, 39.76; H, 4.30; N, 7.37; S, 8.62.

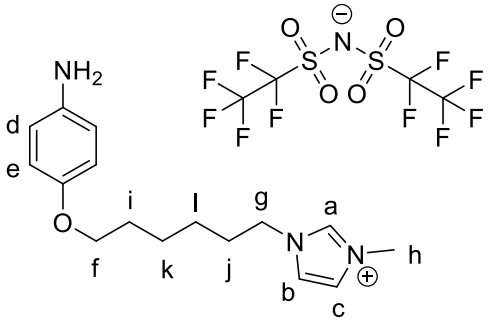

4I

1-(6-(4-aminophenoxy)hexyl)-3-methyl-1H-imidazol-3-ium bis(pentafluoroethyanesulfonylimide **4I**:

Trifluoroacetic acid (1.50 mL, 22.21 eq) was added to a stirring solution of **4H** in DCM (28 mL). The reaction was stirred at 298 K for 1 h then quenched with 30 mL of saturated $NaHCO_3$. The organic layer was removed, washed with water (3 x 30 mL), and concentrated via rotary evaporation. This afforded the pure product as a yellow oil (198.20 mg, 0.30 mmol, 76%). ^{1}H NMR (400 MHz, 298K CD_3CN): δ = 8.78 (s, 1H, H_a), δ = 7.26 (s, 1H, H_b), δ = 7.22 (s, 1H, H_c), δ = 6.71 (d, 2H, J = 8.8 Hz, H_d), δ = 6.62 (d, 2H, J = 8.8 Hz, H_e), δ = 4.16 (t, 2H, J = 7.5 Hz,H_f), δ = 3.86 (t, 2H, J = 6.2 Hz,H_g), δ = 3.80 (s, 3H, H_h), δ = 1.84 (m, 2H, H_i), δ = 1.69 (m, 2H, H_j), δ = 1.46 (m, 2H, H_k), δ = 1.36 (m, 2H, H_l). ^{13}C NMR (100 MHz, CD_3CN): δ 152.2, 142.6, 136.7, 124.6, 123.2, 116.5, 116.4, 69.0, 50.4, 36.8, 30.5, 29.8, 26.3, 26.0 ppm; ^{19}F NMR (377 MHz, $CDCl_3$, referenced to hexafluorobenzene in a C_6F_6 capillary): δ = -79.84 (NPf_2^-), -118.12 (NPf_2^-). HR-MS (ESI) found: 274.19 $[M\text{-}NPf_2]^+$; $C_{16}H_{24}N_3O$ requires: 274.39. Elemental analysis (%) calculated for $C_{20}H_{24}F_{10}N_4O_5S_2$: C, 36.70; H, 3.70; F, 29.03; N, 8.56; S, 9.80. Found: C, 36.88; H, 3.72; N, 8.58; S, 9.57.

4.8.2 Self-assembly of alkylimidazolium-functionalized cages

Cage **4.1**:

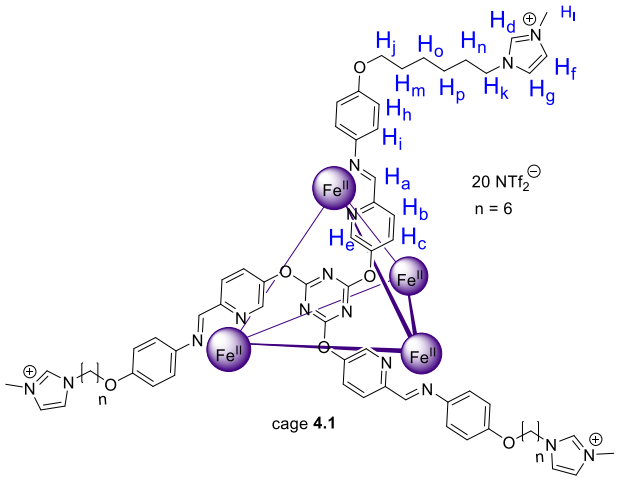

Trialdehyde **4A** (2.67 mg, 6.00 µmol), aniline **4I** (9.98 mg, 18.00 µmol, 3.00 eq), and $Fe(NTf_2)_2$ (3.70 mg, 6.00 µmol, 1.00 eq) were dissolved in CH_3CN (0.5 mL) and heated at 50 °C for 18 h. Diethyl ether (3 mL) was added and the cage precipitated out of solution as a yellow oil. The cage was isolated *via* centrifugation and dried under vacuum, yielding pure cage **4.1** as a purple glass-like solid (13.00 mg, 1.21 µmol, 81% yield). ^{1}H NMR (400 MHz, 298 K, CD_3CN): δ = 9.25 (s, 1H, H_{aEmpty}), δ = 9.02 (s, 1H, H_{aFull}), δ = 8.70 (d, 1H, J = 8.83 Hz, H_{bEmpty}), δ = 8.64 (d, 1H, J=8.83 Hz, H_{bFull}), δ = 8.51 (dd, 1H, J=8.83, 1.53 Hz, H_{cEmpty} and H_{cFull}), δ = 8.39 (s, 1H, H_d), δ = 7.68 (s, 1H, H_{eEmpty}), δ = 7.57 (s, 1H, H_{eFull}), δ = 7.35 (s, 1H, H_f), δ = 7.33 (s, 1H, H_g), δ = 6.78 (d, 2H, J=8.60 Hz, H_{hEmpty}), δ = 6.77 (d, 2H, J=8.60 Hz, H_{hFull}), δ = 5.62 (d, 2H, J=8.60 Hz, H_{iEmpty}), δ = 5.57 (d, 2H, J=8.60 Hz, H_{iFull}), δ = 4.12 (t, 2H, J=7.32 Hz, H_j), δ = 3.96 (m, 2H, H_k), δ = 3.81 (s, 3H, H_l), δ = 1.85 (m, 2H, H_m), δ = 1.75 (m, 2H, H_n), δ = 1.47 (m, 2H, H_o), δ = 1.37 (m, 2H, H_p). ^{13}C NMR (126 MHz, CD_3CN): δ 172.9, 172.6, 172.5, 160.5, 160.4, 156.8, 153.9, 152.6, 148.9, 144.3, 144.2, 136.7, 135.0, 134.4, 132.7, 132.1, 124.6, 124.6, 124.5, 124.1, 123.2, 123.1, 122.1, 115.7, 69.2, 50.4, 36.8, 30.8, 30.4, 29.6, 29.5, 26.5, 26.3, 25.9 ppm. ^{19}F NMR (377 MHz, $CDCl_3$: δ = -75.07 (encapsulated NTf_2^-), -80.12 (free NTf_2^-).

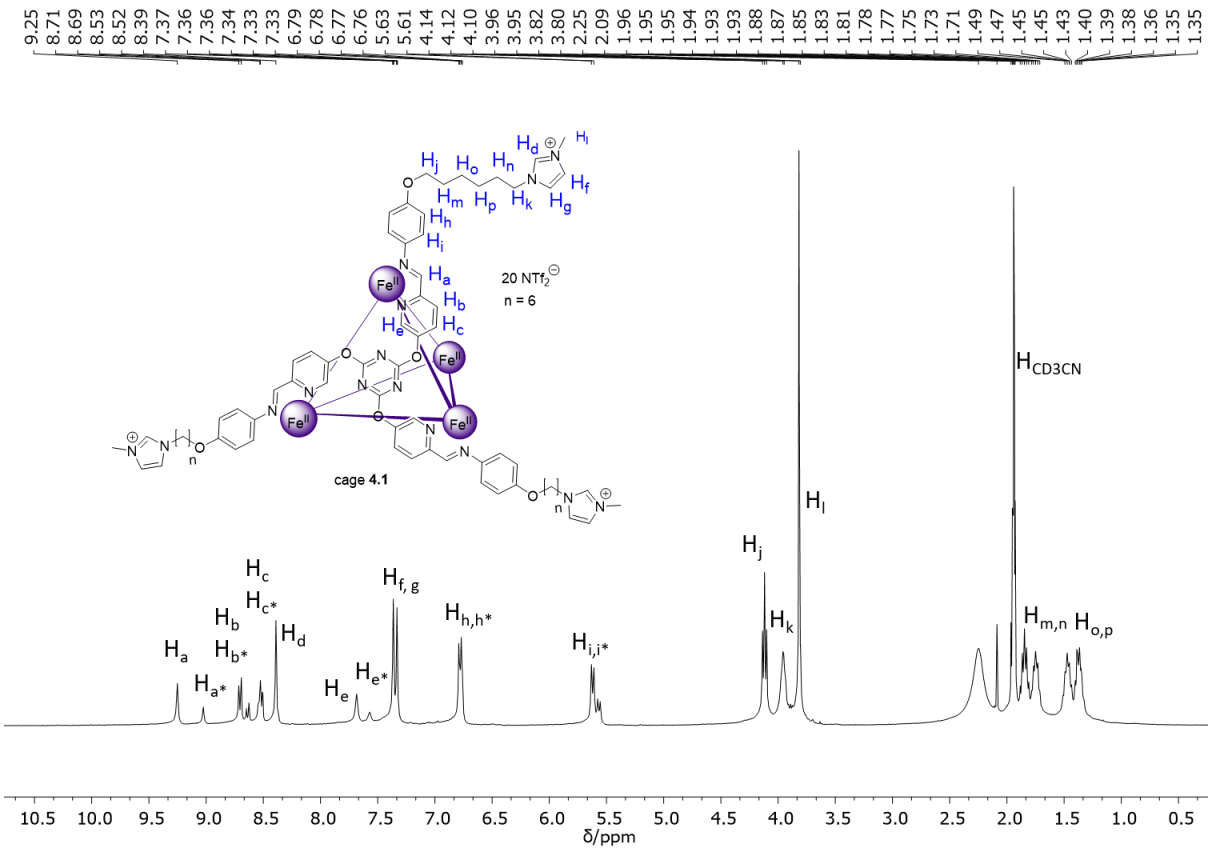

Figure 4.15: ^{1}H NMR (400 MHz, CD_3CN) spectrum of cage **4.1**. Labels with an asterisk (*) indicate cage peaks with bound NTf_2^-.

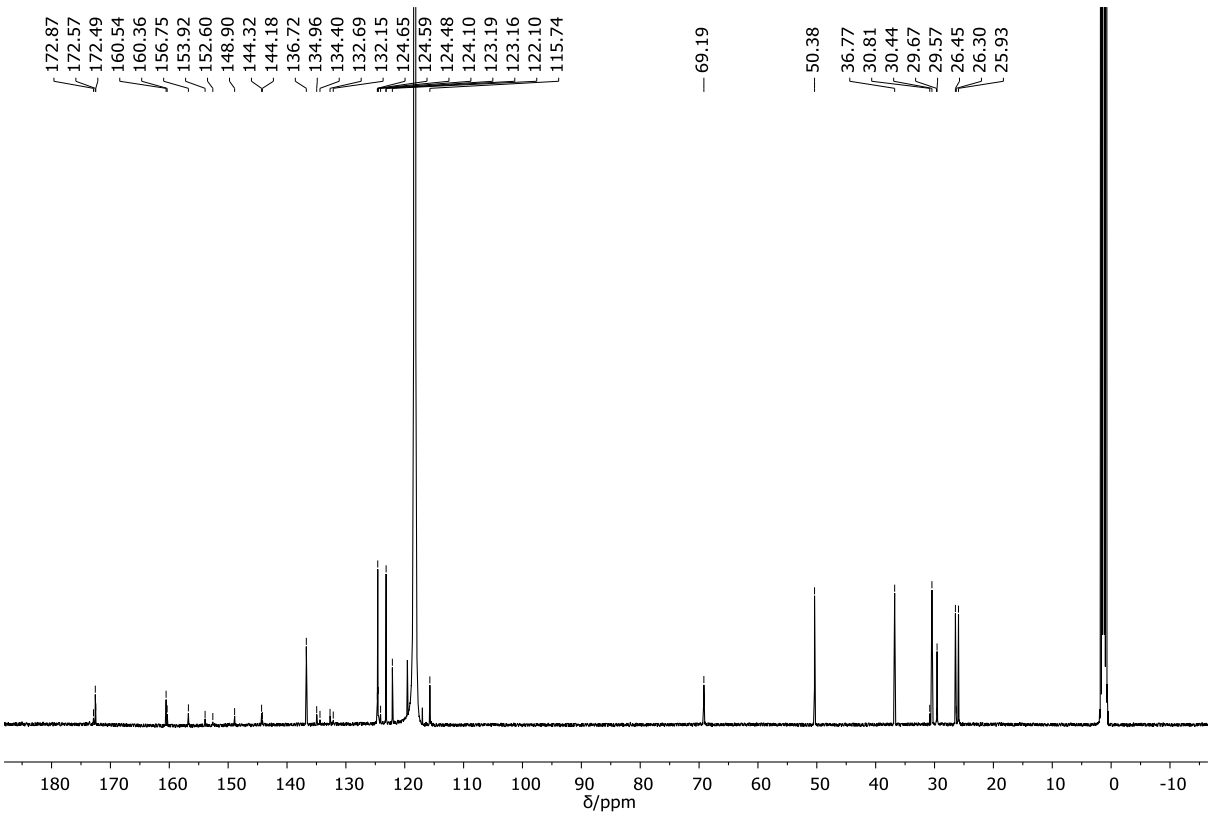

Figure 4.16: ^{13}C NMR (125 MHz, CD_3CN) spectrum of cage **4.1**.

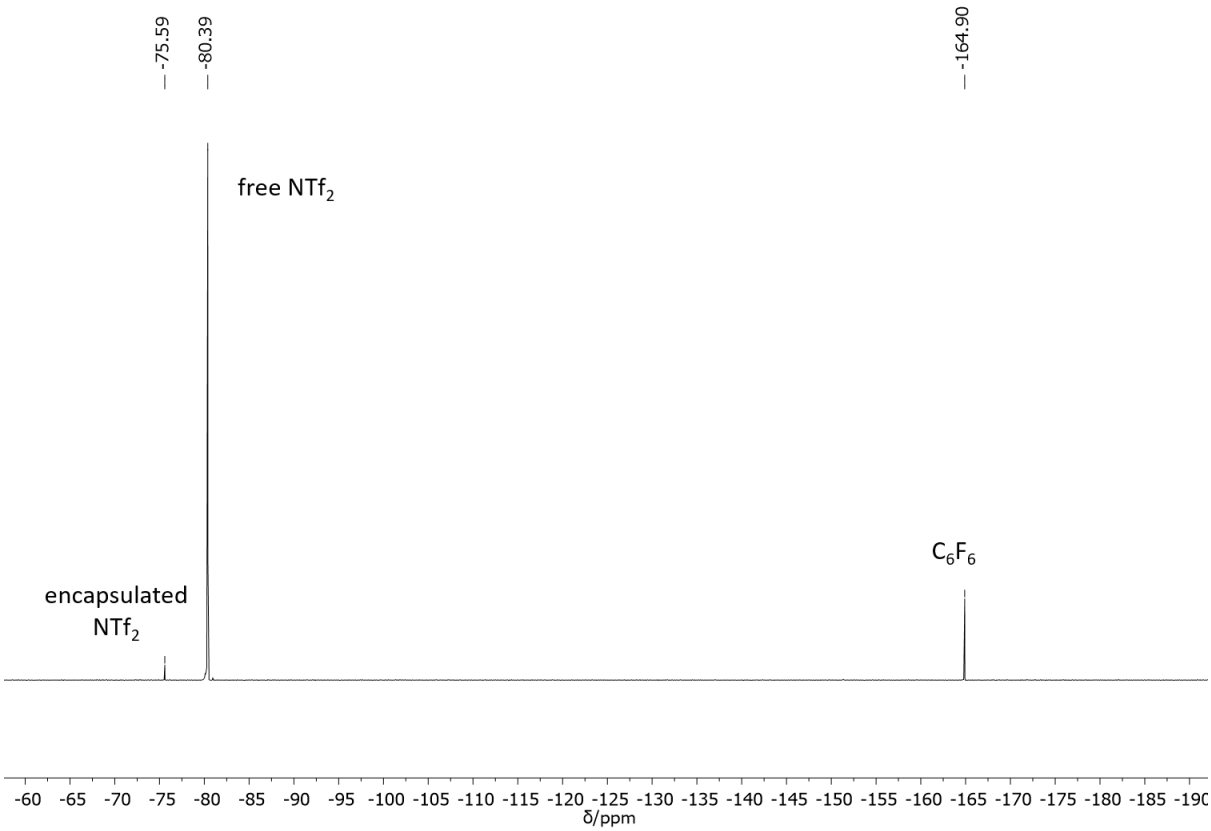

Figure 4.17: ^{19}F NMR (377 MHz, CD_3CN) spectrum of cage **4.1**.

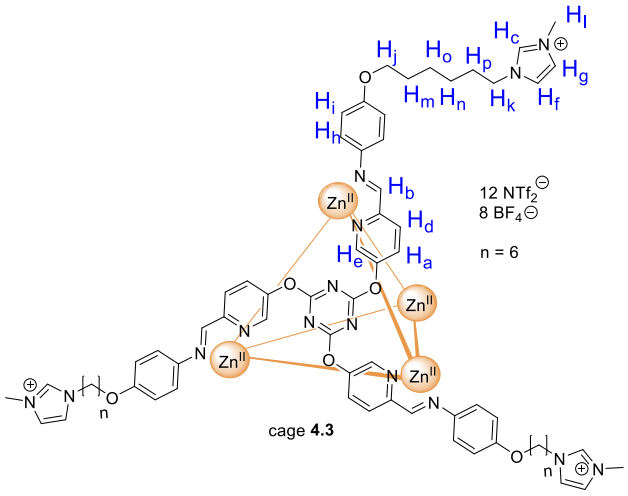

Cage **4.3**:

Trialdehyde **4A** (15.30 mg, 34.43 µmol), aniline **4I** (67.71 mg, 103.29 µmol, 3.00 eq), and $Zn(BF4)_2$ (8.23 mg, 34.43 µmol, 1.00 eq) were dissolved in CH_3CN (2.5 mL) and heated at 50 °C for 18 h. Diethyl ether (3 mL) was added and the cage precipitated out of solution as a yellow oil. The cage was isolated via centrifugation and dried under vacuum, yielding pure cage **4.3** as a yellow glass-like solid (72.00 mg, 6.94 µmol, 81% yield). ^{1}H NMR (400 MHz, 298 K, CD_3CN): δ = 8.58 (dd, 1H, J = 2.5 Hz and 8.65 Hz, H_a), 8.55 (s, 1H, H_b), 8.44 (s, 1H, H_c), 8.30 (d, 1H, J = 8.6 Hz, H_d), 7.82 (d, 1H, J = 2.1 Hz, H_e), 7.40 (s, 1H, H_f), 7.36 (s, 1H, H_g), 6.83 (d, 2H, J = 8.9 Hz, Hh), 6.50 (m, 2H, J = 8.8 Hz, H_i), 4.15 (t, 2H, J = 7.6 Hz, H_j), 3.97 (t, 2H, J = 6.3 Hz, H_k), 3.84 (s, 3H, H_l), 1.87 (m, 2H, H_m), 1.77 (m, 2H, H_n), 1.50 (m, 2H, H_o), 1.39 (m, 2H, H_p). ^{13}C NMR (126 MHz, CD_3CN): δ 172.7, 162.6,

160.4, 152.1, 145.4, 143.6, 140.4, 136.8, 131.4, 124.5, 124.2, 123.2, 116.1, 69.0, 50.3, 36.7, 30.4, 29.5, 26.4, 25.9 ppm. ^{19}F NMR (377 MHz, $CDCl_3$: δ = -79.81 (NPf_2^-), -118.18 (NPf_2^-), -151.11 (BF_4^-), -151.16 (BF_4^-).

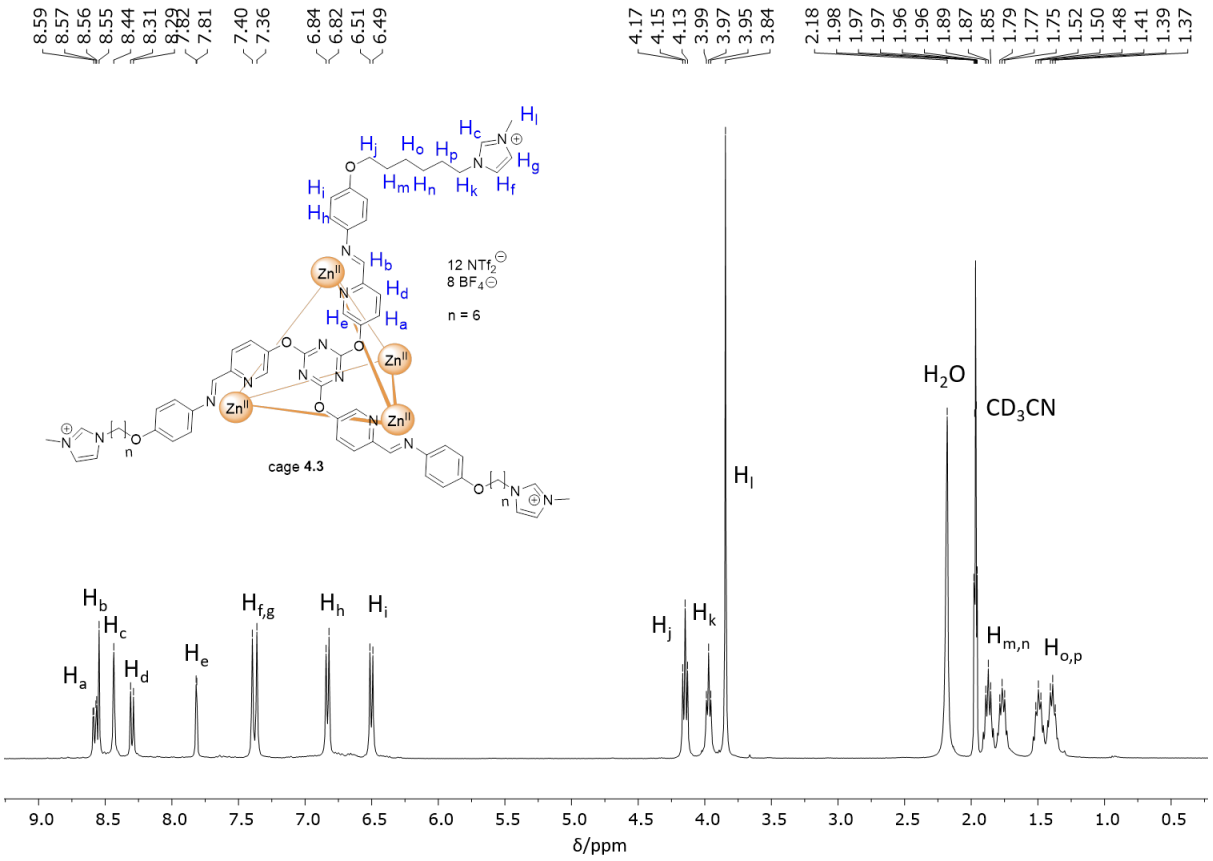

Figure 4.18: ^{1}H NMR (400 MHz, CD_3CN) spectrum of cage **4.3**.

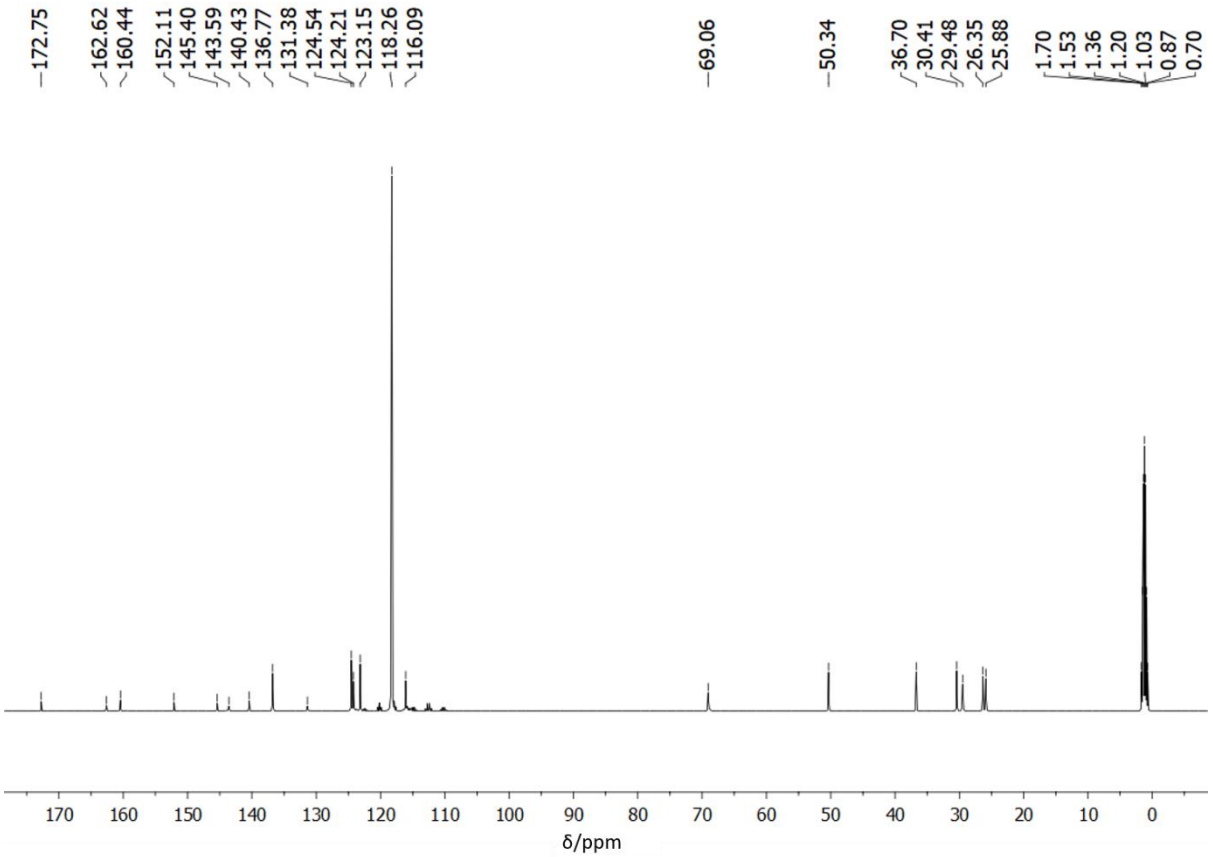

Figure 4.19: ^{13}C NMR (126 MHz, CD_3CN) spectrum of cage **4.3**.

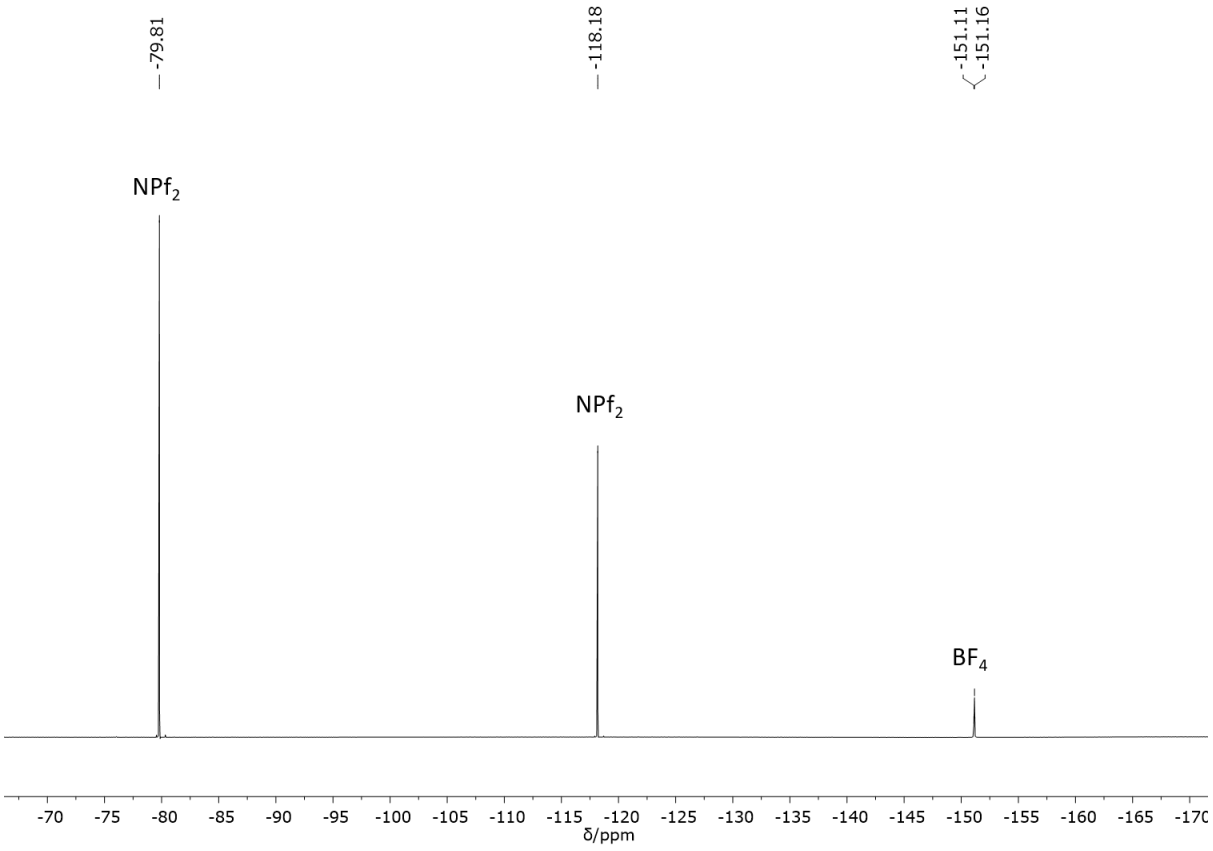

Figure 4.20: ^{19}F NMR (377 MHz, CD_3CN) spectrum of cage **4.3**.

4.8.3 Synthesis of PL4.3

PL4.3 was synthesized *via* the follow method. [hmim][BF_4] (20 mg) was added as a solution in CH_3CN to neat cage **4.3**. The solution was stirred at 298 K for 18h after which the solvent was removed under vacuum, yielding **PL4.3** as a viscous yellow fluid. The porous liquid was then used directly for host-guest experiments and characterization without further purification.

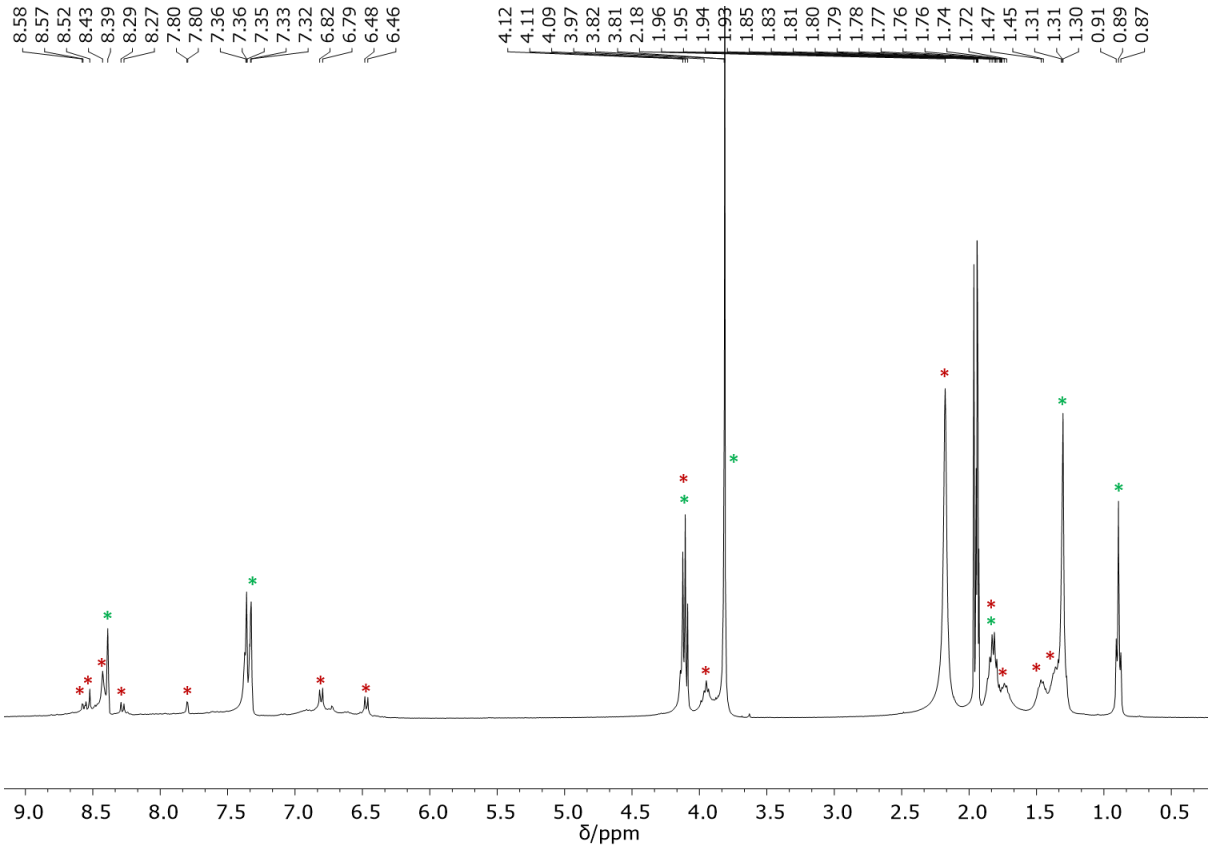

Figure 4.21: ^{1}H NMR (400 MHz, CD_3CN) spectrum of **PL4.3**.

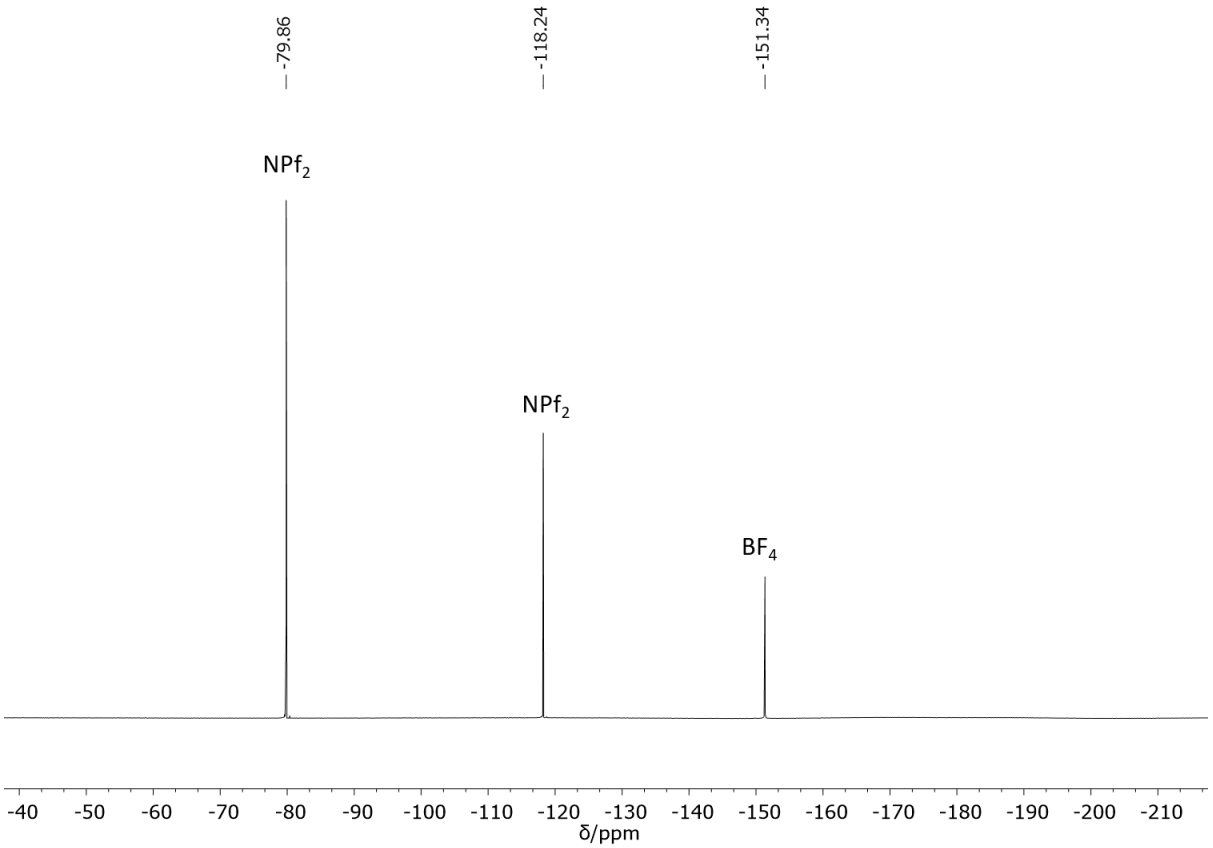

Figure 4.22: ^{19}F NMR (377 MHz, CD_3CN) spectrum of cage **PL4.3**.

4.8.4 PL4.3 interactions with aromatic guests

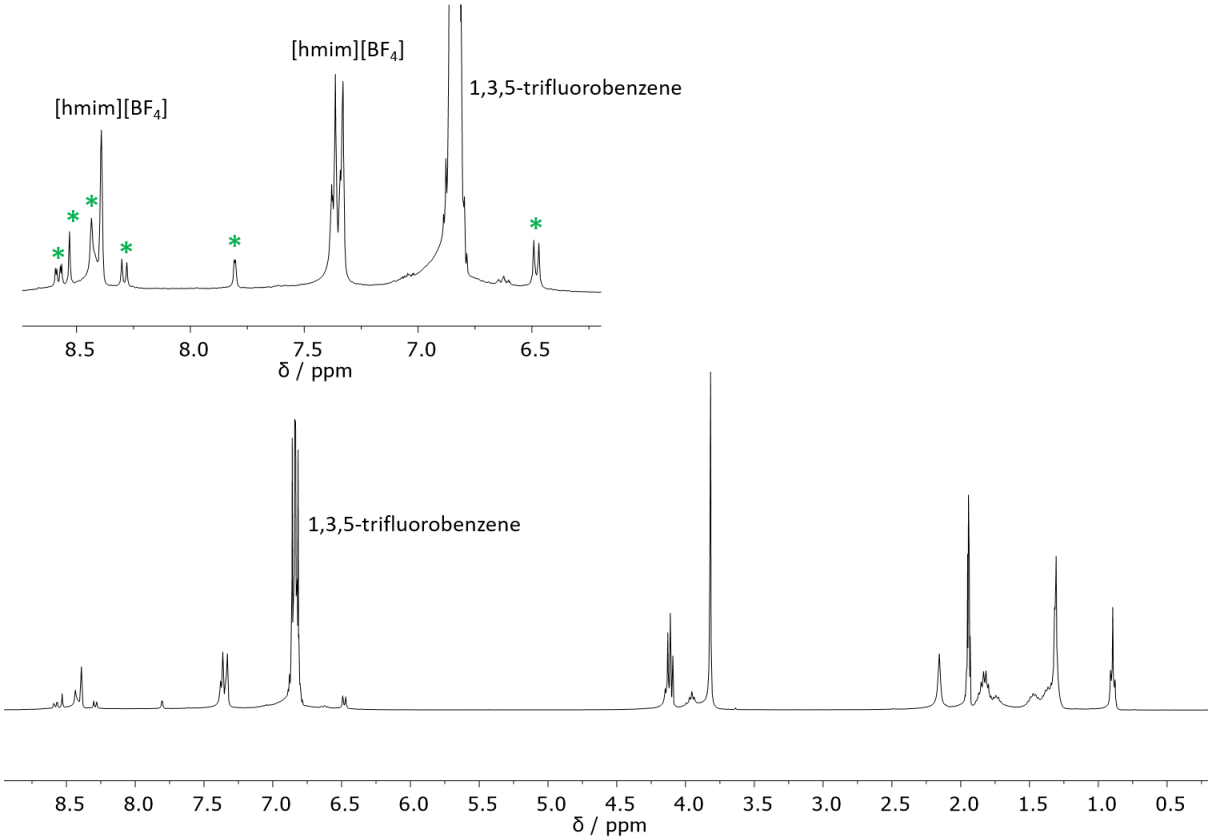

Figure 4.23: ^{1}H NMR (400 MHz, CD_3CN) spectrum of **PL4.3** with 1,3,5-trifluorobenzene. Peaks of cage **4.3** are indicated with green asterisks (*).

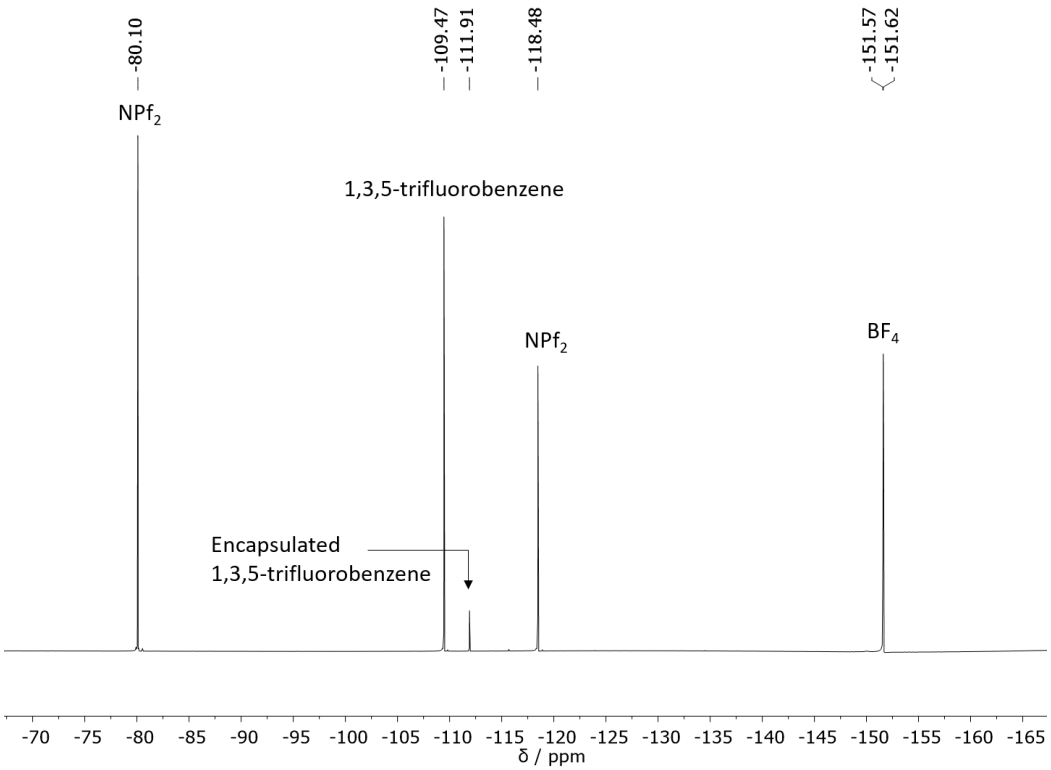

Figure 4.24: ^{19}F NMR (377 MHz, CD_3CN) spectrum of **PL4.3** with 1,3,5-trifluorobenzene.

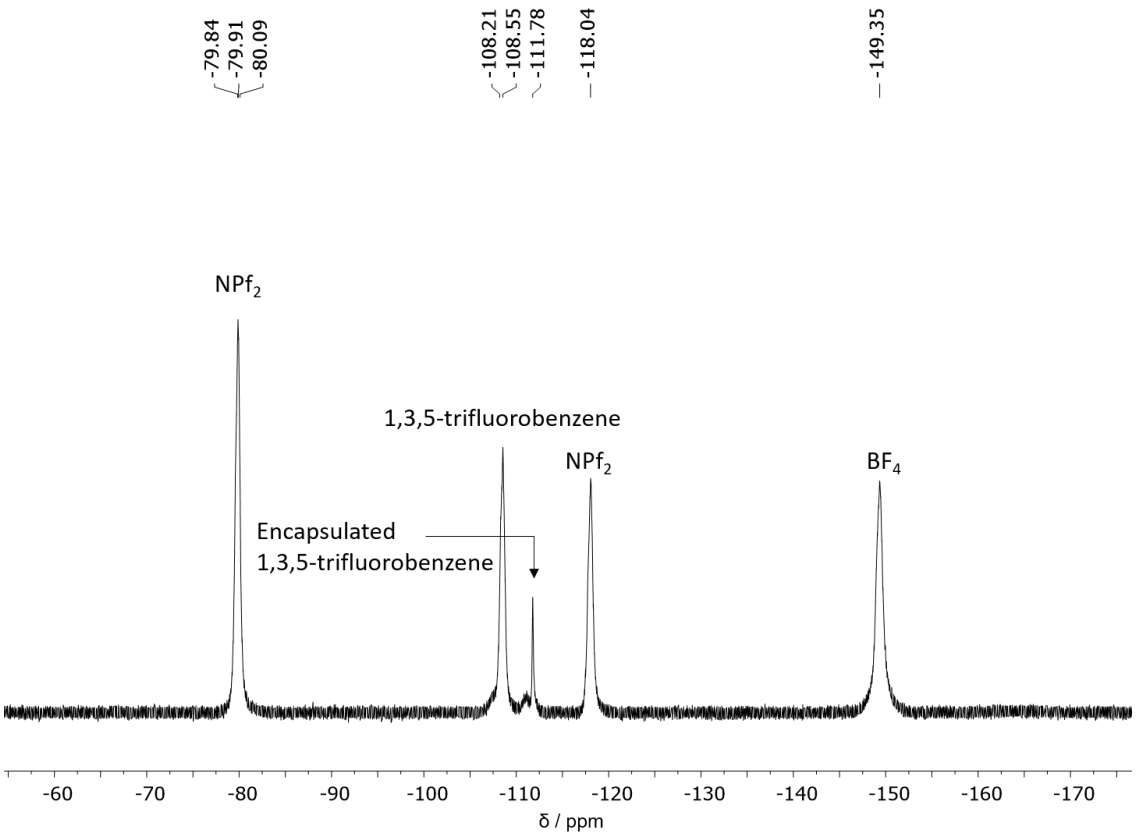

Figure 4.25: VT- ^{19}F NMR (377 MHz, 343, K) spectrum of neat **PL4.3** with 1,3,5-trifluorobenzene.

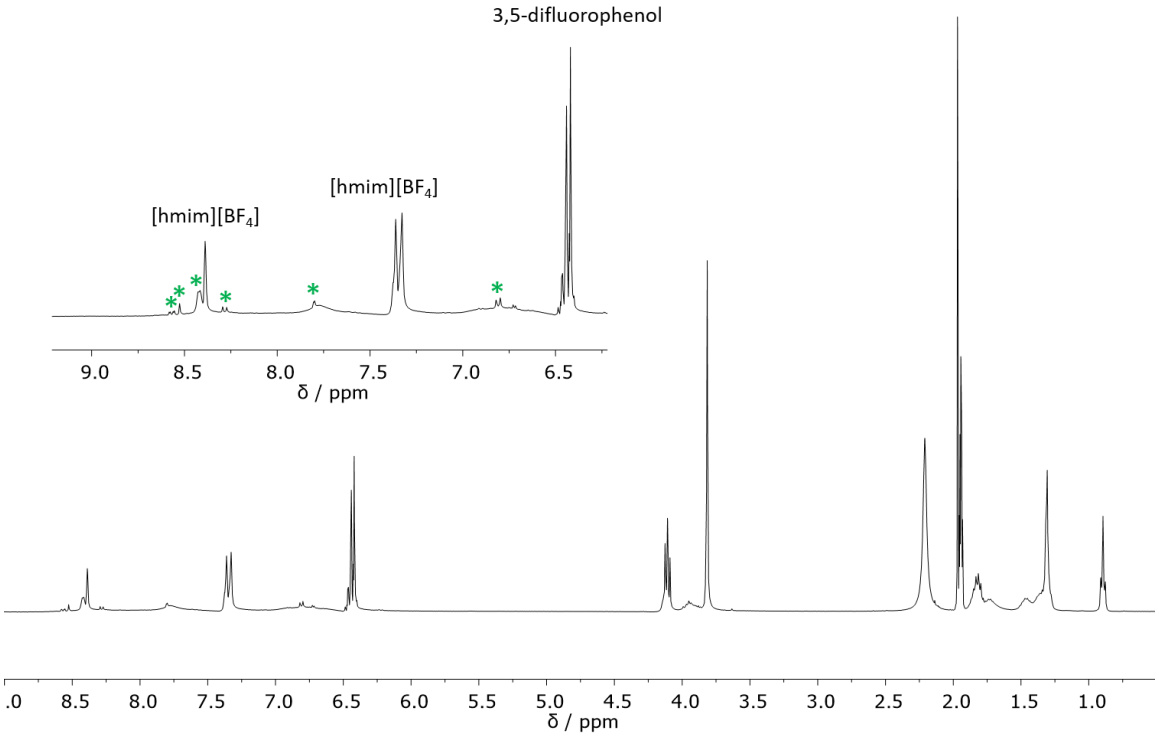

Figure 4.26: ^{1}H NMR (400 MHz, CD_3CN) spectrum of **PL4.3** with 3,5-difluorophenol. Peaks of cage **4.3** are indicated with green asterisks (*). Includes blow-section of the aromatic region.

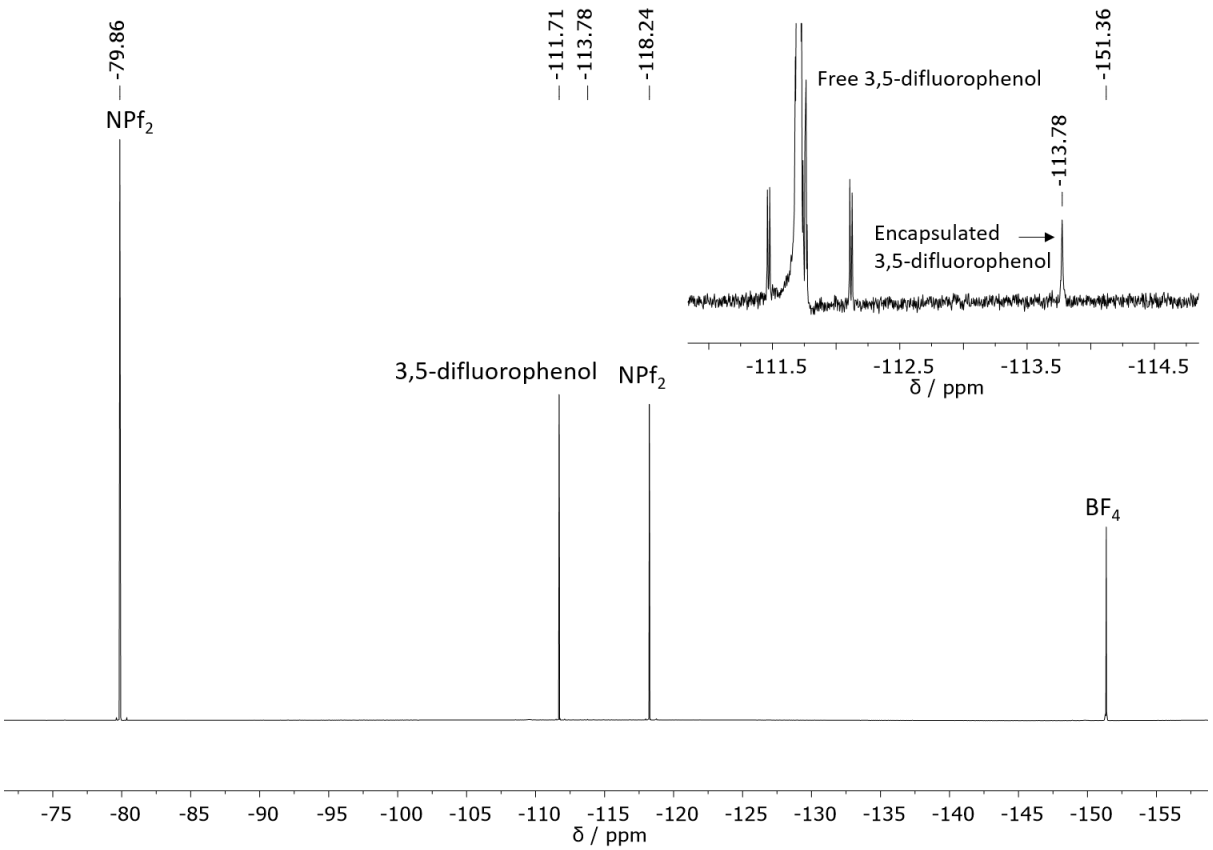

Figure 4.27: ^{19}F NMR (377 MHz, CD_3CN) spectrum of **PL4.3** with 3,5-difluorophenol. Includes blow-section of the encapsulated guest.

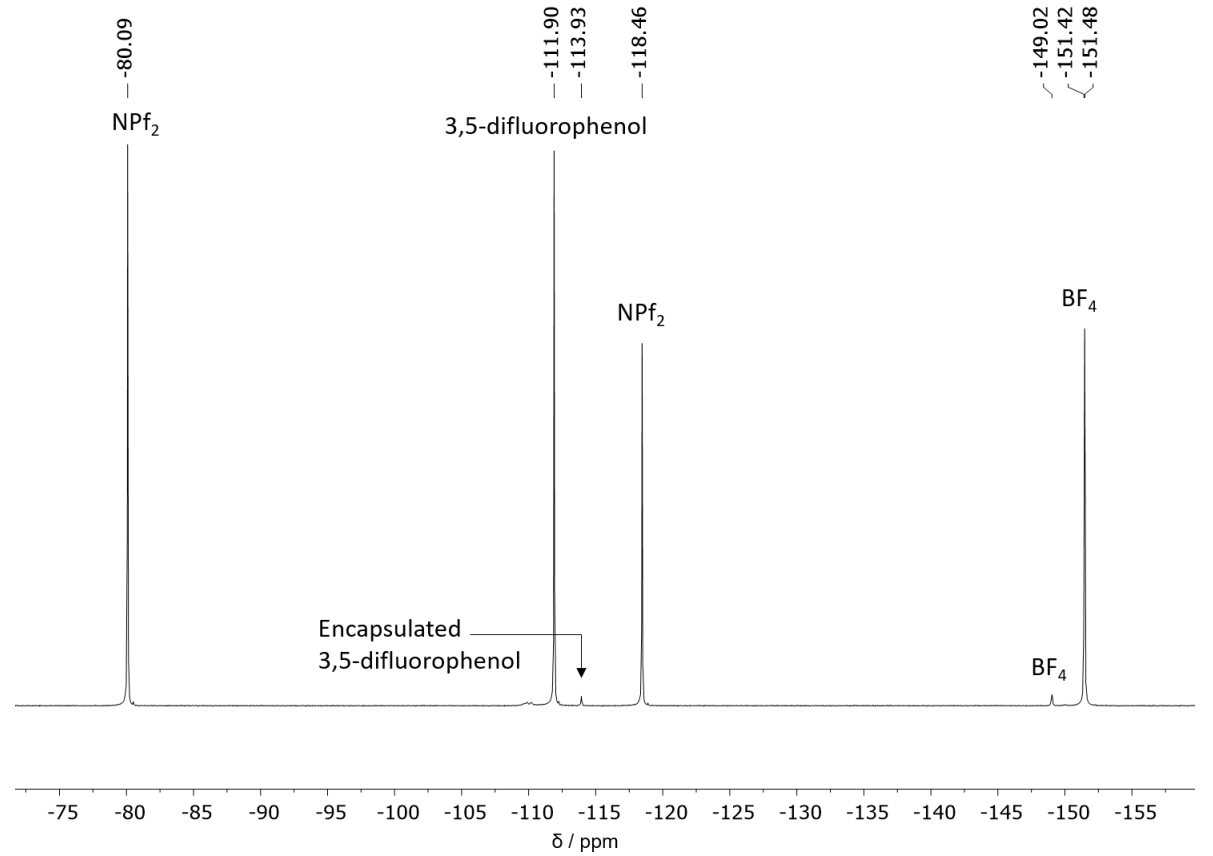

Figure 4.28: VT-^{19}F NMR (377 MHz, 343 K) spectrum of neat **PL4.3** with 3,5-difluorophenol.

4.9 References

(1) Bilbeisi, R. A.; Clegg, J. K.; Elgrishi, N.; Hatten, X. De; Devillard, M.; Breiner, B.; Mal, P.; Nitschke, J. R. *J. Am. Chem. Soc.* **2012**, *134* (11), 5110–5119.

(2) Giri, N.; Del Pópolo, M. G.; Melaugh, G.; Greenaway, R. L.; Rätzke, K.; Koschine, T.; Pison, L.; Gomes, M. F. C.; Cooper, A. I.; James, S. L. *Nature* **2015**, *527* (7577), 216–220.

(3) Grommet, A. B.; Bolliger, J. L.; Browne, C.; Nitschke, J. R. *Angew. Chemie - Int. Ed.* **2015**, *54* (50), 15100–15104.

(4) Castilla, A. *Unpublished*.

(5) Kleywegt, G. J.; Alwyn Jones, T. *Acta Crystallogr. Sect. D Biol. Crystallogr.* **1994**, *50* (2), 178–185.

(6) Łachwa, J.; Bento, I.; Duarte, M. T.; Lopes, J. N. C.; Rebelo, L. P. N. *Chem. Commun.* **2006**, (23), 2445–2447.

CHAPTER 5

PEG-Imidazolium-Functionalized Cages as Type I Porous Liquids

5.1 Introduction

The research presented in Chapter 4 of this thesis showed that functionalizing cages with alkylimidazolium chains significantly lowered the melting temperatures of the resulting capsules. However, none of these cages were liquid at room temperature. Sheng Dai was previously successful in synthesizing a Type I porous liquid by functionalizing the surface of a hollow silica sphere with a positively charged organosilane corona that was charge-balanced with a negative PEG-tailed sulfonate canopy.[1] Dai later extended this method to porous carbons.[2] While both of these porous liquids were functionalized with long alkyl chains in addition to PEG_{1000} chains, it is evident that the PEG_{1000}-based anions played an important role in depressing the melting points of both the silica spheres as well as the porous nanocarbons. Therefore, we hypothesized that using PEG_{1000} moieties in place of the hexyl chain in ligand **4E** would be more effective at depressing the melting point of the system. PEG_{1000} consists of a mixture of polyethylene glycol chains with an overall molecular weight averaging at 1000 g/mol. This assortment of different length chains could further hinder the stacking of cages under solvent-free conditions, leading to a lower melting point of the system.

Therefore, we hypothesized that cages self-assembled from PEG_{1000}-imidazolium-functionalized anilines would be liquid at room temperature. The imidazolium group previously featured in Chapters 3 and 4 would still be appended to the terminal of the PEG_{1000} chain to prevent the long PEG tails from penetrating and occupying the cage cavity. The resulting empty liquid coordination cage would then qualify as a Type I permanently porous liquid. Additionally, this new aniline could be combined with other aldehyde subcomponents to yield a wide range of new liquid cages of different sizes and structures *via* subcomponent self-assembly. The resulting materials could then be characterized by DSC/TGA and rheology to understand their fluid properties, as well as PALS to approximate their porosity. Potential applications of these materials include guest separation and gas sequestration.

5.2 Synthesis of PEG-Imidazolium-Functionalized Anilines

To achieve the goal of an ionic liquid cage, an aniline functionalized by a PEG_{1000} chain terminating in an imidazolium group was designed (Scheme 5.1). Additionally, a shorter equivalent was synthesized with pentaethylene glycol instead of PEG_{1000} (**5F'**). We

hypothesized that the lack of polydispersity in pentaethylene glycol would simplify the characterization of **5F'**. We were also interested in understanding the relationship between the length of the PEG chains and the melting point of the resulting cage. While **5F** and **5F'** can be charge-balanced by a variety of different anions, NTf_2^- was chosen because of its hydrophobic nature, which greatly increased the solubility of the ligand in organic solvents thus making ionic liquids **5F** and **5F'** easier to extract and purify. Studies on ionic liquids also show that ionic liquids containing NTf_2^- are generally less viscous than their counterparts charge-balanced with less fluorous anions.[3] Therefore, we hypothesized that using NTf_2^- anions in our system would also result in a less viscous ionic liquid cage.

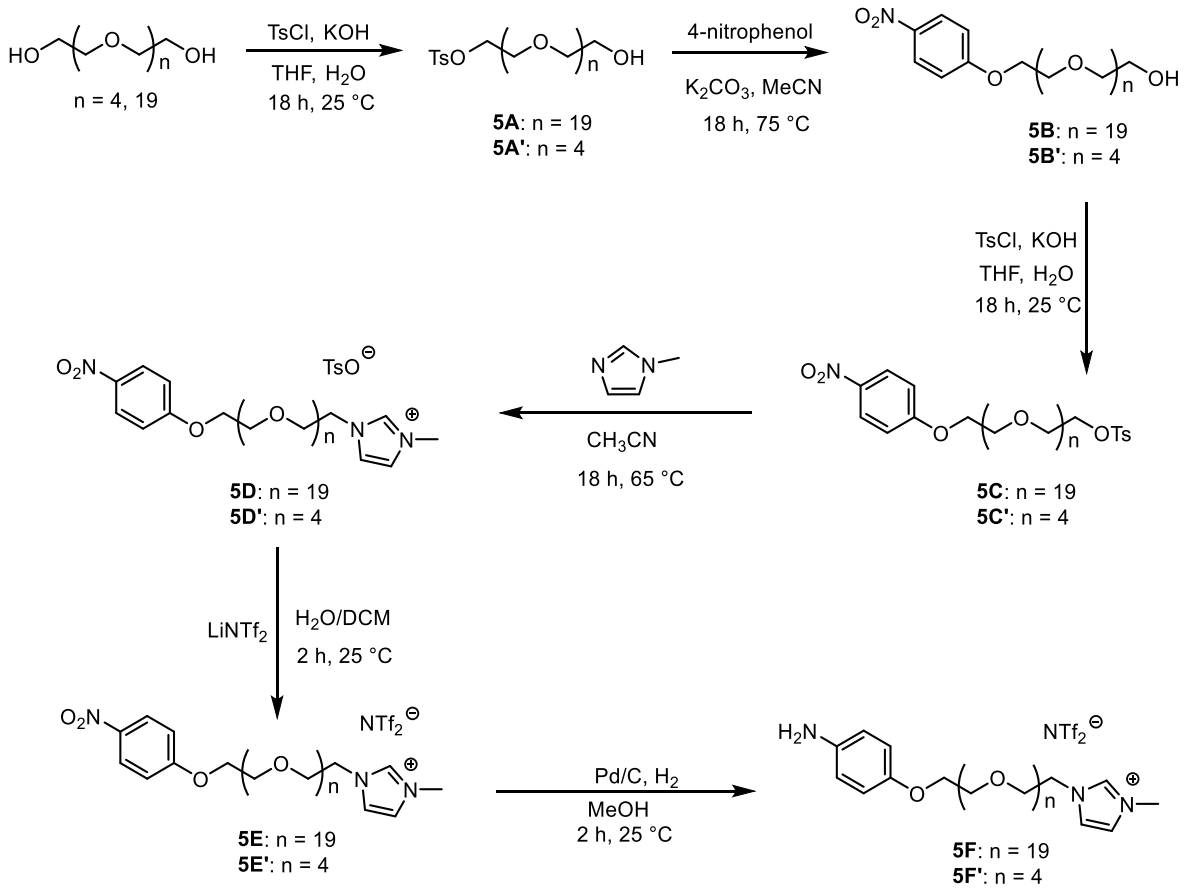

Scheme 5.1: Synthetic scheme of anilines **5F** and **5F'**.

5.3 Self-assembly of Ionic Liquid Cages

5.3.1 Self-assembly of cages 5.1, 5.2 and 5.3

Anilines **5F** and **5F'** were assembled with a number of C_2 and C_3 symmetric aldehyde ligands previously known to form singular discrete coordination cages. Ligand **5H** was chosen

because it self-assembles into a discrete face-capped tetrahedron due to its rigid molecular structure.[4] When synthesized in the presence of NTf_2^-, the cavity of the tetrahedron remains empty because the anion is too sterically hindered to occupy the cage cavities. Since Type I permanently porous liquids are comprised of rigid hosts with empty cavities, the empty liquid tetrahedral cage assembled from trialdehyde **5H** could qualify as a porous liquid.

Trialdehyde **5H** was synthesized and assembled with *p*-toluidine and $Zn(NTf_2)_2$ to form tetrahedral coordination cage **5.1** *via* a previously published procedure.[4] Trialdehyde **5H** was then assembled with $Zn(NTf_2)_2$ and aniline **5F** and heated in a microwave reactor for 10 minutes at 100 °C, resulting in highly viscous liquid cage **5.2** (Scheme 5.2). The same conditions were used to assemble **5H** with aniline **5F'** and the resulting cage **5.3** was a glass-like solid at room temperature. More details on the synthesis of these cages can be found in the experimental section of this chapter (Section 5.11.2).

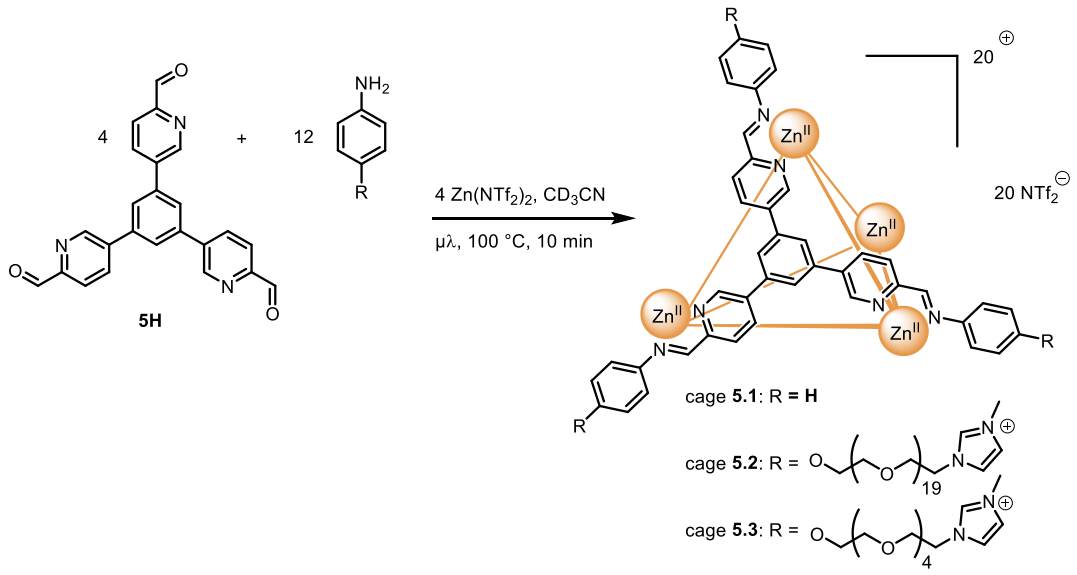

Scheme 5.2: Self-assembly of cages **5.1**, **5.2**, and **5.3.** Cage **5.1** was assembled *p*-toluidine. Cage **5.2** was assembled with the PEG_{1000}-imidazolium aniline **5F** and cage **5.3** was assembled with the shorter pentaethylene glycol-imidazolium aniline **5F'**.

Molecular modelling was used to visualize cages **5.2** and **5.3** (Figure 5.1). Molecular models (MM2 and MM3 force fields) of cages **5.2** and **5.3** were prepared using SCIGRESS version FJ 2.6 (EU 3.1.9) Build 5996.8255.20141202. These models were based on the X-ray crystal structure of cage **5.1.**[4] The model of cage **5.2** showed that the PEG_{1000} chains were considerably longer than those present in cage **5.3**. We hypothesized that the combination of

polydispersity and the increased length of PEG_{1000} resulted in cage **5.2** behaving as a liquid at room temperature while cage **5.3** remained a solid.

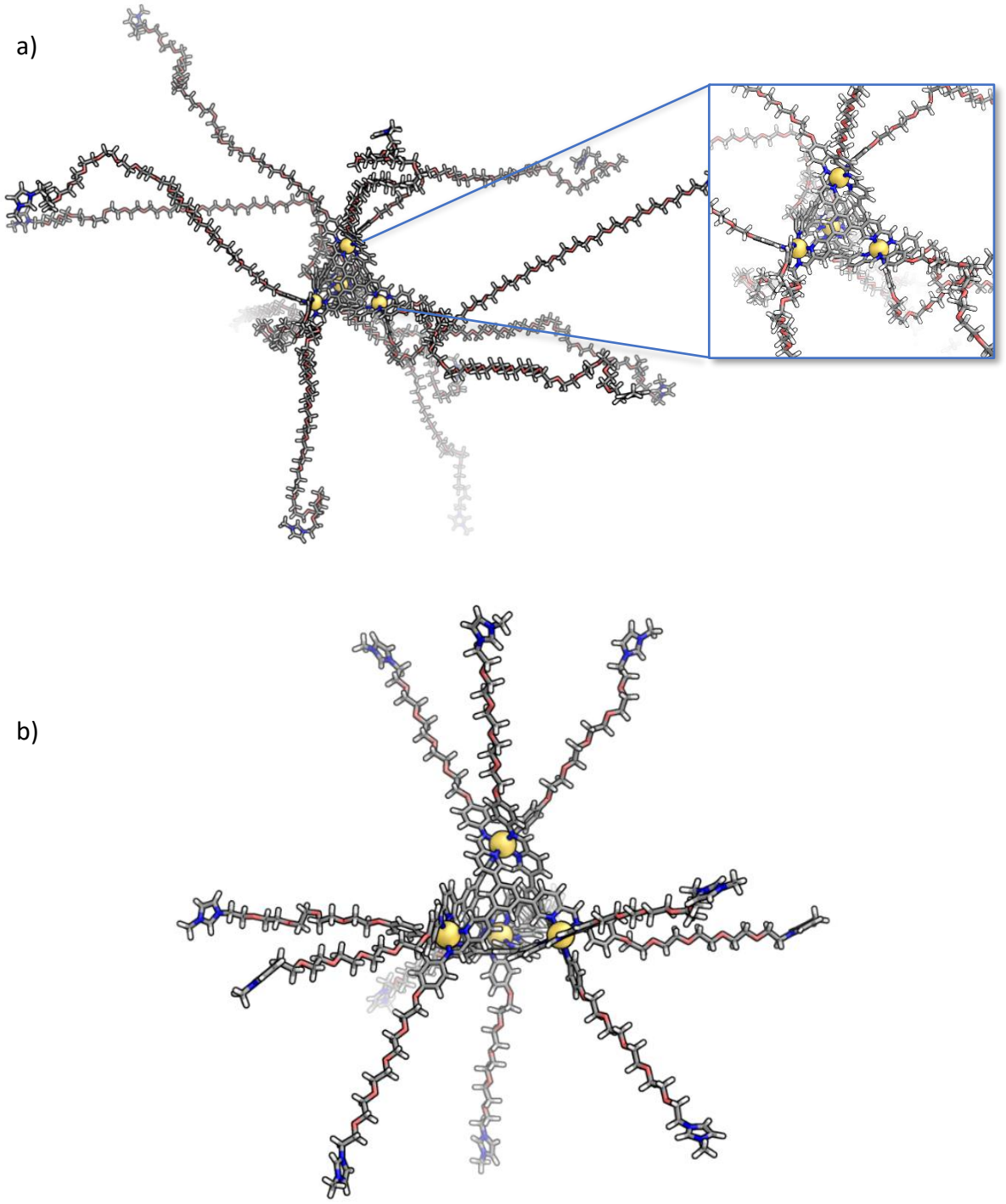

Figure 5.1: a) Molecular model of cage **5.2** created with SCIGRESS. Includes blow-up section of the cage scaffold. b) Molecular model of cage **5.3** created with SCIGRESS.

Cages **5.1**, **5.2** and **5.3** were all characterized by ^{1}H and ^{19}F NMR spectroscopy in CD_3CN. The ^{1}H NMR signals for cage **5.1** matched previously reported values.[4] Similarly, the ^{1}H NMR signals in the aromatic region for cages **5.2** and **5.3** were fairly consistent with the signals of cage **5.1** due to the analogous scaffold of the three cages (Figure 5.2). Small discrepancies in chemical shifts were observed for the three spectra, but these differences were attributed to the PEG functional groups on cages **5.2** and **5.3**. For example, the aniline peak in the ^{1}H NMR spectrum of cage **5.1** manifesting at ~6.4 ppm is shifted further downfield in the spectra for cage **5.2** and **5.3** (~6.8 ppm) due to the electron-donating effects from the PEG chains. The presence of only one set of aromatic signals in all three spectra suggested that no guests were encapsulated in the cages in slow exchange on the NMR chemical shift timescale. Additionally, a single unencapsulated NTf_2^- peak was present in the ^{19}F NMR spectra of **5.1**, **5.2**, and **5.3**, further indicating that the pores of the cages remained unoccupied.

To determine whether cage **5.2** remained intact in the neat state, the liquid cage was characterized *via* ^{1}H and F^{19} NMR spectroscopy under solvent-free conditions. Cage **5.2** was scraped into the opening a 3 mm NMR tube (Scheme 5.3). However, due to the high viscosity of the cage, the sample remained at the top of the NMR tube. The NMR tube was deposited in a centrifuge tube (15 mL) containing a plug of cotton wool in the bottom to cushion the NMR

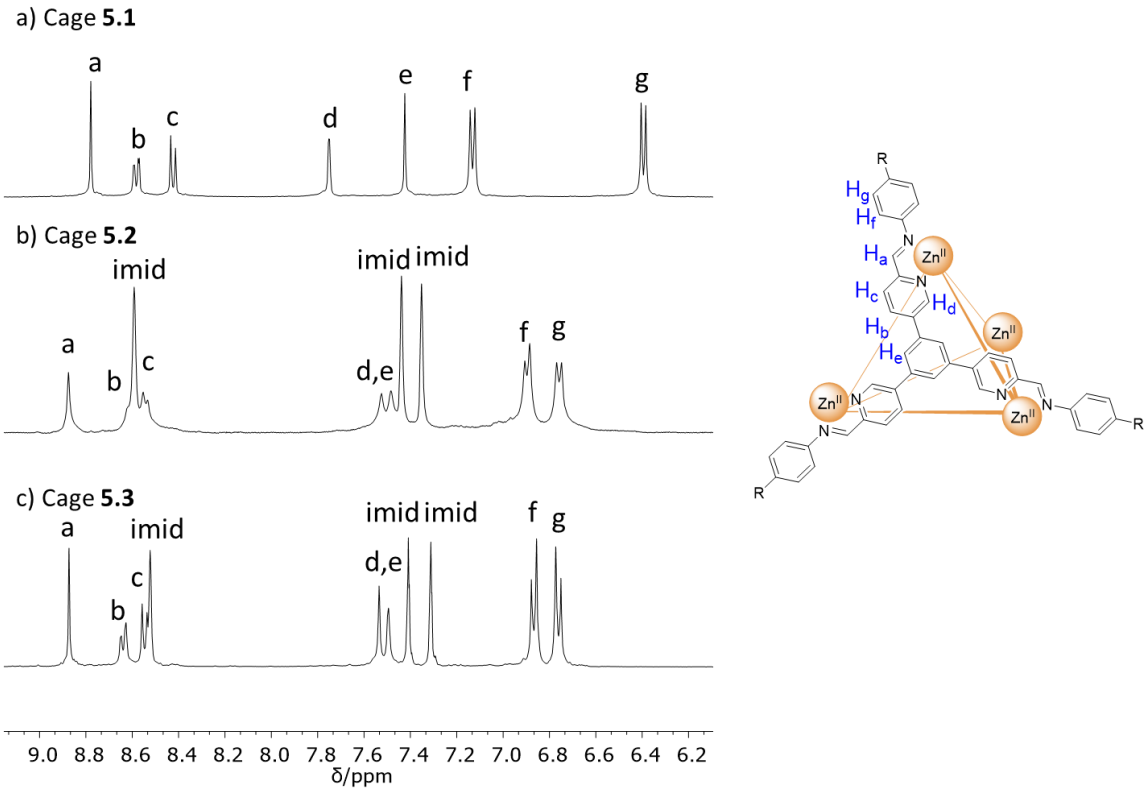

Figure 5.2: Partial ^{1}H NMR (400 MHz, 298 K, CD_3CN) spectra of a) cage **5.1**, b) cage **5.2** and c) cage **5.3**.

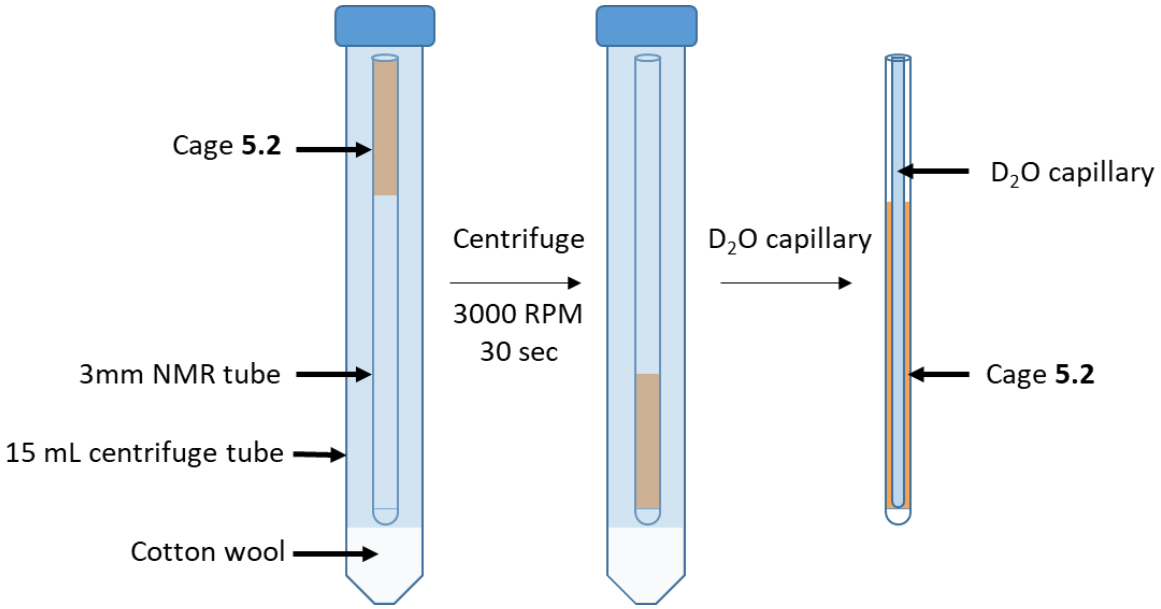

Scheme 5.3: Setup for the preparation of neat NMR of liquid cage samples. The cage was scraped into the top of a 3 mm NMR tube before being centrifuged at 3000 RPM for 5 minutes. A D_2O capillary was inserted to introduce a deuterium signal for locking and to push the material up the sides of the NMR tube.

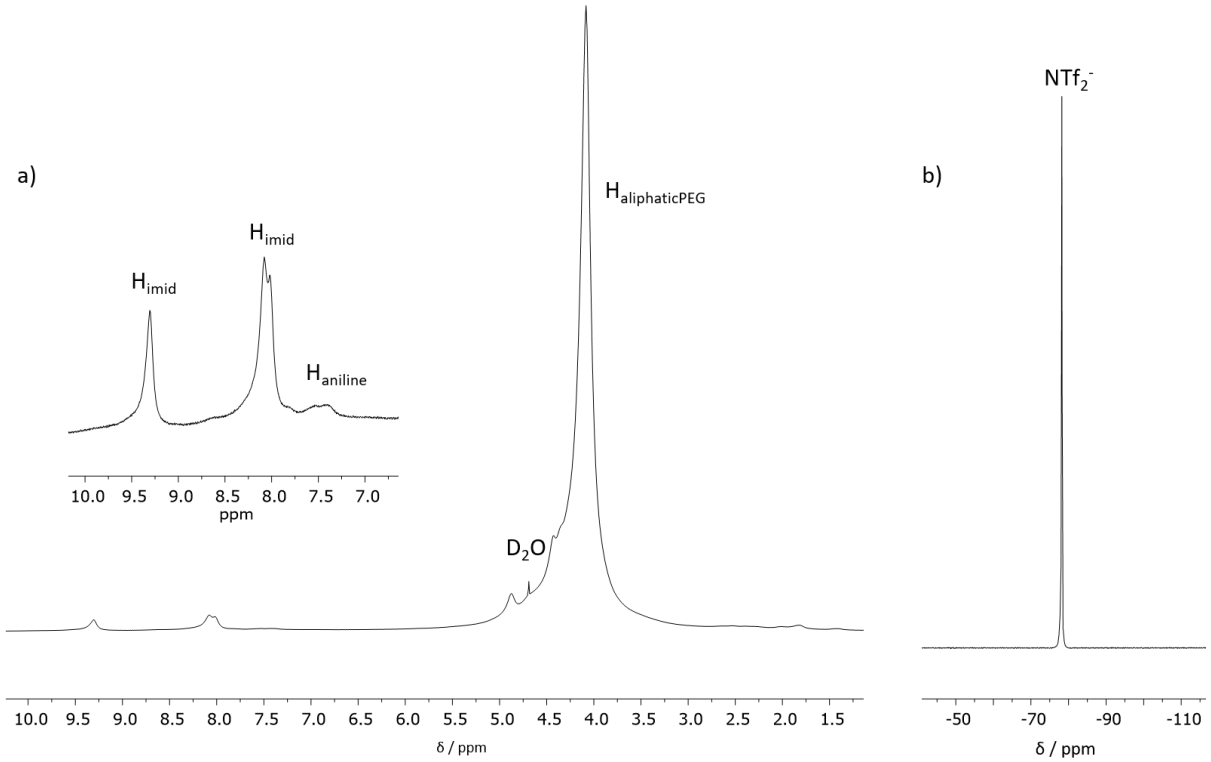

Figure 5.3: a) VT-^{1}H NMR (400 MHz, 343 K) spectrum of cage **5.2** and b) partial VT-^{19}F NMR (377 MHz, 343 K) spectrum of cage **5.2**.

tube. A second centrifuge tube with a cotton wool plug and an empty 3 mm NMR tube was prepared as a counterweight. The sample was centrifuged at 3000 RPM for 5 minutes which resulted in the viscous sample sliding to the bottom of the NMR tube. A D_2O capillary was inserted into the NMR tube to introduce an external deuterated species to the sample for locking, and the addition of the capillary resulted in the cage sample being pushed up the sides of the NMR tube. This sample containing the capillary was then analyzed *via* VT-NMR at 343 K. The increased temperature lowered the viscosity, which increased the tumbling in the sample, resulting in less broad signals.

The neat VT-^{1}H and VT-^{19}F NMR spectra of cage **5.2** at 343 K (Figure 5.3) were broad but consistent with the results obtained in CD_3CN solution, although only the aniline peaks of the cage could be observed in the aromatic region due to the broadness of the signals. Conversely, the imidazolium and PEG peaks were clearly observable. The VT-^{19}F NMR spectrum of cage **5.2** contained a single signal consistent with free NTf_2^-. No other fluorine signals were observed, which we attributed to the lack of encapsulated anions.

One unexpected observation of the self-assemblies of cages **5.1-5.3** was that they could not be reproducibly and consistently assembled. While the self-assemblies occasionally yielded a single discrete structure, oftentimes the ^{1}H NMR spectrum showed two sets of aromatic peaks (Figure 5.4). The major species was consistent with the spectrum of the empty cage, but the minor species appeared to be consistent with the formation of a host-guest complex. No encapsulated guest was observed by ^{19}F NMR, and no guests were deliberately introduced to these self-assemblies. The unknown guest could not be removed from the cage by washing the neat cage with diethyl ether or exposing the cage to vacuum.

A series of control experiments were performed where cage **5.2** was assembled from different sources of trialdehyde **5H**, aniline **5F** and $Zn(NTf_2)_2$ to determine whether any of the subcomponents were inadvertently introducing an impurity that could bind within the cavity. All samples of cage **5.2** generated from these control experiments contained both free cage and the unknown host-guest complex. Interestingly, free cage **5.2** could be selectively synthesized after the source of CD_3CN was changed. Initially, CD_3CN was purchased from Sigma-Aldrich and all samples of **5.2** analyzed in CD_3CN from this supplier showed both free cage and unknown host-guest complex. Yet, when cage **5.2** was analyzed in CD_3CN purchased from Fluorochem, only empty cage **5.2** was observed by ^{1}H NMR. Therefore, we concluded that the CD_3CN from Sigma-Aldrich contained an impurity that was being encapsulated when exposed

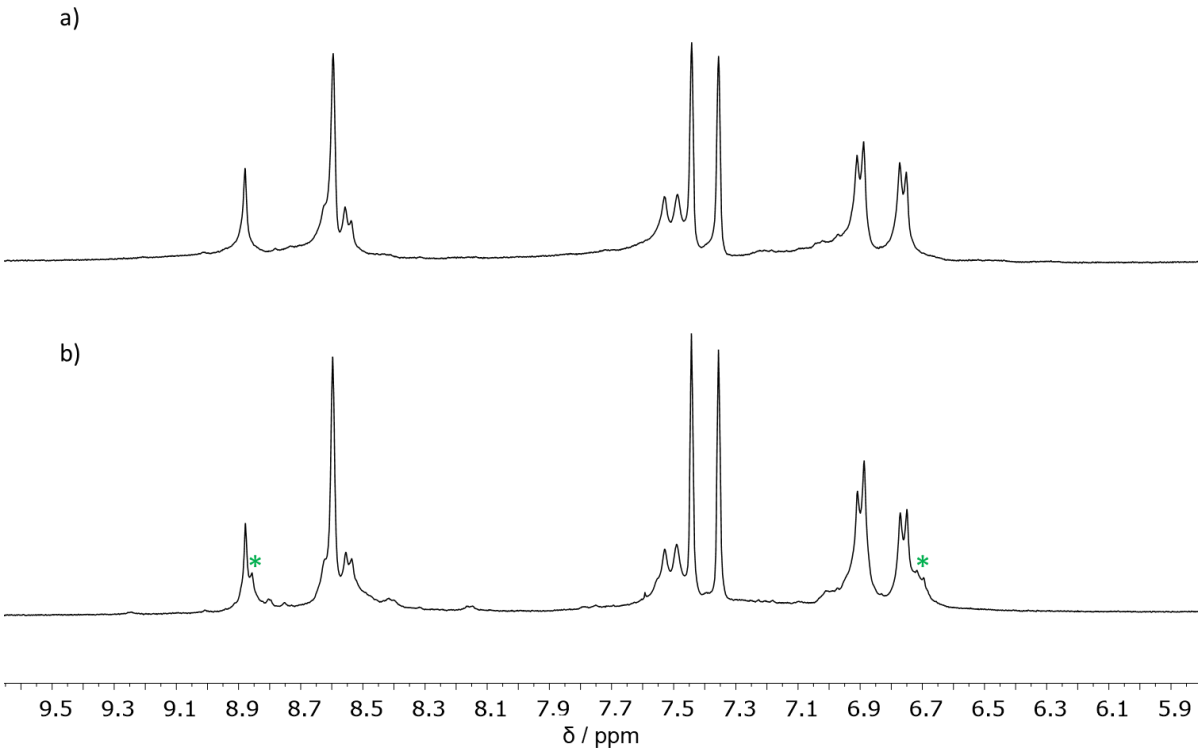

Figure 5.4: Partial ^{1}H NMR (400 MHz, 298 K, CD_3CN) spectra of cage **5.2**. a) Cage **5.2** dissolved in CD_3CN from Fluorochem. b) The same sample of cage **5.2** dissolved in CD_3CN from Sigma Aldrich. Signals arising from the unknown host-guest complex are labelled with green asterisks (*).

to cage **5.2**. While the identity of the impurity remains unknown, we hypothesize that the guest is anionic because it was unobservable by both ^{1}H and ^{19}F NMR. Cage **5.1** is also known to strongly bind anions.[4] Therefore, cages **5.1**, **5.2** and **5.3** should not be characterized in CD_3CN purchased from Sigma-Aldrich.

After finalizing the synthetic method, cages **5.1, 5.2** and **5.3** were then analyzed by LR-ESI-MS. Cage **5.1** exhibited a charge distribution consistent with literature values.[4] Cage **5.2** was not stable under the conditions for ESI-MS and therefore could not be characterized by this technique. However, LR-ESI-MS was successfully conducted on cage **5.3** (Figure 5.5), and the charge distribution was consistent with the proposed $Zn^{II}_4L_4$ stoichiometry – a result that was then confirmed by HR-ESI-MS (Figure 5.6). Due to the consistencies between the ^{1}H NMR spectra of cages **5.2** and **5.3**, we concluded that both cages shared the same stoichiometry.

While these characterization techniques confirmed the successful formation of discrete capsules **5.2** and **5.3**, they did not shed light on the material properties of these two cages. Although cage **5.2** seemed to exhibit fluid-like behavior at room temperature, the precise nature

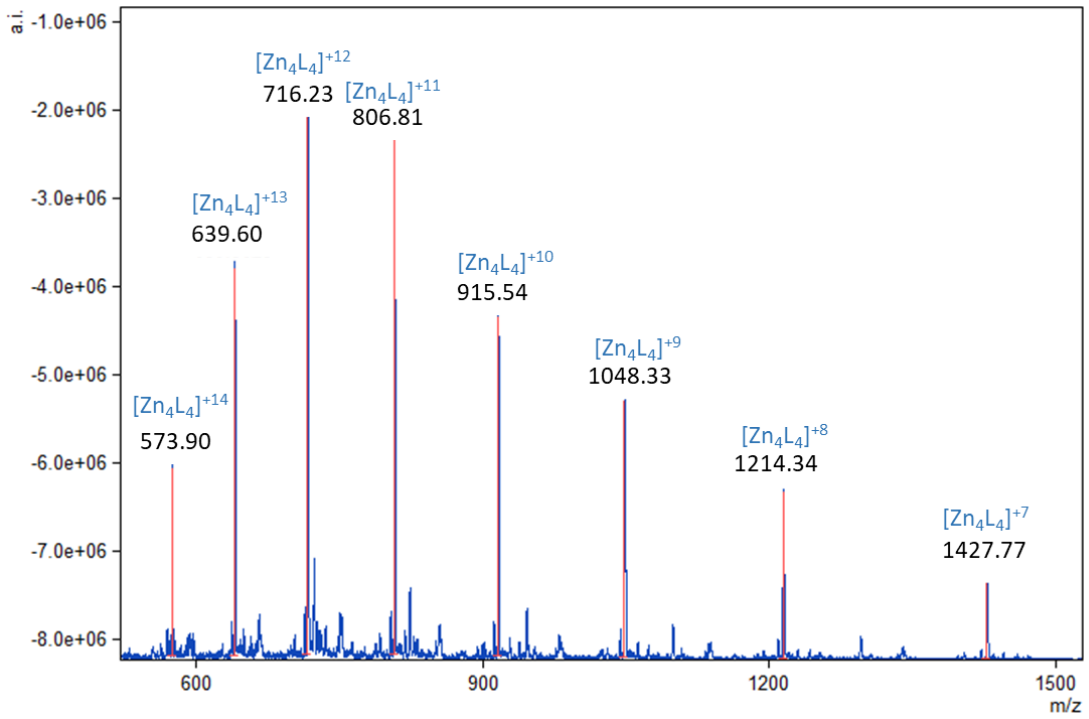

Figure 5.5: LR-ESI-MS of cage **5.3**. Charge distribution consistent with proposed structure.

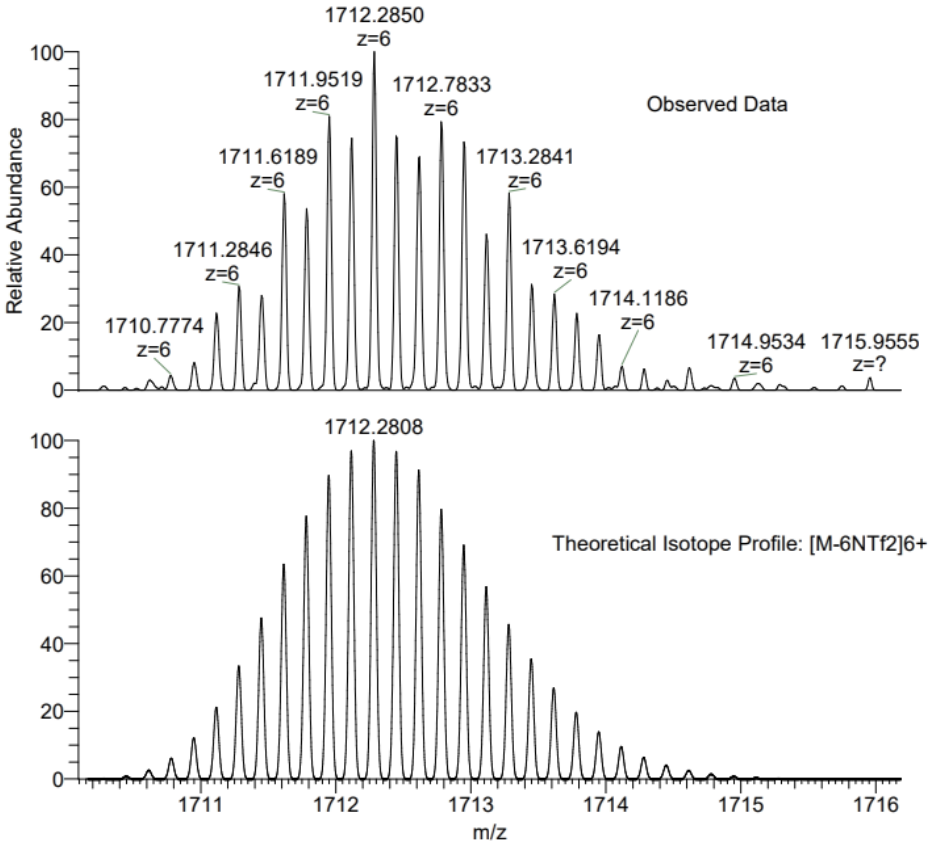

Figure 5.6: HR-ESI-MS of cage **5.3**. Top: observed isotope pattern for $[Zn_4L_4]^{6+}$; bottom: theoretical isotope pattern for $[Zn_4L_4]^{6+}$. The experimental results were consistent with the theoretical calculations.

of its liquid properties needed further investigation. Following the molecular scale characterization of the cages in solution and the gas phase, an analysis of the material properties of these cages in the solvent-free state was undertaken. The results of these experiments are shown in Sections 5.6 and 5.7. Additional experiments to confirm that the pores of these cages remained empty in the neat state are described in Section 5.4 and 5.5.

5.3.2 Self-assembly of other liquid cages

To investigate the scope of different cage assemblies that could be rendered liquid using this strategy, we also investigated the assembly of anilines **5F** and **5F'** with a variety of other aldehyde subcomponents. We were interested in whether the PEG-imidazolium-functionalized anilines could yield other liquid cages with different architectures and stoichiometries. Therefore, we chose aldehydes **4A**, **5I** and **5J** (Scheme 5.4). Results from Chapter 4 indicate that aldehyde **4A** could be self-assembled into a face-capped tetrahedral cage with alkylimidazolium anilines and iron salts; therefore, we were interested in determining whether **4A** could yield a similar cage with anilines **5F** and **5F'**. On the other hand, all imidazolium-functionalized cages to date have been based on face-capped tetrahedra. As a result, we chose aldehydes **5I** and **5J** because previous research demonstrated that these two subcomponents can self-assemble into an edge-bridged $Fe^{II}_8L_{12}$ cubic cage and an edge-bridged $Fe^{II}_4L_6$ tetrahedral cage, respectively.[5,6] The synthetic method used to assemble cages **5.2** and **5.3** was used to successfully generate cages **5.4-5.9** based on aldehydes **4A, 5I** and **5J**. The NMR spectra and MS data obtained from these cages are presented in Section 5.11.2-5. Like cage **5.2**, the new cages assembled with **5F** were not stable under MS conditions. Therefore, only the pentaethylene glycol-functionalized cages characterized with MS.

These experiments indicated that aniline **5F** could be used to generate a wide range of liquid cages *via* subcomponent self-assembly. Moving forward, we chose to focus on cage **5.2** instead of investigating every single liquid cage. Cage **5.2** was chosen because cage **5.1** is known to encapsulate a range of anionic and neutral guests.[4] In contrast, the known host-guest properties of the unfunctionalized versions of cages **5.4-5.9** are limited to very few anions and neutral molecules.[5,6] Therefore, to better understand guest uptake in neat cages under solvent-free conditions, we chose the cage scaffold known to bind the largest variety of guests. Nevertheless, we would be interested in investigating the material properties and host-guest behaviors of liquid cages **5.4**, **5.6** and **5.8** in the future.

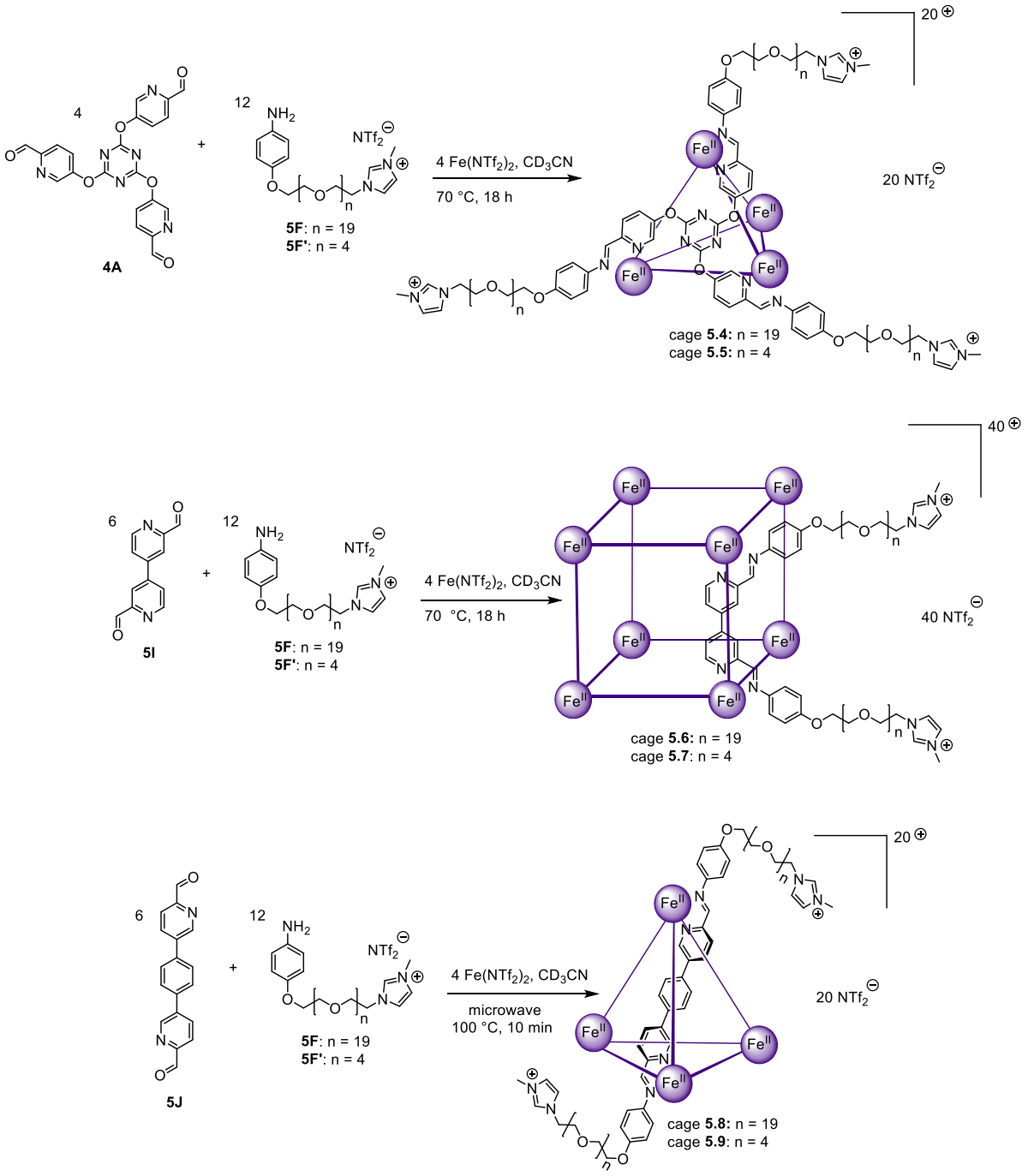

Scheme 5.4: Self-assembly of cages **5.4-5.9** based on aldehydes **4A**, **5I** and **5J**.

5.4 NMR Analysis of Cage 5.2

One of the main challenges in synthesizing new porous liquids is ensuring that the host cavities remain empty and are not occupied inter- or intramolecularly. In the case of liquid coordination cages, the cage cavities could potentially be filled with solvent molecules that the

cage is exposed to during self-assembly in solution. Therefore, to investigate whether the pores of cage **5.2** were occupied by CH_3CN, we conducted a series of NMR control experiments. Based on known cases of neutral guest binding by cage **5.1**, where binding occurs in slow exchange on the NMR chemical shift timescale and peaks for encapsulated guests appear below 0 ppm in the ^1H NMR spectrum, we hypothesized that if an encapsulated CH_3CN signal was present, it would appear upfield of 0 ppm. Therefore, we prepared a solution of cage **5.2** in non-deuterated CH_3CN (2 mM) and added an internal CD_3CN reference capillary for locking. The sample was prepared in CH_3CN rather than CD_3CN because ^1H NMR could be used to identify any encapsulated non-deuterated solvent peak. This sample was analyzed by ^1H NMR with a large spectral width spanning 15 to -15 ppm to better observe any potential encapsulated CH_3CN peaks (Figure 5.7). However, no encapsulated solvent peaks were observed, indicating that the cage either did not bind CH_3CN, or that encapsulation was fast on the NMR chemical shift timescale and therefore unobservable.

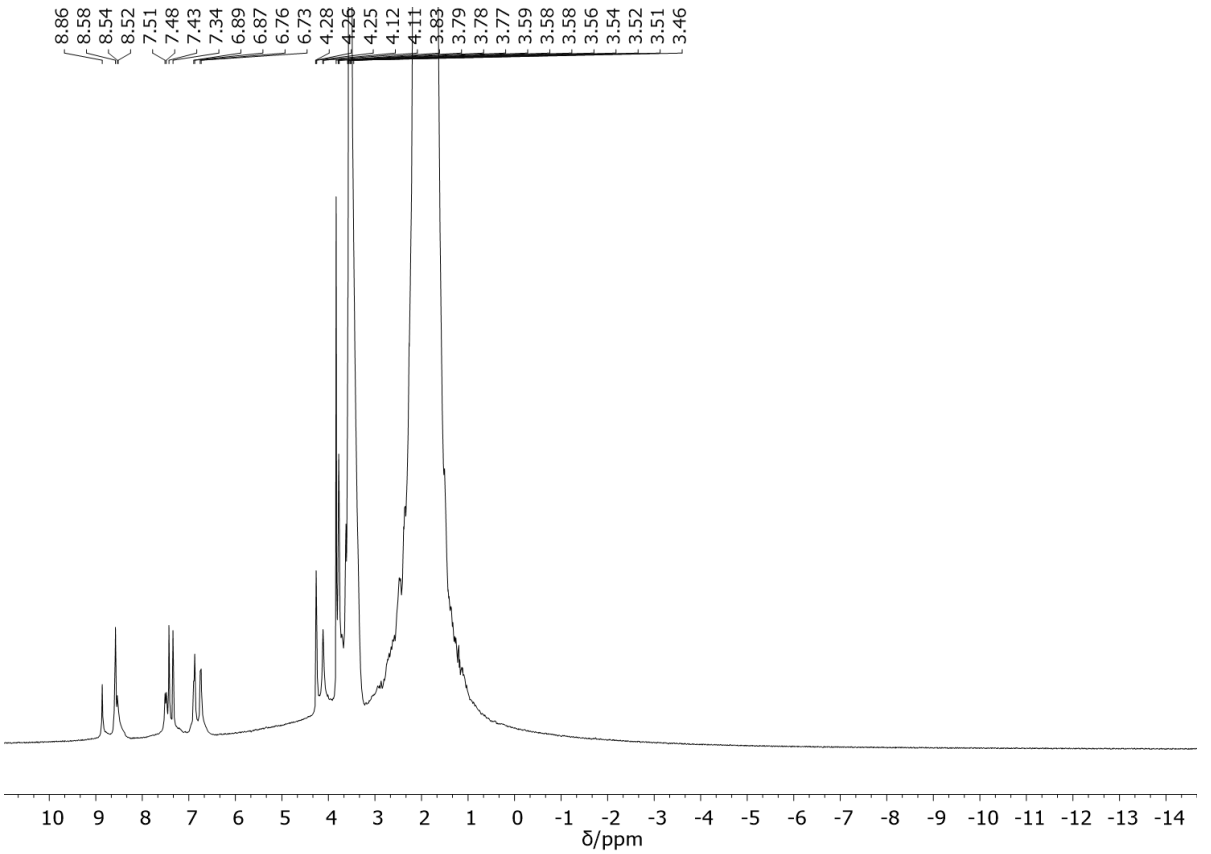

Figure 5.7: ^1H NMR (400 MHz, 298 K, CH_3CN) spectrum of cage **5.2** dissolved in CH_3CN with a CD_3CN reference capillary. No peaks consistent with guest encapsulation were observed upfield of 0 ppm.

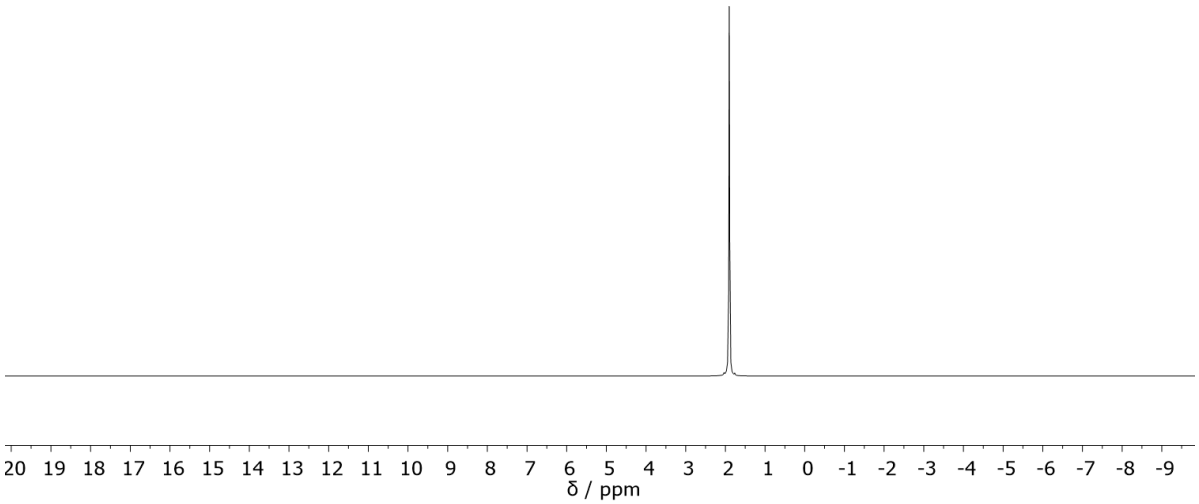

Figure 5.8: ^{2}H NMR (400 MHz, 298 K, CD_3CN) spectrum of cage **5.2** in CD_3CN. No CD_3CN encapsulation was observed.

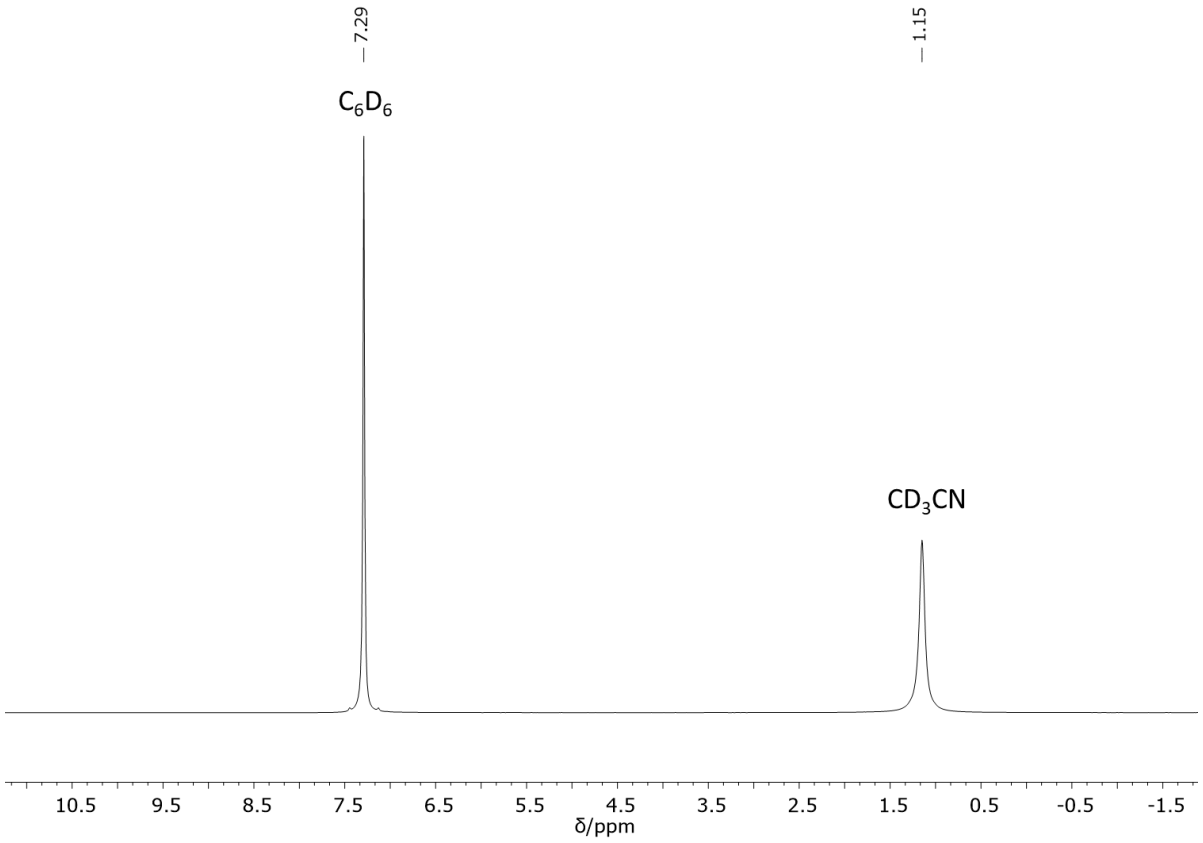

Figure 5.9: VT-^{2}H NMR NMR (400 MHz, 333 K, CD_3CN) spectrum of neat cage **5.2** containing 30 wt% CD_3CN. A reference capillary with 10 wt% C_6D_6 in CH_3CN was added. No guest encapsulation was observed.

Although an encapsulated CH_3CN peak would be expected to appear below 0 ppm, cage **5.2** gives rise to many signals in the ^1H NMR spectrum and an encapsulated solvent peak could be obscured by one of the cage peaks. We therefore undertook analysis of cage **5.2** by ^2H NMR in CD_3CN solution and in the neat state with 30 wt% CD_3CN, to allow for the identification of encapsulated CD_3CN peaks that might overlap with signals from cage **5.2**, as the non-deuterated cage would not produce any ^2H NMR signals. A solution of cage **5.2** (2 mM in CD_3CN) was analyzed by ^2H NMR and no encapsulated CD_3CN peaks were observed in the spectrum (Figure 5.8). This experiment was repeated under solvent-free conditions, in which 30 wt% of CD_3CN was added to 100 mg of cage **5.2** and stirred overnight before being analyzed by neat VT-^2H NMR using the NMR setup described in Section 5.3.1 (Figure 5.9). An external capillary reference containing 10 wt% C_6D_6 in non-deuterated CH_3CN was used. The resulting spectrum did not contain any encapsulated CD_3CN peaks – a result consistent with the observations made in the solution-state. Therefore, we concluded that no potential encapsulated CH_3CN peaks were obscured by the peaks of cage **5.2** in the ^1H NMR spectrum. The combined results from the ^1H and ^2H NMR experiments allow us to infer that CH_3CN is either not encapsulated by cage **5.2**, or that it exchanges rapidly on the NMR chemical shift timescale.

5.5 PALS Analysis of Cage 5.2

One of the key points of engineering intrinsic porosity into liquids is ensuring that the host cavities remain empty in the neat state. In the field of porous liquids, the presence of empty cavities is often demonstrated through molecular simulations and/or positron annihilation lifetime spectroscopy.[1,7,8] Positron annihilation lifetime spectroscopy (PALS) is a technique that can approximate the void sizes of different materials by monitoring the lifetime of *ortho*-positroniums (*o*-Ps), and is commonly used in the field of porous liquids. After synthesizing 1 gram of cage **5.2**, we sent the sample to our collaborator Dr. Cara Doherty who then conducted the PALS experiment and processed the data. The setup and conditions used for these experiments can be found in Section 2.6.

The average lifetime of cage **5.2** was determined to be 2.34 ns, which corresponds to an average diameter of 0.63 nm free space (Figure 5.10). The lifetime of the porous cage had a relatively low intensity value of 2.9% that may be due to *o*-Ps inhibition which is often

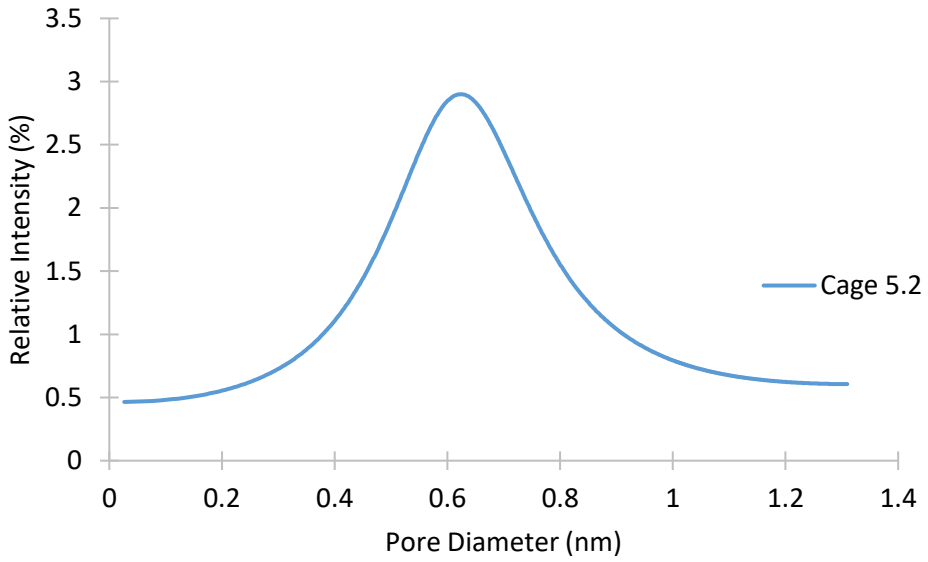

Figure 5.10: The pore size distribution neat cage **5.2**. The PSD was adapted using the PAScual software[9].

seen in materials with functional groups that scavenge the positrons. If this is the case, the lifetimes remain indicative of the average pore size.

Using the crystal structure of previously-published cage **5.1**, a void volume of 130 Å^3 was calculated using VOIDOO.[4] This value corresponds to a sphere of diameter 6.28 Å – a value consistent with the PALS value of 6.29 ± 0.008 Å. This consistency led us to conclude that cage **5.2** was empty under solvent-free conditions. Using the PALS data, we calculated the amount of free space per gram of neat cage **5.2**. The molar mass (*M*) of cage **5.2** was calculated to be 19865.91 g mol^{-1} (assuming an average of 20 -CH_2CH_2O- repeat units per PEG chain, as in our case). **Equation 5.1** was derived from the molar mass of cage **5.2**, Avogradro's constant and the volume of the cage **5.1**. The equation was then used to calculate the number of cages present in a sample of cage **5.2**, with each cage contributing 130 Å^3 of free space (*V*), resulting an estimated 3.94 mm^3 of free space per gram of neat cage **5.2**.

$$V_{total} = \frac{V \times h \times m}{M} \qquad \textbf{Equation 5.1}$$

Equation 5.1. Equation to calculated total free volume (V_{total}) of a sample of liquid cage **5.2** where *V* = volume of cage **5.1** (Å^3), *h* = Avogadro's constant, *m* = mass of cage **5.2** (g) and *M* = molar mass of cage **5.2** (g/mol)."

5.6 Thermal Analysis of Cage 5.2

While cage **5.2** appeared to behave like a fluid at 298 K, we were interested in the phase behavior of the material. We hypothesized that the liquid cage would undergo a glass transition below room temperature because the pentaethylene glycol analogue cage **5.3** appears to be a glass-like solid. Therefore, cage **5.2** was characterized by DSC and TGA (Figure 5.11) under argon. The DSC curve featured a reversible T_g with an onset temperature of -37.6 ± 0.4 °C and -49.5 ± 0.9 °C, implying solidification below this temperature. The onset of the glass transition temperature was defined by the intersection point between the heat flow before the glass transition and the change in heat flow during the glass transition. However, this phase change could not definitively be assigned as glass transition even though the shape of the feature was consistent with that of a glass transition. To confirm the solidification of the cage into a glass, additional characterization would need to be conducted with low-temperature powder X-ray diffraction. The absence of a crystalline diffraction pattern at temperatures below the phase change temperature would indicate the formation of a glass phase. The TGA trace of cage **5.2** showed no significant loss of mass from 25-300 °C, above which decomposition was observed, indicating high thermal stability and that a negligible amount of solvent remained in the neat material. The onset of T_{decomp} was defined as the temperature at which 5 wt% of mass was lost after the plateau immediately prior to decomposition.

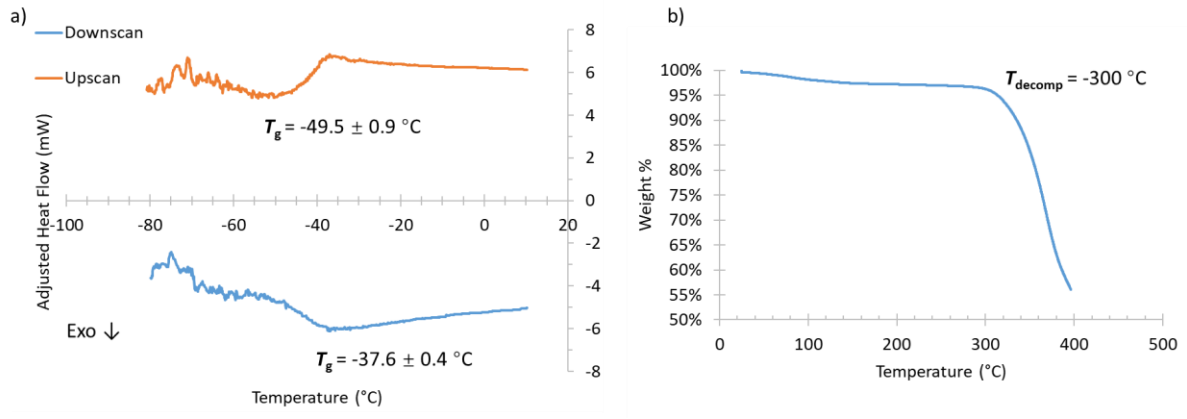

Figure 5.11: a) DSC curve of cage **5.2**. A reversible phase change was present in both the downscan (-38.2 °C) and upscan (-44.5 °C). Cage **5.2** (18.043 mg) was cooled at 10 °C/min to -150 °C then heated at 10 °C/ min to 400 °C. b) TGA curve of cage **5.2**. Neat cage **5.2** (18.578 mg) was heated at 10 °C/min to 400 °C. No significant mass loss was observed until 300 °C when the cage decomposed.

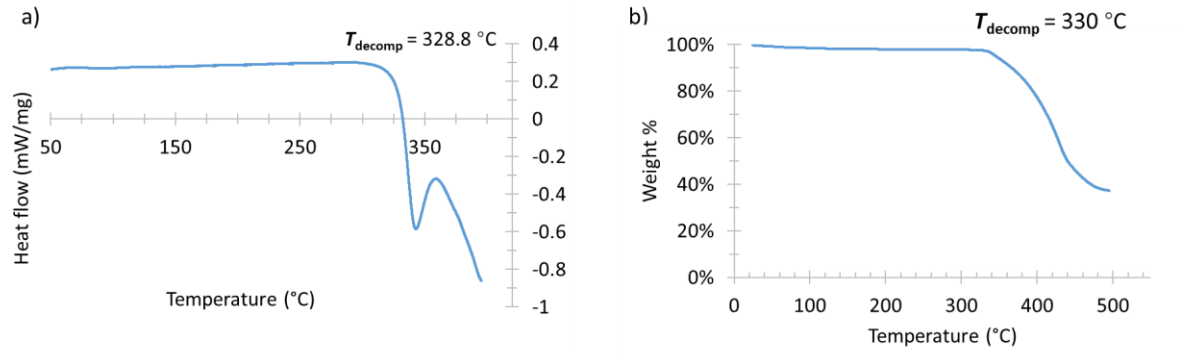

Figure 5.12: a) DSC curve for cage **5.3**. The sample decomposed at 328.8 °C. The sample was heated at 10 °C/min to 400 °C. b) TGA curve of cage **5.3**. Neat cage **5.3** (6.011 mg) was heated at 10 °C/min to 400 °C. No significant mass loss was observed until the cage began to rapidly decompose at 330 °C.

Cage **5.3** was also analyzed *via* DSC and TGA (Figure 5.12). Since cage **5.3** appeared to be a solid at room temperature, low-temperature DSC was not conducted. A sample of **5.3** was heated at 10 °C/min from 25-400 °C. The resulting DSC trace did not contain any significant features other than a clear decomposition point at 328.8 °C. However, an exceptionally broad glass transition could have present but unobservable. Faster heating rates generally increase sensitivity, particularly for thermal events like a glass transition; the experiment could be repeated with a more aggressive heat ramp in order to resolve any broad phase transitions that would be otherwise unobservable. Like cage **5.2**, the TGA trace of **5.3** was also featureless except for a clear decomposition point at 330 °C indicating high thermal stability of the material and an absence of residual solvent.

5.7 Rheology of Cage 5.2

DSC results indicated that cage **5.2** was a liquid at room temperature because it underwent a glass transition below 0 °C. To better understand the fluid properties of this porous liquid, cage **5.2** was analyzed by rheology. These experiments were conducted and processed by Christopher Parkins. An oscillatory-dependent experiment in which the angular frequency was increased from 0.1 to 100 1/s at 1% strain indicated that the G'' (loss modulus) was greater than G' (storage modulus) throughout the measurement – a result consistent with materials exhibiting fluid behavior (Figure 5.13a). The experiment also showed that both G' and G'' were strongly dependent on frequency, with more than 3 orders of magnitude change in G' over the probed frequency range. Furthermore, oscillatory strain measurements over the range of 0.1–

1000% at a fixed angular frequency of 10 rad/s (Figure 5.13b) demonstrated that at above 100% strain, the G´ value dramatically decreased but the material continued to exhibit fluid-like behavior where G´´ was greater than G´.

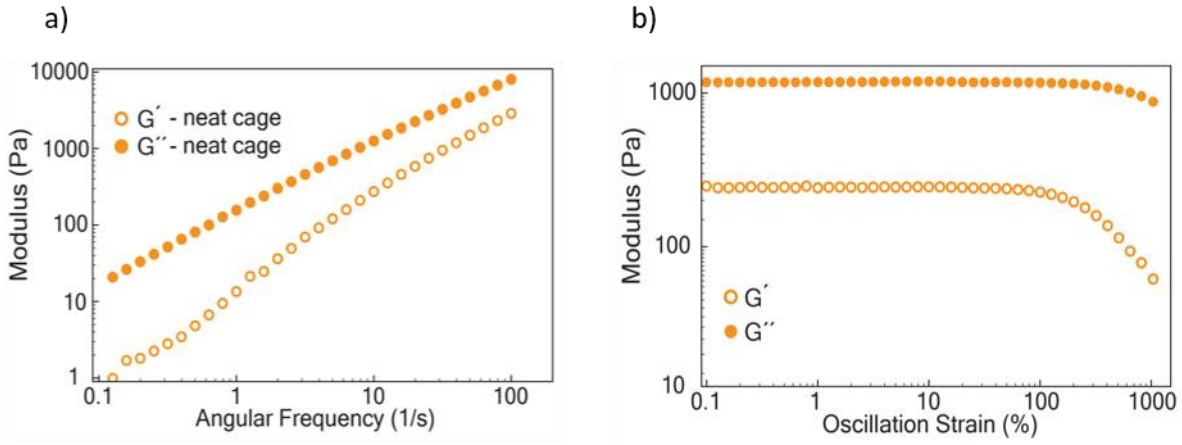

Figure 5.13: a) Oscillatory-dependent rheology of cage **5.2** at 25 °C showed liquid behavior with G´´ (loss modulus) greater than G´ (storage modulus) throughout the measurement. b) Frequency dependent oscillatory rheology measurement indicating that **5.2** remained fluid under all measured frequency regimes (G´´ > G´).

To investigate the temperature-dependent behavior, a temperature sweep was performed at 1% strain and 10 rad/s, highlighting the reversible fluidity of cage **5.2** at temperatures ranging from 20-100 °C, and showing that the viscosity of cage **5.2** decreased as the temperature increased (Figure 5.14). Additionally, the change in viscosity was reversible because the sample returned to its more viscous state upon cooling. Within the temperature range tested, cage **5.2** continued to behave as a fluid with G´´ consistently greater than G´.

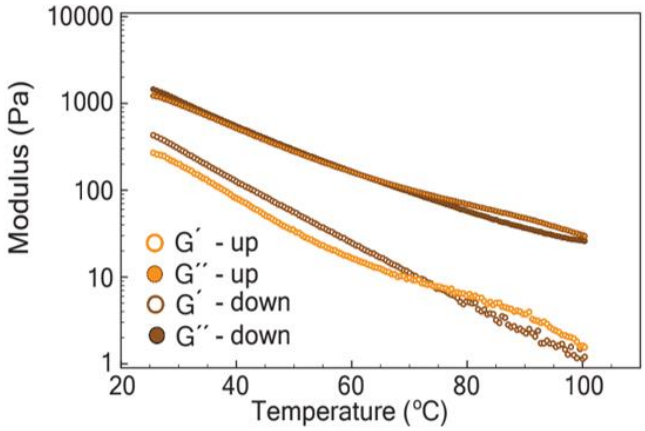

Figure 5.14: Oscillatory temperature ramps at 5 ˚C/min measured at 10 rad/s and 1% strain between 25-100 ˚C, showing that the viscosity of cage **5.2** decreased as temperature increased.

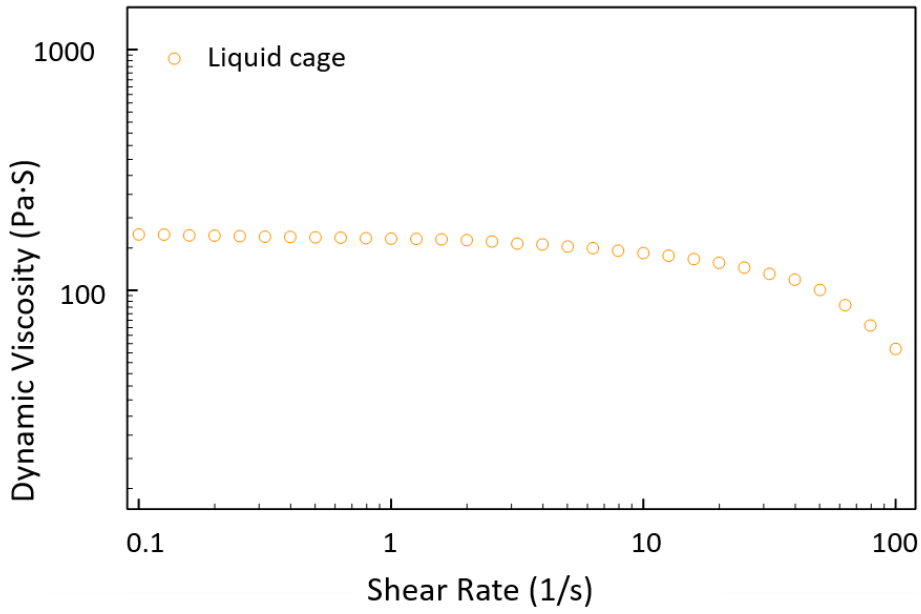

Figure 5.15: Shear dependent rheology; increase in shear rate on neat cage **5.2** causes a drop in the viscosity of the material on account of the mechanical disruption of the structured fluid.

Further rheological studies were performed, and shear-rheology was used to probe the mechanical properties of neat cage **5.2**. Upon increasing the shear rate from 0.1 to 1 1/s, the material expressed behavior indicative of a Newtonian fluid (the viscosity was independent of shear rate) as the dynamic viscosity remained constant in this range. Beyond a shear rate of 1 1/s, neat cage **5.2** exhibited non-Newtonian shear thinning behavior and the viscosity dramatically decreased (Figure 5.15). This type of shear thinning, or thixotropy, has been previously observed in ionic liquids and is correlated with the cation's ability to hydrogen bond.[10] Imidazolium ionic liquids have been shown to form strong hydrogen bonds,[11] which could contribute to shear thinning. Therefore, cage **5.2** behaved in a consistent manner with previously reported imidazolium based ionic liquids.

To better understand the thixotropic behavior of the material, an alternating flow ramp experiment where shear rate was increased from 1 to 100 1/s then immediately from 100 to 1 1/s showed a deviation between the up- and down-shearing cycles, with hysteresis being observed (Figure 5.16). This hysteresis is often seen in concentrated dispersions because the viscosity of the material does not reach a steady value immediately after application of stress and requires time for the system to stabilize. We hypothesized that this hysteresis was observed in our system due to the coulombic repulsions of the cages. In this case, cage **5.2** could be considered as a homogenous dispersion of coordination cages in a PEG-imidazolium ionic liquid. After the material was exposed to stress *via* the rotation of the plate, the capsules in the liquid could be moved closer to their neighboring capsules than they were initially positioned.

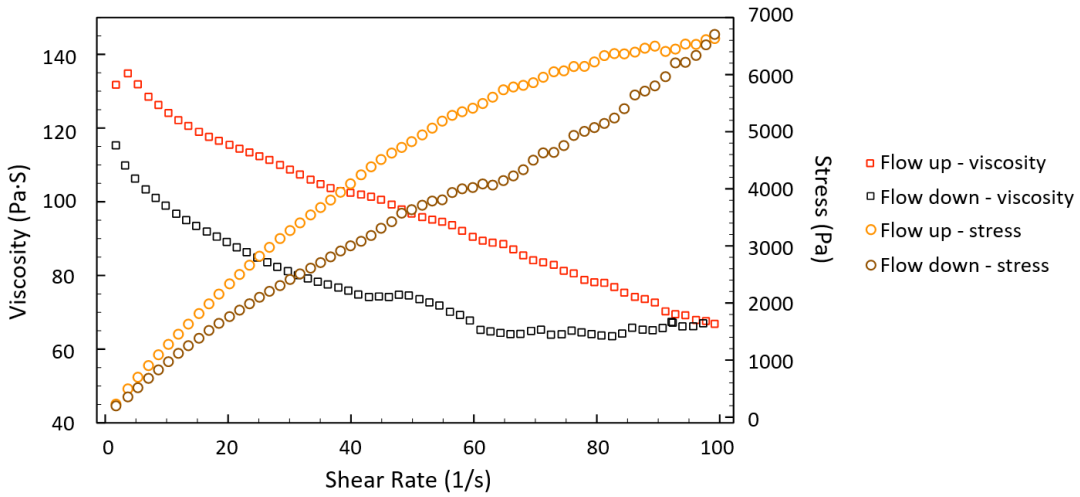

Figure 5.16: An alternating flow ramp experiment where shear rate was increased from 1 to 100 s^{-1} then immediately from 100 to 1 s^{-1} to investigate the thixotropic behavior of the material. The area between the curves is representative of the time-dependent shear recovery hysteresis.

However, due to coulombic repulsion, the system would not be in a stable state when these positively charged capsules are in close proximity to each other. Therefore, we postulate that the hysteresis was caused by the material restructuring itself so maximum distance was maintained between each individual cationic capsule.

5.8 Host-Guest Chemistry of Cage 5.2

5.8.1 Encapsulation of small alcohols in cages 5.2 and 5.3 in CH_3CN solution

Unfunctionalized cage **5.1** was reported to bind *t*-butanol in slow exchange with weak affinity.[4] To explore whether cages **5.2** and **5.3** exhibited similar binding behavior, the cages were introduced to *n*-butanol, *s*-butanol, *i*-butanol, *t*-butanol, *n*-propanol, and *i*-propanol in CD_3CN solution. Initial guest screening was conducted in the solution-state to conserve material. Furthermore, the resolution of NMR spectra obtained in CD_3CN was much higher than the resolution of spectra recorded in the neat state. The chosen alcohol guest (10 µL) was added to a 2 mM CD_3CN solution of cage **5.2** (0.5 mL). The experiment was then equilibrated at 298 K for 18 h before the ^1H NMR spectrum was recorded (Figure 5.17). The same method was used for alcohol binding in cage **5.3** (Figure 5.18). The ^1H NMR spectra of both cages showed upfield shifted encapsulated alcohol peaks below 0 ppm. Comparison of the integrated intensities of these bound guest signals to cage framework peaks demonstrated that *t*-butanol

was the strongest binding guest. Conversely, *i*-butanol, *i*-propanol, *n*-propanol, and *s*-butanol were bound within the cages with weaker affinities. Lastly, *n*-butanol was not observed to be encapsulated in either cage. Based on these guest binding preferences, we hypothesized that branched alcohols might present a better shape match for the cavity of cage **5.2** than their linear isomers, leading to stronger binding (Scheme 5.5).

We hypothesized that the binding mechanism of **5.2** and **5.3** involve the fast rearrangement of the cage scaffold – a behavior that was observed in a previous publication featuring cage **5.1**.[4] The enclosed nature of cage **5.1** does not allow guests to diffuse through the cage apertures. While smaller guests may be encapsulated *via* deformation of the cage framework, larger guests are likely only able to enter the cavity upon the dissociation of metal-ligand bonds. Since cages **5.2** and **5.3** share the same scaffold as cage **5.1**, we hypothesized that the two former cages would encapsulate guests *via* similar mechanisms to cage **5.1**.

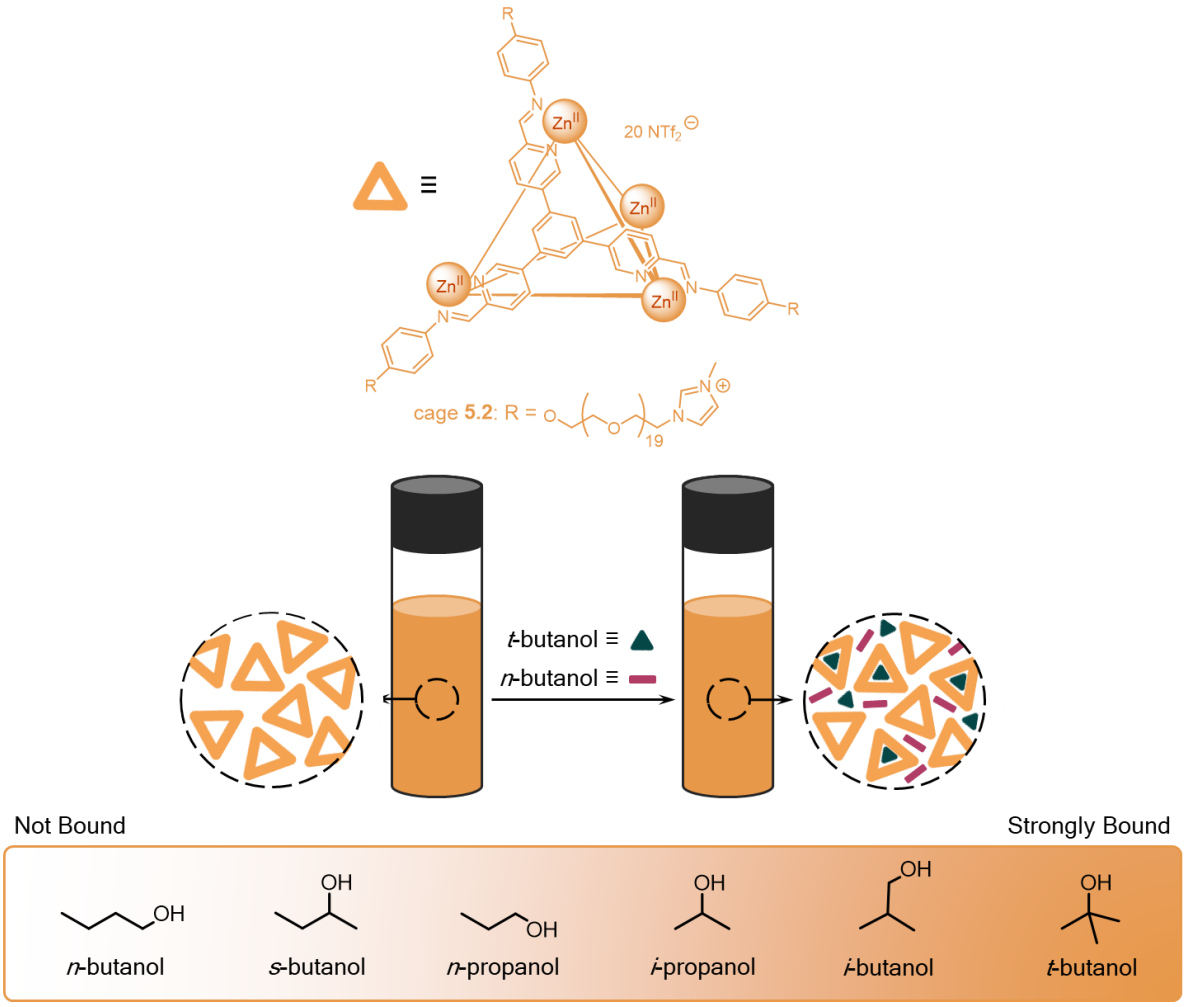

Scheme 5.5: Cage **5.2** encapsulated a variety of small alcohols but bound branched isomers more strongly than their linear counterparts. The cage also selectively encapsulated *t*-butanol when introduced to a 1:1 mixture of *t*-butanol and *n*-butanol.

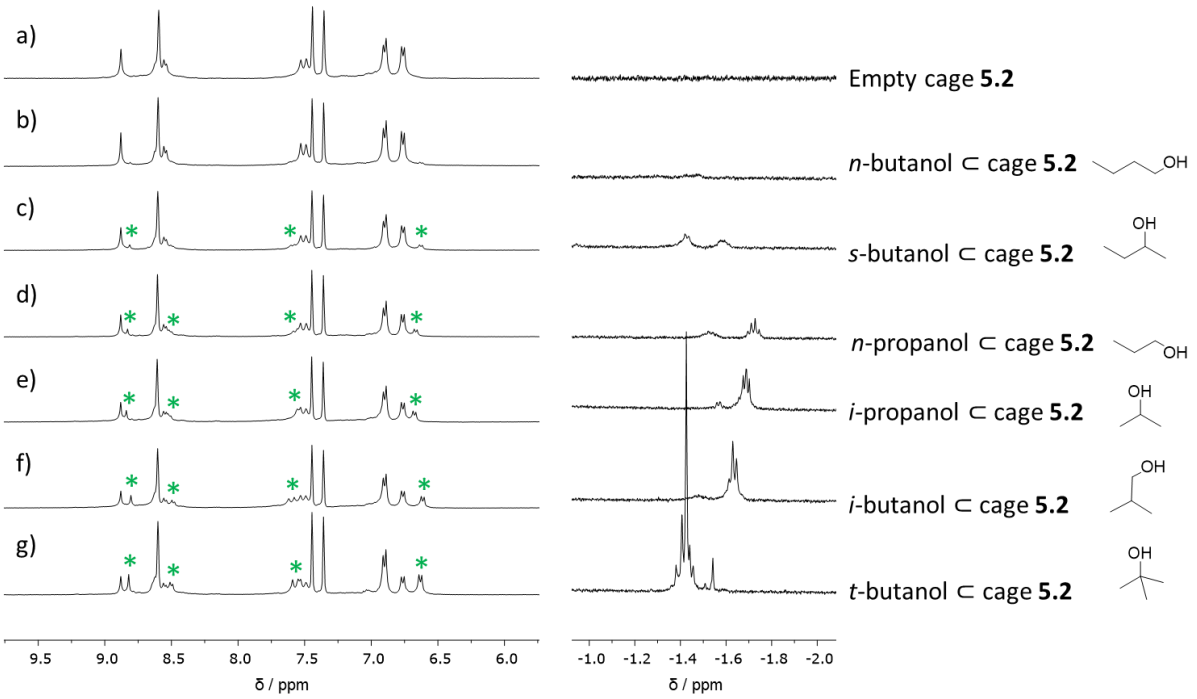

Figure 5.17: Partial ^{1}H NMR (400 MHz, 298 K, CD_3CN) spectra of cage **5.2** host-guest complexes. a) No added guest (free cage), b) *n*-butanol, c) *s*-butanol, d) *n*-propanol, e) *i*-propanol, f) *i*-butanol, g) *t*-butanol. Intensities have been scaled for clarity. Peaks correlated with host-guest complex formation have been denoted with a green asterisk (*).

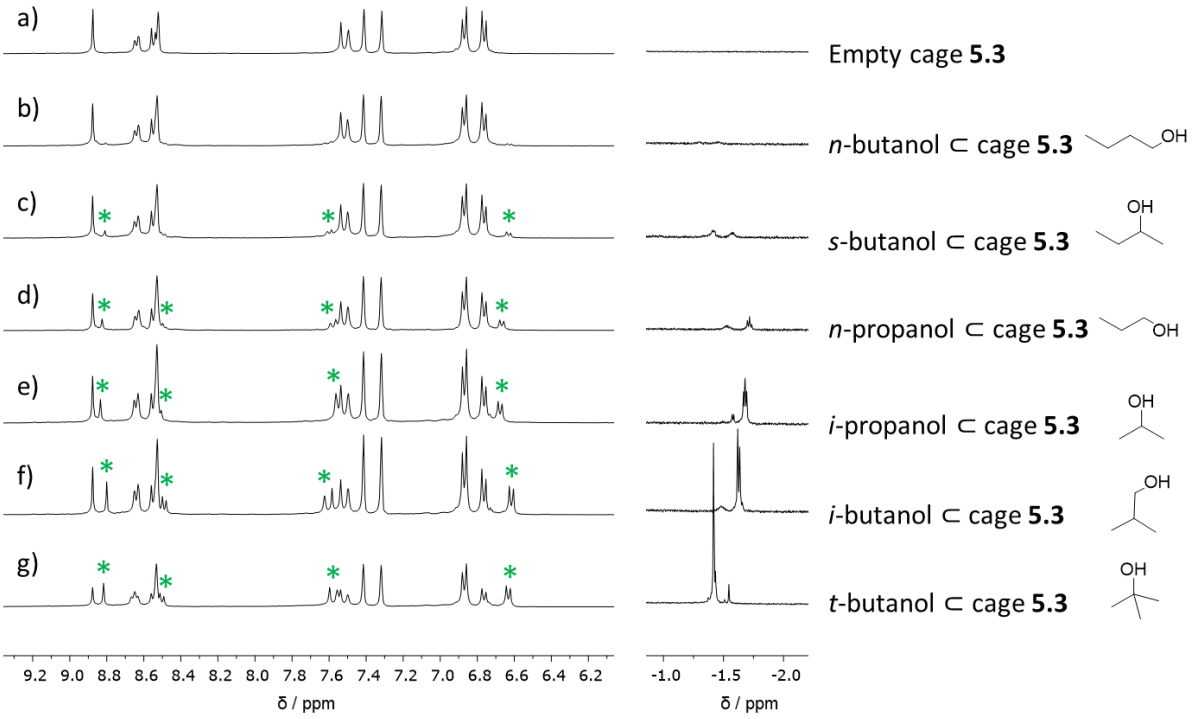

Figure 5.18: Partial ^{1}H NMR (400 MHz, 298 K, CD_3CN) spectra of cage **5.3** host-guest complexes. a) No added guest (free cage), b) *n*-butanol, c) *s*-butanol, d) *n*-propanol, e) *i*-propanol, f) *i*-butanol, g) *t*-butanol. Intensities have been scaled for clarity. Peaks correlated with host-guest complex formation have been denoted with a green asterisk (*).

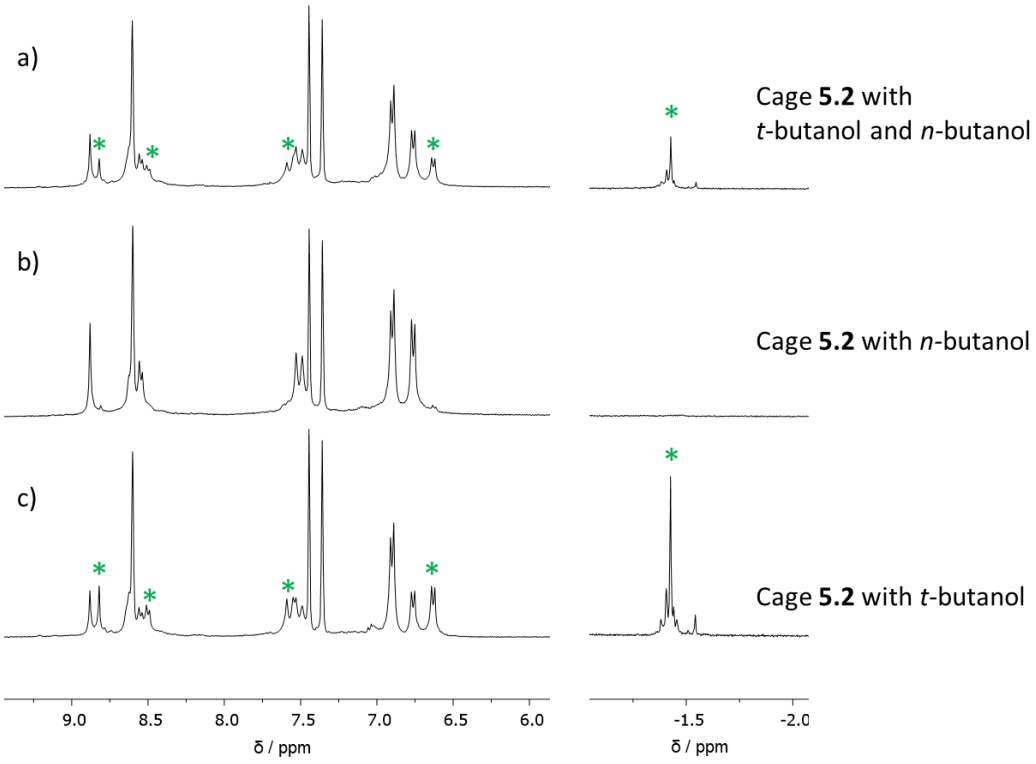

Figure 5.19: Partial ^{1}H NMR (400 MHz, 298 K, CD_3CN) spectra of cage **5.2** selectively encapsulating *t*-butanol in the presence of a 1:1 mixture of *t*-butanol (5 µL) and *n*-butanol (5 µL). a) *T*-butanol ⊂ **5.2** selectively forming in the mixture of both alcohols, b) *n*-butanol ⊂ **5.2**, c) *t*-butanol ⊂ **5.2**. Peaks correlated with host-guest complex formation have been denoted with a green asterisk (*).

To test the hypothesis of branched alcohol isomers having a better shape match for the cavity of cage **5.2**, we introduced a 1:1 mixture of *t*-butanol (5 µL) and *n*-butanol (5 µL) to a 2mM solution of cage **5.2** in CH_3CN (0.5 mL). The experiment equilibrated at 298 K for 18 h and then was analyzed by ^{1}H NMR spectroscopy (Figure 5.19). The spectrum showed that no *n*-butanol was encapsulated, and that *t*-butanol was the only guest within the pore. A smaller amount of *t*-butanol was encapsulated in this sample when compared to the host-guest experiment with only *t*-butanol. However, this difference was due to the smaller amount of *t*-butanol added to the mixed guest experiment. Therefore, cage **5.2** was able to selectively encapsulate a more branched alcohol isomer over its linear counterpart. While this behavior could be applied as potential separation technique, the host-guest complex currently cannot be isolated from the empty cage.

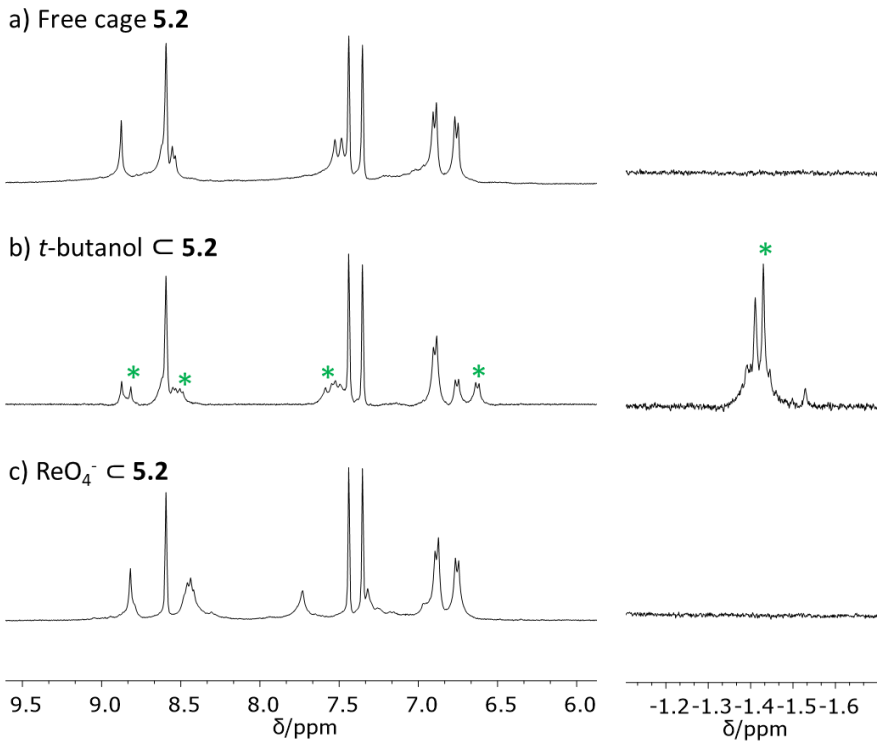

Figure 5.20: Partial ^{1}H NMR (400 MHz, 298 K, CD_3CN) spectra of ReO_4^- displacing encapsulated *t*-butanol in cage **5.2**. a) Free cage **5.2**, b) *t*-butanol ⊂ **5.2**, c) ReO_4^- ⊂ **5.2**. Peaks correlated with *t*-butanol ⊂ **5.2** have been denoted with a green asterisk (*). Region below 0 ppm was zoomed in for clarity.

To demonstrate that the alcohol guests were binding within the cavity of cage **5.2** instead of externally, we conducted a control experiment to show that perrhenate (ReO_4^-), known to be a high affinity guest for parent cage **5.1**, could displace *t*-butanol bound within the cage. *T*-butanol ⊂ **5.2** was synthesized by adding *t*-butanol (10 µL) to a 2 mM solution of cage **5.2** in CD_3CN (0.5 mL). The sample equilibrated for 18 h at 298 K. ^{1}H NMR showed the characteristic aromatic peak splitting of successful host-guest complex formation as well as the encapsulated alcohol peak upfield of 0 ppm (Figure 5.20b). Upon confirming the generation of *t*-butanol ⊂ **5.2**, tetrabutylammonium perrhenate (0.49 mg, 1 µmol) was added to the sample. This amount of (ReO_4^-) was chosen because it is equimolar to the amount of cage **5.2** present in the experiment and should result in the empty cage undergoing full conversion to the host-guest complex. The host-guest system was then allowed to equilibrate for 18 h at 298 K. Upon analysis by ^{1}H NMR, the spectrum showed that the encapsulated guest peak upfield of 0 ppm was no longer present (Figure 5.20c). The aromatic peaks were no longer split and were shifted when compared to the free cage. These results demonstrated that the strongly binding ReO_4^- displaced *t*-butanol from the cavity of cage **5.2**. Therefore, we hypothesized that the

displacement observed in this experiment indicated that the alcohol guests are binding within the cavity of cage **5.2** and not externally.

5.8.2 Encapsulation of small alcohols in neat liquid cage 5.2

After screening in CH_3CN, each alcohol guest was analyzed twice under solvent-free conditions to determine whether liquid cage **5.2** behaved similarly in the neat state. The first analysis was done on a sample containing 10 wt% guest while the second analysis was performed on a sample containing neat cage with 30 wt% guest. Cage **5.2** (~150 mg) was dissolved in CH_3CN (1 mL) and transferred to a tared vial (1 dram) with a stir bar. The solvent was removed under reduced pressure for 2 h. The alcohol guest (10 wt% of cage **5.2**) was added to the vial containing neat cage **5.2**. The experiment was stirred at 298 K for 18 h before the product mixture analyzed by neat NMR using the setup described in Section 5.3.1. This experiment was repeated for the same alcohol with 30 wt% guest.

For the initial solvent-free experiments, 10 wt% of each alcohol guest was added to its respective cage sample (Figure 5.21). Upon analysis *via* VT-^{1}H NMR, it was evident that the behavior of the host-guest complexes in the neat state was consistent with the observations made in the solution-state. Cage **5.2** still bound branched alcohols more strongly than their linear counterparts in the neat state. When these experiments were repeated with 30 wt% of each guest, the results were the same – the cage showed preferential binding toward more branched alcohols (Figure 5.22). However, the excess of guest in the latter samples diluted the host-guest mixture, resulting in a less viscous material. Therefore, the ^{1}H NMR spectra obtained from the host-guest complexes formed with 30 wt% guest exhibited significantly less peak broadening due to an increase in cage tumbling.

The selectivity experiment between *t*-butanol and *n*-butanol was also repeated under solvent-free conditions (Figure 5.23). 5 wt% of each guest was added to a neat sample of cage **5.2** and stirred overnight at 298 K. The sample was then transferred into a neat NMR apparatus and analyzed *via* ^{1}H NMR. At 298 K, no encapsulated guest was observed due to the high viscosity of the sample. When heated to 343 K, a small encapsulated *t*-butanol peak was visible upfield of 0 ppm. This experiment was repeated with 15 wt% of each guest and analyzed with the same method. Again, no encapsulated guest peak was observable at 298 K but an encapsulated *t*-butanol peak was visible upon heating the sample to 343 K. This experiment demonstrated that the neat cage also selectively encapsulated the more branched alcohol isomer – a phenomenon that is consistent with its behavior in the solution-state.

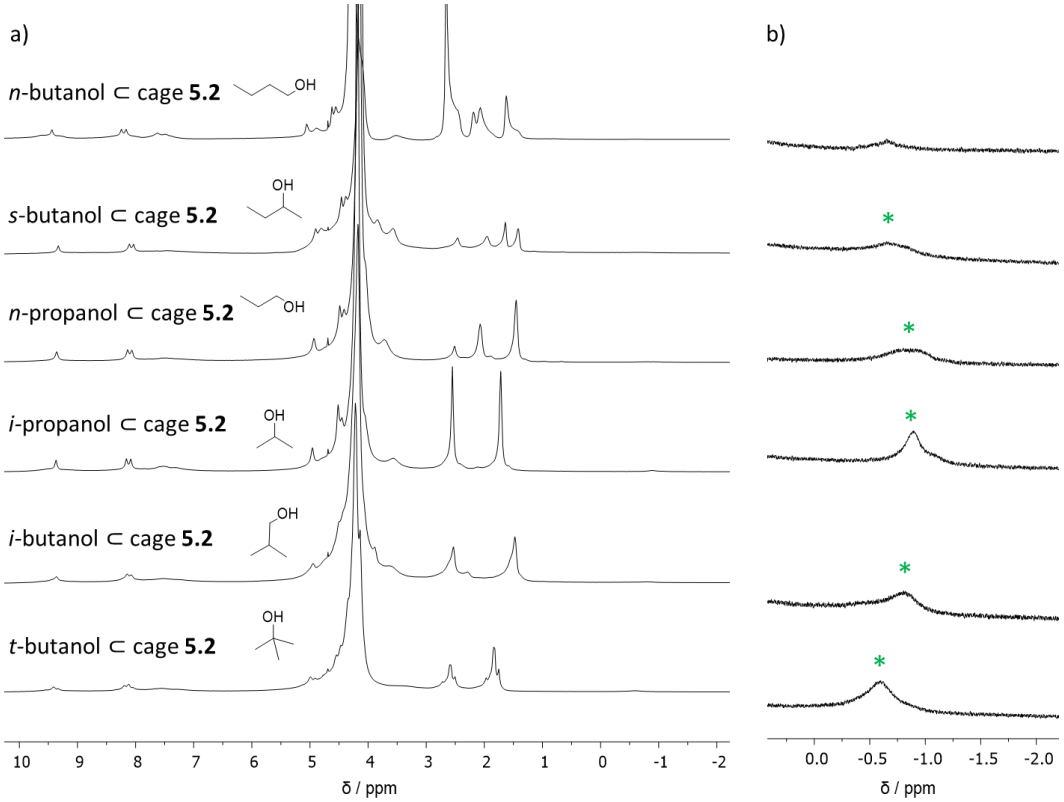

Figure 5.21: a) VT-^{1}H NMR of neat cage **5.2** and 10 wt% guest (400 MHz, 343 K). The NMR signal was locked on a D_2O capillary. b) Partial VT-^{1}H NMR of neat host-guest complexes upfield of 0 ppm. Peaks correlated with host-guest complex formation have been denoted with a green asterisk (*).

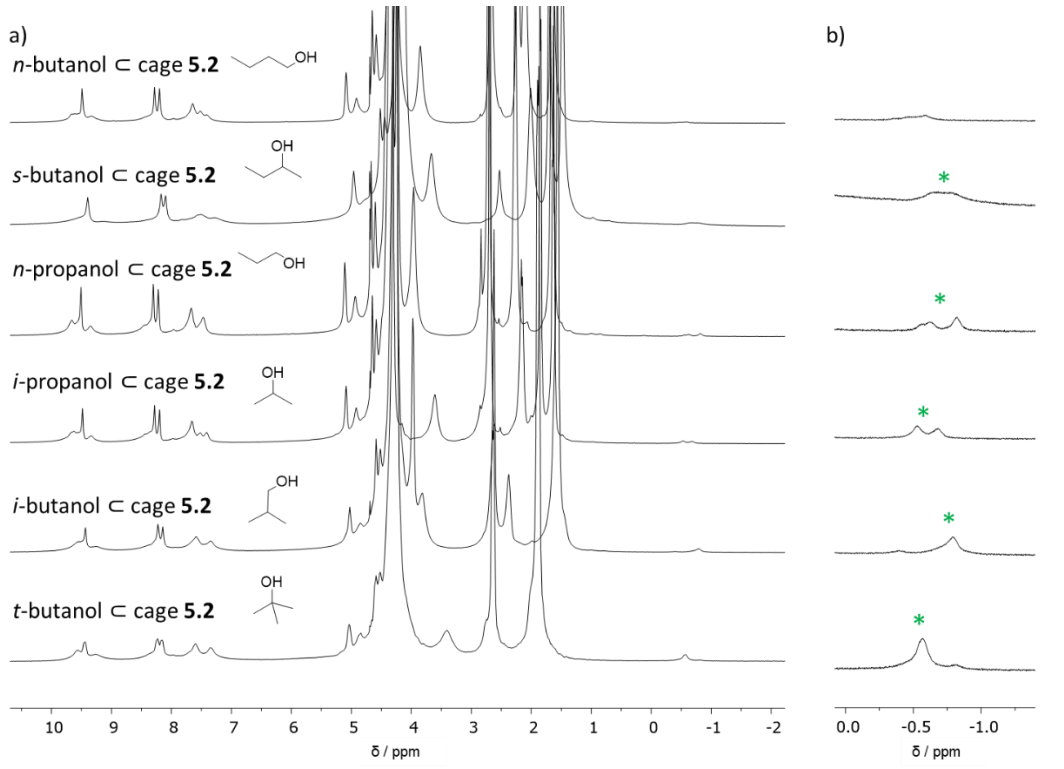

Figure 5.22: a) VT-^{1}H NMR of neat cage **5.2** and 30 wt% guest (400 MHz, 343 K). The NMR signal was locked on a D_2O capillary. b) Partial VT-^{1}H NMR of neat host-guest complexes upfield of 0 ppm. Peaks correlated with host-guest complex formation have been denoted with a green asterisk (*).

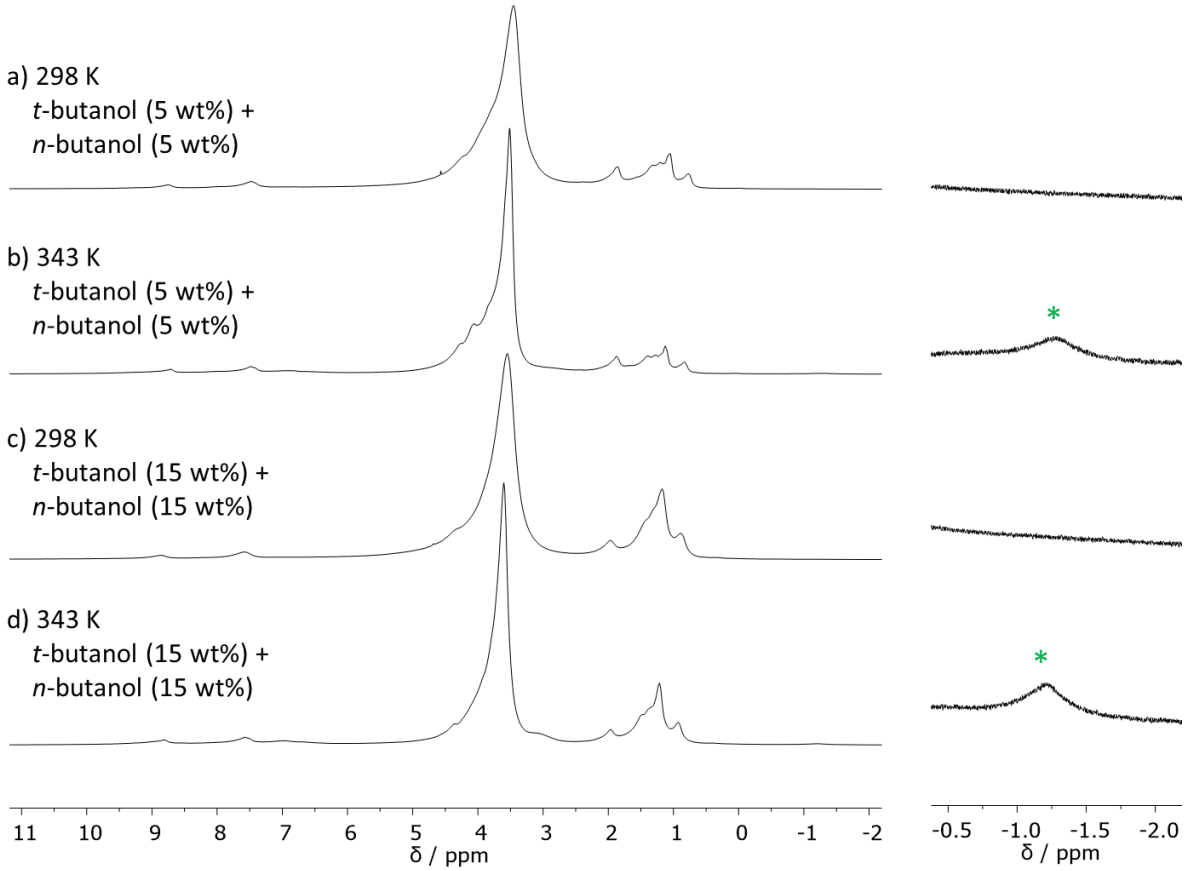

Figure 5.23: VT-^{1}H NMR of neat cage **5.2** and a 1:1 mixture of *t*-butanol and *n*-butanol (400 MHz). The NMR signal was locked on a D_2O capillary. Peaks correlated with host-guest complex formation have been denoted with a green asterisk (*). a) Partial ^{1}H NMR of **5.2** and 5 wt% *t*-butanol and 5 wt% *n*-butanol at 298 K, b) partial VT-^{1}H NMR of **5.2** and 5 wt% *t*-butanol and 5 wt% *n*-butanol at 343 K, c) partial VT-^{1}H NMR of **5.2** and 15 wt% *t*-butanol and 15 wt% *n*-butanol at 298 K, and d) partial VT-^{1}H NMR of **5.2** and 15 wt% *t*-butanol and 15 wt% *n*-butanol at 343 K.

5.8.3 Sequestration of CFCs in cage 5.2

Trichlorofluoromethane ($CFCl_3$, CFC-11), dichlorodifluoromethane (CF_2Cl_2, CFC-12), and chlorotrifluoromethane (CF_3Cl, CFC-13) are three of the most abundant and long-lived ozone depleting agents, with one gram of each in the atmosphere being equivalent to 4750, 10900, and 14400 grams of CO_2, respectively, in global warming effects.[12] $CFCl_3$ alone contributes 25% of all chlorine reaching the stratosphere. Although $CFCl_3$ emissions had been declining consistently since the late 1980s, an unexpected but steady increase of this environmental contaminant began in 2012 and continues today.[13,14] Recovery of the ozone layer is dependent on a sustained reduction in the emissions of these three CFCs. MOFs,[15] ionic liquids,[16] and anion cages[17] have all been shown to adsorb, dissolve or encapsulate CFCs. Our material may be able to combine the benefits of ionic liquids and cages by mediating the

dissolution and encapsulation of CFCs within a single-component fluid phase. Therefore, novel means of selectively and reversibly binding these CFCs could thus lead to new processes for their remediation.

Parent cage **5.1** was previously shown to bind dichloromethane and chloroform with weak affinity.[4] It was hypothesized that cage **5.2** could be a good candidate to sequester CFCs that are similar in size and shape to DCM and $CHCl_3$. Therefore, CF_3Cl, CF_2Cl_2 and $CFCl_3$ were chosen as guests for the cage. Initially the host-guest experiments were conducted in CD_3CN because screening for suitable guests was easier in the solution-state. However, these experiments were repeated with the neat cage.

Two different experimental setups were used for the host-guest studies conducted in CD_3CN. Due to the fact that $CFCl_3$ was a volatile liquid at room temperature, it could be measured in a syringe and directly injected. Therefore, $CFCl_3$ (10 µL) was introduced to 0.5 mL of a 2 mM CD_3CN solution of cage **5.2**. The sample was equilibrated at 298 K for 18 h before being analyzed by ^1H and ^{19}F NMR with a 1,3,5-tris(trifluoromethyl)benzene reference capillary. A slightly different setup was used for host-guest experiments with CF_2Cl_2 and CF_3Cl because of their gaseous nature. CF_2Cl_2 or CF_3Cl (100 mL, gaseous) was bubbled through 0.5 mL of a 2 mM CD_3CN solution of cage **5.2**. The sample was equilibrated at 298 K for 18 h before being analyzed by ^1H and ^{19}F NMR with a 1,3,5-tris(trifluoromethyl)benzene reference capillary.

The ^1H NMR spectra obtained of the CFC ⊂ **5.2** complexes were compared against that of free cage **5.2** (Figure 5.24). $CFCl_3$ ⊂ **5.2** and CF_2Cl_2 ⊂ **5.2** both demonstrated the characteristic peak splitting in the aromatic region indicative of successful host-guest complex formation. Peak deconvolution was conducted on the ^1H NMR spectrum of $CFCl_3$ ⊂ **5.2** showing that 20% of cages remained empty. The same peak deconvolution method was applied to the ^1H NMR spectrum of CF_2Cl_2 ⊂ **5.2** and the calculations showed that 39% of cage **5.2** remained empty. No peak splitting was observed for CF_3Cl ⊂ **5.2** in the ^1H NMR spectrum because the guest was too weakly bound. This difference in uptake indicated that the cage bound $CFCl_3$ with the highest affinity and CF_3Cl with the lowest affinity, indicating size-selectivity toward larger CFCs that fit within its cavity. The size-selective behavior of cage **5.2** was also observed by ^{19}F NMR (Figure 5.25). However, due to the signal-to-noise ratio, it was difficult to accurately integrate the encapsulated guest peaks in the ^{19}F NMR spectra. Therefore, the amounts of bound $CFCl_3$ and CF_3Cl seen by ^{19}F NMR were not compared quantitatively.

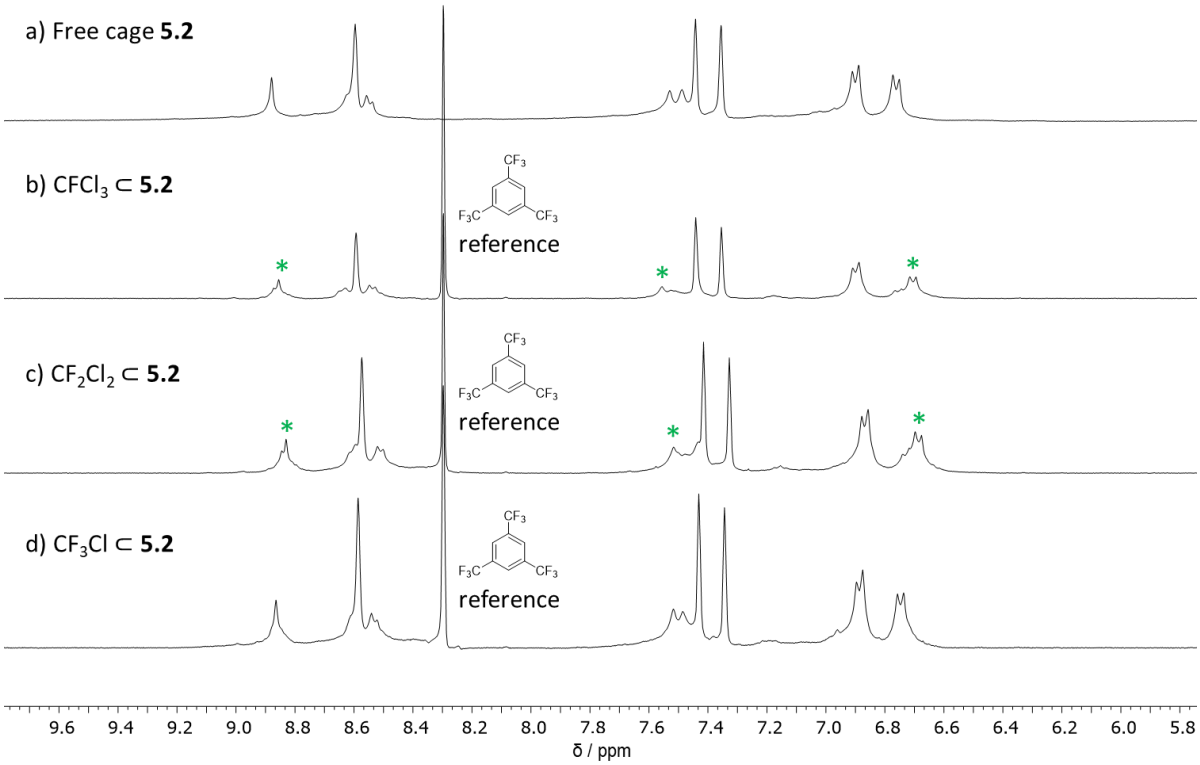

Figure 5.24: Partial ^{1}H NMR (400 MHz, 298 K, CD_3CN) of cage **5.2** and its host-guest complexes in CD_3CN. a) Free cage **5.2**, b) $CFCl_3 \subset$ **5.2**, c) $CF_2Cl_2 \subset$ **5.2**, d) $CF_3Cl \subset$ **5.2**. Peaks correlated with the formation of CFC $\subset$ **5.2** were labelled with a green asterisk (*). No host-guest peaks were observed for $CF_3Cl \subset$ **5.2**.

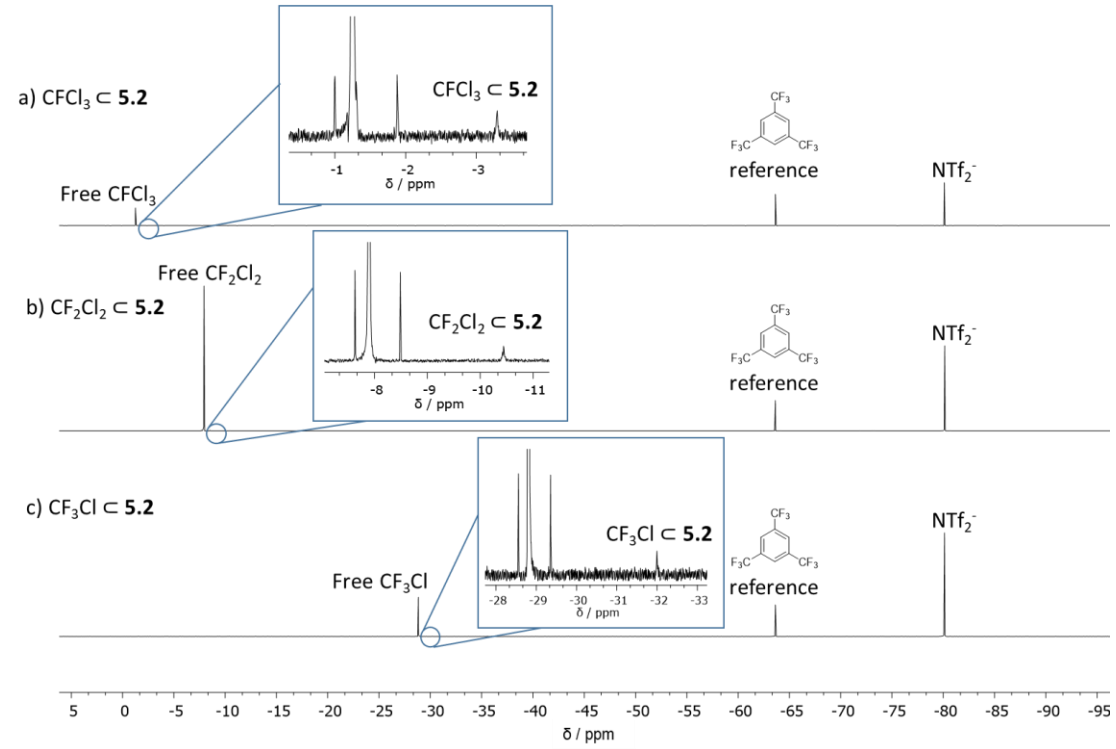

Figure 5.25: ^{19}F NMR (377 MHz, 298 K, CD_3CN) of a) $CFCl_3 \subset$ **5.2**, b) $CF_2Cl_2 \subset$ **5.2**, c) $CF_3Cl \subset$ **5.2**. Includes blow-up section of peaks indicative of host-guest complex formation.

After successfully demonstrating the encapsulation of these three CFCs in the solution-state, the host-guest experiments were repeated under solvent-free conditions. Similar to the experiments conducted in the solution-state, two experimental setups were used due to the different phases of the guests. For $CFCl_3$, a sample of cage **5.2** (20 mg) was transferred into a shell vial (5 mL) containing a small stir bar. A screw-cap vial (4 dram) was filled with 0.1 mL of cold $CFCl_3$ before the shell vial was placed in the screw-cap vial and the entire system was sealed (Figure 5.26a). The sample was stirred at 298 K for 18 h before the sample was prepared for ^{1}H and ^{19}F NMR analysis. The contents of the inner shell vial were dissolved in CD_3CN (0.5 mL) before being quickly transferred to a 5 mM NMR tube and immediately analyzed by ^{1}H and ^{19}F NMR with a 1,3,5-tris(trifluoromethyl)benzene reference capillary. These experiments could not be analyzed by neat NMR because heating the sample to increase tumbling would result in guest evaporation.

CF_2Cl_2 and CF_3Cl was also encapsulated in cage **5.2** in the neat state. For consistency, we chose a similar experimental setup to the one used in the gaseous CFC encapsulation experiments (Figure 5.26b). A sample of cage **5.2** (20 mg) was transferred into a shell vial (5 mL) containing a small stir bar. The shell vial containing the cage was deposited in a larger vial (6 dram) and the system was closed with a septum. A balloon was then filled with CF_2Cl_2 or CF_3Cl (~100 mL, gaseous) and used to purge the stoppered vial containing cage **5.2**. The balloon was removed and the system was stirred at 298 K for 18 h before the sample was prepared for ^{1}H and ^{19}F NMR analysis in the same manner as the protocol used for the synthesis of $CFCl_3 \subset$ **5.2**.

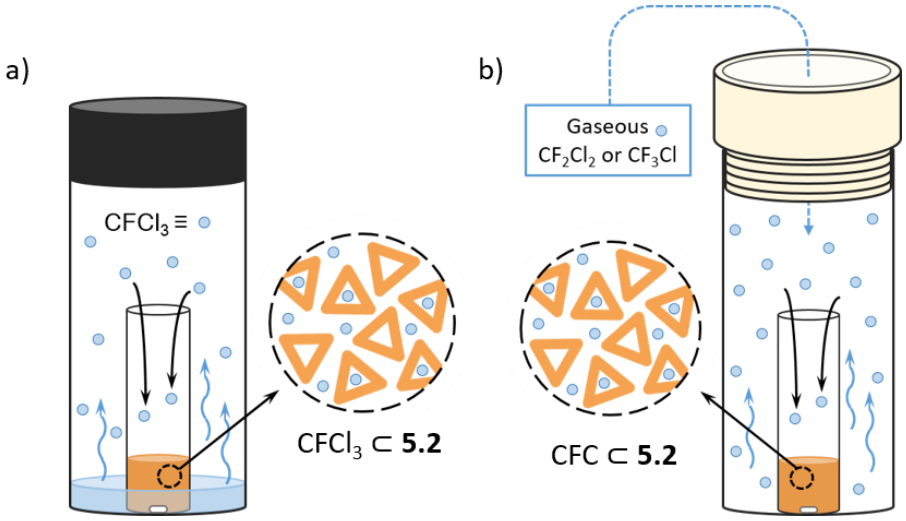

Figure 5.26: a) Gaseous $CFCl_3$ encapsulation experimental setup. Due to the low boiling point of $CFCl_3$ (24 °C), the CFC vaporized over 18 h and was dissolved and encapsulated in **5.2**. b) Gaseous CF_2Cl_2 and CF_3Cl encapsulation experimental setup. A balloon filled with the guests was used to transfer the guests into the system.

The size-selective behavior of cage **5.2** for binding larger CFCs more strongly was still observed in the solvent-free state. ^{1}H NMR spectra for $CFCl_3 \subset$ **5.2** and $CF_2Cl_2 \subset$ **5.2** both demonstrated the characteristic peak splitting in the aromatic region indicative of successful host-guest complex formation (Figure 5.27). Peak deconvolution was conducted on the ^{1}H NMR spectrum of $CFCl_3 \subset$ **5.2** showing that 4.7% of cages remained empty. The same peak deconvolution method was applied to the ^{1}H NMR spectrum of $CF_2Cl_2 \subset$ **5.2** and the calculations showed that 43.8% of cage **5.2** remained empty. No peak splitting was observed for $CF_3Cl \subset$ **5.2** in the ^{1}H NMR spectrum because the guest was too weakly bound. This difference in ratio between free and occupied cage confirmed that **5.2** showed size-selectivity toward larger CFCs.

The size-selective behavior of cage **5.2** was also observed by ^{19}F NMR (Figure 5.28). By comparing the size of the encapsulated peaks of $CFCl_3 \subset$ **5.2** and $CF_3Cl \subset$ **5.2** against the 1,3,5-tris(trifluoromethyl)benzene reference capillary, we determined that cage **5.2** encapsulated approximately one order of magnitude more $CFCl_3$ than it encapsulated CF_3Cl. Additionally, the integrations of free and encapsulated guest were compared for each CFC and the ratios confirmed this order of binding strength. Therefore, although the cage solvated differing amounts of CFC, the size-selective trend in amount of guest encapsulated in the cage was still consistent with the data seen in the ^{1}H NMR analysis.

$CFCl_3 \subset$ **5.2** could not be analyzed in its neat state via VT-NMR due to the low boiling temperature of the guest. The experiments previously described rely on dissolving the neat $CFCl_3 \subset$ **5.2** sample in CD_3CN and rapidly analyzing it using solution-phase ^{1}H and ^{19}F NMR. However, these experiments do not exclude the possibility that the guest could have physically adsorbed to the surface of the liquid cage, and then been rapidly encapsulated in solution after the addition of the CD_3CN. Thus, these experiments alone do not demonstrate that the $CFCl_3$ was encapsulated under solvent-free conditions.

To address this point, a control experiment was conducted. A sample of neat cage **5.2** (20 mg) which had not been exposed to gaseous $CFCl_3$ was prepared. The cage was dissolved in CD_3CN, and immediately prior to NMR analysis 10 μL $CFCl_3$ was added to the NMR tube. The sample was then analyzed by ^{19}F NMR, and a spectrum was collected every minute for 1 h (Figure 5.29). Throughout the 1 h period, the quantity of encapsulated $CFCl_3$ in the control experiment steadily increased. The results were compared to the data obtained from the experiment in which the guest was encapsulated in neat cage. The spectra showed that the

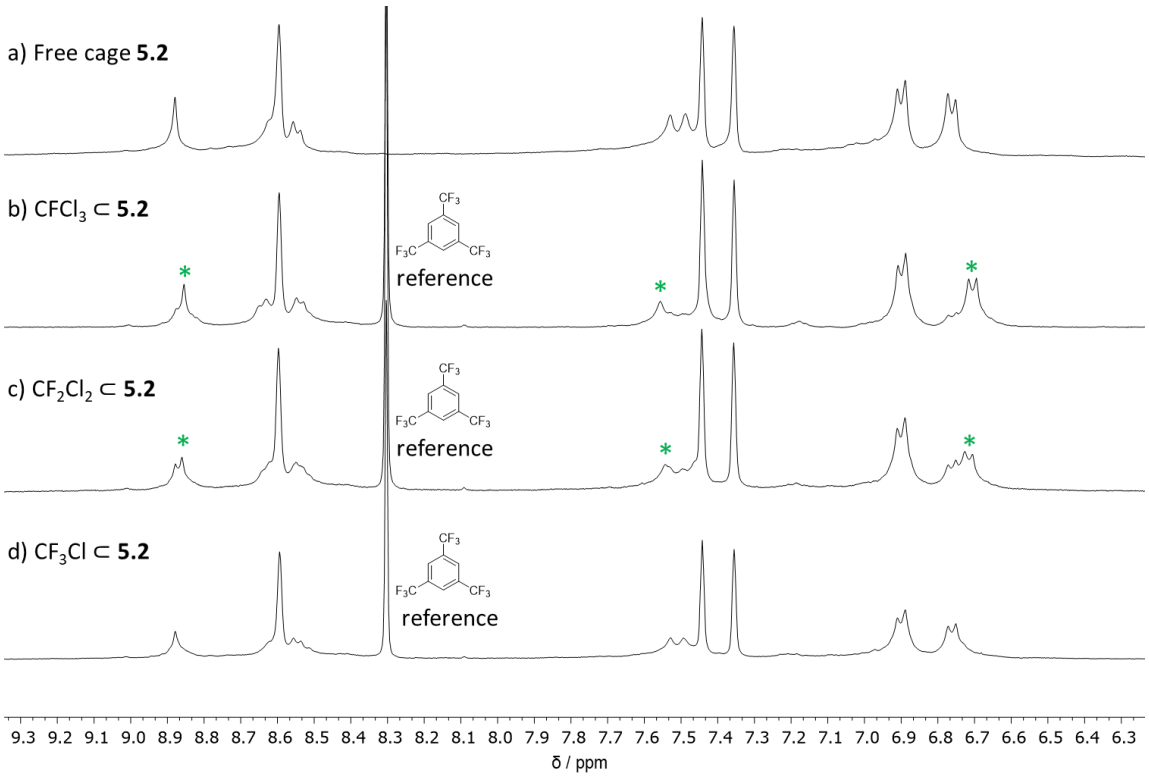

Figure 5.27: Partial ^{1}H NMR (400 MHz, 298 K, CD_3CN) spectra of cage **5.2** and its host-guest complexes synthesized under solvent-free conditions but analyzed in CD_3CN. a) free cage **5.2**, b) $CFCl_3 \subset$ **5.2**, c) $CF_2Cl_2 \subset$ **5.2**, d) $CF_3Cl \subset$ **5.2**. Peaks correlated with the formation of CFC $\subset$ cage **5.2** were labelled with a green asterisk (*). No host-guest peaks were observed for $CF_3Cl \subset$ **5.2**.

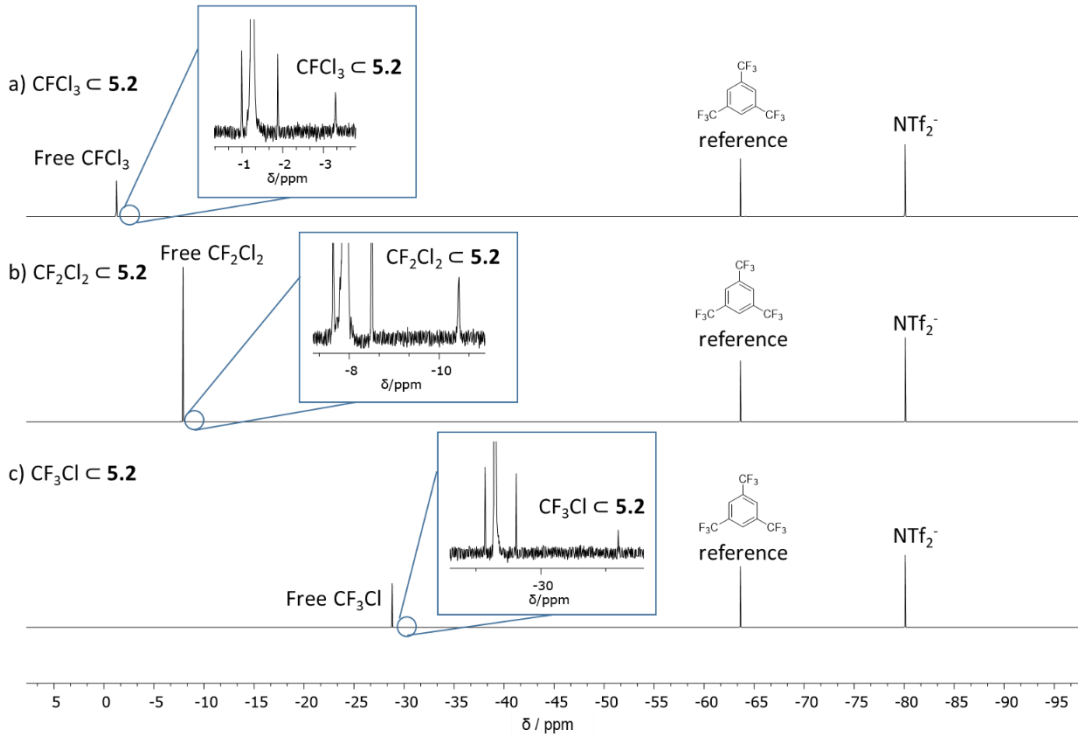

Figure 5.28: ^{19}F NMR (377 MHz, 298 K, CD_3CN) of cage **5.2** and its host-guest complexes synthesized under solvent-free conditions but analyzed in CD_3CN. a) $CFCl_3 \subset$ **5.2**, b) $CF_2Cl_2 \subset$ **5.2**, c) $CF_3Cl \subset$ **5.2**. Includes blow-up section of peaks indicative of host-guest complex formation.

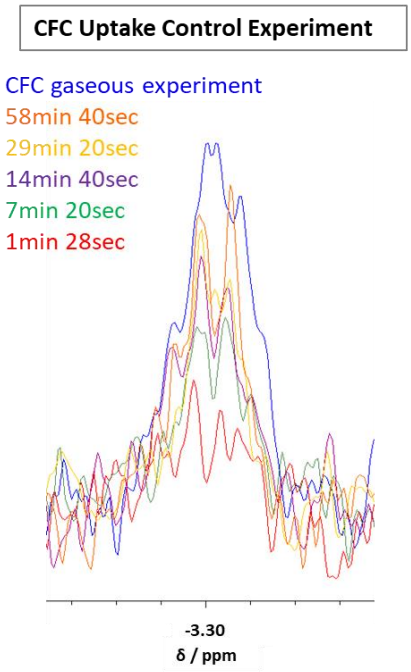

Figure 5.29: Partial ^{19}F NMR (377 MHz, 298 K, CD_3CN) of $CFCl_3 \subset$ **5.2**. After 1 h of equilibration, the integration of the encapsulated guest peak from the control experiment was still smaller than the encapsulated guest peak from the solvent-free CFC binding experiment.

initial quantity of $CFCl_3$ encapsulated by the cage exposed to gaseous $CFCl_3$ overnight was larger than in the control sample. This result indicated that the kinetics of guest uptake are sufficiently slow that it is possible to distinguish between the quantity of $CFCl_3$ that could have been encapsulated by the cage in CD_3CN (in the short space of time between dissolution and analysis) and $CFCl_3$ encapsulated by the cage during solvent-free host-guest experiments.

5.8.4 Molecular modelling and volume calculations of guests

The percent occupancy of cage **5.2** by different guests was calculated by dividing the volume of the guest by the volume of cage **5.2** to determine whether the host-guest behavior of cage **5.2** followed Rebek's 55% rule.[18] The volume of cage **5.1** was previously calculated using VOIDOO on the crystal structure of the empty capsule (Figure 5.30).[19] Cage **5.2** shares an analogous cage scaffold to cage **5.1**, thus we inferred the two cages to share the same volume of 130 Å^3.[4] All guests shown in Table 5.1 were encapsulated within cages **5.2** and **5.3** in CH_3CN solution, and all were also encapsulated within neat cage **5.2**.

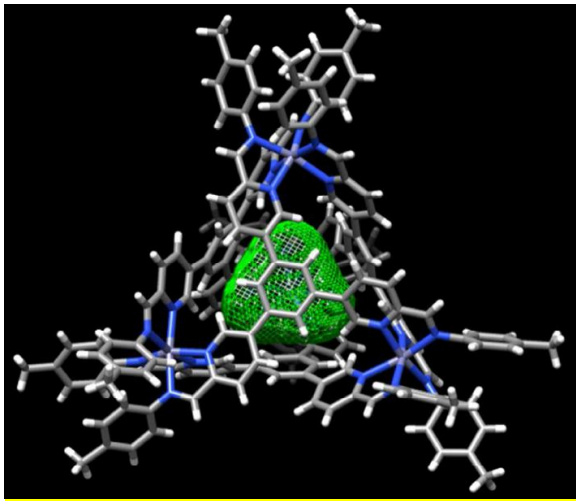

Figure 5.30: VOIDOO-calculated void space within the crystal structure of cage **5.1**. Figure adapted from reference [4].

Table 5.1. Table of the volumes of the guests encapsulated in cages **5.2** and **5.3**, their percent occupancies of the host cavity, and the percentage of cage **5.2** converted to the host-guest complex when exposed to these guests (calculated by peak deconvolution of the ^{1}H NMR spectrum).

Guest	V(Å^3)	% occupation of host cavity	% of cage **5.2** converted to host-guest complex
n-propanol	76	58.5%	18.3%
i-propanol	76	58.5%	32.4%
n-butanol	96	73.8%	3.2%
i-butanol	95	73.1%	38.5%
s-butanol	95	73.1%	13.5%
t-butanol	95	73.1%	54.4%
CF_3Cl	59	45.4%	N/A
CF_2Cl_2	73	56.2%	56.2%
$CFCl_3$	79	60.8%	95.3%

While the occupancy proportions are greater than the 55% optimum suggested by Rebek et al.,[18] these guests were observed to weakly bind in cages **5.2** and **5.3** – a phenomenon that is consistent with previously reported trends for cage **5.1**, where anions that occupied more than 55% of the cage cavity were encapsulated. Interestingly, the volume calculated for every butanol isomer was equal to 95 ± 1 Å^3. However, experimental results show that cages **5.2** and **5.3** preferentially bound the more branched alcohol isomers. Therefore, these calculations are consistent with our hypothesis that these cages bind alcohols shape-selectively amongst guests

of the same size. The calculated volumes of the CF_3Cl, CF_2Cl_2 and $CFCl_3$ also indicate that these three guests were not the same size, lending further evidence to support our hypothesis that cages **5.2** and **5.3** show size-selective binding of the CFCs. Many guests larger than Rebek's optimum were studied herein because smaller guests would be gasses under ambient conditions, whereas in the present work we have chosen to mainly focus on condensed-phase guests.

5.8.5 Recovering and reusing cage 5.2

To maximize the usage of a liquid cage sample, we were interested in whether cage **5.2** could be recovered from host-guest experiments and then subsequently reused without further purification. We discovered that CFCs and alcohols encapsulated in cage **5.2** could be removed from the cavity when the host-guest complex was exposed to vacuum due to weak host-guest interactions. To determine how many times the cage could be recycled without decomposing, we chose *t*-butanol and $CFCl_3$ as model guests for recycling experiments. *T*-butanol could be removed from *t*-butanol ⊂ cage **5.2** under reduced pressure. The clean cage could then be recovered and reused without subsequent purification.

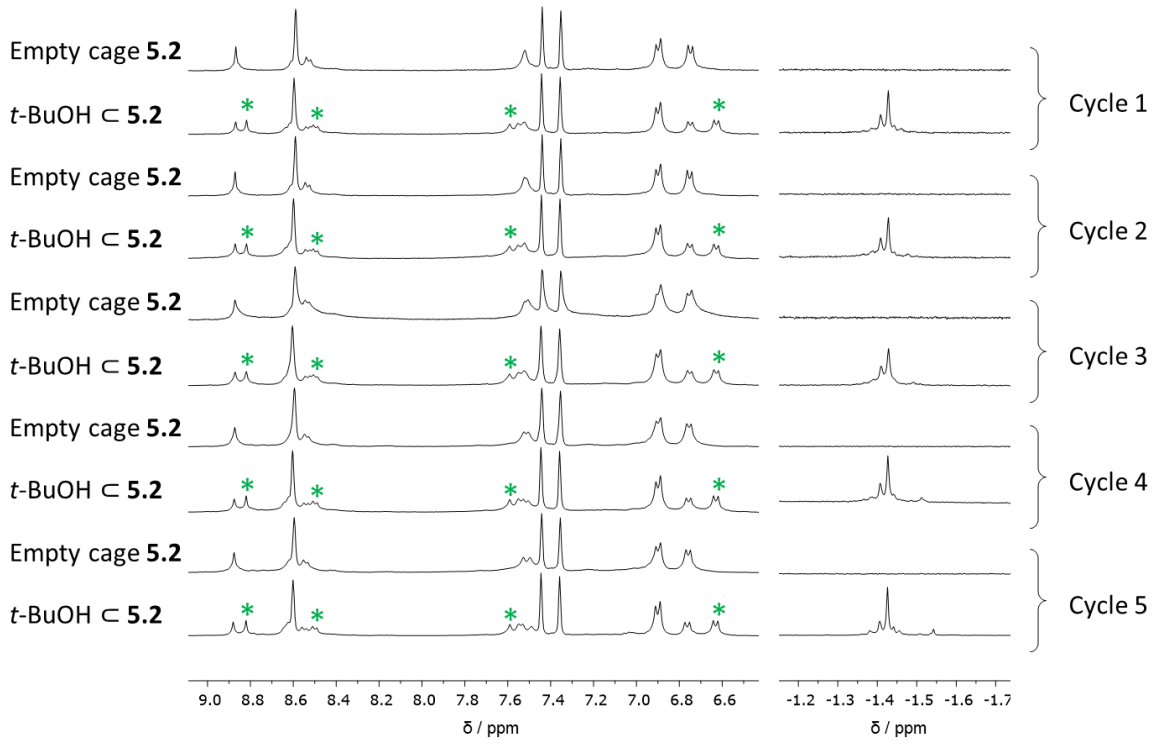

Figure 5.31: Recycling experiment for *t*-butanol ⊂ cage **5.2**. Partial ^{1}H NMR (400 MHz, 298 K, CD_3CN) spectra demonstrated that the guest could be encapsulated and then removed from the cage cavity 5 times without the cage showing significant signs of decomposition. Peaks correlated with the

formation of *t*-butanol ⊂ cage **5.2** were labelled with a green asterisk (*). The peaks below 0 ppm were indicative of encapsulated guest.

T-butanol (10 µL) was introduced to 0.5 mL of a 2 mM CD_3CN solution of cage **5.2**. The sample equilibrated at 298 K for 18 h and was then analyzed by ^1H NMR which confirmed the successful formation of the host-guest complex. The sample was then exposed to vacuum for 2 h, upon which the solvent and guest were removed. The residue was dissolved in CD_3CN and analyzed again by ^1H NMR to confirm the successful removal of the guest from the cage cavity. Upon confirmation that the free cage was regenerated, another 10 µL of *t*-butanol was added. We show below that *t*-butanol could be added and removed from cage **5.2** up to 5 times without signs of cage decomposition (Figure 5.31). These recycling experiments were repeated with $CFCl_3$ and the results indicated that clean cage **5.2** could also be repeatedly recovered from $CFCl_3 \subset$ **5.2** up to 5 times without significant cage decomposition (Figure 5.32).

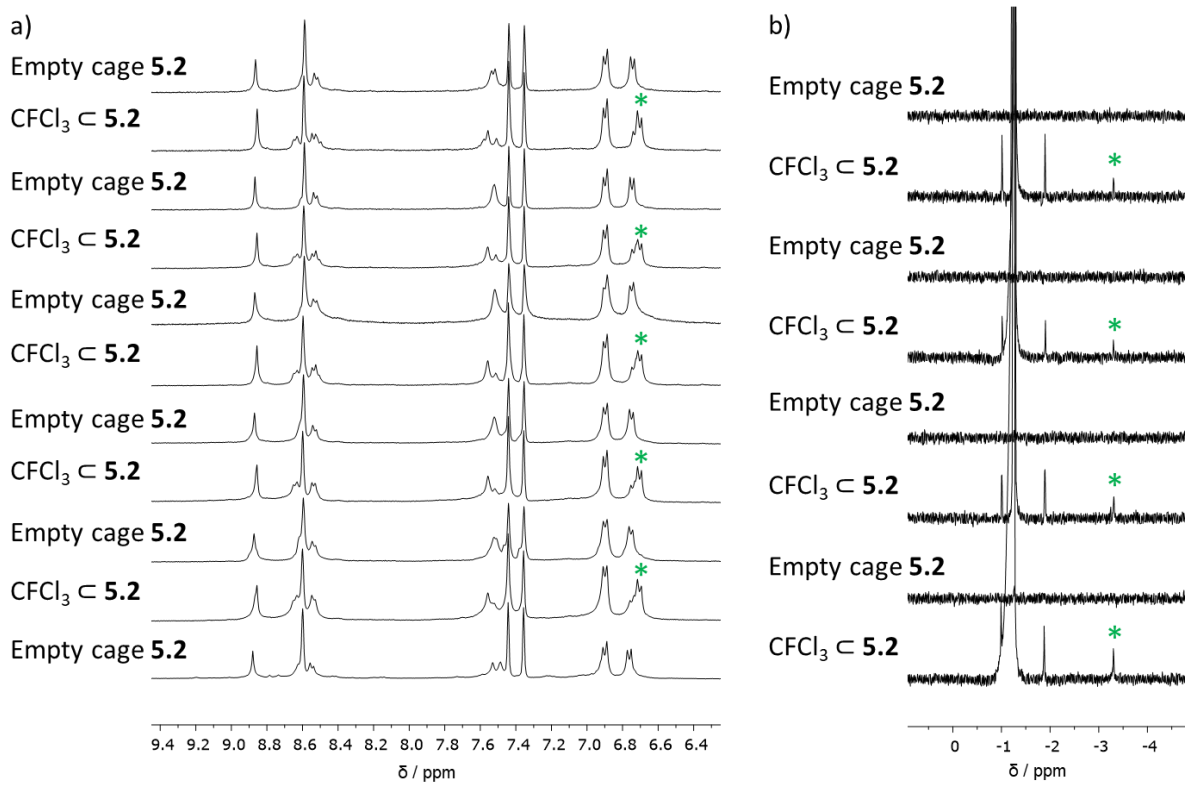

Figure 5.32: Recycling experiment for $CFCl_3 \subset$ cage **5.2**. a) Partial ^1H NMR (400 MHz, 298 K, CD_3CN) spectra demonstrated that the guest could be encapsulated and then removed from the cage cavity 5 times without the cage showing significant signs of decomposition. b) Partial ^{19}F NMR (377 MHz, 298 K, CD_3CN) spectra confirmed that the guest could be encapsulated and removed from the cavity of the cage. Peaks correlated with the formation of $CFCl_3 \subset$ cage **5.2** were labelled with a green asterisk (*).

5.9 Comparison of Cage 5.2 to Type II Porous Liquids

5.9.1 Cage 5.1 dissolved in a PEG_{1000}-imidazolium ionic liquid

While empty liquid cages qualify as Type I porous liquids, a Type II porous liquid based on coordination cages could potentially be prepared by directly dissolving a coordination cage in an ionic liquid. However, we hypothesized that our design of a liquid coordination cage maximized the porosity per quantity of the material, and that direct solvation of a cage in an ionic liquid could not generate a porous liquid with a pore concentration comparable to the liquid cage. To test this hypothesis, the following experiment was conducted. The weight percent of the cage scaffold present in liquid cage **5.2** was estimated to be 25.7%. This value was calculated by dividing the molecular weight of cage **5.1** (5142.8 g/mol) by the molecular weight of cage **5.2** (inferred to be 20,000 g mol^{-1} based upon the mean PEG molecular weight). We hypothesized that dissolving 25 wt% of cage **5.1** in a PEG_{1000}-imidazolium ionic liquid could potentially result in a system that is analogous to the neat liquid coordination cage. Therefore, cage **5.1** (25 wt%) was dissolved in 75 wt% of the PEG_{1000} ionic liquid and stirred for 18 h at 298 K, resulting in a heterogeneous mixture of cage and ionic liquid (Figure 5.33). We thus concluded that non-functionalized cage **5.1** does not dissolve in an analogous ionic liquid to generate a system with comparable porosity to our liquid coordination cage, helping to clarify the need for the synthetic complexity of cage **5.2**.

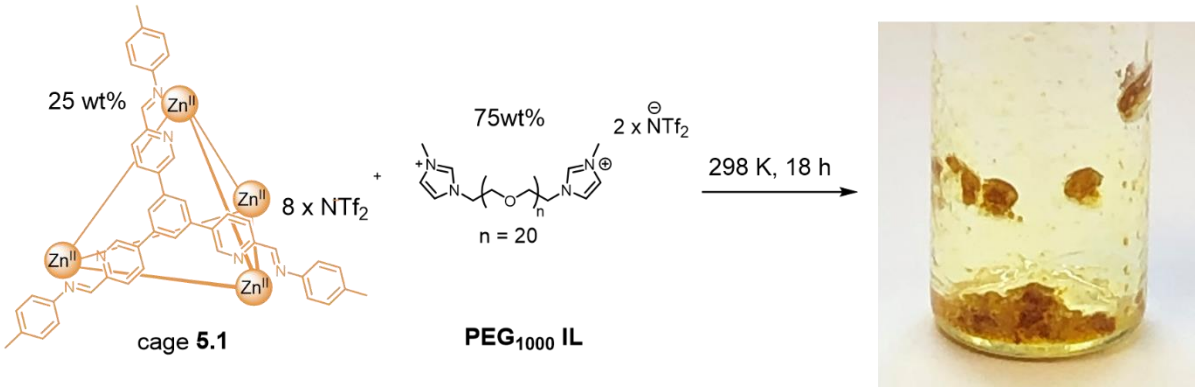

Figure 5.33: Cage **5.1** (25 wt%) suspended in PEG_{1000} ionic liquid (75%).

5.9.2 Stability of cage 5.2 under solvent-free conditions

A key difference between Type I and Type II porous liquids is their complexity. While a liquid coordination cage is more synthetically challenging to produce than dissolving a cage in an ionic liquid, we reduce the complexity of the overall system by eliminating the need for

an additional solvent. This simplification can be useful. For example, the stability of a Type I porous liquid would be solely dependent on the host while the stability of a Type II liquid would be dependent on both the host and the solvent. An example of stability issues with Type II porous liquids was previously observed in the host component of a Type II porous liquid from the Cooper group.[20] The cage was shown to be unstable in the sterically hindered solvent

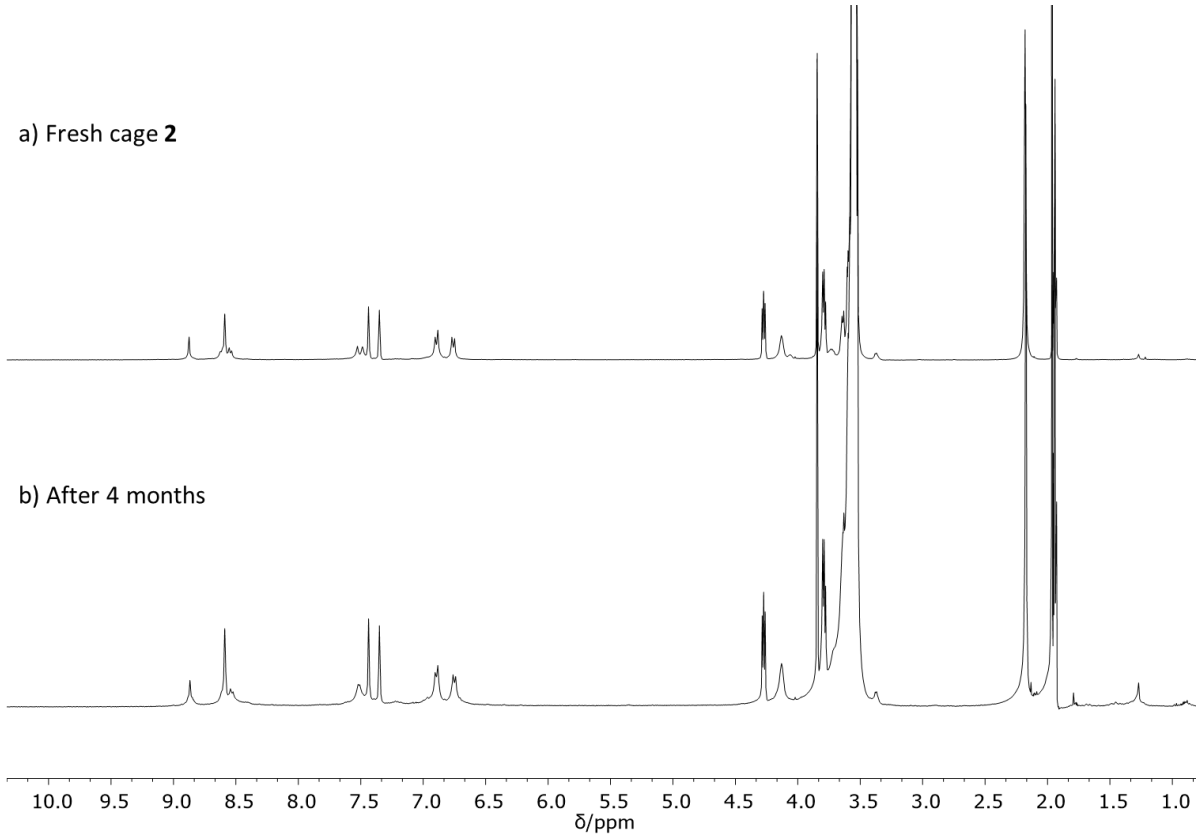

Figure 5.34: ^{1}H NMR (400 MHz, 298 K, CD_3CN) spectra of a) cage **5.2** after initial purification. b) Same sample of cage **5.2** after it was left under solvent-free conditions for 4 months.

over 30 days because the decomposition of the solvent generated acid which then compromised the structural integrity of the cage. In contrast, samples of our liquid coordination cage were kept in the neat state for months with no evidence of decomposition. The ^{1}H NMR spectrum of cage **5.2** in CD_3CN taken immediately after its synthesis and purification was compared against a ^{1}H NMR spectrum of the same sample after 4 months and minimal decomposition was observed (Figure 5.34).

5.10 Conclusions and Future Work

In this chapter, we present the first examples of Type I permanently porous liquids based on coordination cages. A new PEG-imidazolium aniline (**5F**) was synthesized and self-assembled with a number of different aldehyde-based subcomponents to give liquid tetrahedral and cubic cages at room temperature. Amongst these cages, cage **5.2** was further characterized with rheology, DSC/TGA and PALS. The rheological measurements indicated that **5.2** demonstrated fluid-like behavior and the results show that the viscosity of the material decreased as the temperatures increased. The TGA trace of **5.2** indicated that it had a high thermal stability and the reversible T_g below 0 °C observed in the DSC curve provided further evidence of the cage's liquid nature. PALS analysis showed that the experimentally determined cavity size of **5.2** was consistent with the calculated value of the cavity size in cage **5.1** – a result consistent with our hypothesis that cage **5.2** was empty in the neat state.

Cage **5.2** was demonstrated to bind CFCs and small alcohols shape-selectively in both the neat and solution-state. Empty cage **5.2** could also be recovered from its various host-guest complexes when exposed to vacuum. Based on these properties, future generations of liquid cage could be adapted into separation techniques used to differentiate between guests of varying shapes and sizes. This technique would be particularly useful in cases where isomers of the same molecule have different overall geometries but similar boiling points because distillation would be less effective than a shape-selective separation method. After successful separation, the guests could be removed from the cage by exposing the host-guest complex to reduce pressure and the empty cage could then be recovered and reused. While cage **5.2** could not be isolated from the host-guest complexes featured in this chapter, we anticipate that using a cage with stronger guest-binding behavior could overcome this problem.

Also, cage **5.2** is one of multiple liquid coordination cages. Future work includes investigating the physical and chemical properties of cages **5.4**, **5.6**, and **5.8**. Our knowledge of liquid coordination cages to this date is limited to only cage **5.2**. Therefore, there are many questions in this field still unanswered. Thus far, cage **5.2** has only been shown to encapsulate guests it already takes up in CH_3CN solution. One major question of interest is whether liquid cages can encapsulate guests in the neat state that would not otherwise be encapsulated in solution. The chemical environment surrounding the capsule of a liquid coordination cage in its neat state is very different from that of the same capsule in acetonitrile solution. Therefore, a variance in binding behavior is possible. Another area worthy of more investigation is

mixtures of liquid coordination cages. All examples of porous liquids to this date only feature a single type of host in the system, but a system with two or more hosts could open up many possibilities in which a combination of different pores could be simultaneously employed in the same material.

5.11 Experimental Methods

5.11.1 Synthesis of PEG-imidazolium-functionalized anilines

The experimental procedure for synthesizing subcomponent **5F** with PEG chain n = 20 is shown below. The synthesis for the n = 5 equivalent of the aniline (**5F'**) followed the same methods but polyethylene glycol (RMM = 1000 Da) was substituted with pentaethylene glycol.

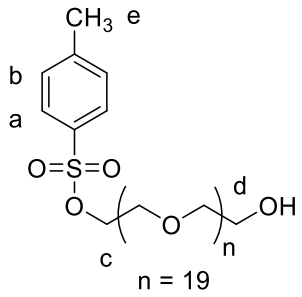

5A

*59-hydroxy-3,6,9,12,15,18,21,24,27,30,33,36,39,42,45,48,51,54,57-nonadecaoxanonapenta contyl 4-methylbenzenesulfonate **5A**:*

A solution of potassium hydroxide (0.49 g, 8.57 mmol, 3 equiv.) in water (7.5 mL) was added slowly to a solution of polyethylene glycol (RMM= 1000 Da, 20.20 g, 21 mmol, 7. equiv.) and 4-toluenesulfonyl chloride (0.55 g, 2.89 mmol, 1 equiv.) in THF (250 mL). The mixture was stirred for 18 h at 298 K. Water (250 mL) was added and the reaction mixture was extracted with DCM (3 x 100 mL). The organic layer was dried over $MgSO_4$, gravity filtered, and the solvent was removed by rotary evaporation. The crude product was purified by flash column chromatography (SiO_2 chloroform/methanol 99:1 to 95:5, v/v) which afforded the desired product **5A** (2.1 g, 78%) as a white wax/oil. ^{1}H NMR (400 MHz, $CDCl_3$): δ = 7.79 (d, J = 8.1 Hz, 2H, H_a), δ = 7.33 (d, J = 8.1 Hz, 2H, H_b), δ = 4.15 (t, J = 4.8 Hz, 2H, H_c), δ = 3.65 (m, 80H, H_d, $H_{aliphaticPEG}$), δ = 2.44 (s, 3H, H_e). ^{13}C NMR (100 MHz, $CDCl_3$): δ = 144.8, 133.0, 129.8 128.00, 72.6, 70.7, 70.6, 70.6, 70.5, 70.3, 69.2, 68.7, 61.7, 21.6 ppm. LR-MS (ESI, CH_3CN): n = 15-20 $[M\text{-}OH]^+$, *m/z* = 861.47, 905.49, 949.52, 993.55, 1037.58, 1081.60.

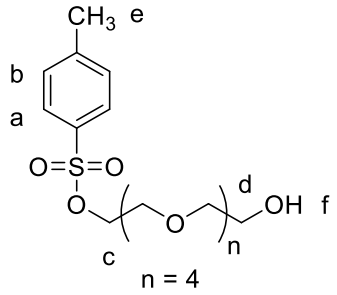

5A'

*14-hydroxy-3,6,9,12-tetraoxatetradecyl 4-methylbenzenesulfonate **5A'***:

^{1}H NMR (400 MHz, $CDCl_3$): δ = 7.79 (d, J = 8.16 Hz, 2H, H_a), δ = 7.33 (d, J = 8.2 Hz, 2H, H_b), δ = 4.15 (t, J = 4.8 Hz, 2H, H_c), δ = 3.65 (m, 21H, H_d, $H_{aliphaticPEG}$), δ = 2.44 (s, 3H, H_e), δ = 2.17 (s, 1H, H_e). ^{13}C NMR (100 MHz, $CDCl_3$): δ = 144.8, 133.0, 129.9, 128.0, 77.5, 77.2, 76.8, 72.5, 72.5, 70.8, 70.6, 70.6, 70.6, 70.5, 70.4, 69.3, 68.7, 61.7, 61.7, 21.7 ppm. HR-MS (ESI) theoretical calculation $C_{17}H_{29}O_8S$, *m/z* = 393.1505 $[M+H]^+$, experimental result *m/z* = 393.1608 $[M+H]^+$.

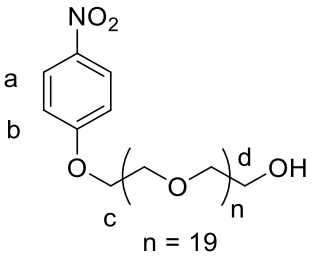

5B

*59-(4-nitrophenoxy)-3,6,9,12,15,18,21,24,27,30,33,36,39,42,45,48,51,54,57-nonadecaoxanonapentacontan-1-ol **5B**:*

A solution of precursor **5A** (1.0 g, 1.00 mmol, 1 equiv.), 4-nitrophenol (278.22 mg, 2.00 mmol, 2 equiv.) and potassium carbonate (691.00 mg, 5.00 mmol, 5 equiv.) in dry CH_3CN (10 mL) was heated at 70 °C under N_2 for 18 h. The yellow suspension was filtered off and the solid was washed with CH_3CN (60 mL). The extract and washes were concentrated via rotary evaporation. The residue was extracted with DCM (3 x 25 mL). The organic phase was washed with water (6 x 150 mL). The organic layer was dried over $MgSO_4$, gravity filtered, and the solvent was removed by rotary evaporation to afford the product **5B** (800 mg, 80%) as a yellow oil. ^{1}H NMR (400 MHz, $CDCl_3$): δ = 8.19 (d, J = 9.3 Hz, 2H, H_a), δ = 6.98 (d, J = 9.3 Hz, 2H, H_b), δ = 4.22 (t, 2H, J = 4.5 Hz, H_c), δ = 3.89 (t, J = 4.5 Hz, 2H, H_d), δ = 3.65 (m, 80H,

$H_{aliphaticPEG}$). ^{13}C NMR (100 MHz, $CDCl_3$): δ = 164.0, 141.7, 126.0, 114.7, 72.7, 71.0, 70.7, 70.7, 70.7, 70.7, 70.4, 69.5, 68.3, 61.8, 53.6 ppm. LR-MS (ESI, CH_3CN): n = 16-25 $[M+H]^+$, *m/z* =844.46, 88.48, 932.51, 975.52, 1020.56, 1064.59, 1108.63, 1152.65, 1196.67, 1240.7.

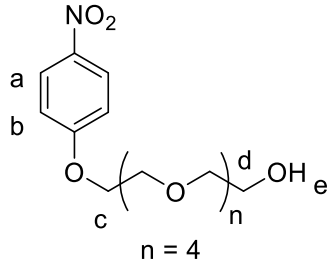

14-(4-nitrophenoxy)-3,6,9,12-tetraoxatetradecan-1-ol ***5B':***

^1H NMR (400 MHz, $CDCl_3$): δ = 8.19 (d, *J* = 9.3 Hz, 2H, H_a), δ = 6.99 (d, *J* = 9.3 Hz, 2H, H_b), δ = 4.23 (t, *J* = 4.5 Hz, 2H, H_c), δ = 3.89 (t, *J* = 4.8 Hz, 2H, H_d), δ = 3.70 (m, 17H, $H_{aliphaticPEG}$), δ = 2.21 (s, 1H, H_e). ^{13}C NMR (100 MHz, $CDCl_3$): δ = 163.9, 141.6, 125.9, 114.6, 72.6, 70.9, 70.9, 70.6, 70.6, 70.6, 70.5, 70.3, 69.4, 68.2, 61.7 ppm. HR-MS (ESI) theoretical calculation $C_{16}H_{26}NO_8$, *m/z* = 360.1658 $[M+H]^+$, experimental result *m/z* = 360.1565 $[M+H]^+$.

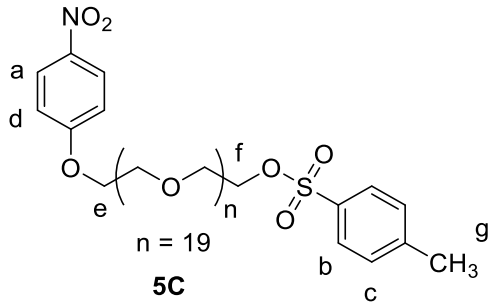

59-(4-nitrophenoxy)-3,6,9,12,15,18,21,24,27,30,33,36,39,42,45,48,51,54,57-nonadecaoxanonapentacontyl 4-methylbenzenesulfonate ***5C:***

A solution of potassium hydroxide (0.84 g, 3.20 mmol, 4 equiv.) in water (5 mL) was added slowly to a solution of precursor **5B** (1.88 g, 0.80 mmol, 1 equiv.) and 4-toluenesulfonyl chloride (1.43 g, 2.00 mmol, 2.5 equiv.) in THF (20 mL). The mixture was stirred for 18 h at 298 K. Water (150 mL) was added and the reaction mixture was extracted with DCM (3 x 100 mL). The organic layer was dried over $MgSO_4$ and the solvent was removed by rotary evaporation. The crude product was purified by flash column chromatography (SiO_2,

DCM/MeOH 100:0 to 90:10, v/v) and afforded the product **5C** (1.21 g, 67%) as yellow oil. ^{1}H NMR (400 MHz, $CDCl_3$): δ = 8.18 (d, 2H, J = 9.3 Hz, H_a), δ = 7.78 (d, J = 8.3 Hz, 2H, H_b), δ = 7.33 (d, J = 8.3 Hz, 2H, H_c), δ = 6.97 (d, J = 9.3 Hz, 2H, H_d), δ = 4.21 (t, J = 4.6 Hz, 2H, H_e), δ = 4.14 (t, J = 4.7 Hz, 2H, H_f), δ = 3.65 (m, 90H, $H_{aliphaticPEG}$), δ = 2.43 (s, 3H, H_g). ^{13}C NMR (100 MHz, $CDCl_3$): δ = 164.0, 145.0, 133.1, 129.9, 128.1, 126.0, 114.7, 71.0, 70.9, 70.8, 70.7, 70.7, 70.6, 69.5, 69.4, 68.8, 68.3, 21.8 ppm. LR-MS (ESI, CH_3CN): n = 14-25 $[M+K]^+$, *m/z* =992.35, 1036.51, 1080.67, 1124.63, 1168.58, 1212.53, 1256.44, 1300.80, 1344.66, 1389.50, 1432.69, 1479.78.

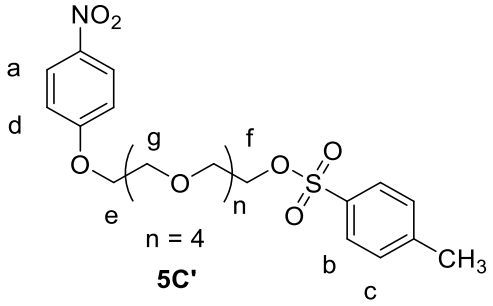

*14-(4-nitrophenoxy)-3,6,9,12-tetraoxatetradecyl 4-methylbenzenesulfonate **5C':***

^{1}H NMR (400 MHz, $CDCl_3$): δ = 8.14 (d, J = 9.2 Hz, 2H, H_a), δ = 7.75 (d, J = 8.3 Hz, 2H, H_b), δ = 7.31 (d, J = 8.3 Hz, 2H, H_c), δ = 6.95 (d, J = 9.2 Hz, 2H, H_d), δ = 4.20 (t, 2H, J = 4.6 Hz, H_e), δ = 4.12 (t, J = 4.7 Hz, 2H, H_f), δ = 3.86 (t, J = 4.8 Hz, 2H, H_g), δ = 3.64 (m, 14H, $H_{aliphaticPEG}$), δ = 2.41 (s, 3H, H_h). ^{13}C NMR (100 MHz, $CDCl_3$): δ = 163.9, 144.9, 141.6, 133.0, 129.9, 128.0, 125.9, 114.7, 70.9, 70.8, 70.6, 70.6, 70.5, 69.4, 69.3, 68.7, 68.3, 21.7 ppm. HR-MS (ESI) theoretical calculation $C_{20}H_{30}N_3O_7$, *m/z* = 514.1747 $[M\text{-}OTs]^+$, experimental result *m/z* = 514.1765 $[M\text{-}OTs]^+$.

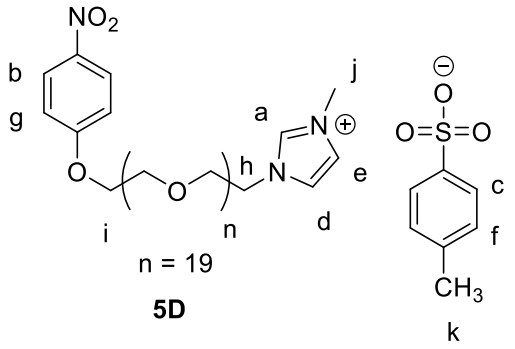

5D

3-methyl-1-(59-(4-nitrophenoxy)-3,6,9,12,15,18,21,24,27,30,33,36,39,42,45,48,51,54,57-nonadecaoxanonapentacontyl)-1H-imidazol-3-ium 4-methylbenzenesulfonate ***5D****:*

1-methylimidazole (167.48 mg 2.04 mmol, 3 equiv.) was added to solution of precursor **5C** (680.20 mg, 0.68 mmol, 1 equiv.) in CH_3CN (5 mL). The mixture was heated at 65 °C under N_2 for 18 h. The solvent was removed by rotary evaporation and the residue was washed with diethyl ether (3 x 75 mL). The bottom layer was dried under vacuum, to afford the desired product **5D** (502.10 mg, 85%) as a yellow oil. The product was used without purification. ^{1}H NMR (400 MHz, $CDCl_3$): δ = 9.78 (s, 1H, H_a), δ = 8.20 (d, J = 9.2 Hz, 2H, H_b), δ = 7.79 (d, J = 8.2 Hz, 2H, $H_{cTosylate}$), δ = 7.65 (s, 1H, H_d), δ = 7.27 (s, 1H, H_e), δ = 7.15 (d, J = 8.0 Hz, 2H, $H_{fTosylate}$), δ = 6.98 (d, J = 9.3 Hz, 2H, H_g), δ = 4.52 (t, J = 4.5 Hz, 2H, H_h), δ = 4.22 (t, J = 4.6 Hz, 2H, H_i), δ = 4.00 (s, 3H, H_j), δ = 3.87 (m, 76H, $H_{aliphaticPEG}$), δ = 2.23 (s, 3H, $H_{kTosylate}$). ^{13}C NMR (100 MHz, $CDCl_3$): δ = 164.0, 143.5, 141.6, 139.3, 138.2, 128.6, 125.9, 125.9, 123.7, 122.7, 114.6, 70.9, 70.6, 70.5, 70.5, 70.4, 70.4, 70.3, 70.2, 70.1, 69.4, 69.1, 68.2, 49.6, 36.3, 21.3 ppm. LR-MS (ESI, CH_3CN): n = 17-25 $[M\text{-}OTs]^+$, *m/z* = 908.37, 952.41, 996.44, 1040.48, 1084.50, 1128.54, 1172.55, 1216.57, 1260.58, 1304.60.

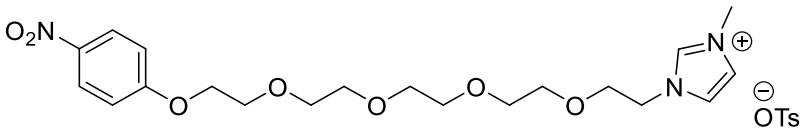

5D'

3-methyl-1-(14-(4-nitrophenoxy)-3,6,9,12-tetraoxatetradecyl)-1H-imidazol-3-ium 4-methylbenzenesulfonate ***5D'****:* The crude product was used in the following step without additional purification or characterization.

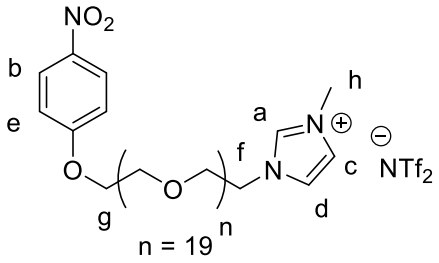

5E

*3-methyl-1-(59-(4-nitrophenoxy)-3,6,9,12,15,18,21,24,27,30,33,36,39,42,45,48,51,54,57-nonadecaoxanonapentacontyl)-1H-imidazol-3-ium bis((trifluoromethyl)sulfonyl)imide **5E**:*

Bis(trifluoromethane)sulfonimide lithium salt (152.63 mg, 0.52 mmol, 1.5 equiv.) was added to solution of precursor **5D** (400.00 mg, 0.34 mmol, 1 equiv.) in water (5 mL). The mixture was stirred for 2 h at room temperature. Dichloromethane (60 mL) was added and the organic phase was washed with water (3 x 25 mL). The organic layer was dried over $MgSO_4$, gravity filtered, and the solvent was removed by rotary evaporation, to afford the desired ligand **5E** (402.10 mg, 90%) as yellow oil. ^{1}H NMR (400 MHz, $CDCl_3$): δ = 8.93 (s, 1H, H_a), δ = 8.19 (d, J = 9.2 Hz, 2H, H_b), δ = 7.58 (s, 1H, H_c), δ = 7.39 (s, 1H, H_d), δ = 6.99 (d, J = 8.3 Hz, 2H, H_e), δ = 4.37 (t, J = 4.4 Hz, 2H, H_f), δ = 4.22 (t, J = 4.6 Hz, 2H, H_g), δ = 3.96 (s, 3H, H_h), δ = 3.87 (m, 76H, $H_{aliphaticPEG}$). ^{13}C NMR (100 MHz, $CDCl_3$): δ = 164.0, 141.6, 137.0, 125.9, 123.5, 123.4, 121.5, 118.3, 114.7, 71.0, 70.7, 70.6, 70.6, 70.6, 70.5, 70.5, 70.4, 70.3, 70.2, 69.4, 68.6, 68.3, 53.6, 49.8, 36.4 ppm. ^{19}F NMR (377 MHz, $CDCl_3$, referenced to hexafluorobenzene in a C_6F_6 capillary): δ = -79.97 (NTf_2^-). LR-MS (ESI, CH_3CN): n = 17-25 $[M\text{-}NTf_2]^+$, *m/z* = 908.37, 952.41, 996.44, 1040.48, 1084.50, 1128.54, 1172.55, 1216.57, 1260.58, 1304.60.

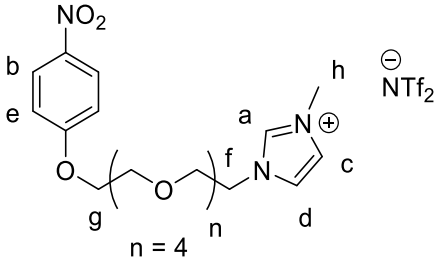

5E

*3-methyl-1-(14-(4-nitrophenoxy)-3,6,9,12-tetraoxatetradecyl)-1H-imidazol-3-ium bis((trifluoromethyl)sulfonyl)imide **5E'**:* ^{1}H NMR (400 MHz, $CDCl_3$): δ = 8.86 (s, 1H, H_a), δ = 8.18 (d, J = 8.3 Hz, 2H, H_b), δ = 7.48 (s, 1H, H_c), δ = 7.2 (s, 1H, H_d), δ = 6.97 (d, J = 8.3 Hz, 2H, H_e), δ = 4.34 (t, J = 4.5 Hz, 2H, H_f), δ = 4.19 (t, J = 4.4 Hz, 2H, H_g), δ = 3.93 (s, 3H, H_h),

δ = 3.87 (m, 16H, $H_{aliphaticPEG}$). ^{13}C NMR (100 MHz, $CDCl_3$): δ = 164.0, 141.8, 137.0, 126.1, 123.7, 123.0, 121.5, 118.3, 114.8, 71.0, 70.6, 70.6, 70.4, 70.3, 70.3, 69.5, 68.6, 68.4, 50.0, 36.5 ppm. ^{19}F NMR (377 MHz, $CDCl_3$, referenced to hexafluorobenzene in a C_6F_6 capillary): δ = -80.12 (NTf_2^-). HR-MS (ESI) theoretical calculation $C_{20}H_{30}N_3O_7$, *m/z* = 424.2084 $[M\text{-}NTf_2]^+$, experimental result *m/z* = 424.2110 $[M\text{-}NTf_2]^+$.

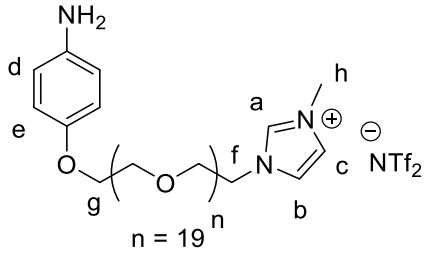

5F

*1-(59-(4-aminophenoxy)-3,6,9,12,15,18,21,24,27,30,33,36,39,42,45,48,51,54,57-nonadecaoxanonapentacontyl)-3-methyl-1H-imidazol-3-ium bis((trifluoromethyl)sulfonyl)imide **5F**:*

A solution of precursor **5E** (500 mg, 1 equiv.), Pd/C (100 mg, 20 wt%) in MeOH (10 mL) was stirred for 6h under H_2. The mixture was filtered through Celite and the solvent was removed by rotary evaporation, affording the final ligand **5F** (435 mg, 87%) as a yellow oil. ^{1}H NMR (400 MHz, $CDCl_3$): δ = 8.60 (s, 1H, H_a), δ = 7.44 (s, 1H, H_b), δ = 7.36 (s, 1H, H_c), δ = 6.70 (d, 2H, *J* = 8.8 Hz, H_d), δ = 6.57 (d, *J* = 8.8 Hz, 2H, H_e), δ = 4.27 (t, *J* = 4.6 Hz, 2H

, H_f), δ = 3.97 (t, *J* = 4.6 Hz, 2H, H_g), δ = 3.84 (s, 3H, H_h), δ = 3.57 (m, 76H, $H_{aliphaticPEG}$). ^{13}C NMR (100 MHz, $CDCl_3$): δ = 152.0, 142.9, 137.7, 124.2, 123.9, 118.3, 116.5, 71.3, 71.2, 71.1, 71.1, 71.0, 71.0, 70.9, 70.5, 69.2, 69.0, 50.5, 36.9 ppm. ^{19}F NMR (377 MHz, $CDCl_3$, referenced to hexafluorobenzene in a C_6F_6 capillary): δ = -79.93 (NTf_2^-). LR-MS (ESI, CH_3CN): n = 14-30 $[M\text{-}NTf_2]^+$, *m/z* = 790.52, 834.48, 878.52, 922.56, 966.57, 1010.60, 1054.67, 1098.73, 1142.71, 1186.74, 123.84, 1274.87, 1318.88, 1362.64, 1406.96, 1450.92, 1495.87; n = 15-29 $[M\text{-}NTf_2\text{+}H]^{2+}$, *m/z* = 417.83, 439.77, 461.80, 483.81, 505.84, 527.87, 549.88, 571.92, 593.88, 615.92, 637.92, 659.96, 681.97, 704.02, 726.01.

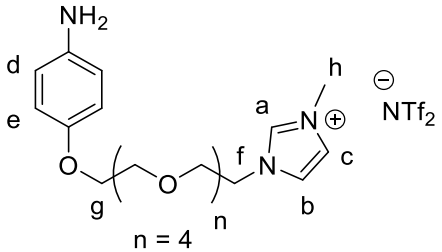

5F'

1-(14-(4-aminophenoxy)-3,6,9,12-tetraoxatetradecyl)-3-methyl-1H-imidazol-3-ium bis((trifluoromethyl)sulfonyl)imide ***5F':*** ^{1}H NMR (400 MHz, $CDCl_3$): δ = 8.53 (s, 1H, H_a), δ = 7.39 (s, 1H, H_b), δ = 7.28 (s, 1H, H_c), δ = 6.67 (d, J = 8.9 Hz, 2H, H_d), δ = 6.58 (d, J = 8.9 Hz, 2H, H_e), δ = 4.22 (t, J = 4.7 Hz, 2H, H_f), δ = 3.95 (t, J = 4.4 Hz, 2H, H_g), δ = 3.81 (s, 3H, H_h), δ = 3.59 (m, 76H, $H_{aliphaticPEG}$). ^{13}C NMR (100 MHz, $CDCl_3$): δ = 152.1, 142.4, 137.6, 124.2, 123.9, 116.8, 116.5, 71.3, 71.1, 71.1, 71.0, 71.0, 70.9, 70.5, 69.2, 69.0, 50.5, 36.9 ppm. ^{19}F NMR (377 MHz, $CDCl_3$, referenced to hexafluorobenzene in a C_6F_6 capillary): δ = -80.52 (NTf_2^-). HR-MS (ESI) theoretical calculation $C_{20}H_{32}N_3O_5$, *m/z* = 394.2342 $[M\text{-}NTf_2]^+$, experimental result *m/z* = 394.2341 $[M\text{-}NTf_2]^+$.

5.11.2 Self-assembly of cages 5.1-5.3

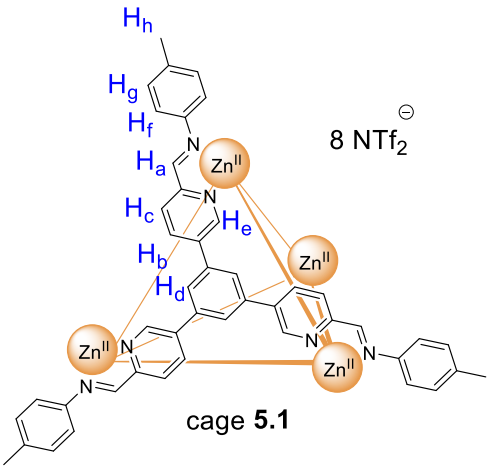

Cage **5.1**:

Cage **5.1** was assembled a *via* published procedure.[4] The NMR analysis of this material was consistent with published results. ^{1}H NMR (400 MHz, CD_3CN): δ = 8.85 (s, 1H, H_a), 8.60 (dd, 1H, J = 8.3, 2.1 Hz, H_b), 8.54 (d, 1H, J = 8.2 Hz, H_c), 7.55 (s, 1H, H_d), 7.52 (d, 1H, J = 2.1 Hz, H_e), 7.16 (d, 2H, J = 8.1 Hz, H_f), 6.48 (d, 2H, J = 8.3 Hz, H_g), 2.38 (s, 3H, H_h).

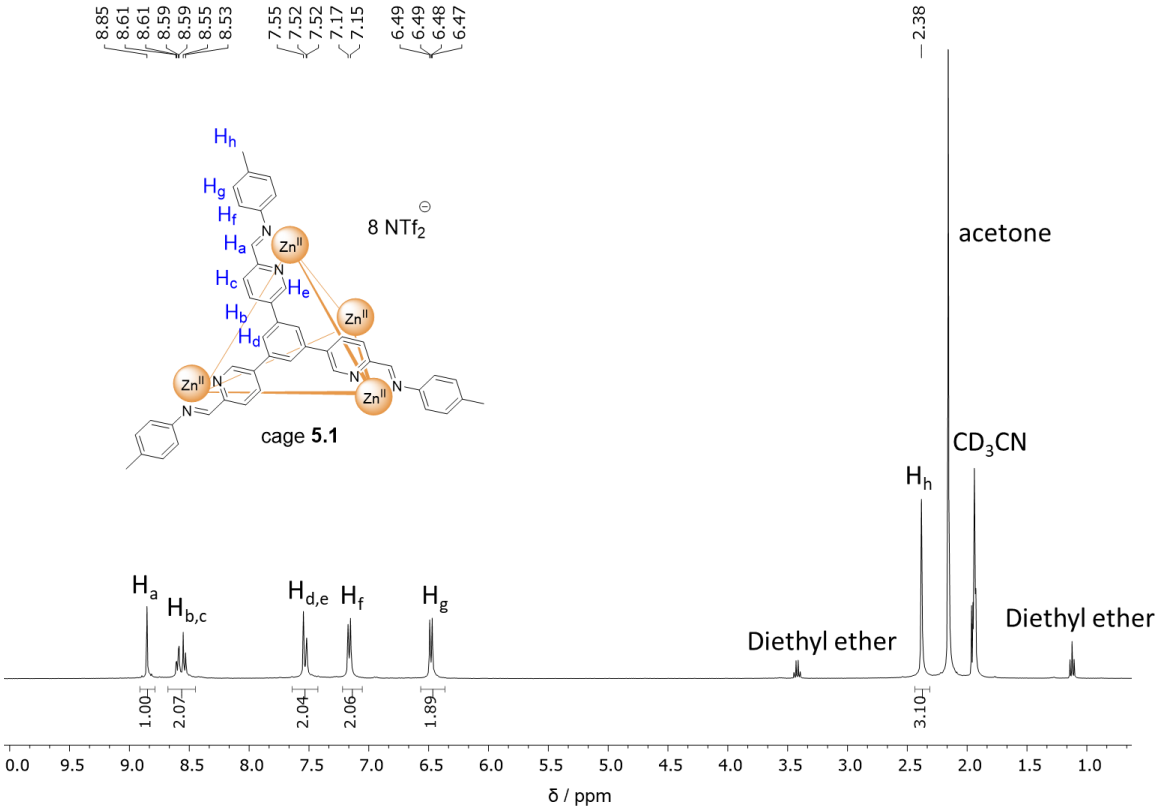

Figure 5.35: ^{1}H NMR (400 MHz, CD_3CN) spectrum of cage **5.1**.

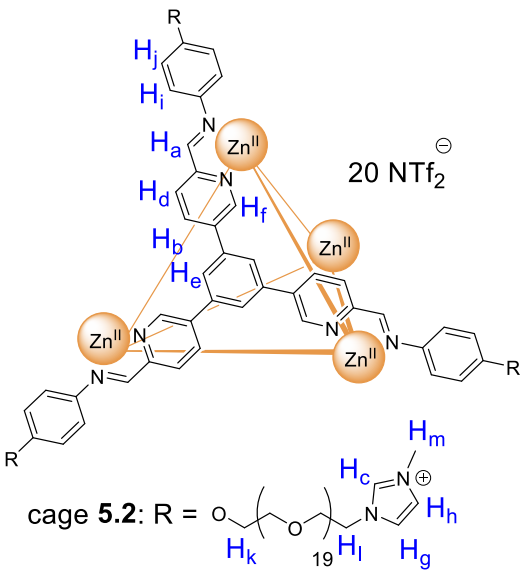

Cage **5.2**

Trialdehyde **5H** (15.72 mg, 0.070 mmol, 4 equiv.) and aniline **5F** (156.00 mg, 0.12 mmol, 12 equiv., added as a stock solution in 3 mL CH_3CN) were combined and heated in a microwave reactor at 100 °C for 10 minutes. $Zn(NTf_2)_2$ (27.53 mg, 0.044 mmol, 4.4 equiv, added as a stock solution in 3 mL CH_3CN) was added to the solution then heated for an additional 10 minutes at 100 °C in the microwave reactor. The cage was precipitated out of solution *via* the addition of diethyl ether (5 mL) and centrifuged. The resulting oil was concentrated under reduced pressure yielding a dark yellow, viscous liquid (172 mg, 88% yield).

^{1}H NMR (400 MHz, CD_3CN): δ = 8.91 (s, 1H, H_a), δ = 8.63 (s, 2H, $H_{b,c}$), δ = 8.57 (d, 1H, J = 8.0 Hz, H_d), δ = 7.56 (s, 1H, H_e), δ = 7.52 (s, 1H, H_f), δ = 7.47 (s, 1H, H_g), δ = 7.39 (s, 1H, H_h), δ = 6.93 (d, J = 8.4 Hz, 2H, H_i), δ = 6.79 (d, J = 8.4 Hz, 2H, H_j), δ = 4.31 (t, J = 4.8 Hz, 2H, H_f), δ = 4.16 (t, J = 4.7 Hz, 2H, H_l), δ = 3.87 (s, 3H, H_m), δ = 3.58 (m, 118H, $H_{aliphaticPEG}$). ^{13}C NMR (125 MHz, CD_3CN): δ = 163.4, 160.5, 148.1, 146.1, 140.9, 139.5, 139.1, 137.7, 132.7, 126.7, 124.8, 124.6, 124.2, 123.8, 122.0, 119.5, 118.3, 117.0, 116.5, 116.3, 71.3, 71.2, 71.1, 71.1, 71.1, 71.0, 71.0, 71.0, 71.0, 71.0, 70.8, 70.0, 69.2, 68.9, 50.4, 36.8 ppm. ^{19}F NMR (377 MHz, CD_3CN, referenced to hexafluorobenzene in a C_6F_6 capillary): δ = -80.52 (NTf_2^-).

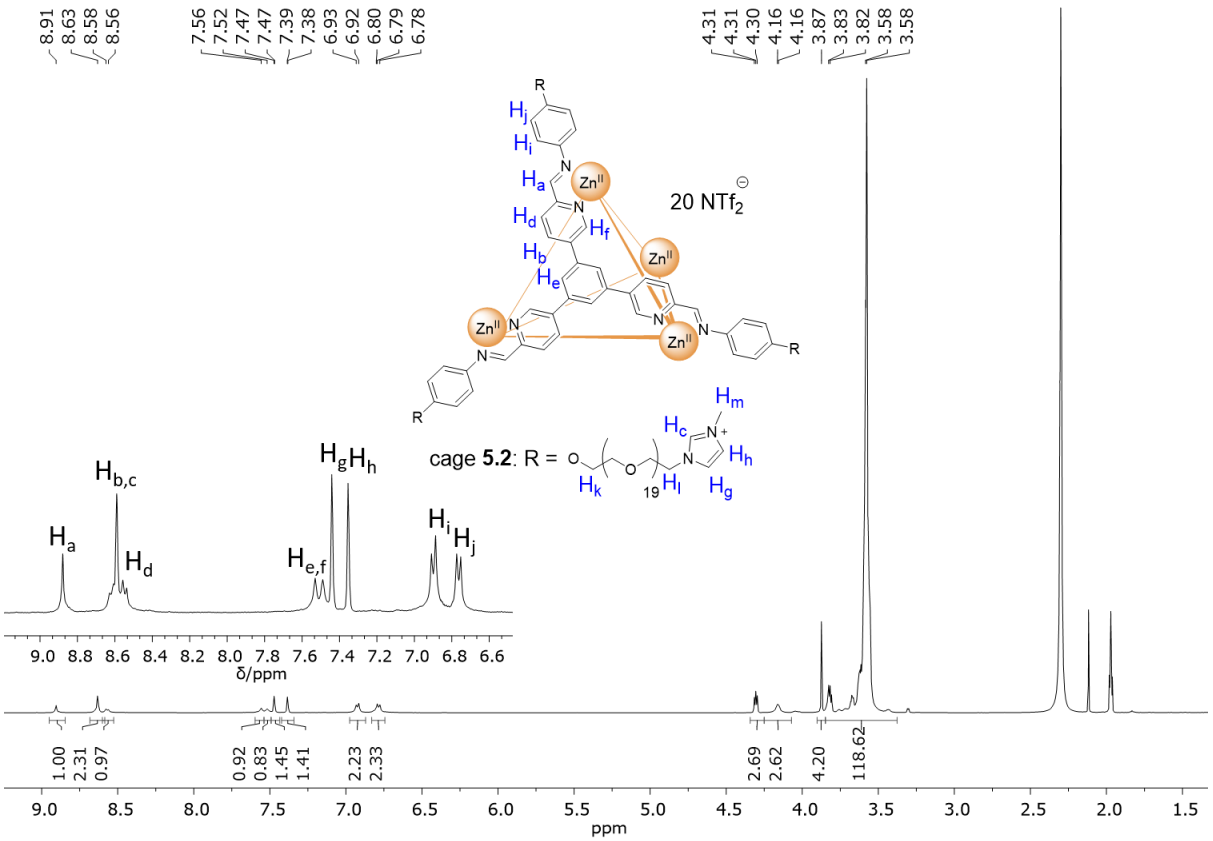

Figure 5.36: ^{1}H NMR (400 MHz, CD_3CN) spectrum of cage **5.2**.

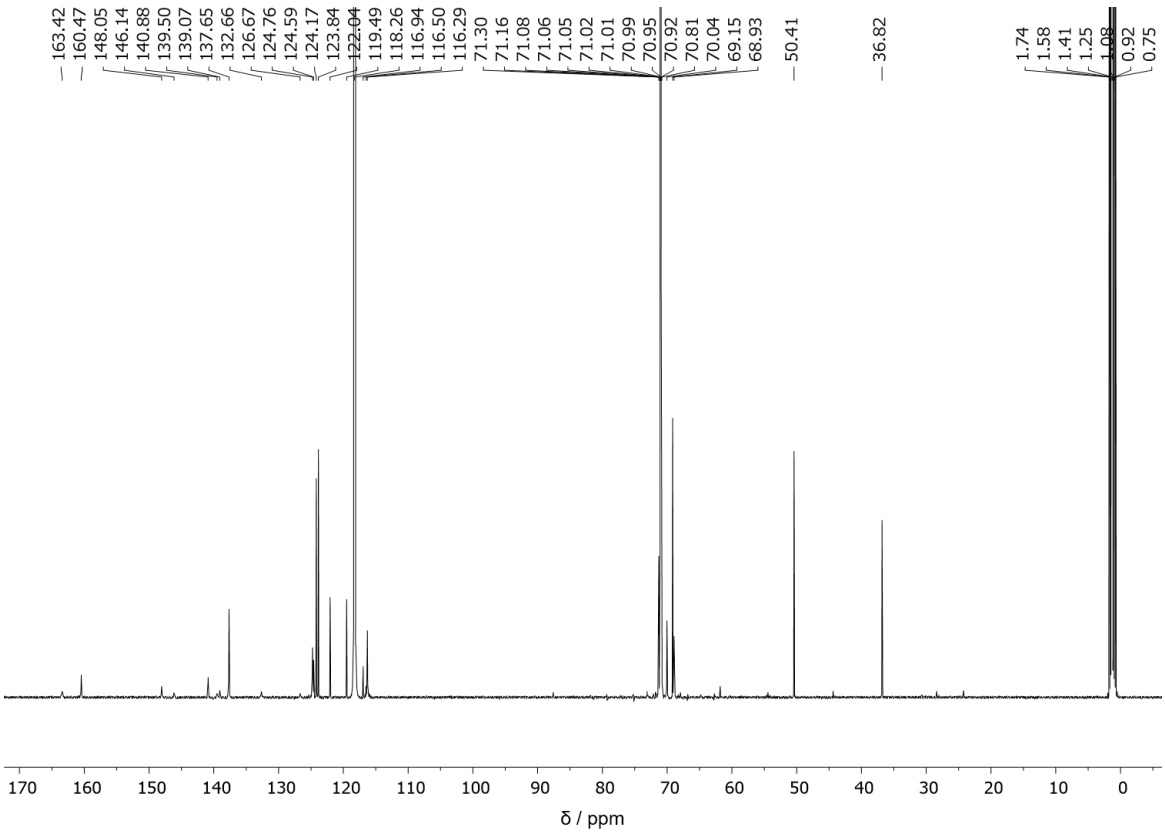

Figure 5.37: ^{13}C NMR (125 MHz, CD_3CN) spectrum of cage **5.2**.

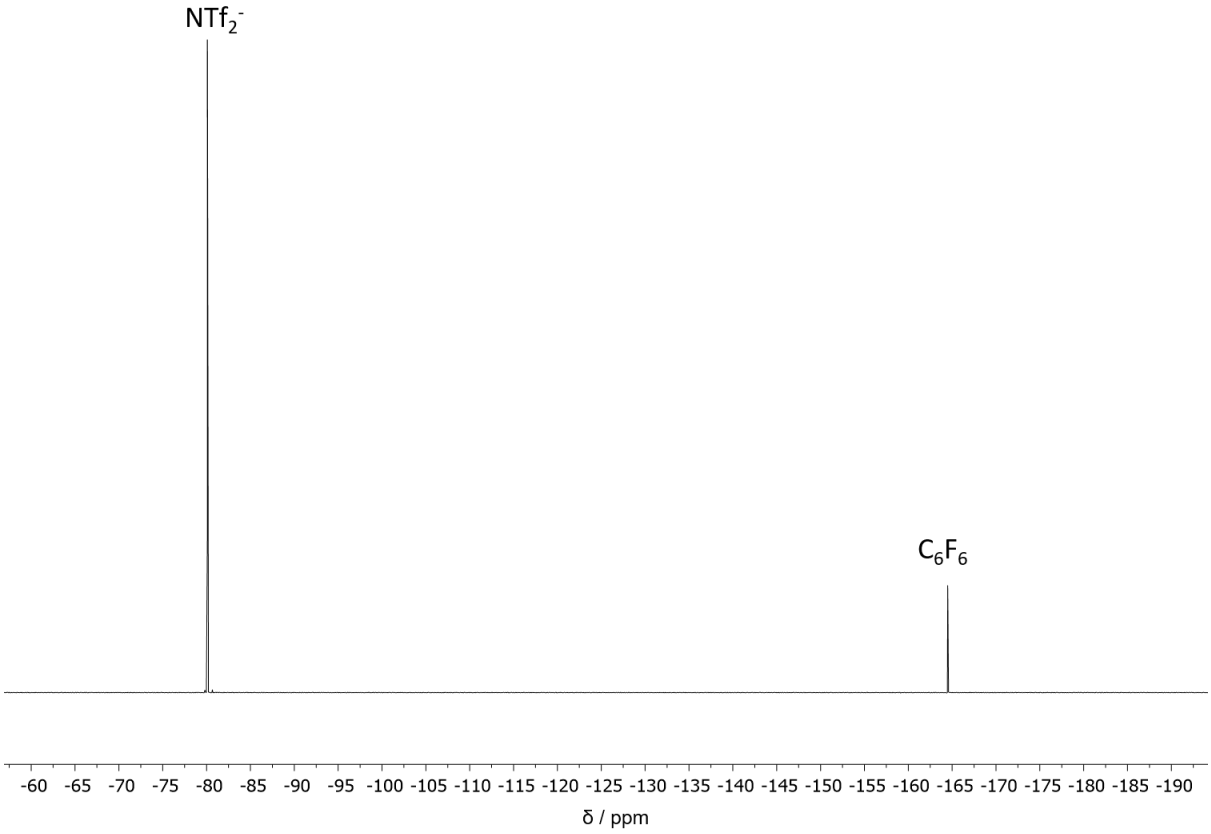

Figure 5.38: ^{19}F NMR (377 MHz, CD_3CN) spectrum of cage **5.2** with a C_6F_6 reference capillary.

Cage **5.3** was synthesized with the same method as cage **5.2** by replacing aniline **5F** with **5F'**.

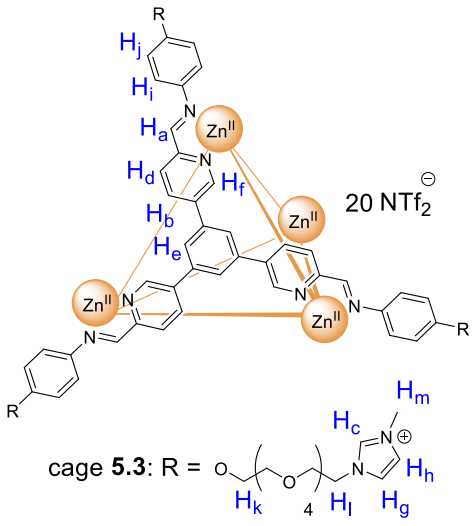

Cage **5.3**:

^{1}H NMR (400 MHz, CD_3CN): δ = 8.88 (s, 1H, H_a), δ = 8.64 (d, J = 8.47 Hz, 1H, H_b), δ = 8.56 (s, 1H, H_c), δ = 8.54 (s 1H, H_d), δ = 7.54 (s, 1H, H_e), δ = 7.50 (s, 1H, H_f), δ = 7.41 (t, J = 1.7 Hz, 1H, H_g), δ = 7.32 (t, J = 1.6 Hz, 1H, H_h), δ = 6.87 (d, J = 9.1 Hz, 2H, H_i), δ = 6.77 (d, J = 9.1 Hz, 2H, H_j), δ = 4.25 (t, J = 4.6 Hz, 2H, H_f), δ = 4.10 (t, J = 4.6 Hz, 2H, H_l), δ = 3.78 (m, 22H, $H_{aliphaticPEG}$). ^{13}C NMR (125 MHz, CD_3CN): δ = 162.6, 159.5, 153.8, 147.1, 145.2, 140.1, 138.6, 138.2, 136.8, 136.5, 131.8, 123.9, 123.2, 123.0, 121.1, 118.6, 115.3, 70.4, 70.1, 70.7, 70.1, 70.0, 70.0, 69.9, 69.1, 68.2, 68.0, 49.5, 35.9 ppm. ^{19}F NMR (377 MHz, CD_3CN, referenced to hexafluorobenzene in a C_6F_6 capillary): δ = -80.52 (NTf_2^-).

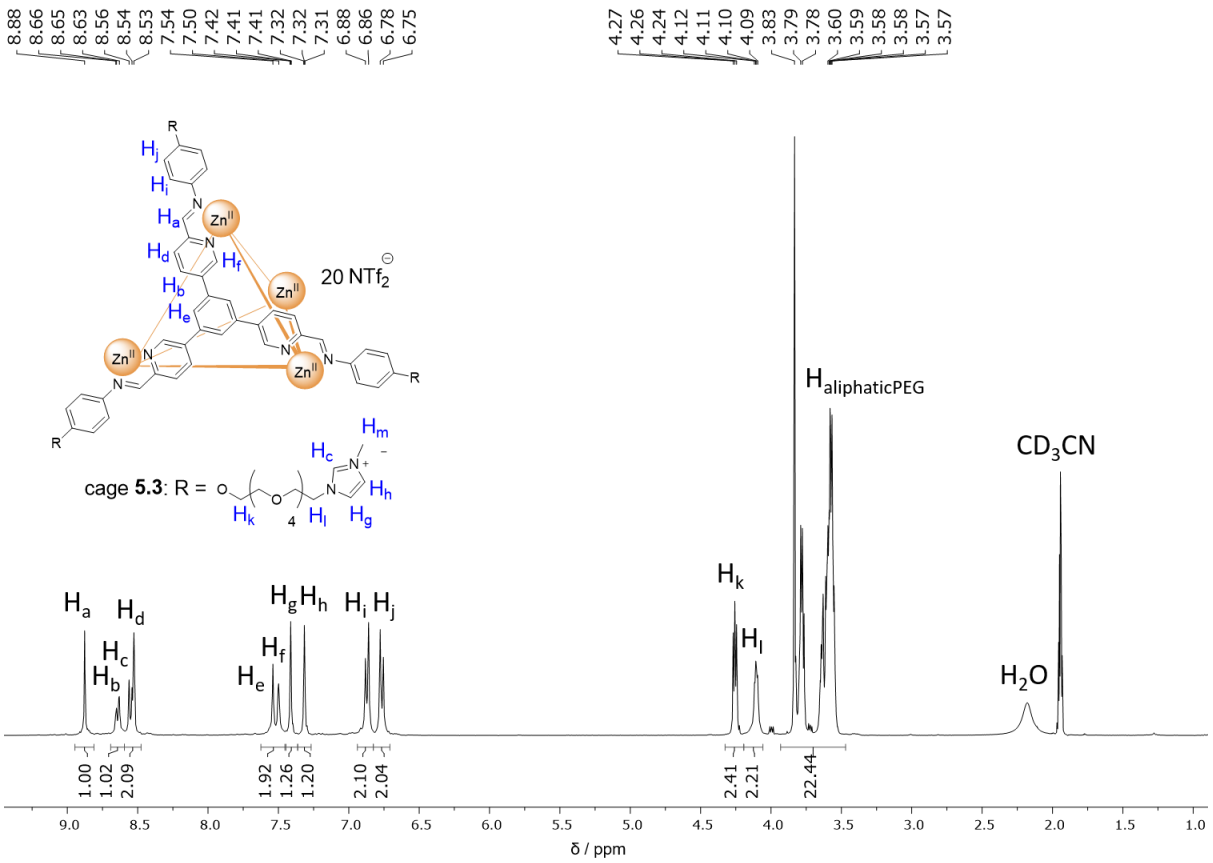

Figure 5.39: ^{1}H NMR (400 MHz, CD_3CN) spectrum of cage **5.3**.

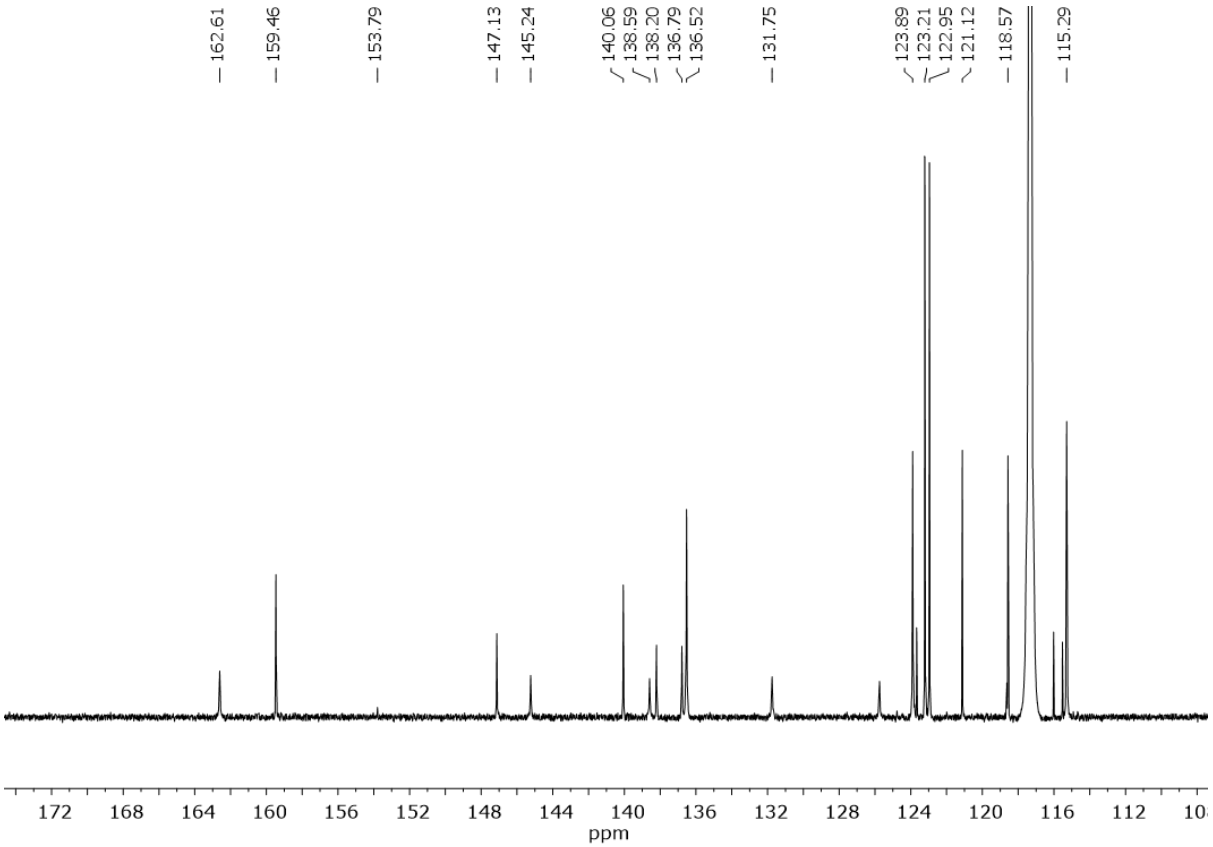

Figure 5.40: ^{13}C NMR (125 MHz, CD_3CN) spectrum of cage **5.3**.

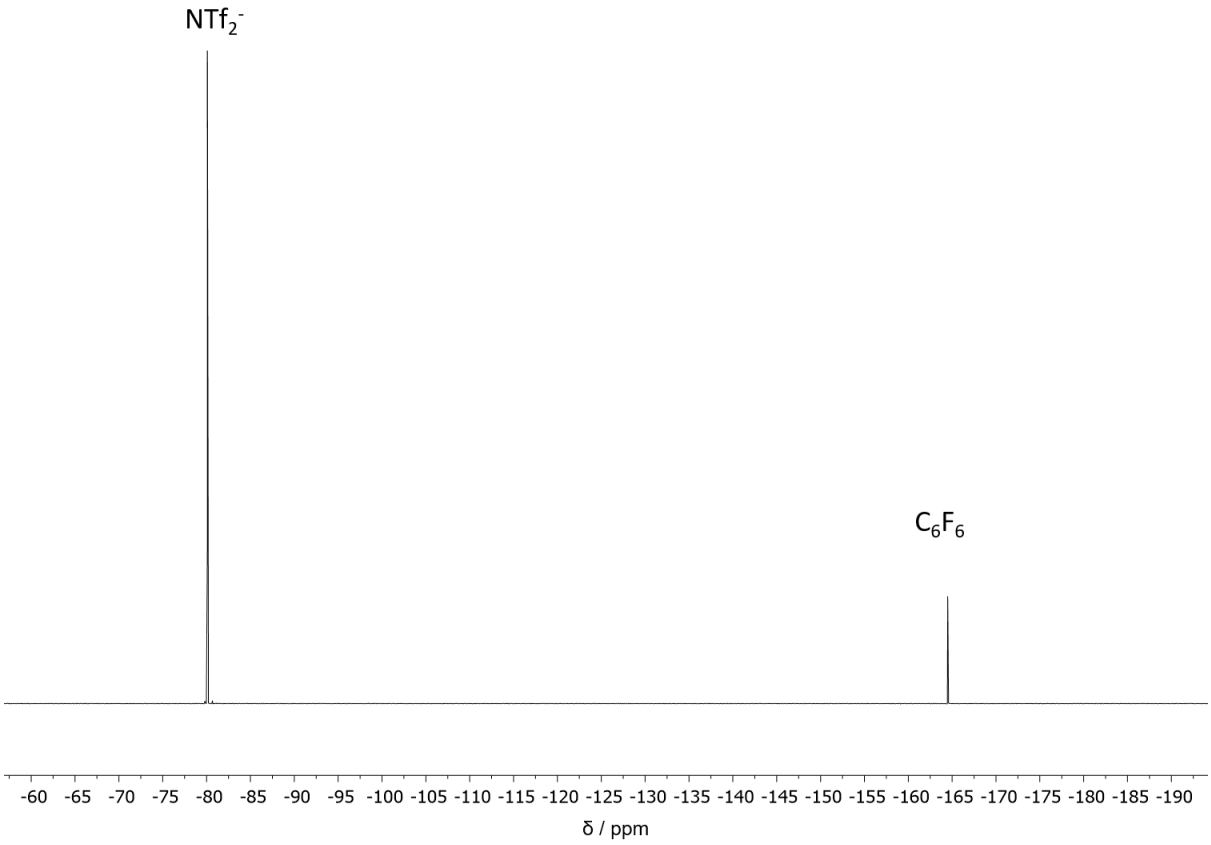

Figure 5.41: ^{19}F NMR (377 MHz, CD_3CN) spectrum of cage **5.3** with a C_6F_6 reference capillary.

5.11.3 Self-assembly of cages 5.4-5.5

Cage **5.4**:

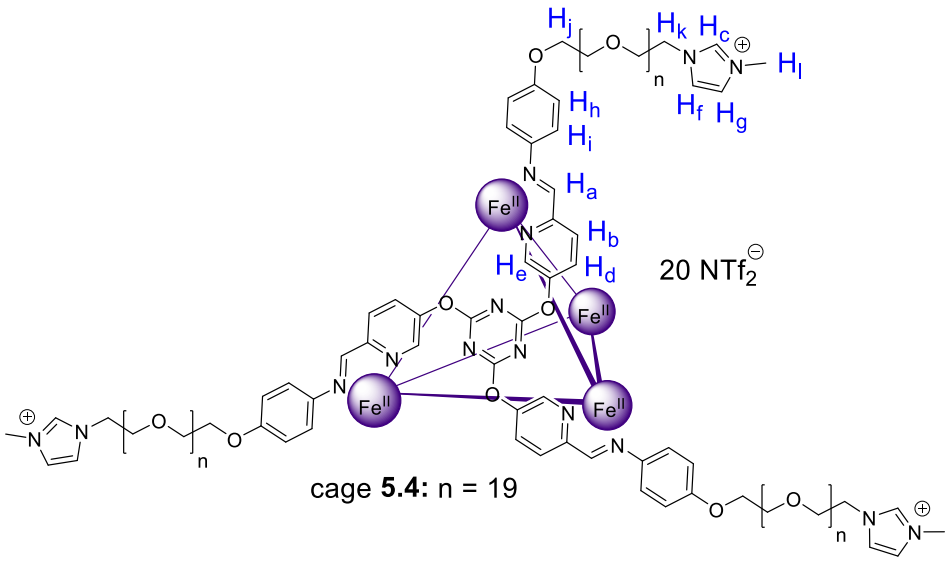

Trialdehyde **4A** (2.67 mg, 6.00 µmol, 4 equiv.), aniline **5F** (15.60 mg, 12.00 µmol, 12 equiv.) and $Fe(NTf_2)_2$ (3.88 mg, 6.30 µmol, 4.2 equiv) were added to 0.5 mL CH_3CN and exposed to 3 evacuation/nitrogen fill cycles. The cage was precipitated out of solution *via* the addition of

diethyl ether (2 mL) and centrifuged. The resulting oil was concentrated under reduced pressure yielding a dark purple, viscous liquid (25.1 mg, 85% yield). ^{1}H NMR (400 MHz, CD_3CN): δ = 9.24 (s, 1H, *H*$_a$), 9.00 (s, 1H, *H*$_a$-NTf2⊂**5.5**), 8.71 (d, 2H, J = 8.8 Hz, *H*$_b$), 8.64 (d, 2H, J = 9.1 Hz, *H*$_b$-NTf2⊂**5.5**), 8.59 (s, 1H, *H*$_c$), 8.53 (d, 2H, *J* = 8.9 Hz, *H*$_d$), 7.66 (s, 1H, *H*$_e$), 7.43 (s, 1H, *H*$_f$), 7.35 (s, 1H, *H*$_g$), 6.83 (d, 2H, J = 8.3 Hz, *H*$_h$), 5.60 (d, 2H, J = 8.3 Hz, *H*$_i$), 5.54 (d, 2H, J = 8.3 Hz, *H*$_i$-NTf2⊂**5.5**), 4.27 (t, 2H, *J* = 4.7 Hz, *H*$_j$), 4.11 (m, 2H, *H*$_k$), 3.84 (s, 3H, *H*$_l$), 3.82 – 3.37 (m, 118H, *H*$_{aliphati}$cPEG). ^{13}C NMR (125 MHz, CD_3CN): δ = 173.0, 172.4, 160.1, 156.7, 153.7, 148.7, 144.3, 137.5, 134.9, 132.7, 124.5, 124.3, 124.0, 123.7, 122.0, 119.4, 116.9, 115.8, 71.1, 70.9, 70.8, 70.8, 70.8, 70.7, 70.6, 69.9, 69.00, 68.8, 50.3, 36.7 ppm. ^{19}F NMR (377 MHz, CD_3CN, referenced to hexafluorobenzene in a C_6F_6 capillary): *δ* = -75.40 (encapsulated NTf_2^-), -80.30 (free NTf_2^-).

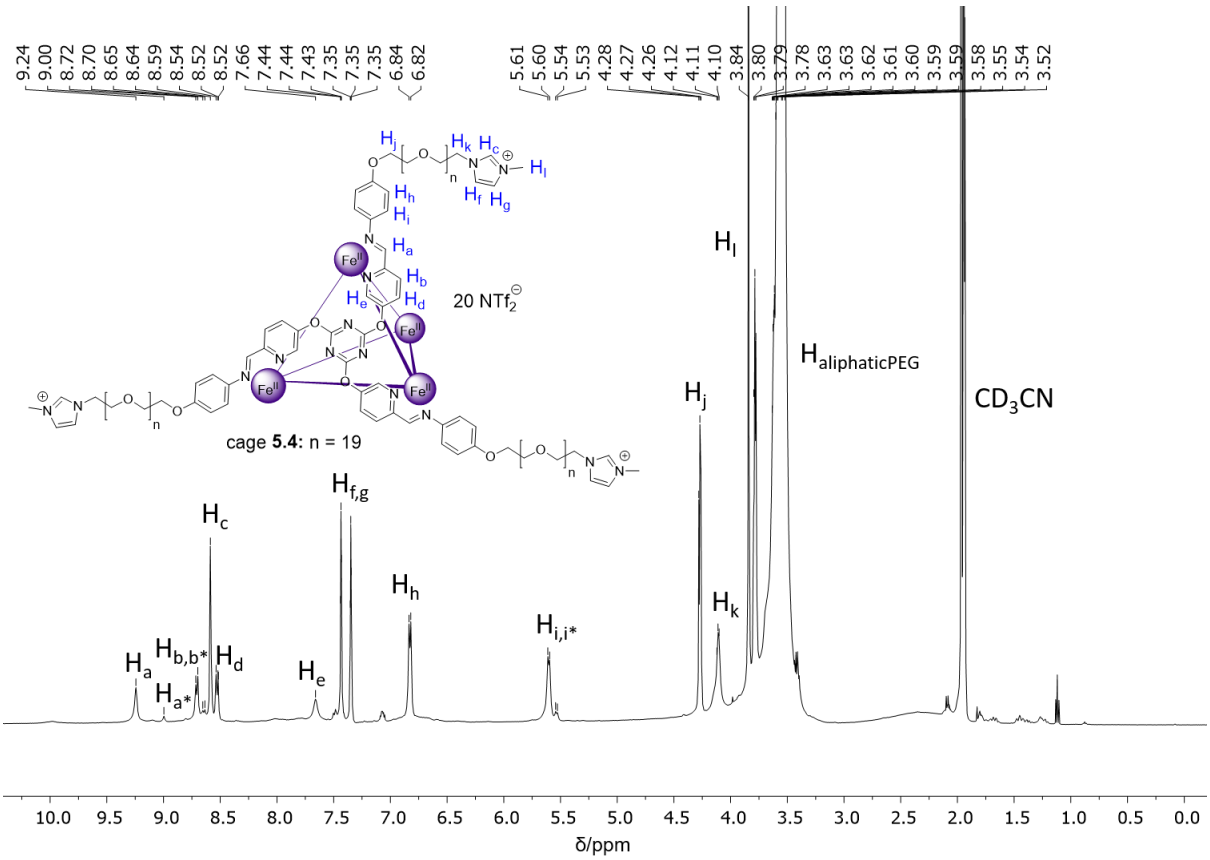

Figure 5.42: ^{1}H NMR (400 MHz, CD_3CN) spectrum of cage **5.4**. Labels with an asterisk (*) indicate NTf2⊂**5.5.**

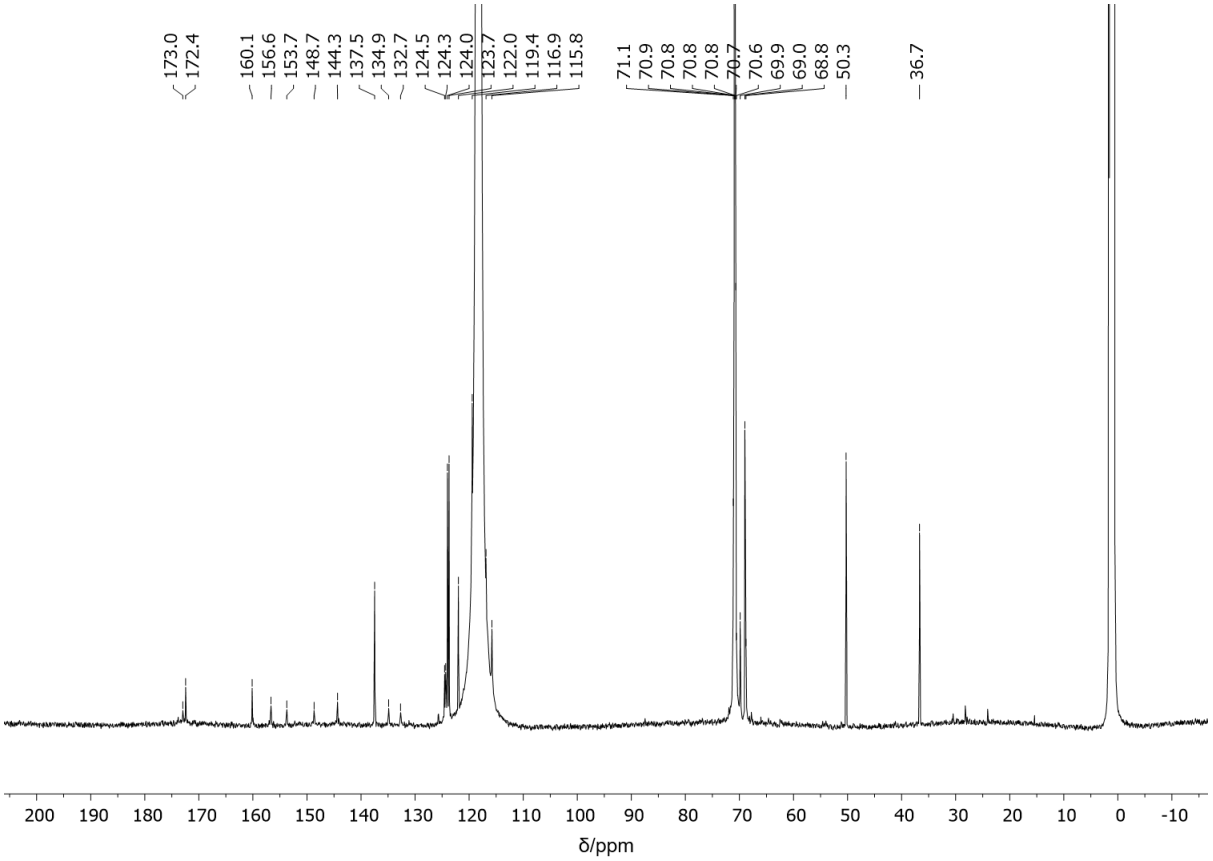

Figure 5.43: ^{13}C NMR (125 MHz, CD_3CN) spectrum of cage **5.4**.

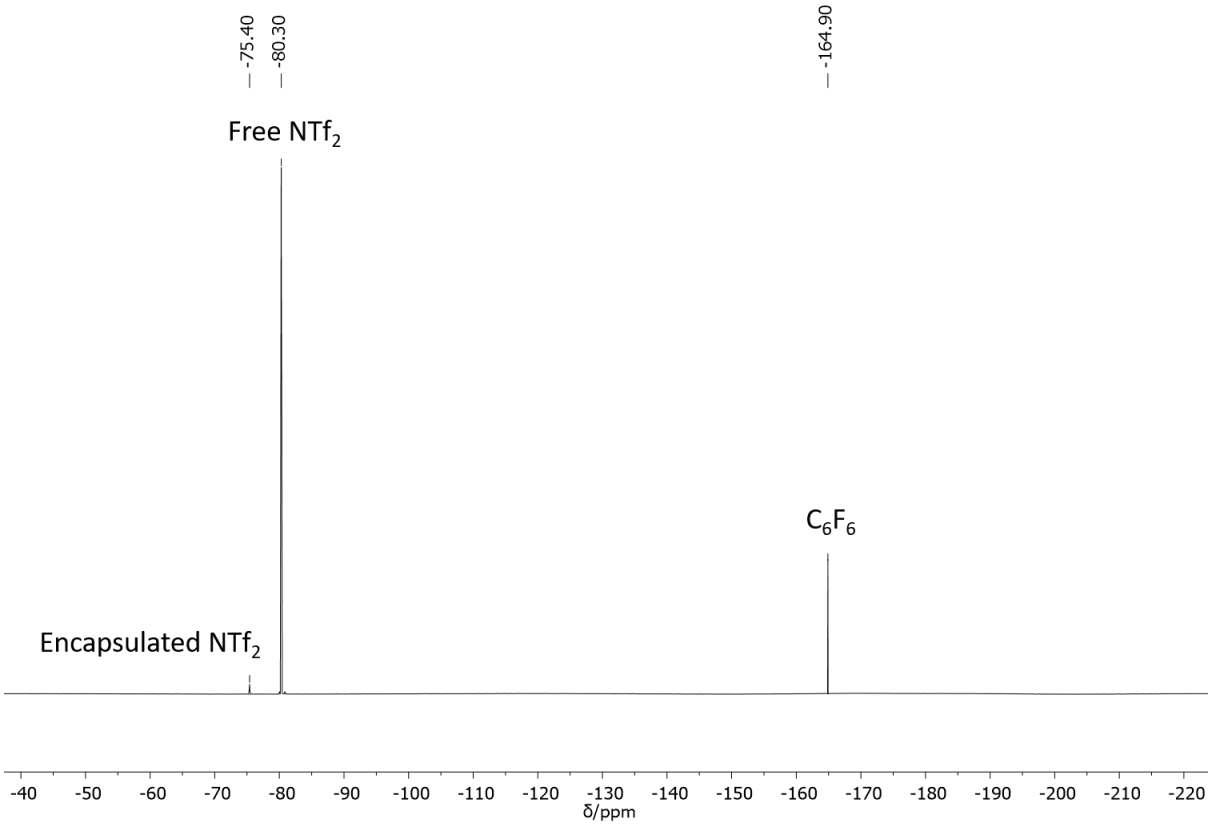

Figure 5.44: ^{19}F NMR (377 MHz, CD_3CN) spectrum of cage **5.4** with a C_6F_6 reference capillary.

Cage **5.5** was synthesized with the same method as cage **5.4** by replacing aniline **5F** with **5F'**.

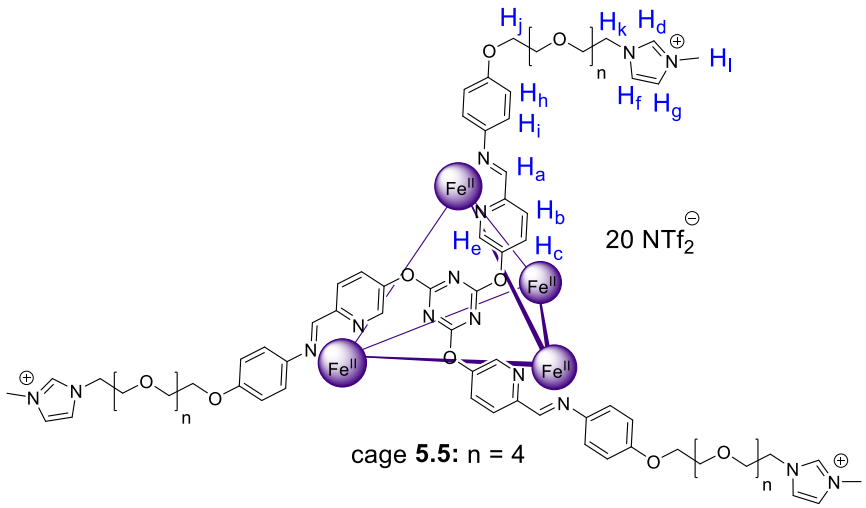

Cage **5.5**:

^{1}H NMR (400 MHz, CD_3CN): 9.28 (s, 1H, H_a), 9.01 (s, 1H, H_a-NTf2⊂**5.5**), 8.72 (d, 2H, J = 8.6 Hz, H_b), 8.65 (d, 2H, J = 9.8 Hz, H_b-NTf2⊂**5.5**), 8.53 (d, 2H, J = 8.7 Hz, H_c), 8.59 (s, 1H, H_d), 7.66 (s, 1H, H_e), 7.50 (s, 1H, H_e-NTf2⊂**5.5**), 7.41 (t, 1H, J = 1.6 Hz, H_f), 7.31 (t, 1H, J = 1.6 Hz, H_g), 6.81 (d, 2H, J = 8.8 Hz, H_h), 5.60 (d, 2H, J = 8.6 Hz, H_i), 5.54 (d, 2H, J = 8.6 Hz, H_i-NTf2⊂**5.5**), 4.25 (t, 2H, J = 5.0 Hz, H_j), 4.11 (m, 2H, H_k), 3.84 (s, 3H, H_l), 3.82 – 3.37 (m, 22H, $H_{aliphatic}$PEG). ^{13}C NMR (125 MHz, CD_3CN): δ = 173.1, 172.7, 172.5, 160.3, 156.8, 154.2, 149.0, 144.7, 137.5, 135.1, 132.9, 124.7, 124.6, 124.2, 123.9, 122.2, 119.6, 118.6, 118.3, 117.1, 115.9, 71.3, 71.1, 71.0, 71.0, 70.8, 70.1, 69.2, 68.9, 50.5, 36.9 ppm. ^{19}F NMR (377 MHz, CD_3CN, referenced to hexafluorobenzene in a C_6F_6 capillary): δ = -75.42 (encapsulated NTf_2^-), -80.40 (free NTf_2^-).

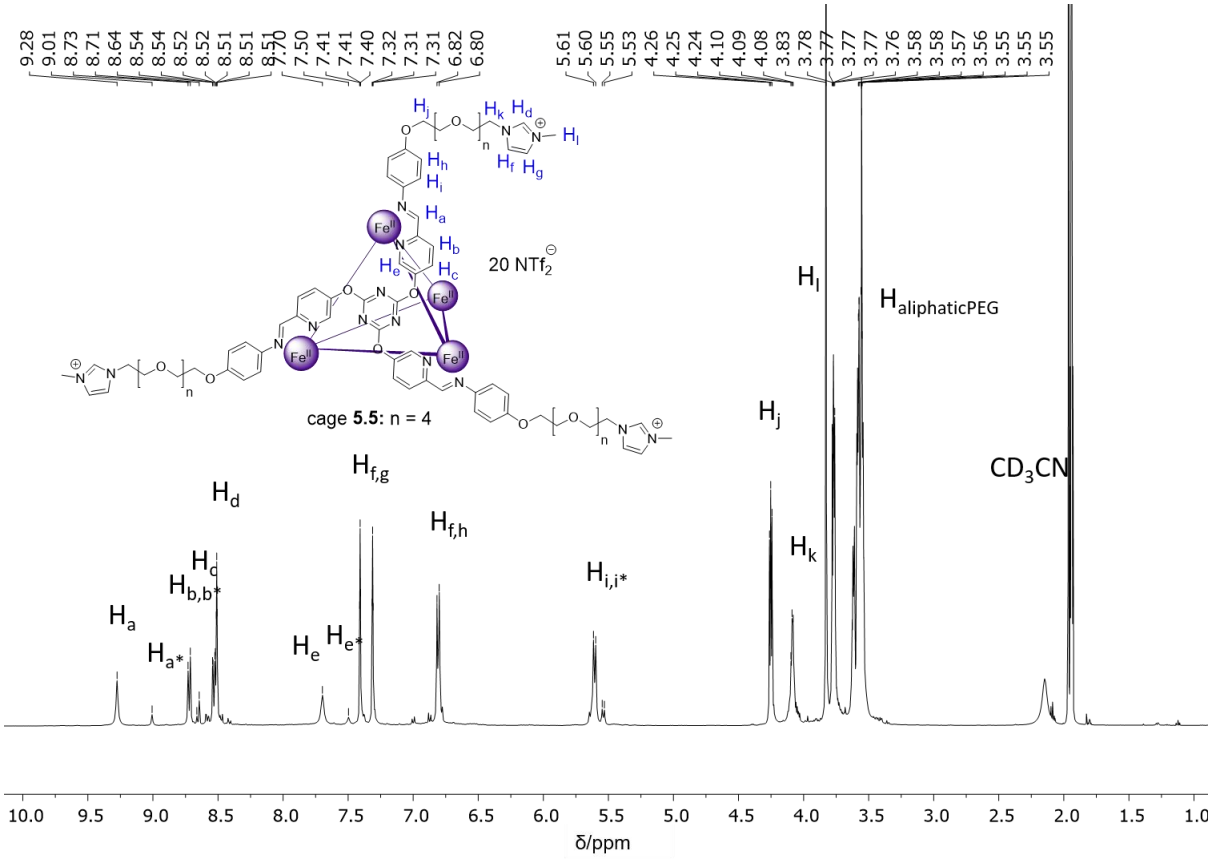

Figure 5.45: ^{1}H NMR (400 MHz, CD_3CN) spectrum of cage **5.5**. Labels with an asterisk (*) indicate cage peaks with bound NTf_2^-.

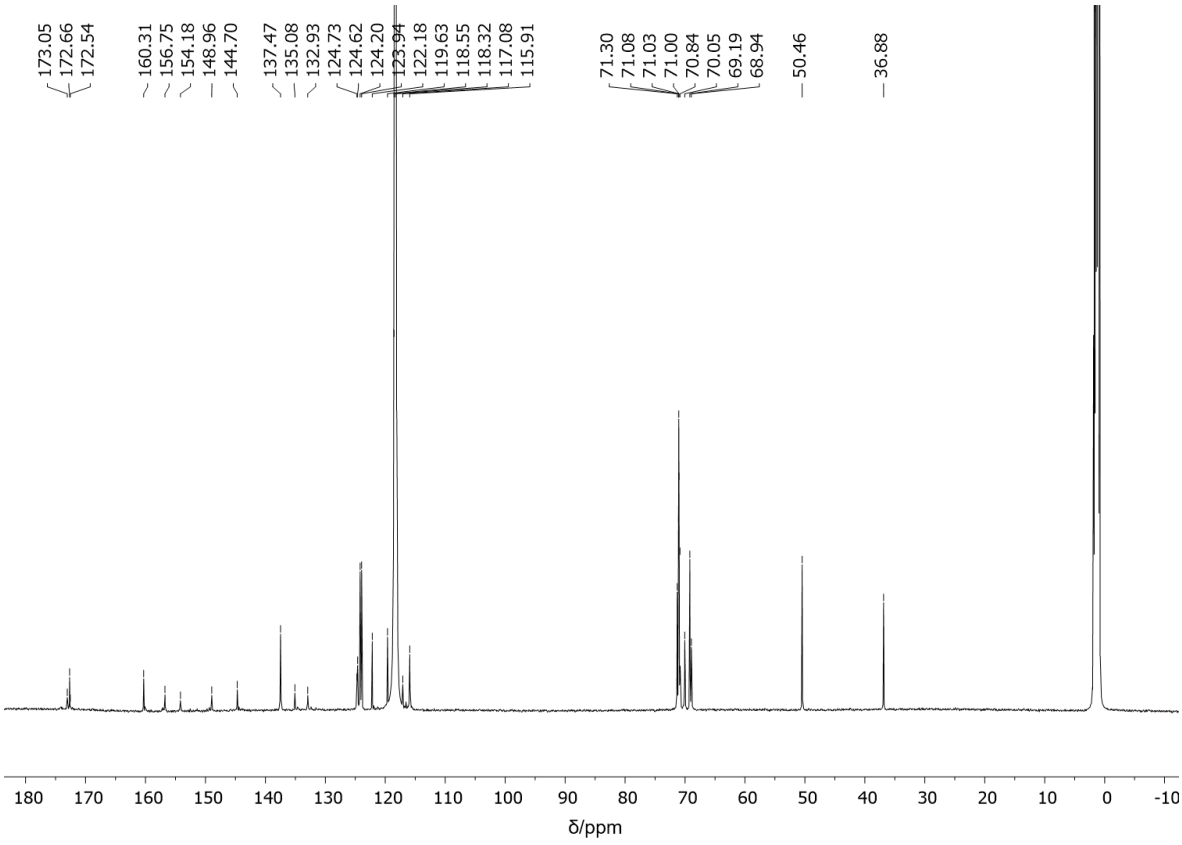

Figure 5.46: ^{13}C NMR (125 MHz, CD_3CN) spectrum of cage **5.5.**

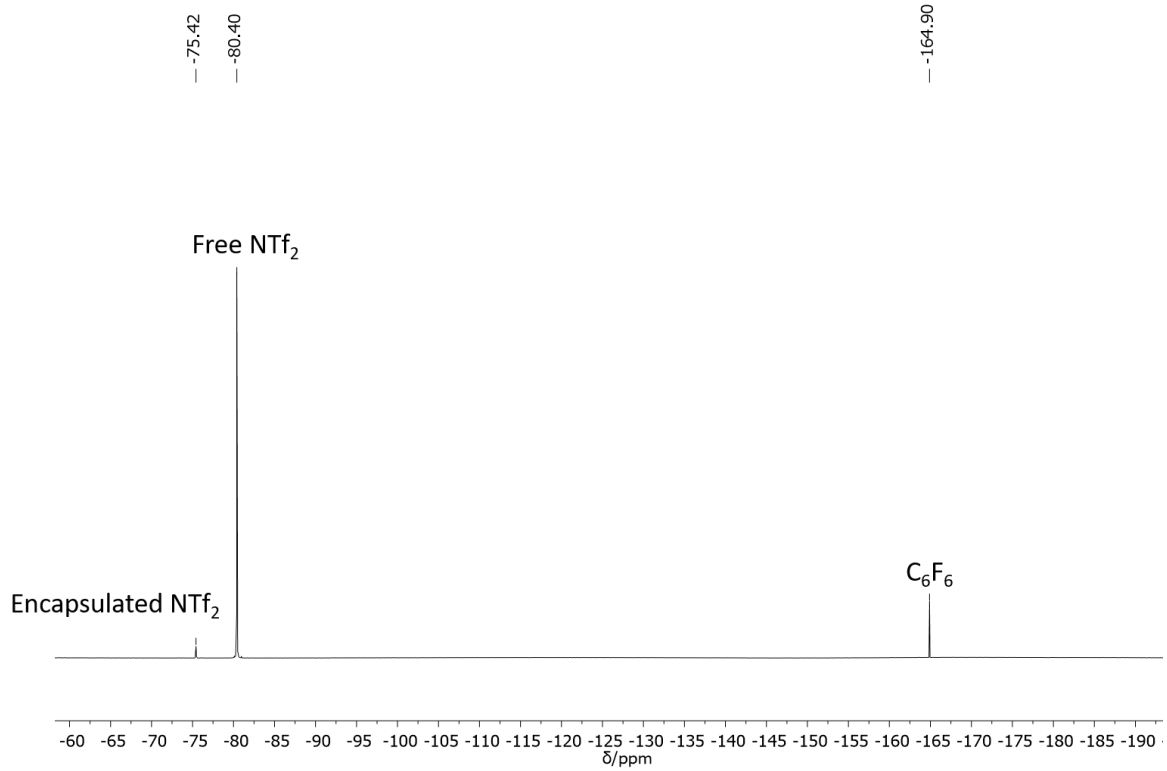

Figure 5.47: ^{19}F NMR (377 MHz, CD_3CN) spectrum of cage **5.5** with a C_6F_6 reference capillary.

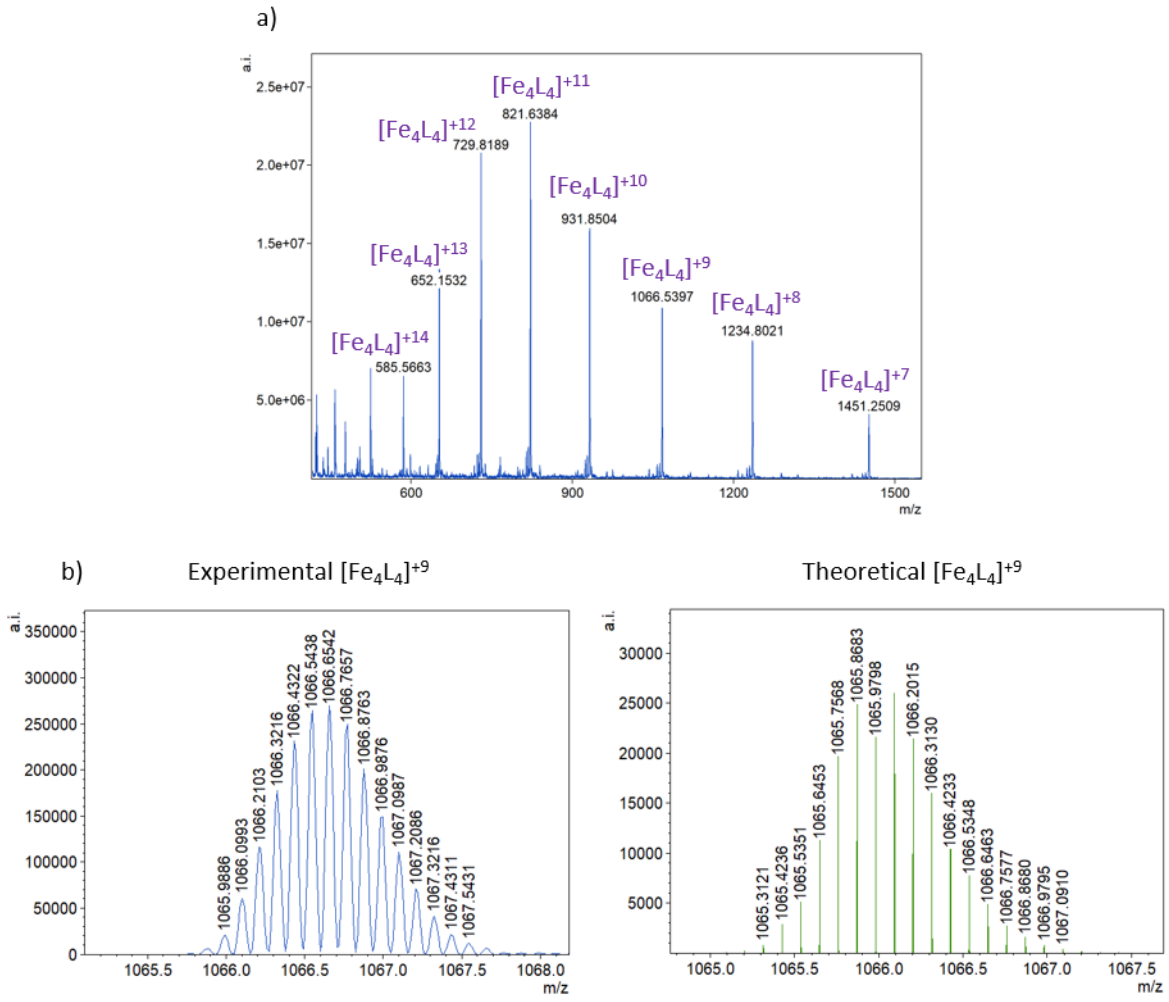

Figure 5.48: a) LR-ESI-MS spectrum of cage **5.5**.; charge distribution consistent with proposed structure. b) HR-ESI-MS spectrum of cage **5.5**; isotope pattern consistent with theoretical calculations.

5.11.4 Self-assembly of cages 5.6-5.7

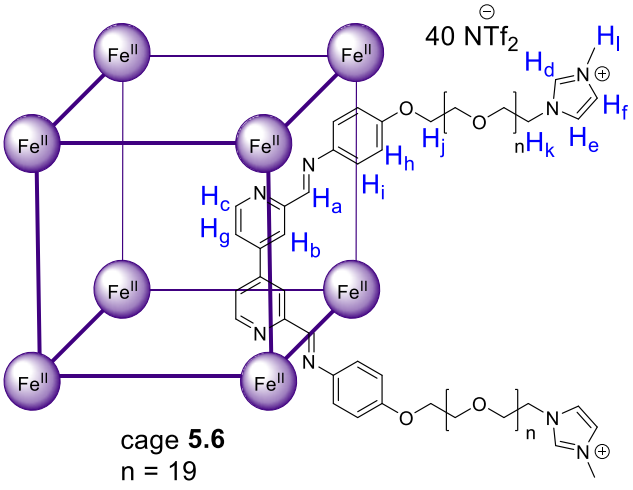

Cage **5.6**:

Dialdehyde **5I** (3.82 mg, 18.00 µmol, 12 equiv.), aniline **5F** (46.80 mg, 36.00 µmol, 24 equiv.) and $Fe(NTf_2)_2$ (7.76 mg, 12.60 µmol, 8.4 equiv) were added to 0.5 mL CH_3CN and exposed to 3 evacuation/nitrogen fill cycles. The mixture was heated at 70 °C for 18 h. The cage was precipitated out of solution *via* the addition of diethyl ether (2 mL) and centrifuged. The resulting oil was concentrated under reduced pressure yielding a dark blue, viscous liquid (25.1 mg, 86% yield). ^{1}H NMR (400 MHz, CD_3CN): δ = 9.20 (s, 1H, H_a), 8.94 (s, 1H, H_b), 8.59 (s, 2H, $H_{c,d}$), 7.44 (t, 1H, J = 2.1 Hz, H_e), 7.35 (t, 1H, J = 2.1 Hz, H_f), 7.22 (s, 1H, H_g), 6.83 (d, 2H, J = 8.3 Hz, H_h), 5.77 (d, 2H, J = 8.5 Hz, H_i), 4.27 (t, 2H, J = 5.0 Hz, H_j), 4.13 (m, 2H, H_k), 3.84 (s, 1H, H_l), 3.96 – 3.22 (m, 120H, $H_{aliphaticPEG}$). ^{13}C NMR (125 MHz, CD_3CN): δ = 174.2, 160.5, 160.2, 152.8, 144.8, 144.6, 137.7, 124.7, 124.2, 124.1, 123.9, 122.1, 119.6, 118.3, 117.0, 116.1, 71.5, 71.4, 71.1, 71.0, 70.9, 70.1, 69.2, 69.0, 50.5, 36.9, 28.4, 24.3 ppm. ^{19}F NMR (377 MHz, CD_3CN, referenced to hexafluorobenzene in a C_6F_6 capillary): δ = -80.36 (free NTf_2^-).

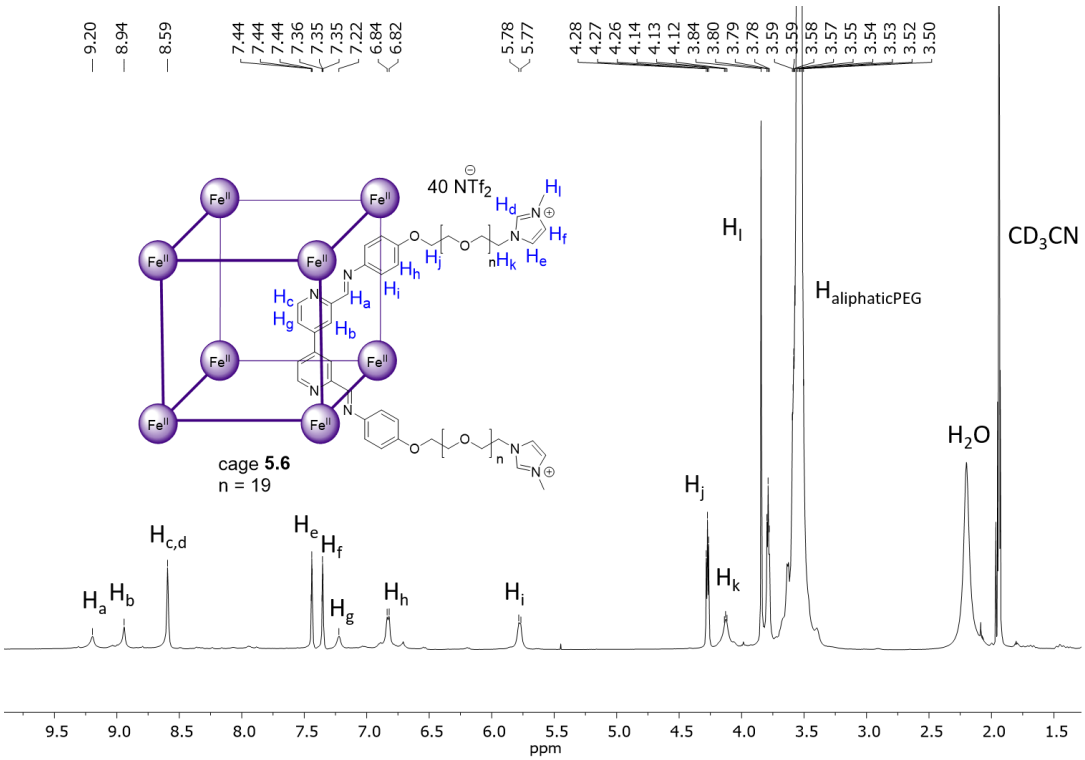

Figure 5.49: ^{1}H NMR (400 MHz, CD_3CN) spectrum of cage **5.6**.

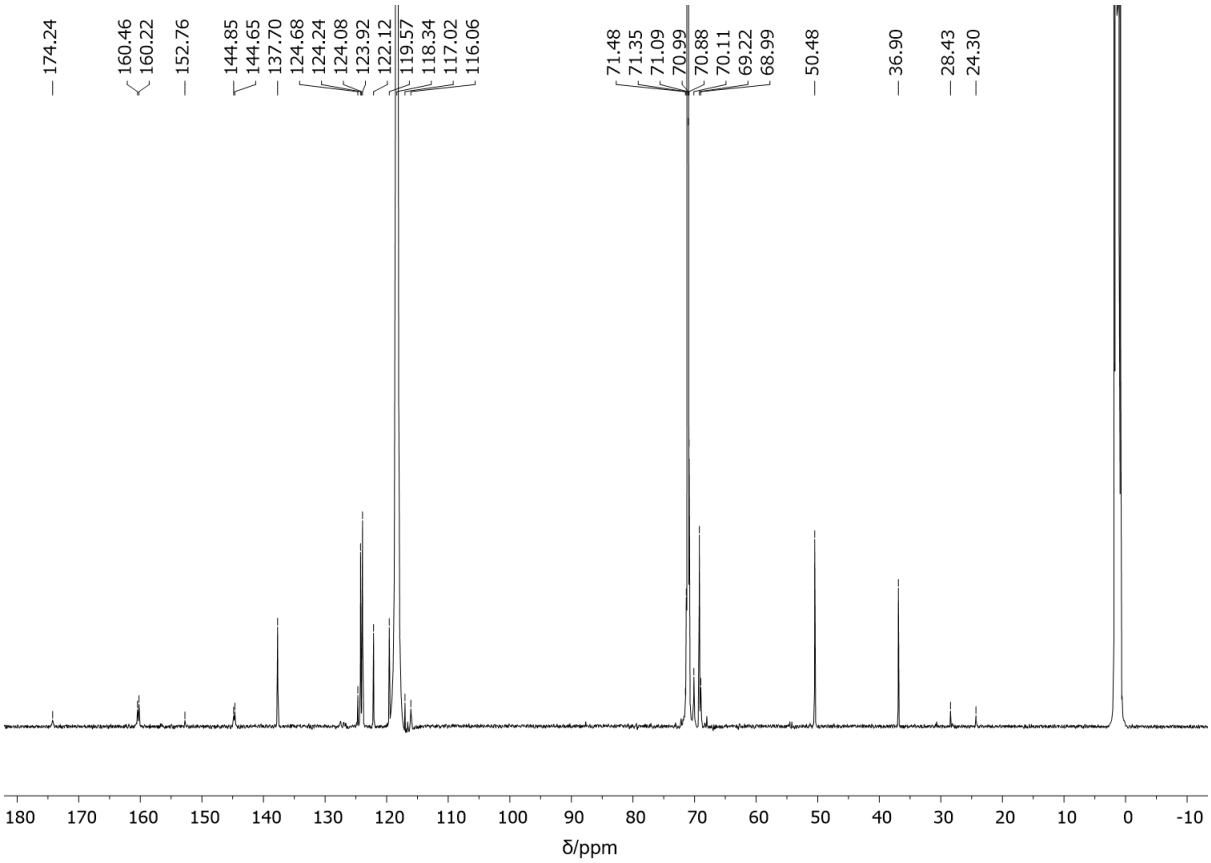

Figure 5.50: ^{13}C NMR (125 MHz, CD_3CN) spectrum of cage **5.6**.

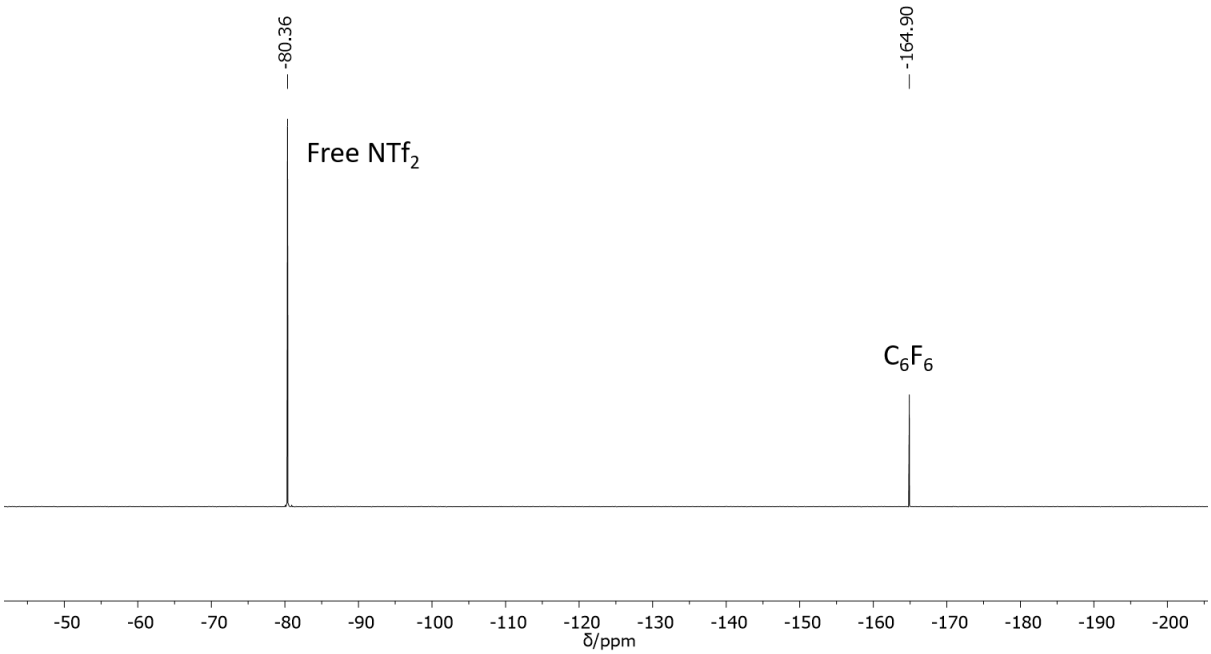

Figure 5.51: ^{19}F NMR (377 MHz, CD_3CN) spectrum of cage **5.6** with a C_6F_6 reference capillary.

Cage **5.7** was synthesized with the same method as cage **5.6** by replacing aniline **5F** with **5F'**.

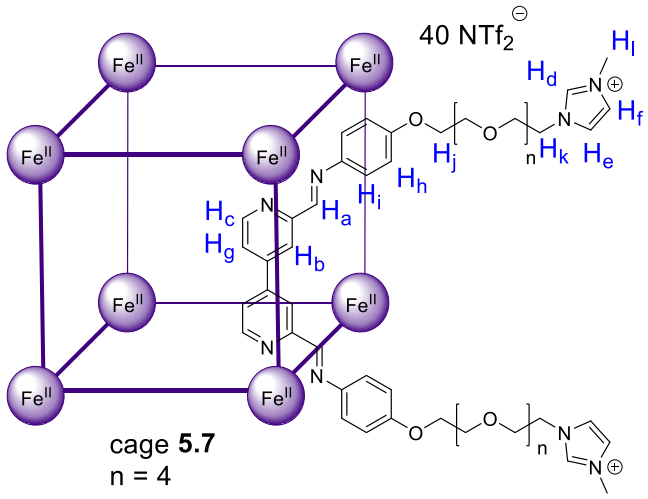

Cage **5.7**:

^{1}H NMR (400 MHz, CD_3CN): δ = 9.20 (s, 1H, *H*$_a$), 8.91 (s, 1H, *H*$_b$), 8.61 (d, 1H, *J* = 6.4 Hz, *H*$_c$), 8.52 (s, 1H, *H*=*d*), 7.40 (t, 1H, *J* = 1.8 Hz, *H*$_e$), 7.30 (t, 1H, *J* = 1.9 Hz, *H*$_f$), 7.23 (d, 1H, *J* = 5.9 Hz, *H*$_g$), 6.80 (d, 2H, *J* = 8.4 Hz, *H*$_h$), 5.75 (d, 1H, *J* = 8.3 Hz, *H*$_i$), 4.24 (t, 2H, *J* = 4.8, *H*$_j$), 4.10 (m, 2H, *H*$_k$), 3.82 (s, 3H, *H*$_l$), 3.94 – 3.36 (m, 16H, *H*$_{aliphaticPEG}$). ^{13}C NMR (125 MHz, CD_3CN): δ = 174.3, 160.4, 160.1, 156.6, 144.8, 144.7, 137.5, 127.5, 127.0, 124.6, 124.2, 123.9, 122.1, 119.5, 118.4, 117.0, 116.0, 71.3, 71.1, 71.0, 71.0, 71.0, 70.9, 70.8, 70.1, 69.2, 68.9, 50.5, 36.9, 30.9 ppm. ^{19}F NMR (377 MHz, CD_3CN, referenced to hexafluorobenzene in a C_6F_6 capillary): δ -80.32 (free NTf_2^-).

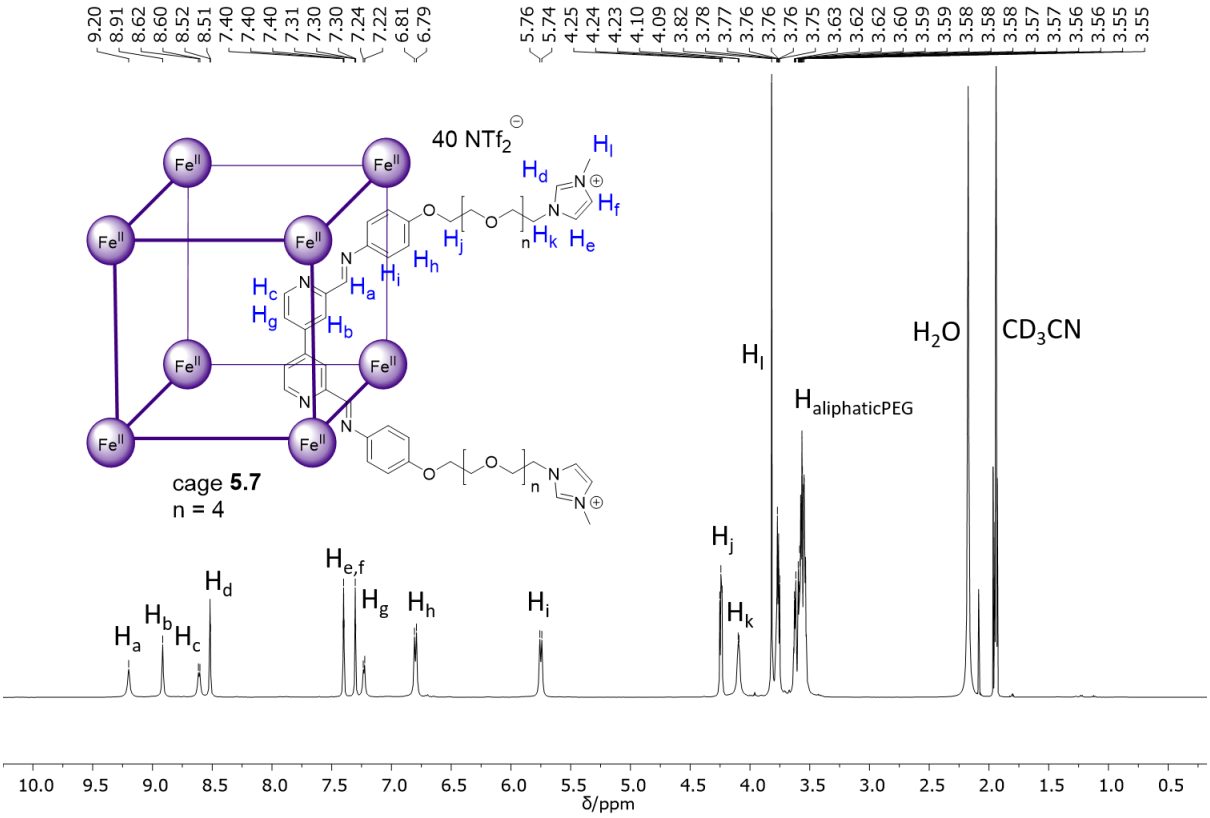

Figure 5.52: ^{1}H NMR (400 MHz, CD_3CN) spectrum of cage **5.7.**

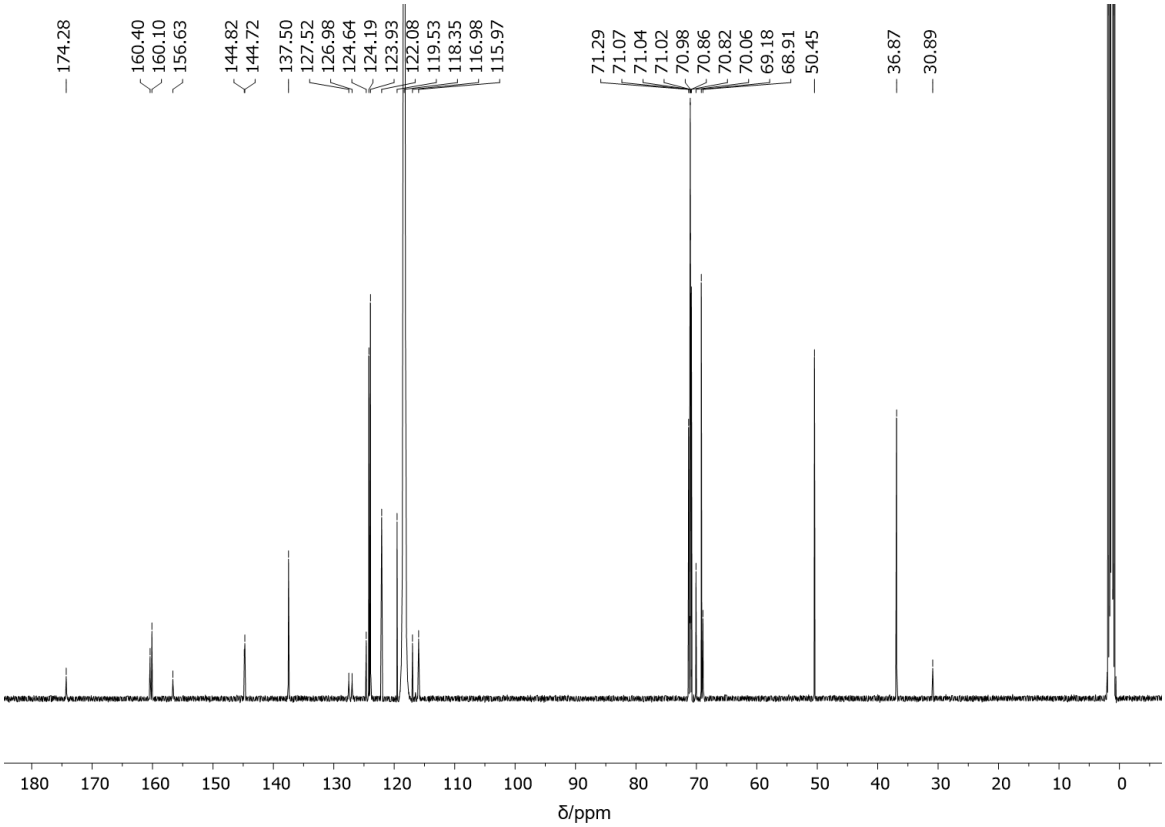

Figure 5.53: ^{13}C NMR (125 MHz, CD_3CN) spectrum of cage **5.7**.

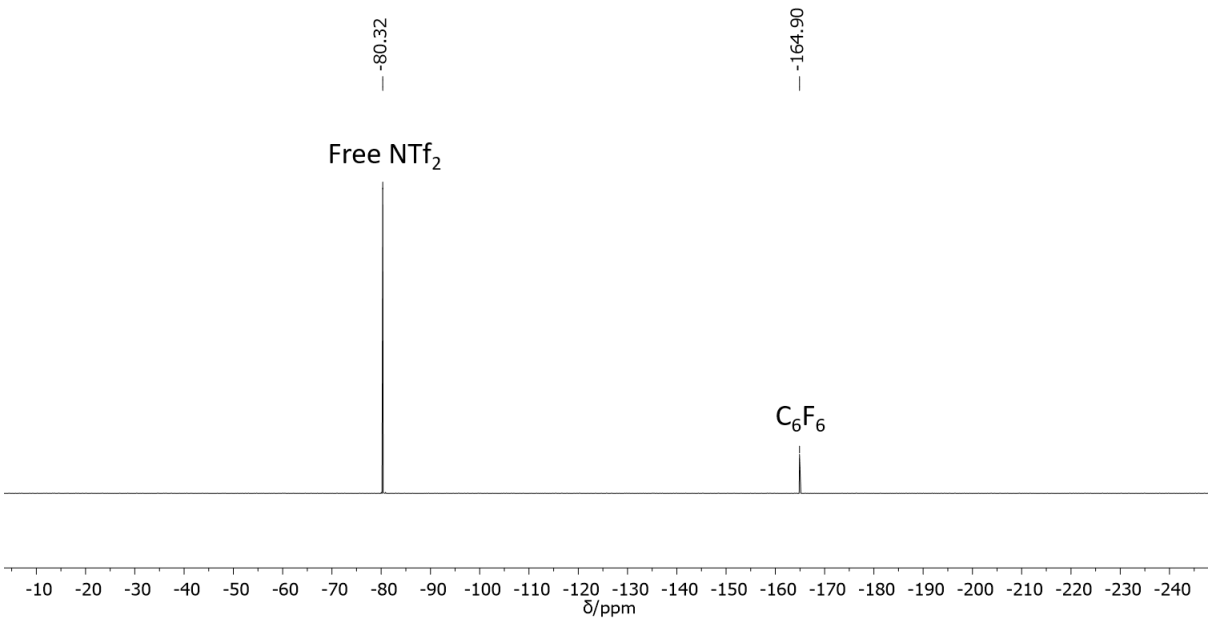

Figure 5.54: ^{19}F NMR (377 MHz, CD_3CN) spectrum of cage **5.7** with a C_6F_6 reference capillary.

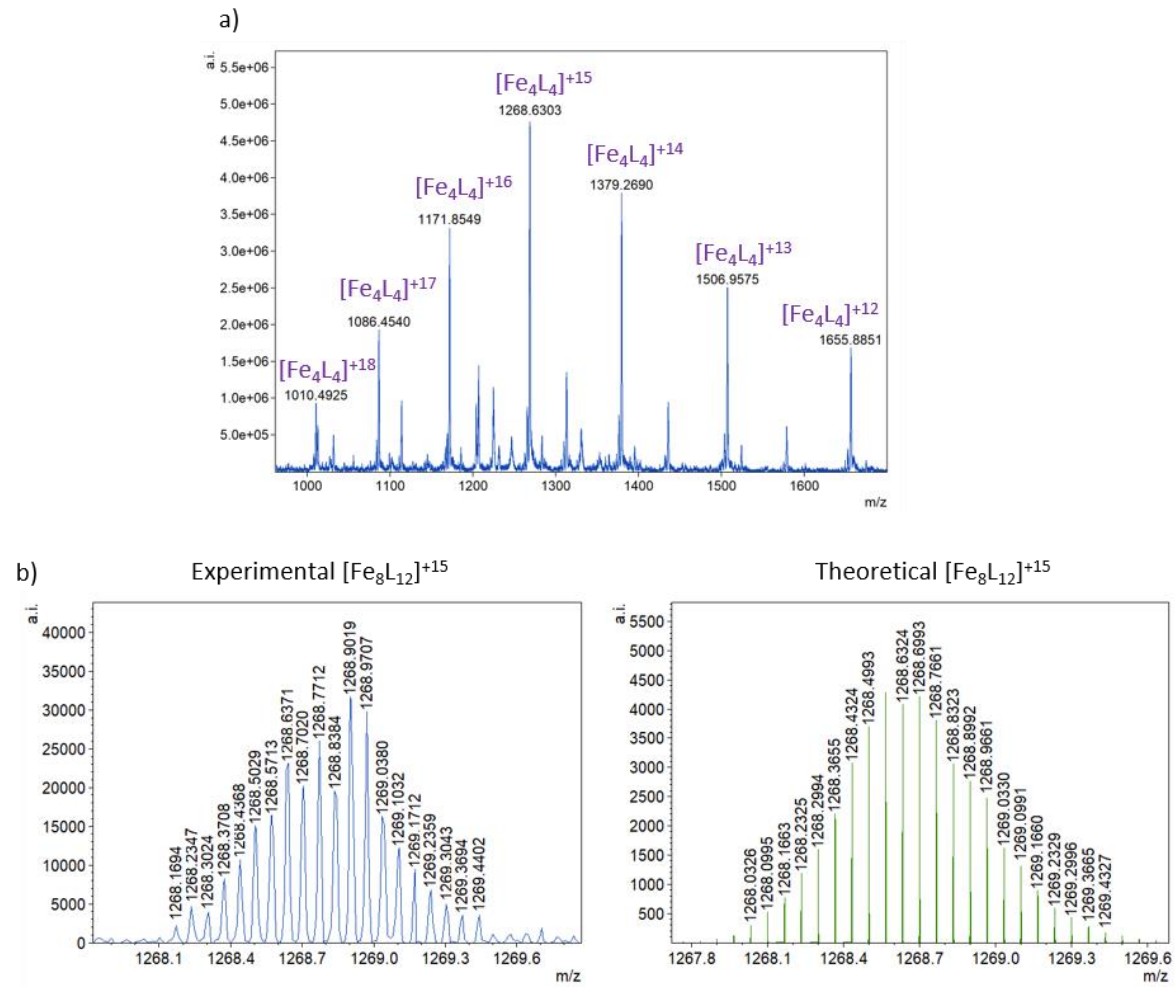

Figure 5.55: a) LR-ESI-MS spectrum of cage **5.7**.; charge distribution consistent with proposed structure. b) HR-ESI-MS spectrum of cage **5.7**; isotope pattern consistent with theoretical calculations.

5.11.5 Self-assembly of cages 5.8-5.9

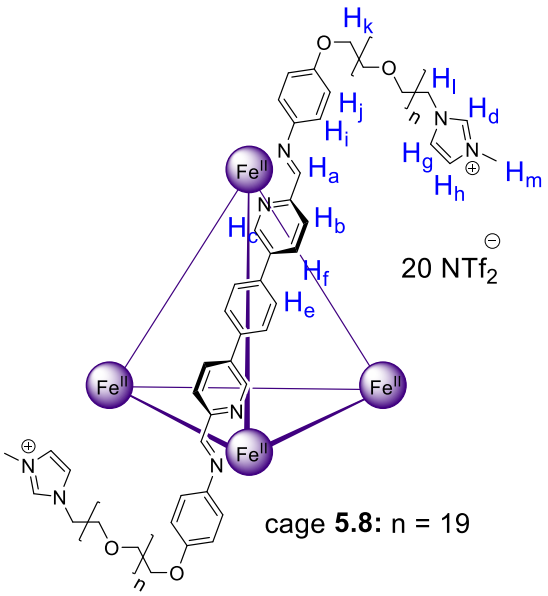

Cage **5.8**:

Dialdehyde **5J** (2.59 mg, 9.00 µmol, 6 equiv.), aniline **5F** (23.40 mg, 18.00 µmol, 12 equiv.) and $Fe(NTf_2)_2$ (3.88 mg, 6.30 µmol, 4.2 equiv) were added to 0.5 mL CH_3CN and exposed to 3 evacuation/nitrogen fill cycles. The mixture was heated in a microwave reactor at 100 °C for 10 minutes. The cage was precipitated out of solution *via* the addition of diethyl ether (2 mL) and centrifuged. The resulting oil was concentrated under reduced pressure yielding a dark blue, viscous liquid (25.1 mg, 86% yield). ^{1}H NMR (400 MHz, CD_3CN): δ = 8.84 (s, 1H, H_a), 8.67 (d, 1H, J = 8.2 Hz, H_b), 8.58 (m, 2H, $H_{c,d}$), 7.47 (m, 2H, $H_{e,f}$), 7.44 (s, 1H, H_g), 7.35 (s, 1H, H_h), 6.80 (d, 2H, J = 8.4 Hz, H_i), 5.71 (d, 2H, J = 8.4 Hz, H_j), 4.27 (t, 2H, J = 4.7 Hz, H_k), 4.12 (m, 2H, H_l), 3.85 (s, 3H, H_m), 3.81 – 3.40 (m, 118H, $H_{aliphaticPEG}$). ^{13}C NMR (125 MHz, CD_3CN): δ = 174.1, 160.0, 158.5, 144.5, 139.9, 137.7, 136.2, 128.7, 124.7, 124.2, 124.1, 123.9, 122.2, 119.6, 118.3, 117.1, 115.9, 71.3, 71.1, 71.1, 71.1, 71.0, 71.0, 71.0, 70.9, 70.8, 70.1, 69.2, 68.9, 50.4, 36.8 ppm. ^{19}F NMR (377 MHz, CD_3CN): δ = -80.38 (free NTf_2^-).

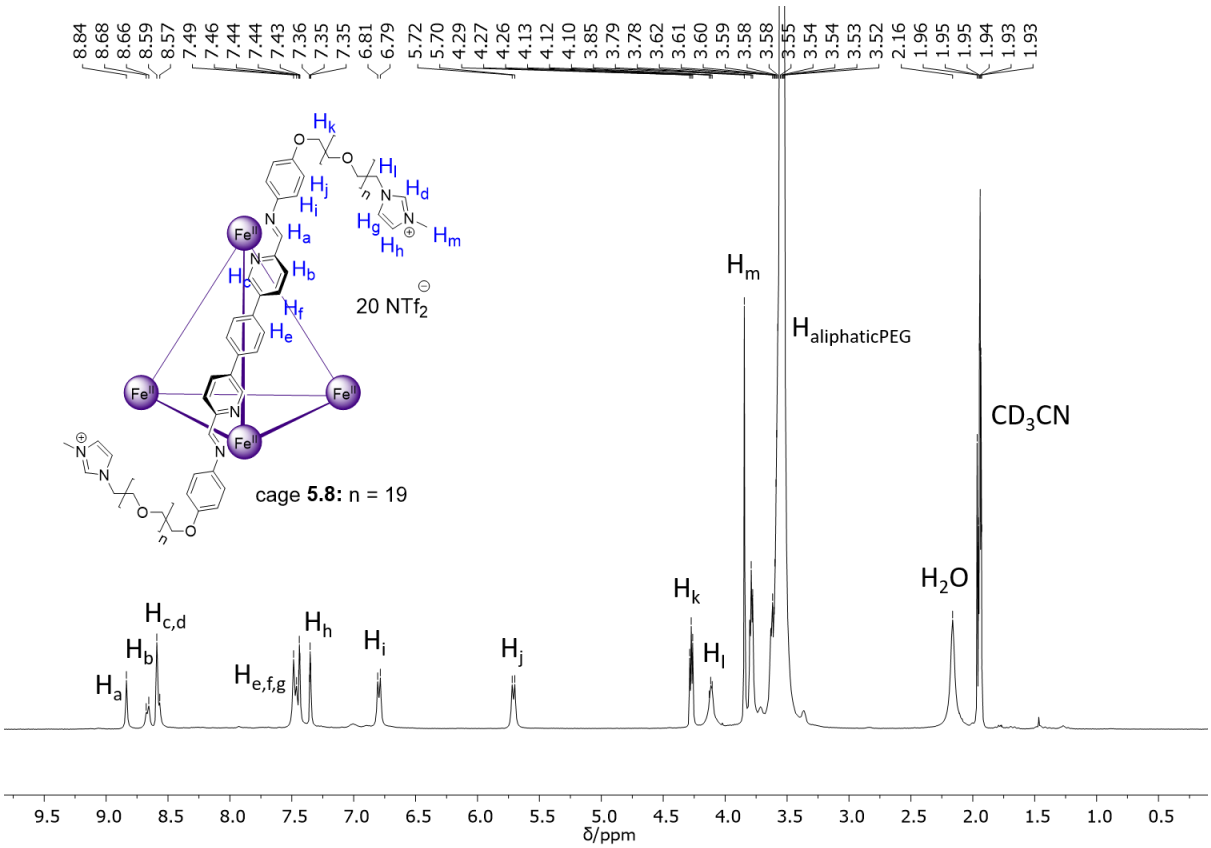

Figure 5.56: ^{1}H NMR (400 MHz, CD_3CN) spectrum of cage **5.8.**

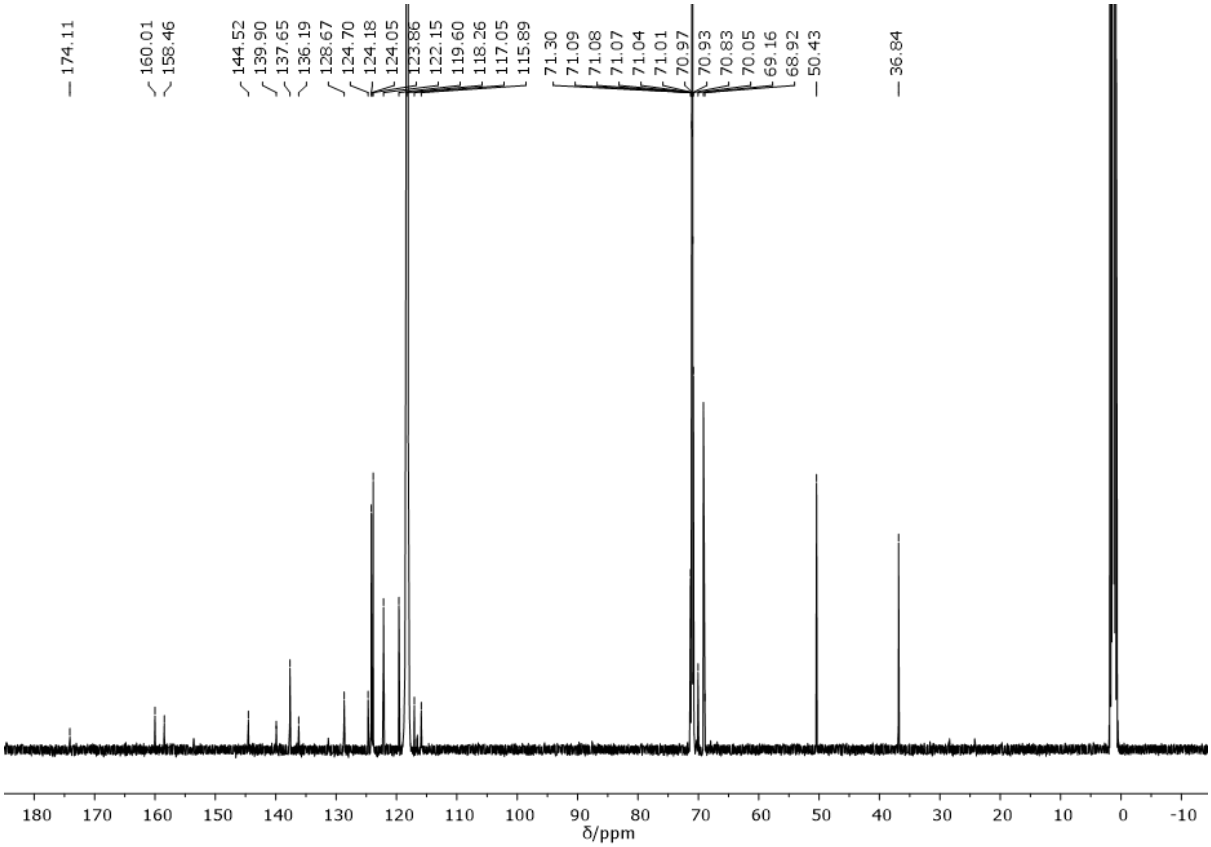

Figure 5.57: ^{13}C NMR (125 MHz, CD_3CN) spectrum of cage **5.8**.

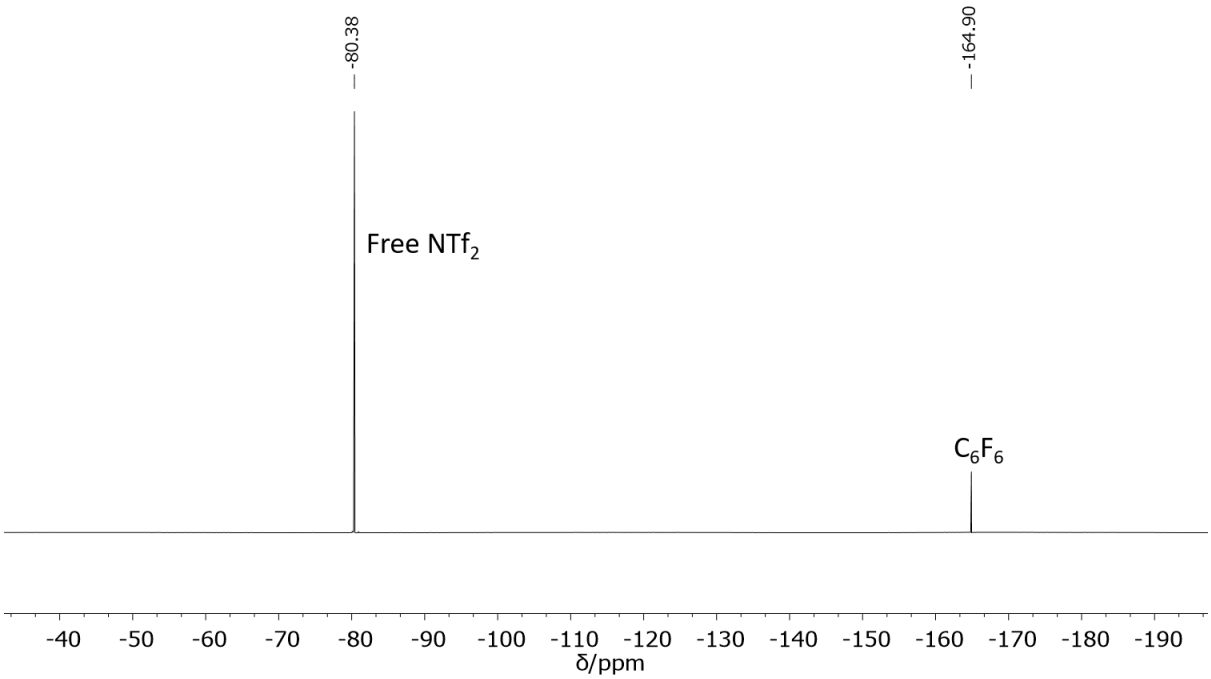

Figure 5.58: ^{19}F NMR (377 MHz, CD_3CN) spectrum of cage **5.8** with a C_6F_6 reference capillary.

Cage **5.9** was synthesized with the same method as cage **5.8** by replacing aniline **5F** with **5F'**.

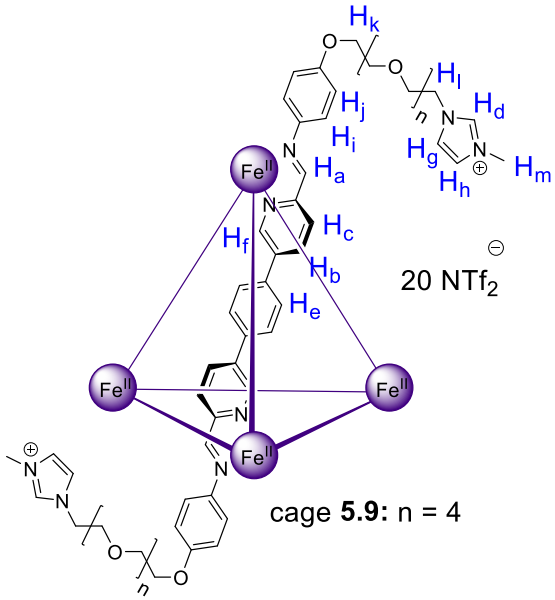

Cage **5.9**:

^{1}H NMR (400 MHz, CD_3CN): δ = 8.83 (s, 1H, H_a), 8.67 (s, 1H, H_b), 8.59 (d, 1H, J = 6.0 Hz, H_c), 8.51 (s, 1H, H_d), 7.49 (s, 1H, H_e), 7.45 (s, 1H, H_f), 7.41 (s, 1H, H_g), 7.31 (s, 1H, H_h), 6.77 (d, 2H, J = 8.4 Hz, H_i), 5.71 (d, 2H, J = 8.4 Hz, H_j), 4.25 (t, 2H, J = 4.8 Hz, H_k), 4.09 (m, 2H, H_l), 3.83 (s, 3H, H_m), 3.80 – 3.42 (m, 17H, $H_{aliphaticPEG}$). ^{13}C NMR (125 MHz, CD_3CN): δ = 174.1, 159.9, 158.5, 153.5, 144.6, 139.9, 137.8, 137.4, 136.2, 131.3, 128.7, 124.7, 124.1, 124.1, 123.9, 122.1, 119.6, 117.0, 115.8, 71.2, 71.0, 71.0, 71.0, 70.9, 70.8, 70.00, 69.1, 68.9, 50.4, 36.8 ppm. ^{19}F NMR (377 MHz, CD_3CN): δ = -80.33 (free NTf_2^-).

s

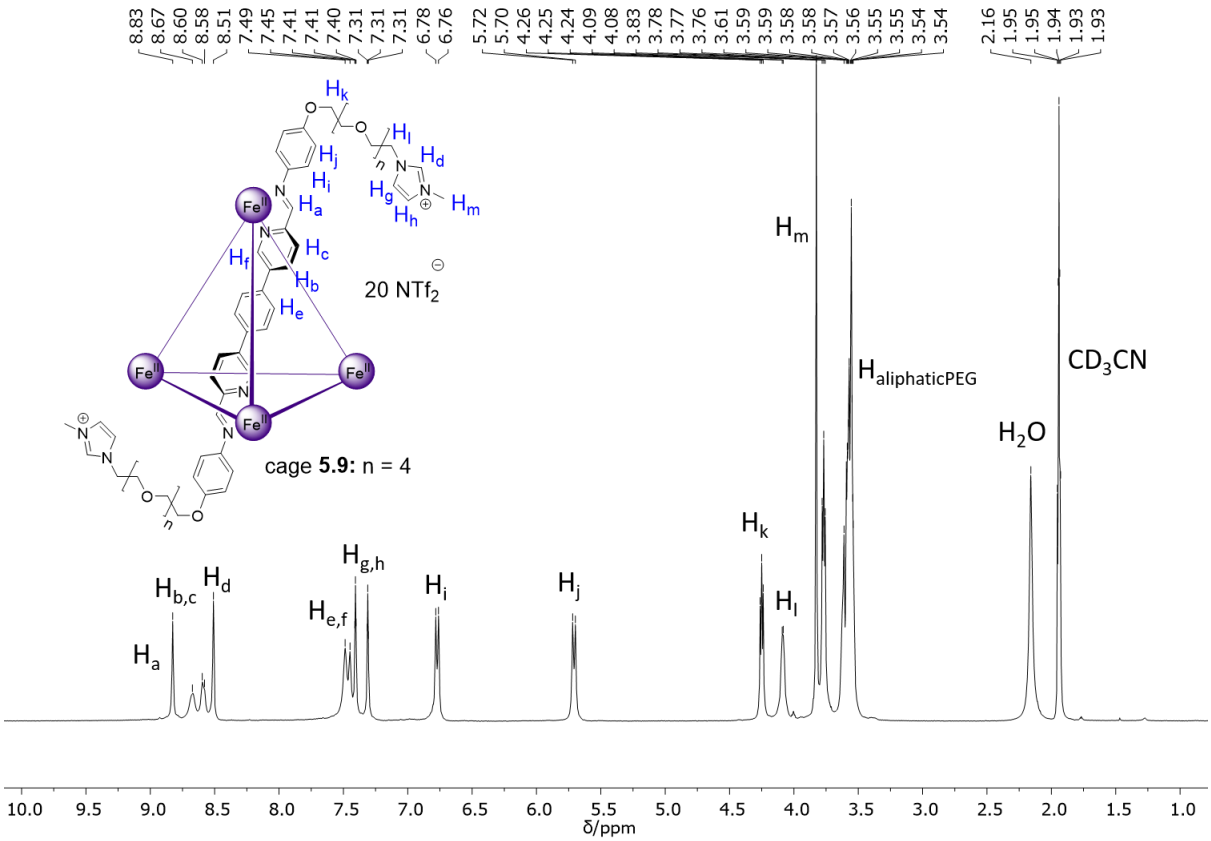

Figure 5.59: ^{1}H NMR (400 MHz, CD_3CN) spectrum of cage **5.9**.

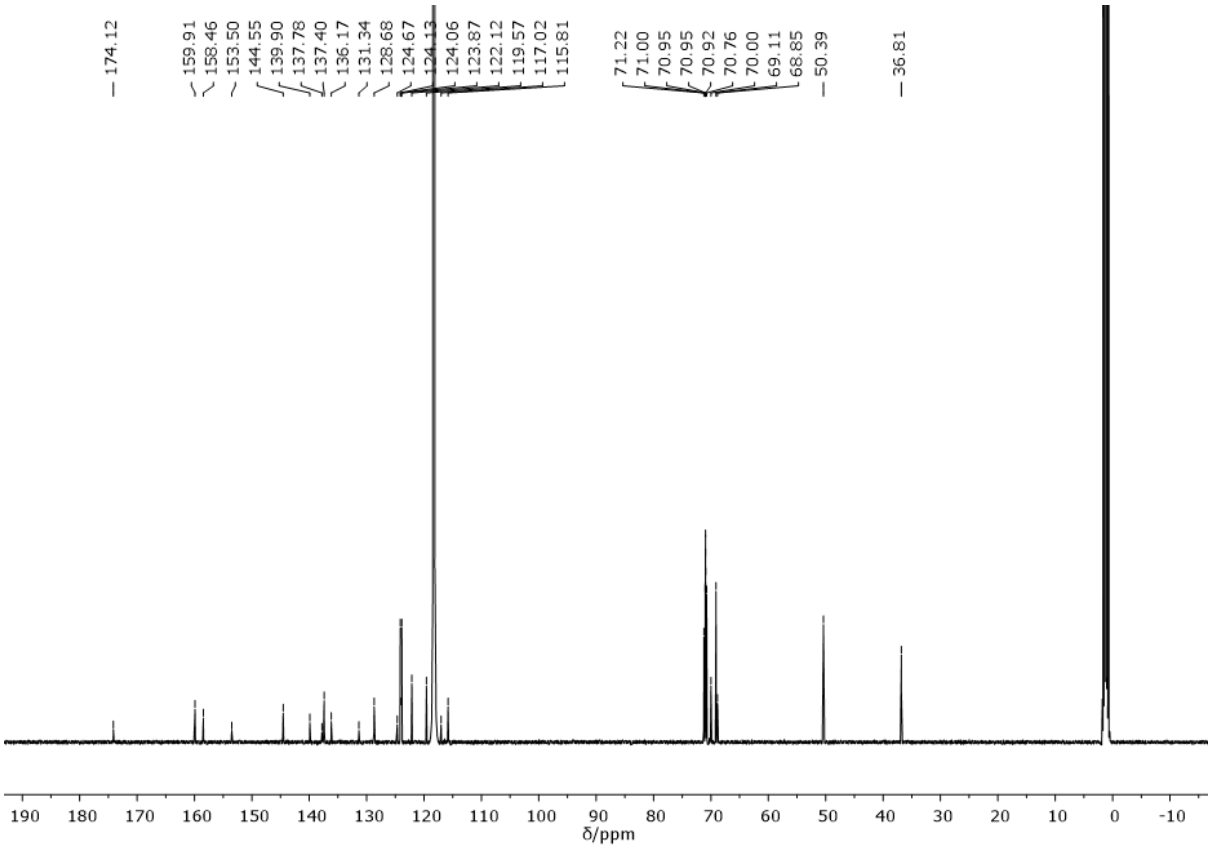

Figure 5.60: ^{13}C NMR (125 MHz, CD_3CN) spectrum of cage **5.9**.

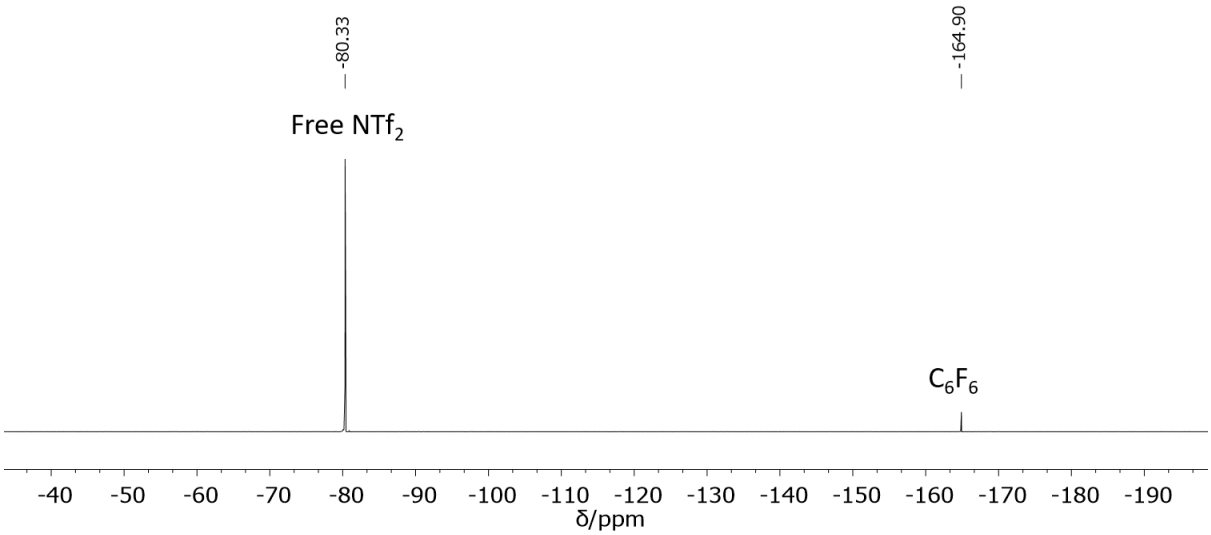

Figure 5.61: ^{19}F NMR (377 MHz, CD_3CN) spectrum of cage **5.9** with a C_6F_6 reference capillary.

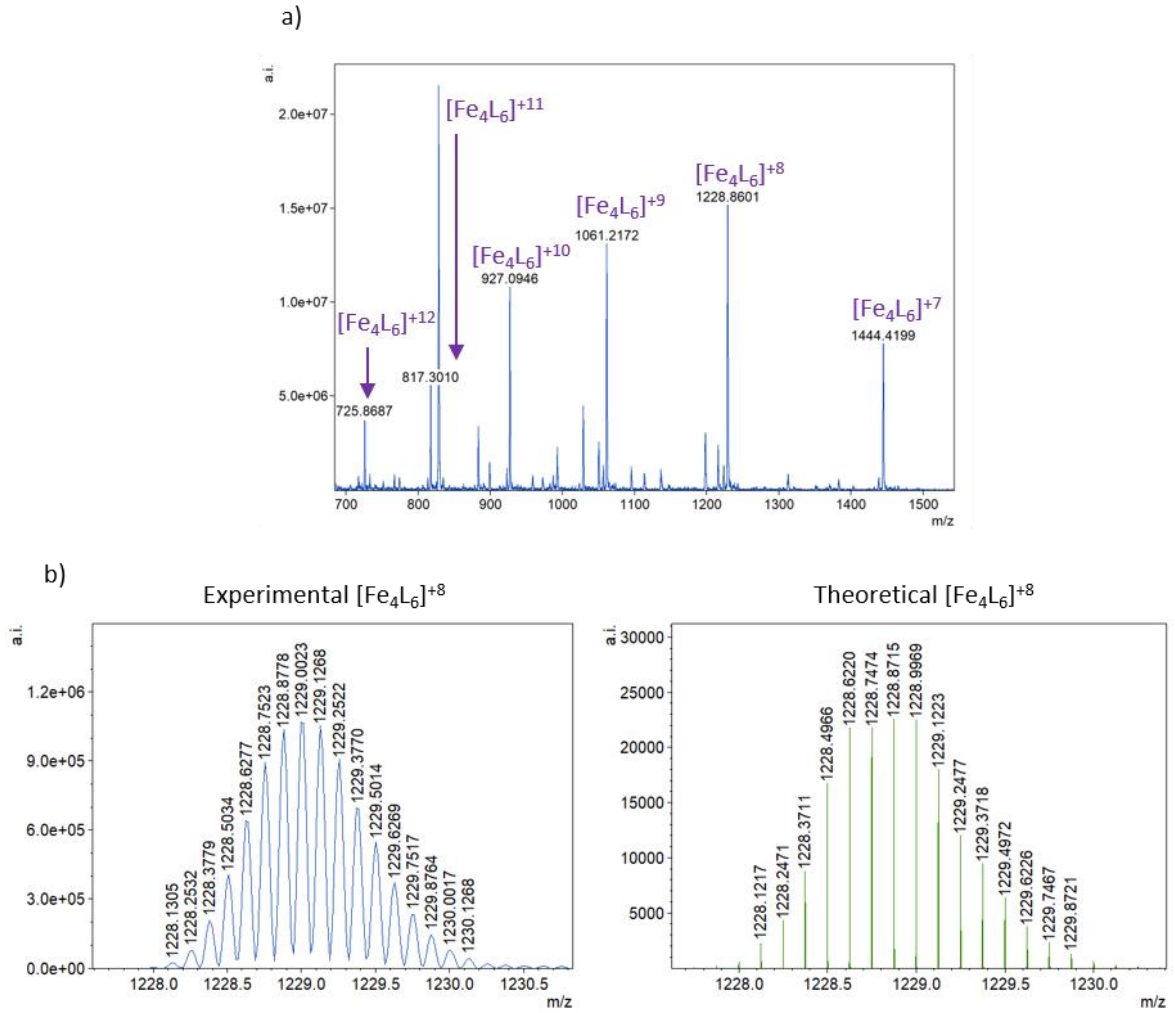

Figure 5.62: a) LR-ESI-MS spectrum of cage **5.9**.; charge distribution consistent with proposed structure. b) HR-ESI-MS spectrum of cage **5.9**; isotope pattern consistent with theoretical calculations.

5.12 References

(1) Zhang, J.; Chai, S. H.; Qiao, Z. A.; Mahurin, S. M.; Chen, J.; Fang, Y.; Wan, S.; Nelson, K.; Zhang, P.; Dai, S. *Angew. Chemie - Int. Ed.* **2015**, *54* (3), 932–936.

(2) Li, P.; Schott, J. A.; Zhang, J.; Mahurin, S. M.; Sheng, Y.; Qiao, Z. A.; Hu, X.; Cui, G.; Yao, D.; Brown, S.; et al. *Angew. Chemie - Int. Ed.* **2017**, *56* (47), 14958–14962.

(3) Maton, C.; De Vos, N.; Stevens, C. V. *Chem. Soc. Rev.* **2013**, *42* (13), 5963–5977.

(4) Castilla, A. M.; Ronson, T. K.; Nitschke, J. R. *J. Am. Chem. Soc.* **2016**, *138* (7), 2342–2351.

(5) Ma, S.; Smulders, M. M. J.; Hristova, Y. R.; Clegg, J. K.; Ronson, T. K.; Zarra, S.; Nitschke, J. R. *J. Am. Chem. Soc.* **2013**, *135* (15), 5678–5684.

(6) Browne, C.; Brenet, S.; Clegg, J. K.; Nitschke, J. R. *Angew. Chemie - Int. Ed.* **2013**, *52* (7), 1944–1948.

(7) Giri, N.; Del Pópolo, M. G.; Melaugh, G.; Greenaway, R. L.; Rätzke, K.; Koschine, T.; Pison, L.; Gomes, M. F. C.; Cooper, A. I.; James, S. L. *Nature* **2015**, *527* , 216–220.

(8) Shan, W.; Fulvio, P. F.; Kong, L.; Schott, J. A.; Do-Thanh, C. L.; Tian, T.; Hu, X.; Mahurin, S. M.; Xing, H.; Dai, S. *ACS Appl. Mater. Interfaces* **2018**, *10* (1), 32–36.

(9) Kansy, J. *Nucl. Instruments Methods Phys. Res. Sect. A Accel. Spectrometers, Detect. Assoc. Equip.* **1996**, *374* (2), 235–244.

(10) Burrell, G. L.; Dunlop, N. F.; Separovic, F. *Soft Matter* **2010**, *6* (9), 2080–2086.

(11) Dong, K.; Zhang, S.; Wang, D.; Yao, X. *J. Phys. Chem. A* **2006**, *110* (31), 9775–9782.

(12) Kunz, T. H.; de Torrez, E. B.; Bauer, D.; Lobova, T.; Fleming, T. H. *Annals of the New York Academy of Sciences*. **2011**, *1223* (1), 1–38.

(13) Montzka, S. A.; Dutton, G. S.; Yu, P.; Ray, E.; Portmann, R. W.; Daniel, J. S.; Kuijpers, L.; Hall, B. D.; Mondeel, D.; Siso, C.; et al. *Nature* **2018**, *557* (7705), 413–417.

(14) Rigby, M.; Park, S.; Saito, T.; Western, L. M.; Redington, A. L.; Fang, X.; Henne, S.; Manning, A. J.; Prinn, R. G.; Dutton, G. S.; et al. *Nature* **2019**, *569* (7757), 546–550.

(15) Chen, T. H.; Popov, I.; Kaveevivitchai, W.; Chuang, Y. C.; Chen, Y. S.; Jacobson, A. J.; Miljanic, O. *Angew. Chemie - Int. Ed.* **2015**, *54* (47), 13902–13906.

(16) Shiflett, M. B.; Yokozeki, A. *Fluid Phase Equilib.* **2007**, *259* (2), 210–217.

(17) Yang, D.; Zhao, J.; Zhao, Y.; Lei, Y.; Cao, L.; Yang, X. J.; Davi, M.; De Sousa Amadeu, N.; Janiak, C.; Zhang, Z.; et al. *Angew. Chemie - Int. Ed.* **2015**, *54* (30), 8658–8661.

(18) Mecozzi, S.; Rebek, J. *Chem. - A Eur. J.* **1998**, *4* (6), 1016–1022.

(19) Kleywegt, G. J.; Alwyn Jones, T. *Acta Crystallogr. Sect. D Biol. Crystallogr.* **1994**, *50* (2), 178–185.

(20) Greenaway, R. L.; Holden, D.; Eden, E. G. B.; Stephenson, A.; Yong, C. W.; Bennison, M. J.; Hasell, T.; Briggs, M. E.; James, S. L.; Cooper, A. I. *Chem. Sci.* **2017**, *8* (4), 2640–2651.

CHAPTER 6

Hetero-Cages as Porous Liquids

6.1 Introduction

In Chapter 5, we presented the successful synthesis of the first liquid coordination cage which has the properties of a Type I permanently porous liquid. However, one of the drawbacks of the system is the relatively low porosity of the material. Due to the high molecular weight of the PEG_{1000} chains, the porous liquid was comprised of only 25 wt% cage. Therefore, we proposed to increase the porosity by replacing the anions in the system with negatively-charged cages. This unique structure will be referred to as a "hetero-cage" henceforth. The anion exchange from a conventional, small molecule-based anion to an anionic cage could not only

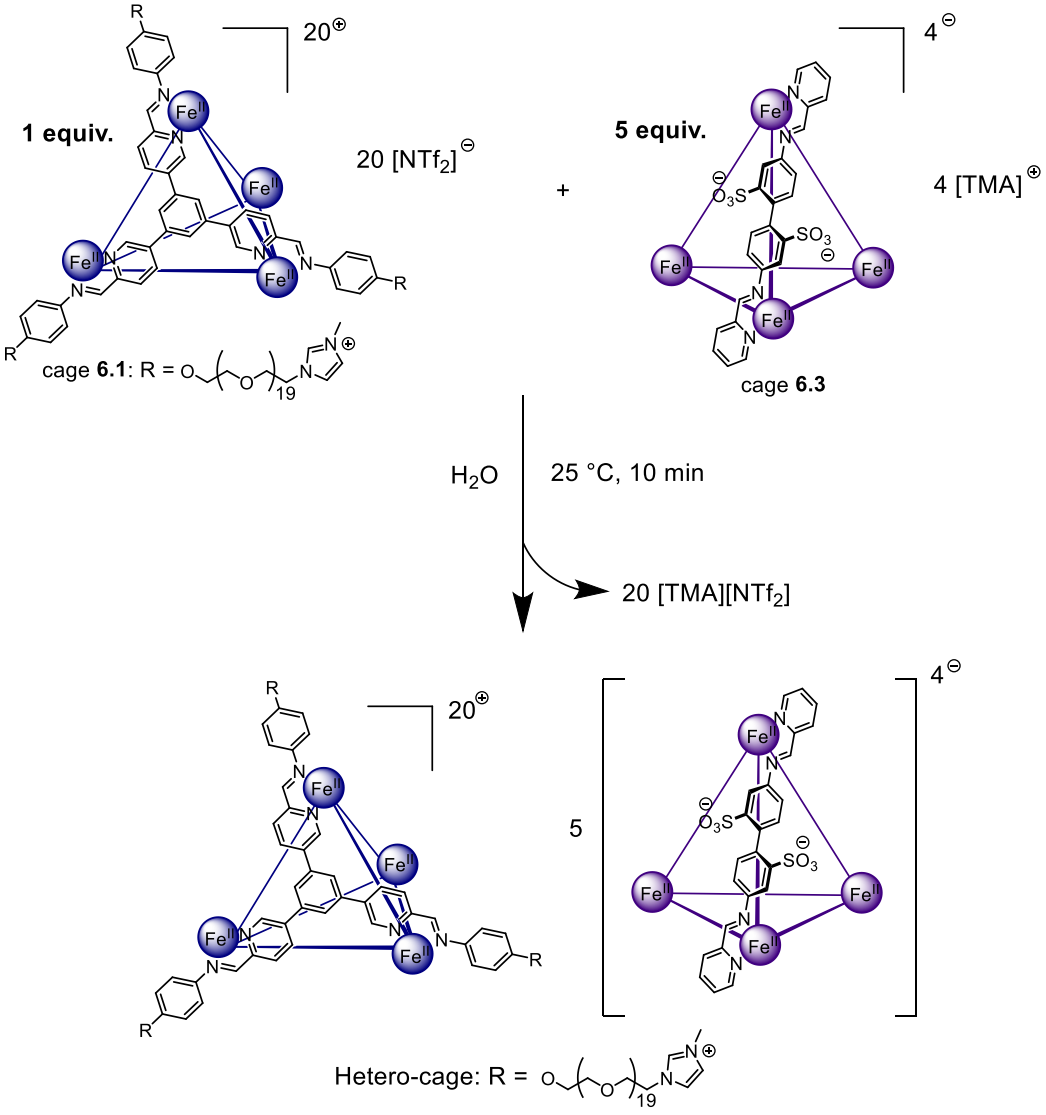

Scheme 6.1: Ion metathesis between cationic liquid cage **6.1** and anionic cage **6.3** to yield a hetero-cage liquid.

result in a liquid with increased porosity compared to the cages in Chapter 5, but also yield a single porous liquid containing two different but discrete pores – a novel concept in the field of porous liquids. When Stuart James proposed the idea of engineering intrinsic porosity into liquids, he conceptualized liquids comprised of one type of host. For example, Type I porous liquids are comprised of a single liquid host while Type II porous liquids are comprised of a single host dissolved in a sterically hindered solvent. However, we hypothesized that a hetero-cage could not only qualify as a Type I porous liquid because it will be comprised of rigid liquid hosts, but also as a Type II porous liquid because the anionic cage could also be considered as solubilized by the liquid cationic cage. Previous research and the results of Chapter 4 indicate that cages have been successfully solubilized in ionic liquids,[1] and we therefore postulate that a solid cage could potentially be dissolved in a liquid coordination cage because the latter material is by definition an ionic liquid.

In this chapter, we investigated the synthesis and characterization of hetero-cage porous liquids comprised of a cationic cage charge-balanced by multiple equivalents of anionic cage. Specifically, we proposed to charge-balance a liquid coordination cage with +20 charge liquid with an anionic cage with -4 charge (Scheme 6.1). Therefore, one equivalent of liquid cage requires 5 equivalents of the solid anionic cage to yield a fully charge-balanced system. Solid anionic cage **6.3** was chosen for its synthetic simplicity because large quantities of it are needed (5 equiv.) in the heterocage synthesis. While cage **5.2** could be employed as the liquid cationic cage in this system, we hypothesized that the labile zinc corners of the cage could result in ligand scrambling. Therefore, we designed cage **6.1** because iron is less labile and could result in a more stable structure.

Upon successful synthesis, the hetero-cage could then be characterized by DSC and TGA; those results contrasted against the DSC and TGA analyses of parent cages **6.1** and **6.3** could clarify how the individual components of the hetero-cage system influence the phase behavior of this new material. While there is no previous research on charge-balancing a cage with a second cage, Bennett et al. have performed a study on the blending of liquid MOFs. Their work demonstrated that mixing two MOFs in the liquid state resulted in a new blended MOF with a tailorable glass transition temperature based on the different ratio of parent MOFs in the sample (Figure 6.1).[2]

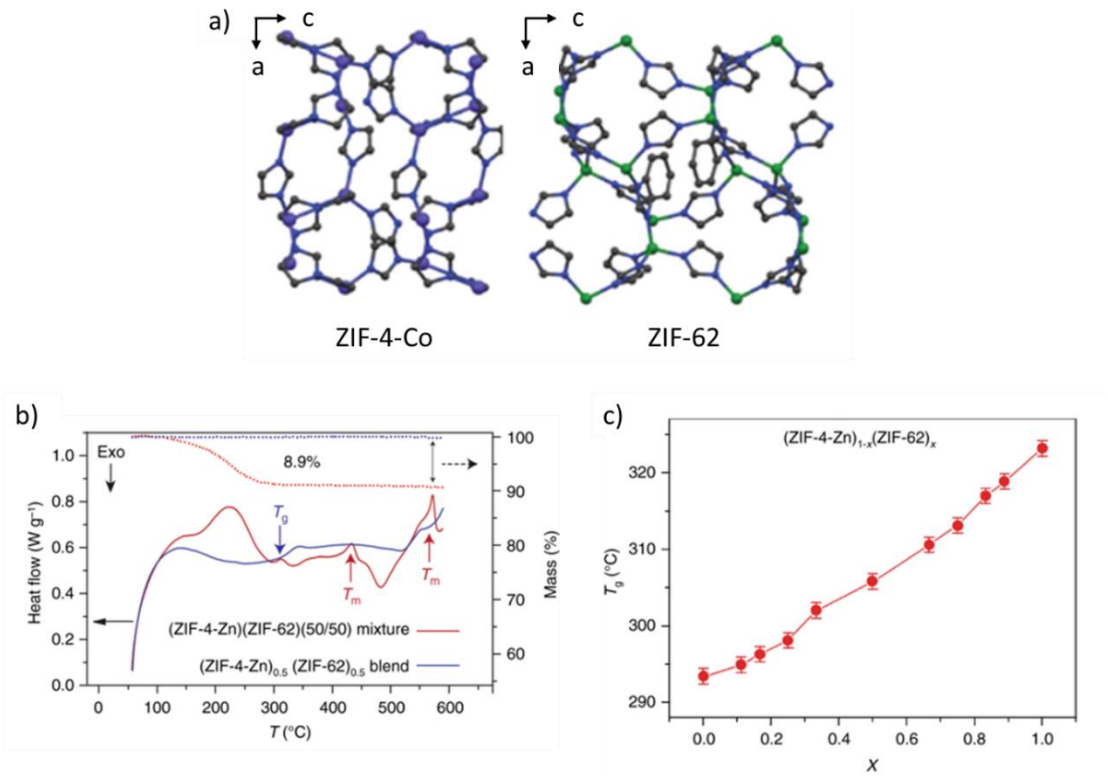

Figure 6.1: a) Structures of ZIF-4-Co and ZIF-62. b) Enthalpy response (red curve) and mass change (dotted curve) in the physical mixture of (ZIF-4-Zn)(ZIF-62)(50/50) during heating at 10 °C/min. Blue curve: reheating curve representing the enthalpy response of the corresponding glass that forms upon quenching, i.e., $(ZIF\text{-}4\text{-}Zn)_{0.5}(ZIF\text{-}62)_{0.5}$ during prior cooling at 10 °C min−1. c) Evolving T_g of the sample series $(ZIF\text{-}4\text{-}Zn)_{1-x}(ZIF\text{-}62)_x$. Figure adapted from reference 2.

We postulated that our system may behave analogously so we proposed synthesizing hetero-cages with a 1:1, 1:3 and 1:5 ratio of cage **6.1** to cage **6.3**. While the 1:1 and 1:3 mixtures of cages **6.1** and **6.3** would not generate a true hetero-cage because residual NTf_2^- anions would be needed to charge-balance **6.1**, the enthalpy responses of these samples could still shed light on how the parent cages influence the phase change behavior of the mixture. While we hypothesized that cage **6.1** would have a glass transition similar to cage **5.2** because the cages share a similar scaffold, the enthalpy responses of the hetero-cages are difficult to predict because the phase behavior of cage **6.3** is unknown.

6.2 Synthesis of Cages 6.1-6.3

Trialdehyde **5H** was self-assembled with aniline **5F** and **5F'** in the presence of $Fe(NTf_2)_2$ to yield cages **6.1** and **6.2**. The subcomponents were combined in CH_3CN and the chamber was subjected to 3 freeze-pump-thaw cycles before heating at 70 °C for 18 h under

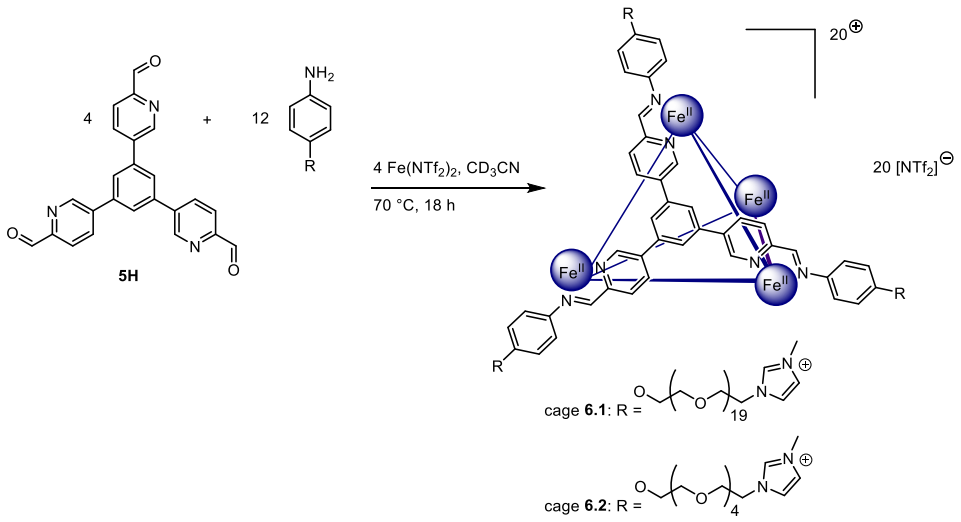

Scheme 6.2: Self-assembly of cages **6.1** and **6.2**. Cage **6.1** was assembled with the PEG_{1000}-imidazolium aniline **5F** and cage **6.2** was assembled with the shorter pentaethylene glycol-imidazolium aniline **5F'**.

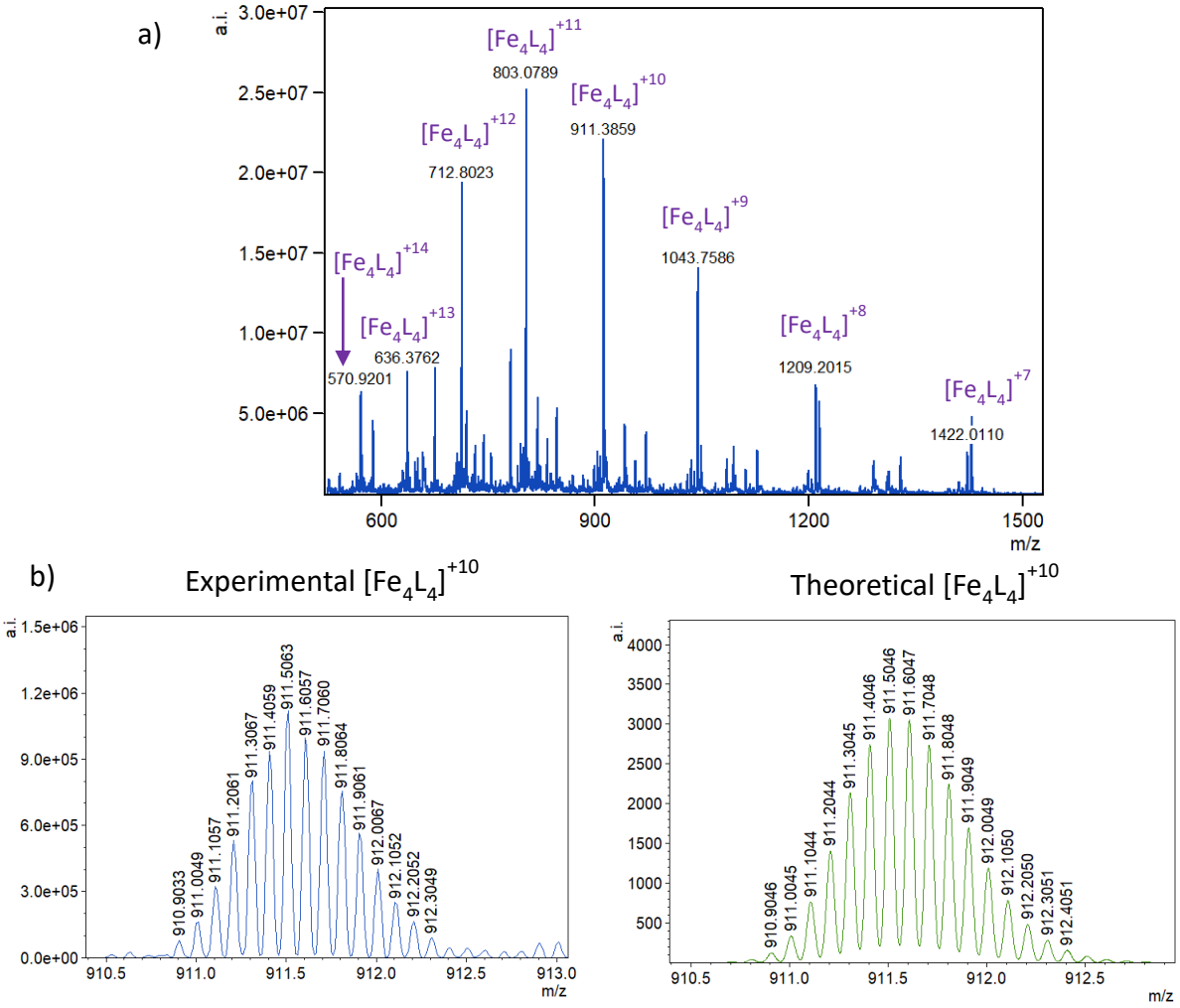

Figure 6.2: a) LR-ESI-MS spectrum of cage **6.2**; charge distribution consistent with proposed structure and b) HR-ESI-MS spectrum of cage **6.2**; isotope pattern consistent with theoretical calculations.

N_2 (Scheme 6.2). The cages were precipitated out of solution with diethyl ether and collected *via* centrifugation. Cage **6.1** was a dark blue viscous liquid at room temperature while cage **6.2** was a glass-like solid. These physical properties of cages **6.1** and **6.2** are qualitatively analogous to those of zinc cages **5.2** and **5.3**, respectively. Both cages **6.1** and **6.2** were analyzed *via* ^{1}H NMR in CD_3CN, and the observed peaks were consistent with the previously published unfunctionalized $Fe^{II}_4L_4$ tetrahedral cage.[4] The ^{19}F NMR spectra of both cages contained a single peak consistent with free NTf_2^-, demonstrating that the cavities of both cage **6.1** and **6.2** remained empty – a result again consistent with cages **5.2** and **5.3**. Cages **6.1** and **6.2** were also analyzed by LR-ESI-MS, but cage **6.1** was found to be unstable under those experimental conditions. However, the mass spectrum of cage **6.2** exhibited a charge-distribution consistent with an $Fe^{II}_4L_4$ structure (Figure 6.2a), a result that was then confirmed by HR-ESI-MS (Figure 6.2b). Based on the NMR results indicating that cage **6.1** and **6.2** shared similar scaffolds**,** we assumed that **6.1** was also a face-capped tetrahedral cage.

In addition to cages **6.1** and **6.2**, anionic cage **6.3** was assembled *via* a published procedure.[3] 4,4'-diaminobiphenyl-2,2'-disulfonic acid, 2-pyridinecarboxaldehye and tetra-methylammonium hydroxide pentahydrate were combined in D_2O and heated at 50 °C for 18 h to yield edge-bridged tetrahedral cage **6.3** (Scheme 6.3). The cage was then precipitated out of solution with CH_3CN and isolated as a dark purple solid. ^{1}H NMR analysis of the cage in D_2O solution was consistent with published results. Cages **6.3** and **6.1** were then subsequently used to synthesize the hetero-cage.

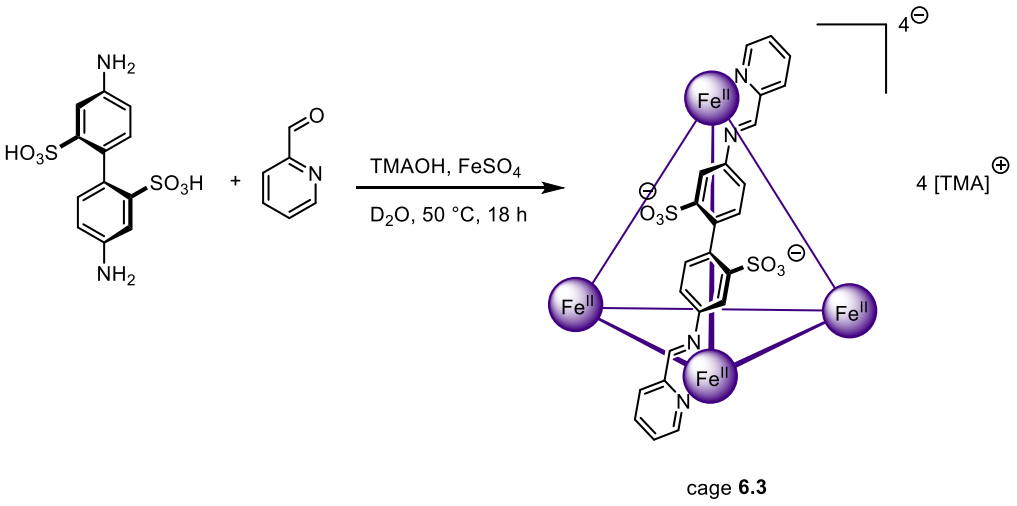

Scheme 6.3: Self-assembly of cage **6.3** from a previously published procedure.[3]

6.3 Synthesis of Hetero-Cages

Hetero-cage samples were synthesized by adding cage **6.3** to a solution of cage **6.1** in cold water (3 mL). The synthesis was conducted in water due to the insolubility of cage **6.3** in organic solvents. Although PEG-imidazolium cages were previously only analyzed in CH_3CN, a preliminary solubility test on cage **6.1** demonstrated that the cage was also soluble in water. Therefore, cage **6.1** was re-characterized *via* ^{1}H NMR in D_2O. The ^{1}H NMR spectrum showed very broad peaks that were consistent in chemical shift to the peaks observed in the ^{1}H NMR spectrum of cage **6.1** dissolved in CD_3CN. To determine whether the cage was stable in water over extended periods of time, a stability experiment was conducted on a sample of cage **6.1** in D_2O, in which a ^{1}H NMR spectrum was taken of the sample every 20 minutes. The ^{1}H NMR spectrum of the sample after 8 hours was consistent with the spectrum of the sample taken immediately after solvation of cage **6.1** in D_2O (Figure 6.3). Therefore, we concluded that the cage was stable for the duration of this experiment. Consequently, we also assumed that cage **6.1** was stable in water during the hetero-cage synthesis.

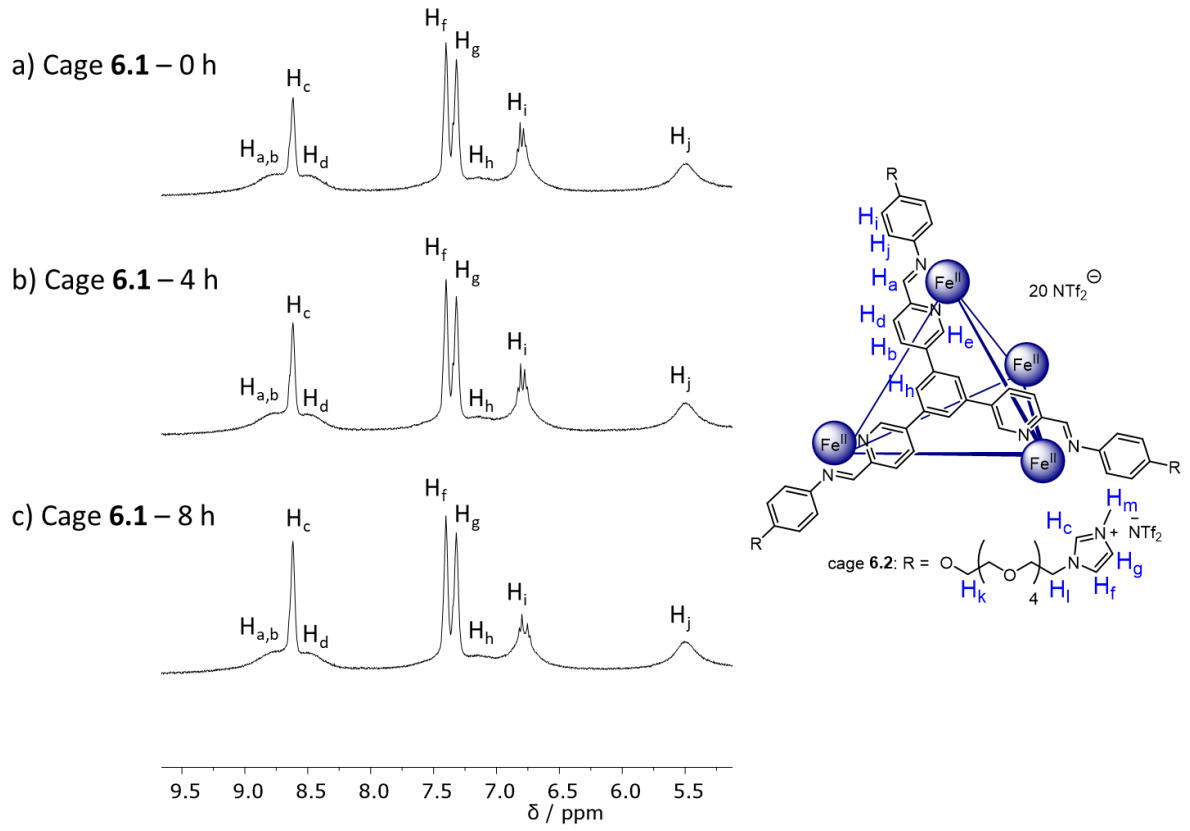

Figure 6.3: Partial ^{1}H NMR (400 MHz, 298 K, D_2O) spectra used to track the stability of cage **6.1** in D_2O. a) Fresh sample of cage **6.1** b) after 4 h and c) after 8 h.

Nevertheless, even though cages **6.1** and **6.3** could be combined in water, the residual TMA^+ and NTf_2^- ions in solution would prevent the cages from solely charge-balancing each other. Therefore, the hetero-cage solution was purified by extracting out TMA^+ and NTf_2^- with cold ethyl acetate (10 x 3 mL); the reaction vessel was submerged in ice water to ensure that the system remained cold during the partition of ethyl acetate and water. The temperature of the system was kept low because cage **6.1** is also soluble in ethyl acetate. However, research has shown that the solubility of PEG-imidazolium ionic liquids can be thermally controlled.[5] At lower temperatures, these ionic liquids exhibit higher solubility in water than organic solvents due to an increase in ordered water molecules around the random-coil conformations of the PEG chains.[6] Similarly, cages functionalized with PEG-imidazolium chains can also be thermally controlled.[7] Solubility tests showed that cage **6.1** also showed increased solubility in water compared to organic solvents at lower temperatures – a result we attributed to the PEG-imidazolium groups appended on the corners of the cage.

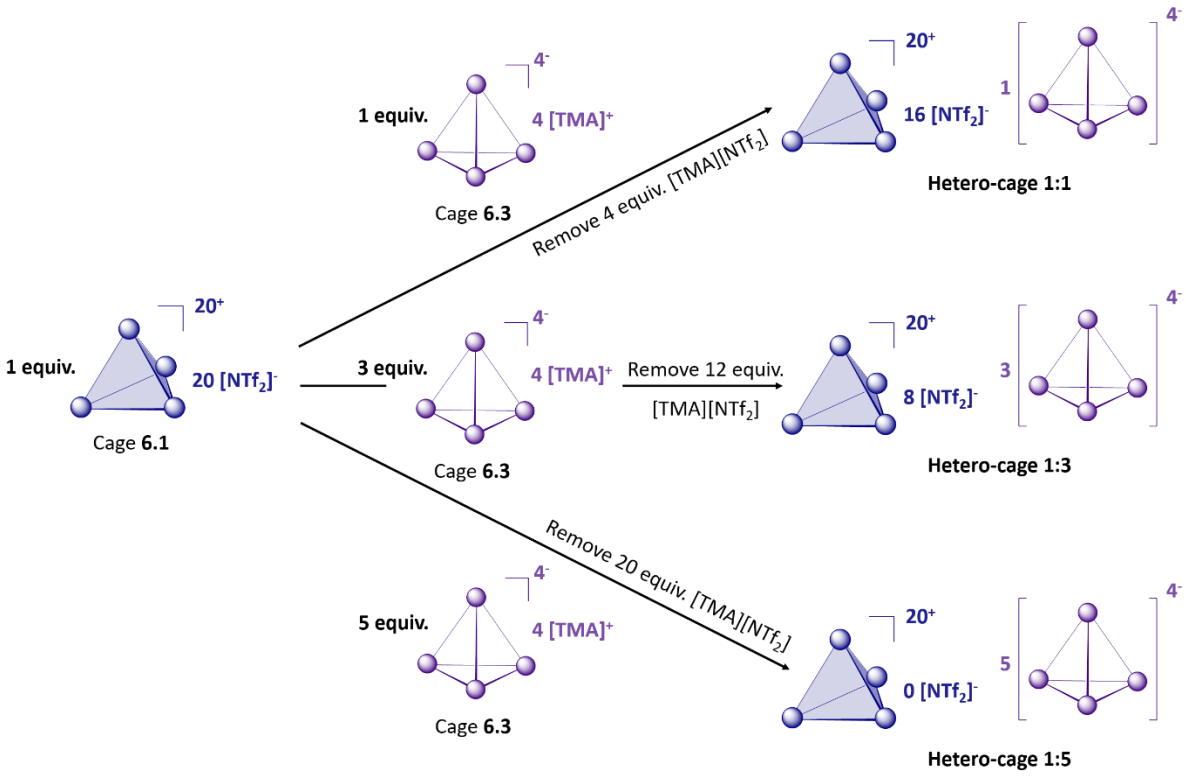

Figure 6.4: Synthetic scheme of the hetero-cage samples with mixtures of cage **6.1** to **6.3** in a 1:1, 1:3 and 1:5 ratio.

Therefore, washing the aqueous hetero-cage solution with cold ethyl acetate and allowing the organic and aqueous layer to partition at low temperatures, resulted in the successful removal of excess TMA^+ and NTf_2^- without extracting out cage **6.1** – a result confirmed by NMR spectroscopy. After the organic washes, water was removed under vacuum at 298 K to yield pure hetero-cage. This experimental process was used to synthesize hetero-cage samples comprised of a 1:1, 1:3 and 1:5 ratio of cage **6.1** to **6.3**. These samples will hereafter be referred to as hetero-cage 1:1 (**HC-1:1**), hetero-cage 1:3 (**HC-1:3**) and hetero-cage 1:5 (**HC- 1:5**) (Figure 6.4). It should be acknowledged that **HC-1:1** and **HC-1:3** are not technically hetero-cages because they contain excess NTf_2^- anions to fully balance the charge of cage **6.1**, but we will use this notation across the series for simplicity.

Hetero-cages **HC-1:1**, **HC-1:3** and **HC-1:5** were analyzed by ^{1}H NMR in D_2O. The results of these spectra were compared against the individual ^{1}H NMR spectra of cages **6.1** and **6.3** in D_2O. While it was difficult to identify the presence of cage **6.1** due to the broadness of its peaks, peaks associated with both cages **6.1** and **6.3** were observed in all three hetero-cage samples (Figure 6.5). A peak integration comparison was used to approximate the actual ratio of cage **6.1** to **6.3** in the sample. Peaks **A** and **B** were chosen to calculate the cage ratio (Figure 6.5). Peak **A** is correlated to cage **6.3** and peak **B** to cage **6.1**.

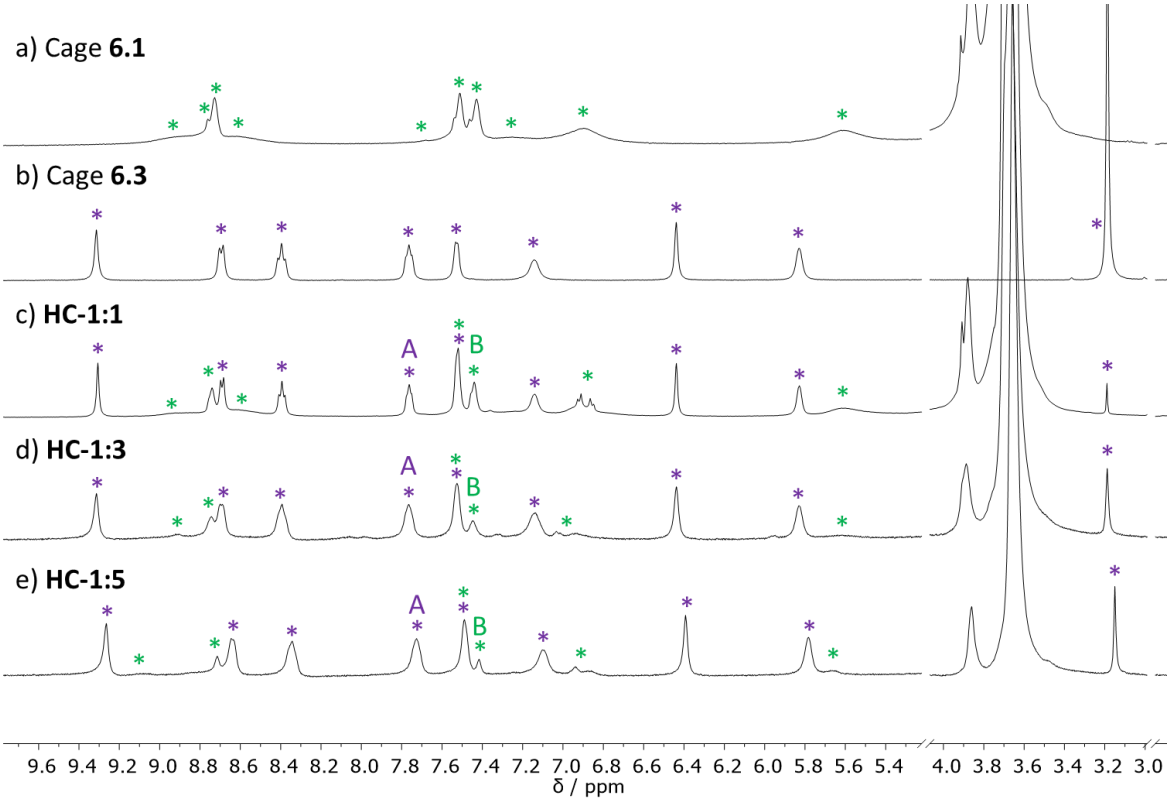

Figure 6.5: Partial ^{1}H NMR (400 MHz, 298 K, D_2O) spectra of a) cage **6.1**, b) cage **6.3**, c) **HC-1:1**, d) **HC-1:3** and e) **HC-1:5**. Peaks from cages **6.1** (*) and **6.3** (*) are labelled with green and purple asterisks, respectively. A and B label the peaks used to calculate the ratios of cage **6.1** to **6.3**.

The areas under peaks **A** and **B** were calculated using the deconvolution method in MestreNova and are reported in Table 1. The peak area ratio was then calculated by dividing the peak area of **A** by the area of **B**. The resulting value was also equal to the ratio of cage **6.3** to **6.1** in the hetero-cage sample. Therefore, the experimental ratio of cage **6.3** to **6.1** in sample **HC-1:1** was 0.9:1.0, indicating that less cage **6.3** was present in the sample than the proposed ratio of 1:1. Conversely, **HC-1:5** contained a ratio of 5.2 equivalents of cage **6.3** to 1.0 equivalent of cage **6.1** – a ratio higher than the intended 5:1 proportion. However, the calculations for sample **HC-1:3** showed that the experimental ratio of cage **6.3** to **6.1** in the sample was 3.0:1.0 – a good match to the proposed ratio.

Table 6.1: Areas of peak A and peak B (see Figure 6.5) are reported. Peak area ratio was calculated by dividing the area of A by the area of B (A : B).

Sample	Peak Area of A	Peak Area of B	Peak Area Ratio (A : B)
HC-1:1	2582.9	2918.1	0.9 : 1
HC-1:3	37725.3	12389.8	3.0 : 1
HC-1:5	36221.5	6924.2	5.2 : 1

The combination of cage **6.1** (1 equiv.) and cage **6.3** (5 equiv.) should yield a completely charge-balanced hetero-cage after the residual [TMA][NTf_2] salt is extracted with ethyl acetate (Figure 6.4). Similarly, **HC-1:1** and **HC-1:3** would contain NTf_2^- anions to balance the charge of cage **6.1** but no TMA^+ cations. Therefore, no TMA^+ signals were expected in any of the ^1H NMR spectra obtained from the hetero-cage samples. However, all three ^1H NMR spectra of the hetero-cages contained a signal at 3.19 ppm, which is consistent with the chemical shift of TMA^+ (Figure 6.5). The experimental ratio of **HC-1:5** indicated that an excess of cage **6.3** was present in the sample. Therefore, one can expect a TMA^+ signal to balance the charge of excess cage **6.3**. However, the TMA^+ signals present in **HC-1:1** and **HC-1:3** were attributed to incomplete purification.

HC-1:1, **HC-1:3** and **HC-1:5** were also analyzed by ^{19}F NMR, and the resulting spectra showed that **HC-1:1** contained more NTf_2^- than **HC-1:3** (Figure 6.6). Conversely, no signal was observed in the ^{19}F NMR spectrum of **HC-1:5** – a result that was consistent with our hypothesis that no NTf_2^- would remain in the sample due to the complete charge-balance between cage **6.1** and **6.3**. Although the experimental ratio of cage **6.1** to cage **6.3** in sample

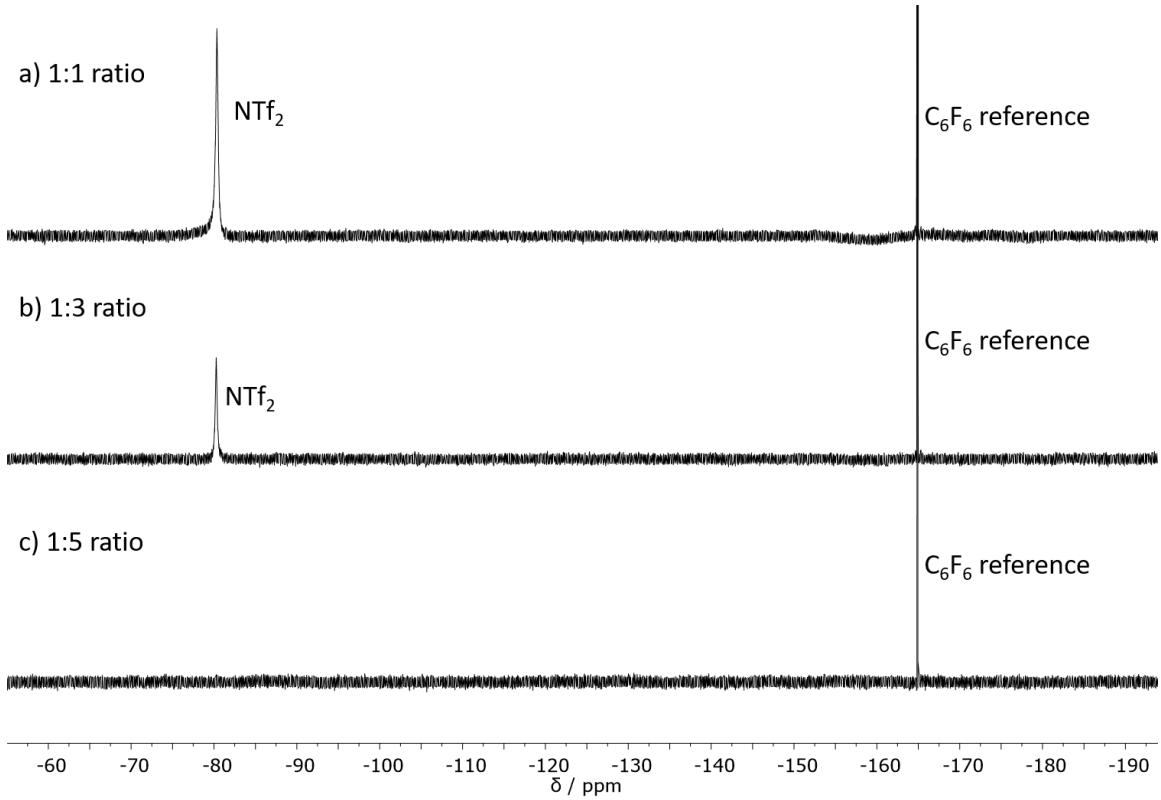

Figure 6.6: ^{19}F NMR (377 MHz, 298 K, D_2O) spectra of **HC-1:1**, **HC-1:3** and **HC-1:5**.

HC-1:5 was previously calculated to be 1.0:5.2, which is not a perfect match for the proposed ratio of 1.0:5.0, the absence of a NTf_2^- signal in the ^{19}F NMR spectrum indicated that enough cage **6.3** was present in sample **HC-1:5** to fully charge-balance cage **6.1**. This trend of less NTf_2^- in hetero-cage samples containing more cage **6.3** was consistent with the proposed ratios of parent cages in these samples.

However, the residual TMA^+ signals observed in the ^1H NMR spectra of **HC-1:1** and **HC-1:3** suggested that remaining NTf_2^- anions were also present in these two samples because the excess TMA^+ cations would need to be charge-balanced by an anionic species. Therefore, we acknowledge that the purification of these systems requires optimization. These hetero-cage samples were subsequently used for preliminary DSC and TGA analysis. While these samples did not contain the exact proposed ratio of cage **6.1** to cage **6.3**, the thermal profiles of these hetero-cages can provide a foundation on which future hetero-cages can be designed. These preliminary thermal analysis studies also provide an opportunity to optimize characterization conditions for these novel materials.

6.4 Thermal Analysis of Hetero-Cages

6.4.1 TGA analysis of cage 6.1, cage 6.3, and hetero-cages

After solution-state NMR analysis of cage **6.1**, cage **6.3**, **HC-1:1, HC-1:3** and **HC-1:5**, the neat samples were characterized with TGA to investigate the thermal stability of these materials (Figure 6.7). All samples were heated at 10 °C until 500 °C. The TGA curve of cage **6.1** contained no features except for a T_{decomp} (303.9 °C). The onset of T_{decomp} was defined as the temperature at which 5 wt% was lost after the plateau immediately prior to decomposition. The cage rapidly decomposed, losing 75 wt% by the end of the scan. The lack of other features below 200 °C indicated that a negligible amount of residual solvent was present in the sample. These results were consistent with the thermal stability of cage **5.2**, the zinc-based equivalent of cage **6.1**.

In contrast, the TGA curve of cage **6.3** showed a 20 wt% loss below 100 °C. We attributed this early mass loss to the presence of water in the sample. Cage **6.3** was synthesized in water, and although the sample was dried under vacuum after its initial assembly, it was stored under ambient conditions prior to thermal analysis. We therefore hypothesized that the hygroscopic cage salt absorbed water from the atmosphere prior to analysis. In addition to the

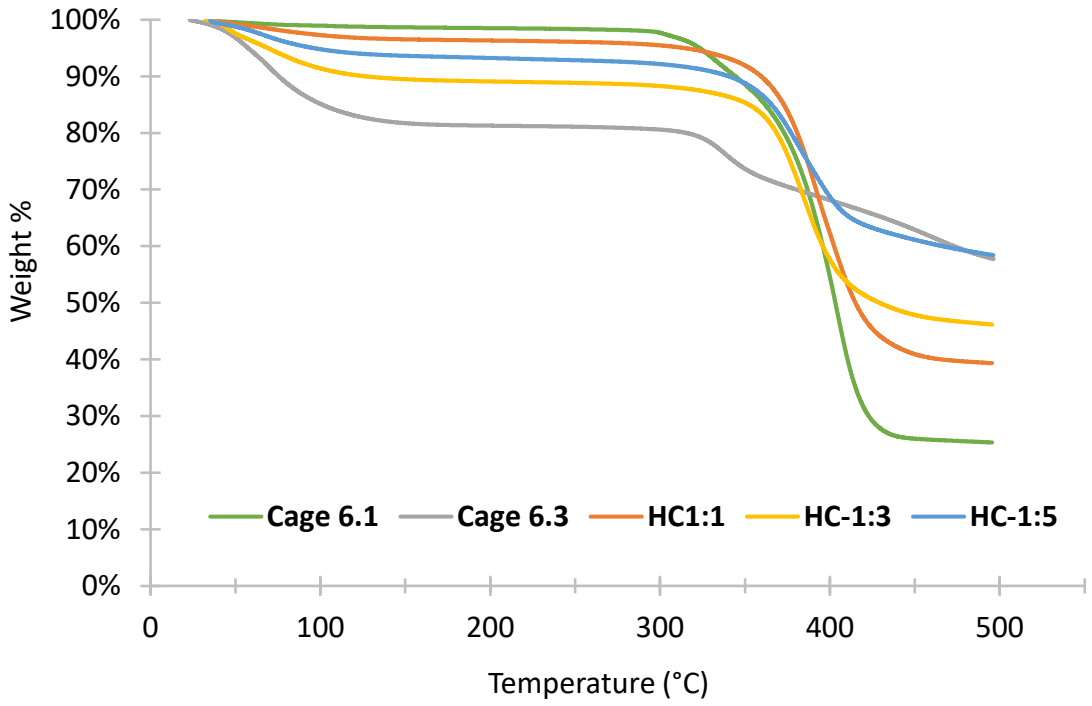

Figure 6.7: TGA curves of cage **6.1**, cage **6.3**, **HC-1:1, HC-1:3** and **HC-1:5**.

loss of solvent below 100 °C, the other feature present in the TGA curve of cage **6.3** was a T_{decomp} at 329.7 °C. However, while cage **6.1** rapidly decomposed to 25 % of its initial mass, the decomposition of cage **6.3** was gradual. By 500 °C, the sample only decomposed to 58% of its original mass. While considerably less mass loss was observed in the same temperature range for cage **6.3** than cage **6.1**, an approximately 20 wt% loss between the plateaued region in the TGA curve of cage **6.3** (150–300 °C) and the end of the TGA scan is still significant. Therefore, we assumed that by 500 °C, cage **6.3** was decomposed. However, in the future this experiment could be repeated with a drier sample of cage **6.3** heated to a higher temperature in order to observe whether any additional features appear above 500 °C, and to determine whether excess moisture affected the thermal stability of the material.

Like cage **6.3**, the TGA curves of **HC-1:1, HC-1:3** and **HC-1:5** exhibited mass loss below 100 °C. We attributed this decrease in mass to the presence of water in the samples due to the hygroscopicity of the hetero-cages. The samples that were dried under vacuum closer to the time of analysis contained less water than samples that were left under ambient conditions. In contrast to the parent cages, **HC-1:1**, **HC-1:3** and **HC-1:5** all decomposed at 350 ± 1 °C – a temperature slightly higher than the decomposition temperatures of cage **6.1** and **6.3** individually. However, samples containing larger amounts cage **6.1** decomposed more rapidly above their T_{decomp} than their counterparts containing more cage **6.3**. For example, sample **HC-1:5** lost 41 wt% by 500 °C, a value identical to that of cage **6.3**. However, **HC-1:3** and **HC-1:1** lost 54 % and 61 % of their initial masses, respectively, at the ends of their scans. This trend is consistent with the observation that cage **6.1** decomposed more rapidly than cage **6.3**; therefore a larger amount of cage **6.1** in the hetero-cage samples could result in faster decomposition. Although the three hetero-cage samples decomposed at different rates, all three curves contained only one T_{decomp} in the temperature range for these experiments. These hetero-cages could be reanalyzed at higher temperatures in the future to determine whether any additional features appear above 500 °C.

6.4.2 DSC analysis of cage 6.1, cage 6.3 and hetero-cages

While **HC-1:3** and **HC-1:5** both appeared to be amorphous solids at room temperature, **HC-1:1** had the consistency of a highly viscous liquid or a soft waxy solid. We hypothesized that the phase change behaviors of these samples would indicate whether the different hetero-

cages are solid or liquid at room temperature. We also wanted to investigate whether the phase behavior of the hetero-cages differed from those of their individual component cages.

Therefore, cage **6.1**, cage **6.3**, **HC-1:1, HC-1:3** and **HC-1:5** were analyzed by DSC (Figure 6.8, Figure 6.9, Table 6.2). The DSC curve of cage **6.1** featured a reversible T_g at -36.9 ± 1.2 °C and -41.7 ± 0.7 °C (Figure 6.8) – a result similar to that of cage **5.2**, The onset of the T_g was defined by the intersection point between the heat flow before the glass transition and the change in heat flow during the glass transition. No other features were observed in this scan. Similarly, the DSC curve of cage **6.3** featured a single sharp T_m at 171.2 °C and no additional features (Figure 6.9). The onset of T_m was defined as the apex of the melting feature. The looping of the melting point feature was an artefact of the experiment and can be caused by a sudden and intense change in enthalpy.[8] This artefact can be prevented in the future by decreasing the sample mass.

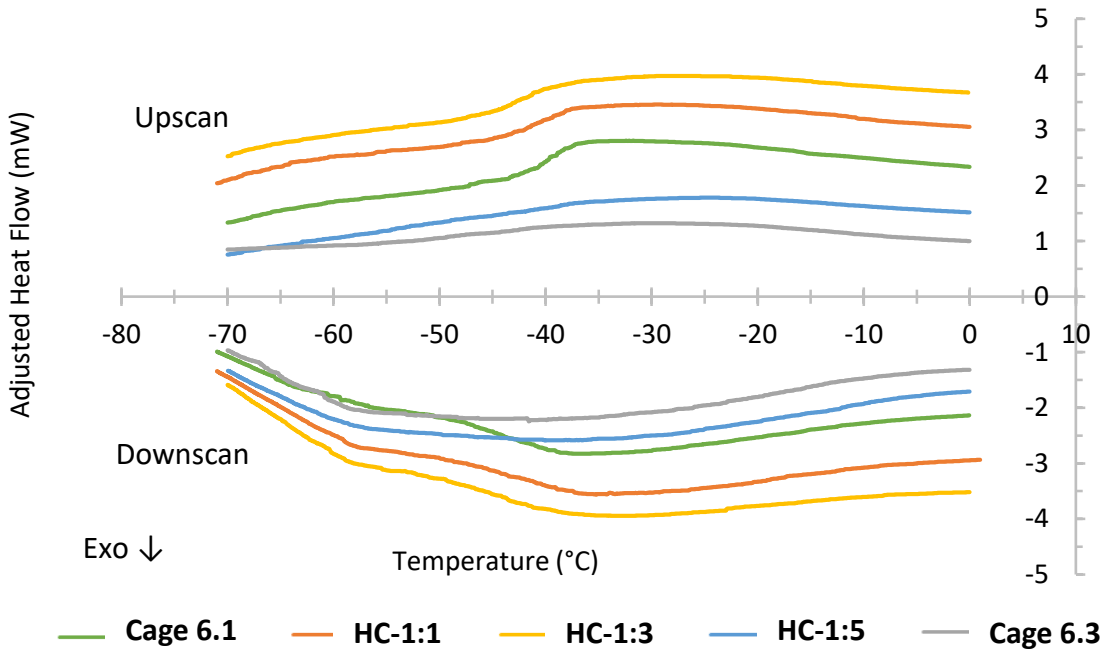

Figure 6.8: Partial DSC curves containing an enlargement of the T_g features of cage **6.1**, **HC-1:1, HC-1:3** and **HC-1:5**. Cage **6.3** did not contain a T_g but is shown as a comparison to **HC-1:5**.

Conversely, all hetero-cage samples contained two features, a reversible T_g at -37 ± 2 °C and -58 ± 1 °C and a T_m between 140-180 °C. The temperature of the glass transition features observed in the hetero-cage samples was consistent with the T_g of cage **6.1** (Figure 6.8). Furthermore, the resolution of the T_g feature was proportional to the amount of cage **6.1** present in the sample. The glass transitions of **HC-1:1** and **HC-1:3** were clearly observable,

but the T_g of **HC-1:5** was poorly resolved. While the broad T_g of **HC-1:5** may have been be overlooked when independently observing the curve, comparing the curve of cage **6.1** against **HC-1:5** showed that the curve of **HC-1:5** contained a more pronounced bend below 0 °C. The poor resolution of this T_g was attributed to the relatively low ratio of cage **6.1** present in sample **HC-1:5**.

Table 6.2: T_g and T_m of cage **6.1**, cage **6.3**, **HC-1:1**, **HC-1:3** and **HC-1:5**.

Sample	T_g (Upscan)	T_g (Dowscan)	T_m
Cage **6.1**	-36.9 ± 1.2 °C	-41.7 ± 0.7 °C	N/A
Cage **6.3**	N/A	N/A	171.2 °C
HC-1:1	-36.3 ± 0.8 °C	-43.2 ± 0.3 °C	142.9 °C
HC-1:3	-36.3 ± 1.1 °C	-43.8 ± 1.1 °C	157.1 °C
HC-1:5	N/A*	N/A*	177.6 °C

*A T_g was observed for **HC-1:5** but an onset was not determined due to the broadness of the feature.

In addition to glass transitions, each hetero-cage sample also contained a melting feature (Figure 6.9). While the T_m of **HC-1:5** (177.6 °C) was sharp and similar to with the T_m of cage **6.3** (171.2 °C), the melting features of **HC-1:1** (142.9 °C) and **HC-1:3** (157.1 °C) were broader and appeared at lower temperatures. We hypothesized that this difference was due to the mixture of cations present in these samples. While the anionic cage **6.3** species present in **HC-1:5** was fully charge-balanced by cationic cage **6.1**, **HC-1:1** and **HC-1:3** both contained a mixture of cage **6.1** and residual TMA^+ as the counterions for cage **6.3**. Therefore, we hypothesized that this mixture of cations with vastly different structures prevented efficient stacking under solvent-free conditions, which depressed the melting points of these samples. The broadness of the melting features was also consistent with previous studies on ionic liquids with different anion mixtures.[9] Additionally, the sharpness of the T_m in **HC-1:5** confirmed the NMR results and supported our hypothesis that cage **6.1** was fully charge-balanced by cage **6.3**. Since a mixture of cations resulted in the T_m of the hetero-cage samples broadening, we hypothesized that a sharp T_m in the DSC curve of **HC-1:5** was indicative of cage **6.1** being charge-balanced by solely cage **6.3**.

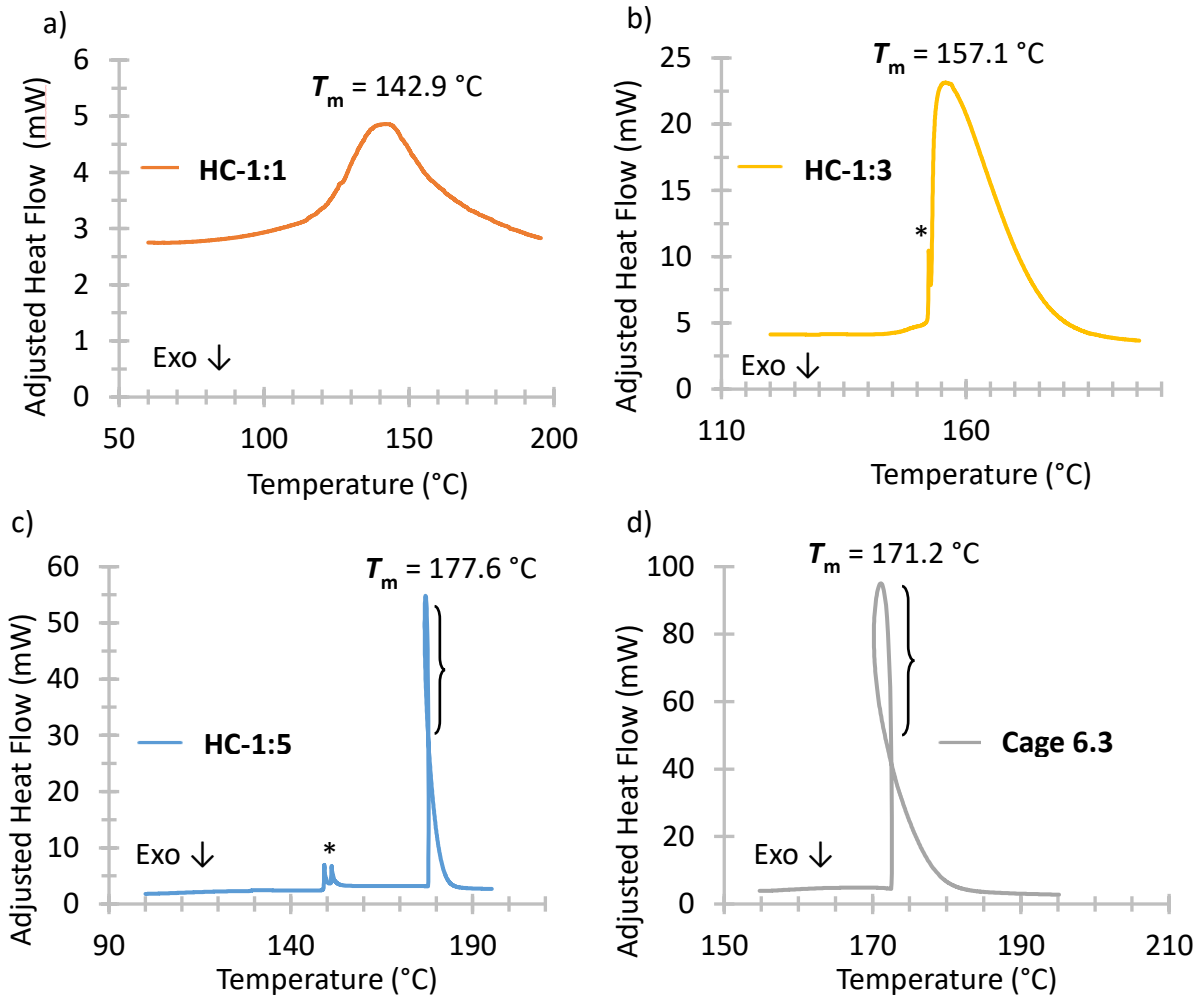

Figure 6.9: Partial DSC curves containing an enlargement of the T_m feature in cage **HC-1:1, HC-1:3, HC-1:5** and cage **6.3**. Artefacts are marked with asterisks (*) and brackets (}).

After consulting the thermal analysis results, we reached the hypothesis that the hetero-cages were comprised of a suspension of solid cage **6.3** in liquid cage **6.1**. Such a mixture could result in both a T_g and a T_m appearing in the same hetero-cage sample. The glass transition of cage **6.1** does not seem to affect the stability of cage **6.3** because the melting feature is still observable after cage **6.1** undergoes its reversible glass transition. Although different ratios of cages **6.1** and **6.3** in the hetero-cage resulted in slightly different DSC curves, combining the two parent cages in solution did not result in a new material with different phase behavior, but rather a composite mixture of cage **6.1** and **6.3**. As a result, this data cannot be used to describe whether the hetero-cage samples are solids or liquids.

6.5 Conclusions and Future Work

In this chapter, we presented the first synthesis and characterization of hetero-cages. We define hetero-cages to be cages that are charge-balanced by a different cage of opposite charge. We hypothesized that charge-balancing cationic liquid cage **6.1** with 5 equivalents of anionic cage **6.3** would result in a novel liquid hetero-cage that would behave as a Type I permanently porous liquid. To better understand how various ratios of parent cage affect the properties of the resulting hetero-cage, we prepared samples with a 1:1, 1:3 and 1:5 ratio of cage **6.1** to cage **6.3**. NMR studies on these hetero-cages confirmed the partial removal of residual counterions and indicated that both component cages in the hetero-cage were stable in solution. The absence of encapsulated counterion signals also confirmed that both cage components of the hetero-cage remained empty.

TGA analysis of the hetero-cages indicated that these materials possessed high thermal stabilities (~350 °C) comparable to those of the individual parent cages. DSC curves of the hetero-cages showed both a reversible T_g consistent with cage **6.1** and a T_m consistent with cage **6.3**. The melting features in **HC-1:1** and **HC-1:3** were broader than those in **HC-1:5** and cage **6.3**. We attributed this broadness to the mixture of cage **6.1** and TMA^+ cations present in the two former samples. Samples containing a lower ratio of cage **6.1** also had less defined glass transition features. Therefore, the different ratios of cage **6.1** and **6.3** in **HC-1:1, HC-1:3** and **HC-1:5** influence the enthalpy responses of the hetero-cages. Also, the simultaneous appearance of a T_m and T_g in the same DSC curve of the hetero-cages suggests that these samples are comprised of a solid suspension of cage **6.3** in liquid cage **6.1**.

Nevertheless, the DSC results indicated that both cage **6.1** and cage **6.3** in the hetero-cage samples are liquid above 200 °C and the TGA data showed that the hetero-cage samples are still stable at this temperature. Therefore, heating a sample of hetero-cage past the T_m of cage **6.3** would result in the liquid blending of cage **6.1** and **6.3**. We hypothesize that a liquid blended hetero-cage would have different enthalpic behavior when compared to the individual parent cages. While, Bennett *et al.* have conducted a similar study on the liquid blending of MOFs,[2] to the best extent of our knowledge, no studies have been conducted on the liquid blending of metal-organic cages.

To achieve the initial goal of synthesizing a liquid hetero-cage, we hypothesize that using a more negatively-charged anionic cage to balance the charge of a cationic liquid cage

would be more effective. The current system requires 5 equivalents of solid anionic cage to charge-balance 1 equivalent of liquid cationic cage; therefore, the resulting hetero-cage is unlikely to behave as a liquid at room temperature due to the large quantities of solid cage it contains. If sulfonate groups were appended to the corners of cage **6.3**, the resulting cage would have an overall charge of -16. Therefore, a 1.25:1.00 mixture of this new cage and cage **6.1** would result in a fully charge-balanced hetero-cage, which we hypothesize is more likely to be liquid at room temperature. This liquid hetero-cage could then act as a Type I permanently porous liquid containing two different cavities – an entirely new concept in the field of liquids with intrinsic porosity. Different combinations of parent cages could yield a variety of hetero-cages with assorted pores in the same liquid material. These liquid hetero-cages could then be potentially tuned for novel extraction and separation applications in the future.

6.6 Experimental Methods

6.6.1 Synthesis of cages 6.1-6.3

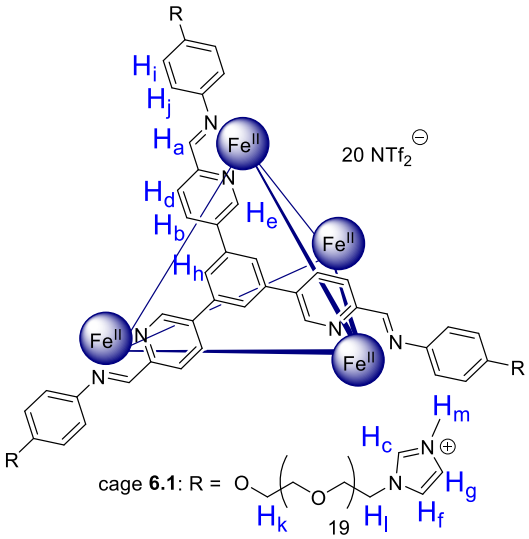

Cage **6.1**:

Trialdehyde **5H** (4.72 mg, 12.00 µmol, 1 equiv.), aniline **5F** (46.80 mg, 36.00 µmol, 3 equiv.) and $Fe(NTf_2)_2$ (8.13 mg, 3.00 µmol, 1.1 equiv.) were combined in 1.5 mL CH_3CN before being subjected to 3 freeze-pump thaw cycles. The sealed flask was then heated at 70 °C for 18 h under N_2. The cage was precipitated out of solution *via* the addition of diethyl ether (5 mL) and centrifuged. The resulting oil was concentrated under reduced pressure yielding a dark blue, viscous liquid (50.8 mg, 90% yield). ^{1}H NMR (400 MHz, 298 K, CD_3CN) δ = 8.98 (s, 1H, H_a), 8.80 (d, J = 8.1 Hz, 1H, H_b), 8.58 (m, 2H, $H_{c,d}$), 7.43 (m, 2H, $H_{e,f}$), 7.35 (s, 1H, H_g), 7.15 (s, 1H, H_h), 6.88 (d, J = 8.6 Hz, 2H, H_i), 5.71 (d, J = 8.7 Hz, 2H, H_j), 4.27 (t, 2H, J = 4.65 Hz H_k), 4.16 (m, 2H, H_l), 3.84 (s, 3H, H_m), 3.82 – 3.75 (m, 76H, $H_{aliphaticPEG}$). ^{13}C NMR (125 MHz, CD_3CN): δ = 175.3, 160.1, 159.8, 152.4, 144.5, 138.57, 137.7, 136.5, 132.8, 126.8, 124.7, 124.2, 124.1, 123.9, 122.2, 116.1, 71.1, 71.0, 71.0, 70.9, 50.5, 36.9 ppm. ^{19}F NMR (377 MHz, CD_3CN, referenced to hexafluorobenzene in a C_6F_6 capillary): δ = -80.01 (NTf_2^-).

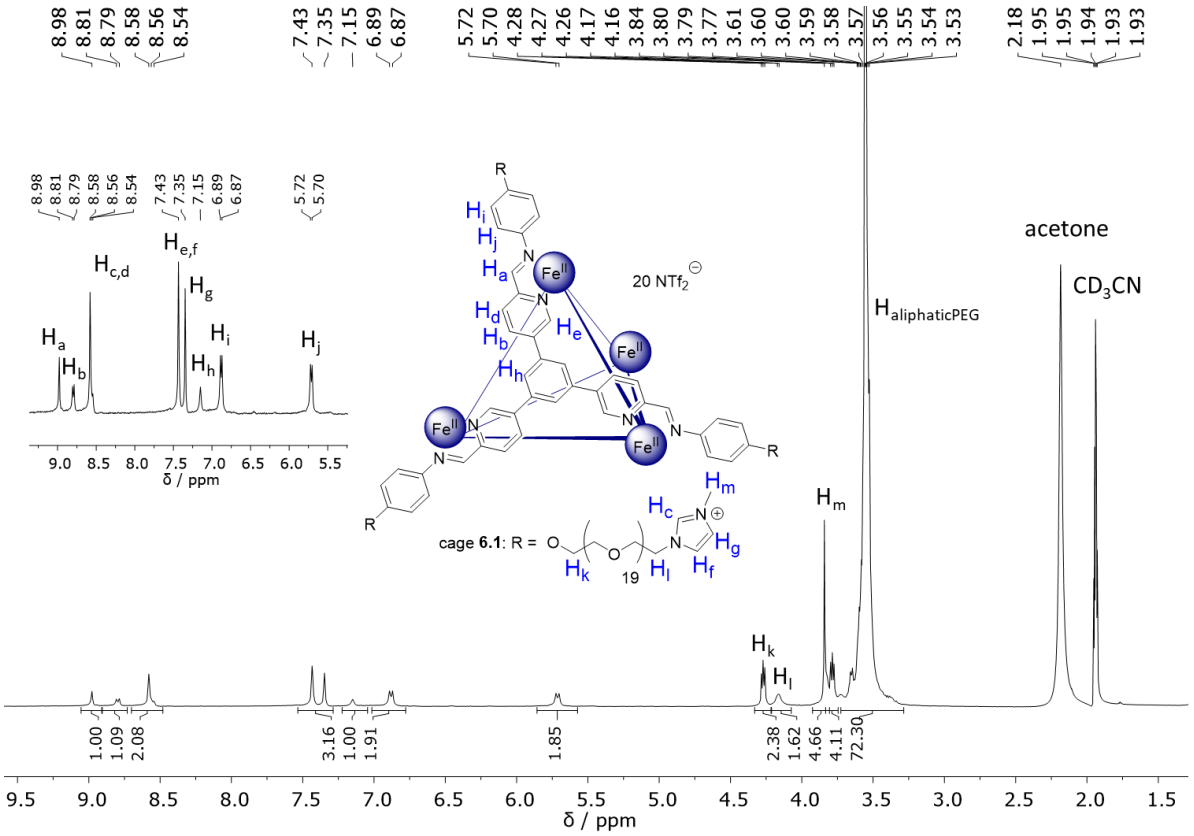

Figure 6.10: ^{1}H NMR (400 MHz, CD_3CN) spectrum of cage **6.1**.

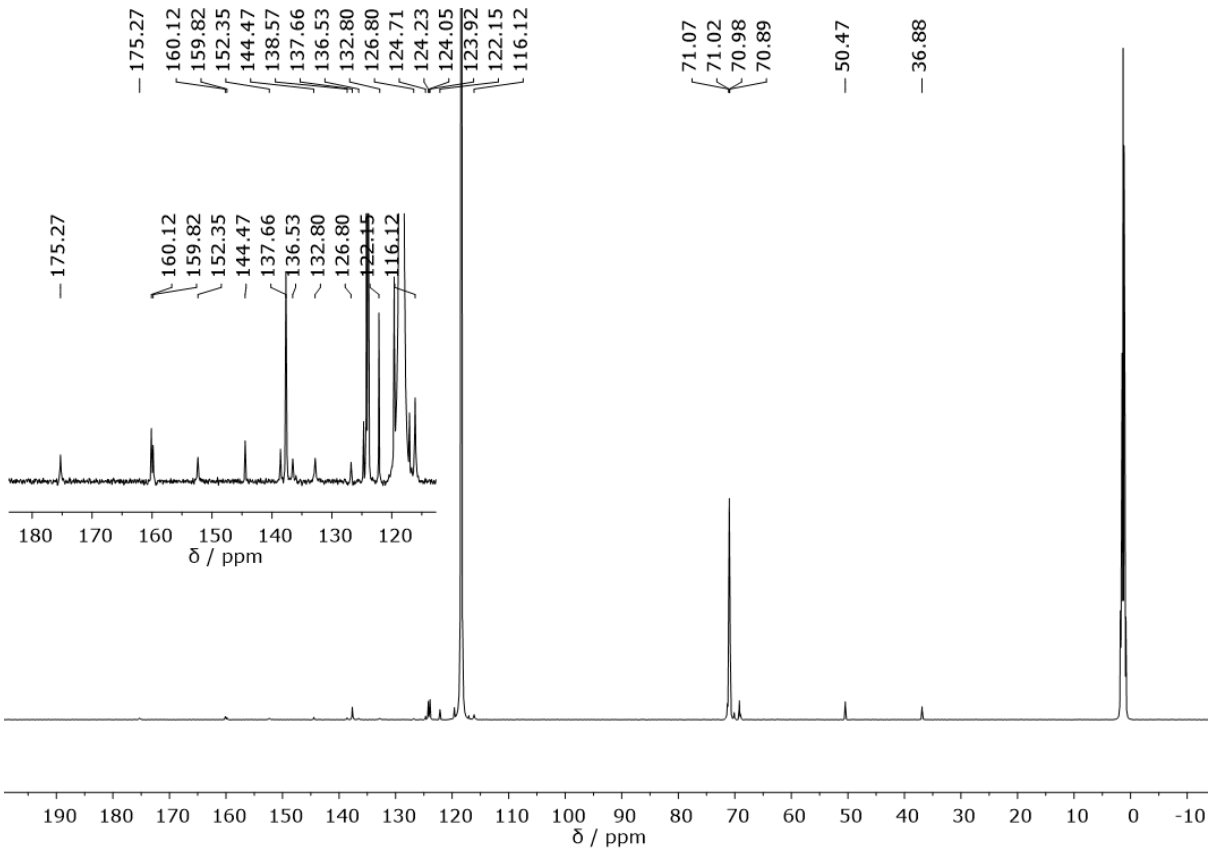

Figure 6.11: ^{13}C NMR (125 MHz, CD_3CN) spectrum of cage **6.1.**

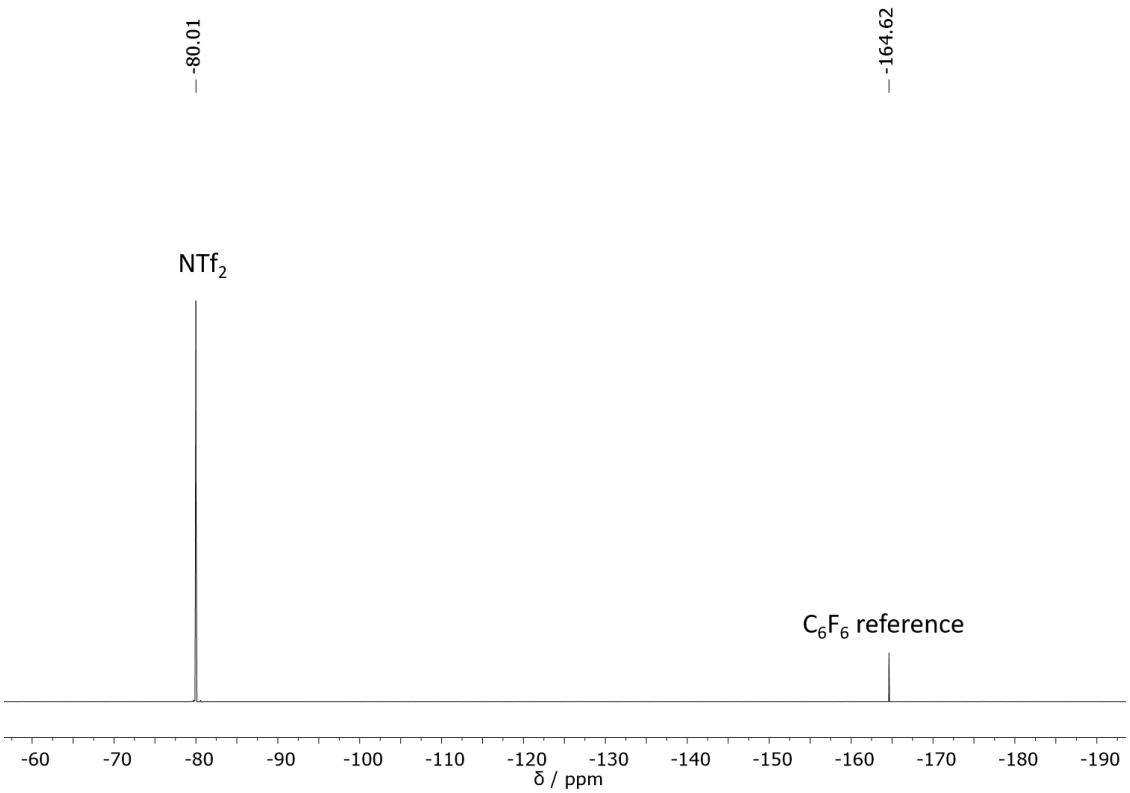

Figure 6.12: ^{19}F NMR (377 MHz, CD_3CN) spectrum of cage **6.1**.

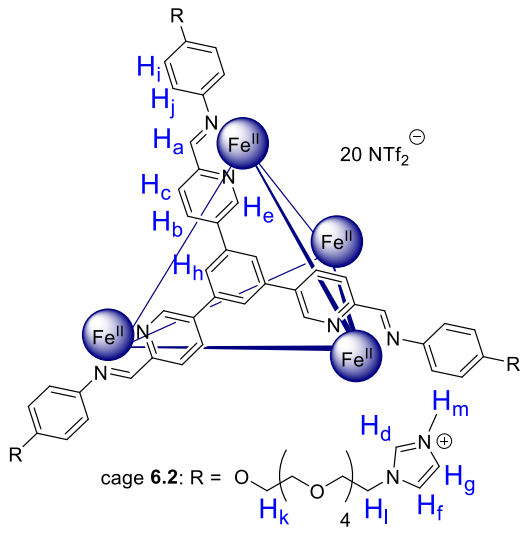

Cage **6.2**

Cage **6.2** was synthesized using the same method as cage **6.1** by replacing aniline **5F** with **5F'**.

^{1}H NMR (400 MHz, 298 K, CD_3CN) δ = 8.98 (s, 1H), 8.80 (d, J = 8.1 Hz, 1H, H_b), 8.58 (d, J = 8.5 Hz, 1H, H_c), 8.52 (s, 2H, H_d), 7.44 (s, 1H, H_e), 7.41 (d, J = 1.9 Hz, 1H, H_f), 7.32 (d, J = 1.9 Hz, 1H, H_g), 7.17 (s, 1H, H_h), 6.86 (d, J = 8.4 Hz, 2H, H_i), 5.72 (d, J = 8.3 Hz, 2H, H_j), 4.25 (t, J = 4.8 Hz, 2H, H_k), 4.14 (m, 1H, H_l), 3.97 – 3.34 (m, 23H, $H_{aliphaticPEG}$). ^{13}C NMR (125 MHz, CD_3CN): δ = 175.1, 159.9, 159.7, 152.19, 144.4, 138.5, 137.4, 137.3, 136.4, 132.6, 126.7, 124.5, 124.0, 123.9, 123.8, 122.0, 119.4, 115.9, 71.2, 71.1, 70.9, 70.9, 70.9, 70.9, 70.8, 70.7, 70.7, 70.7, 69.9, 69.0, 68.8, 50.3, 36.7 ppm. ^{19}F NMR (377 MHz, CD_3CN, referenced to hexafluorobenzene in a C_6F_6 capillary): δ = -80.01 (NTf_2^-).

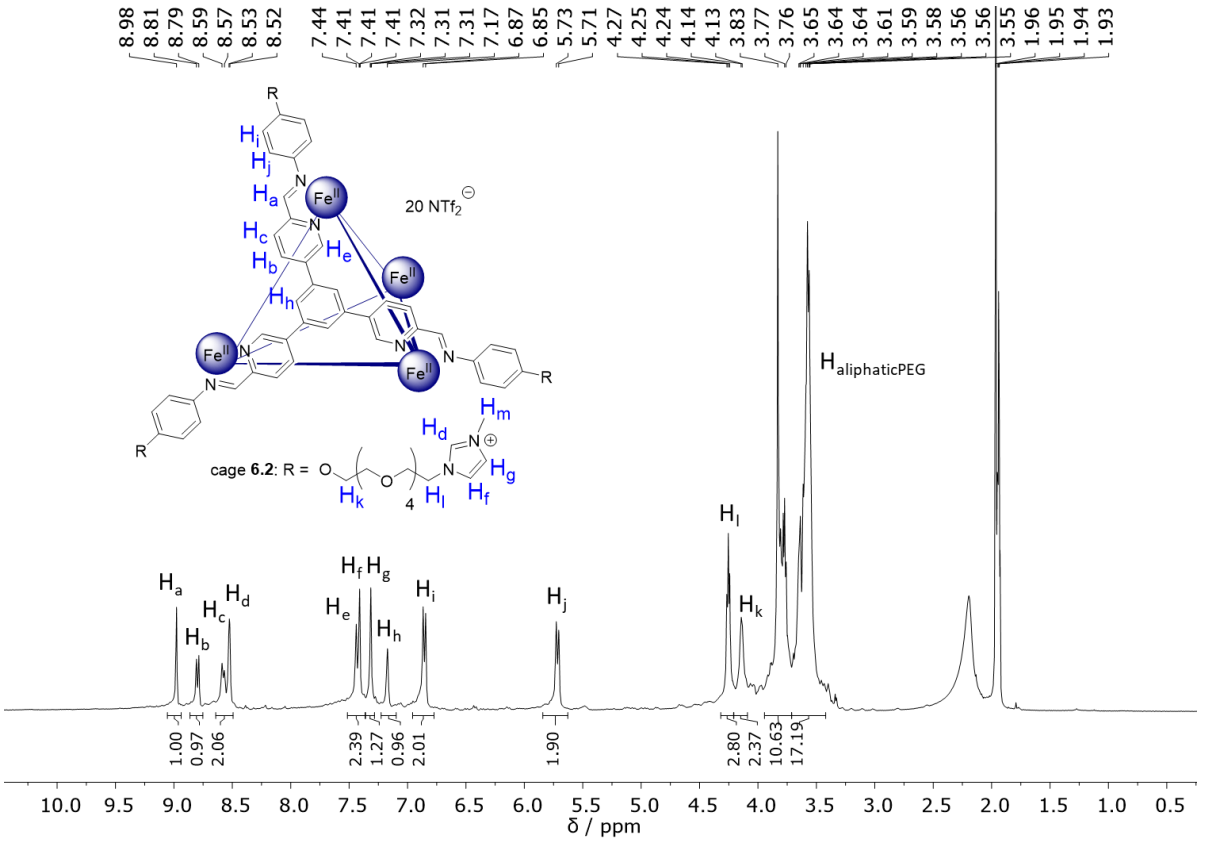

Figure 6.13: ^{1}H NMR (400 MHz, CD_3CN) spectrum of cage **6.2**.

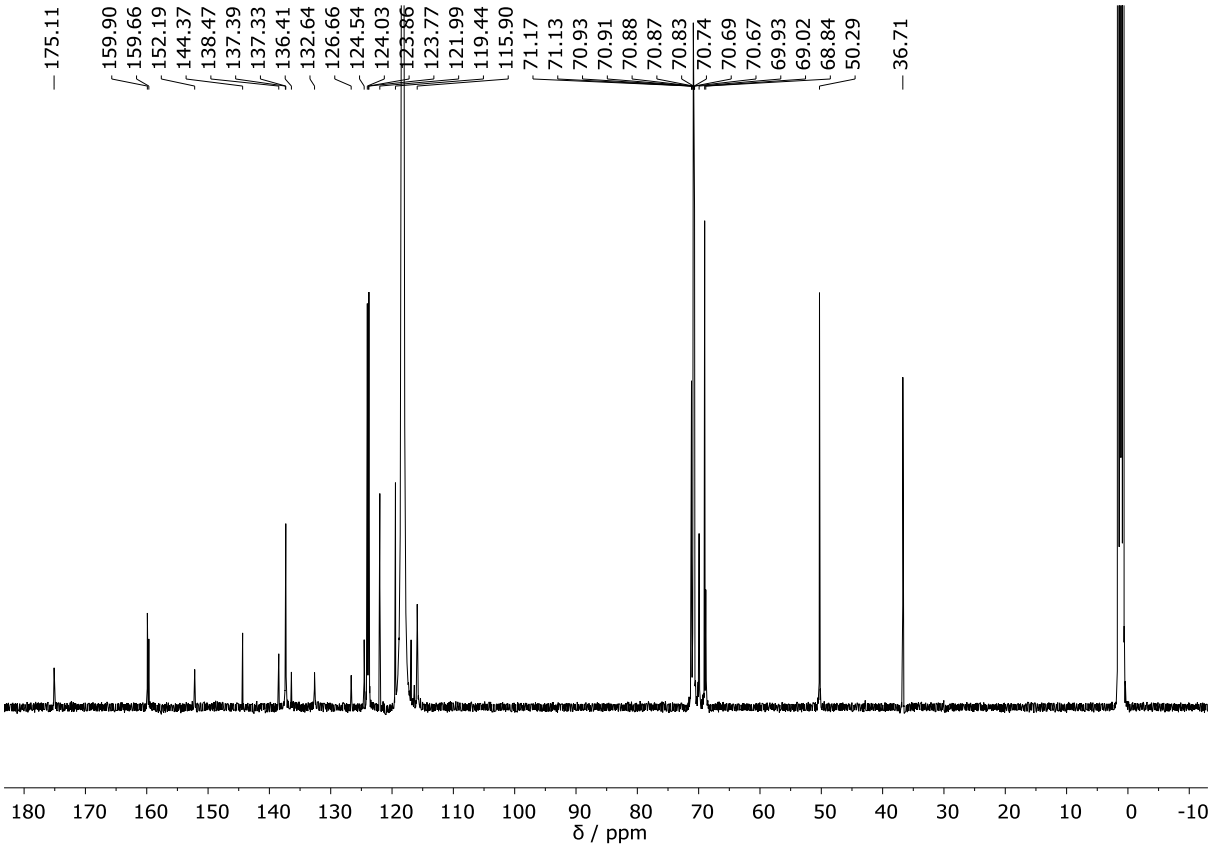

Figure 6.14: ^{13}C NMR (125 MHz, CD_3CN) spectrum of cage **6.2.**

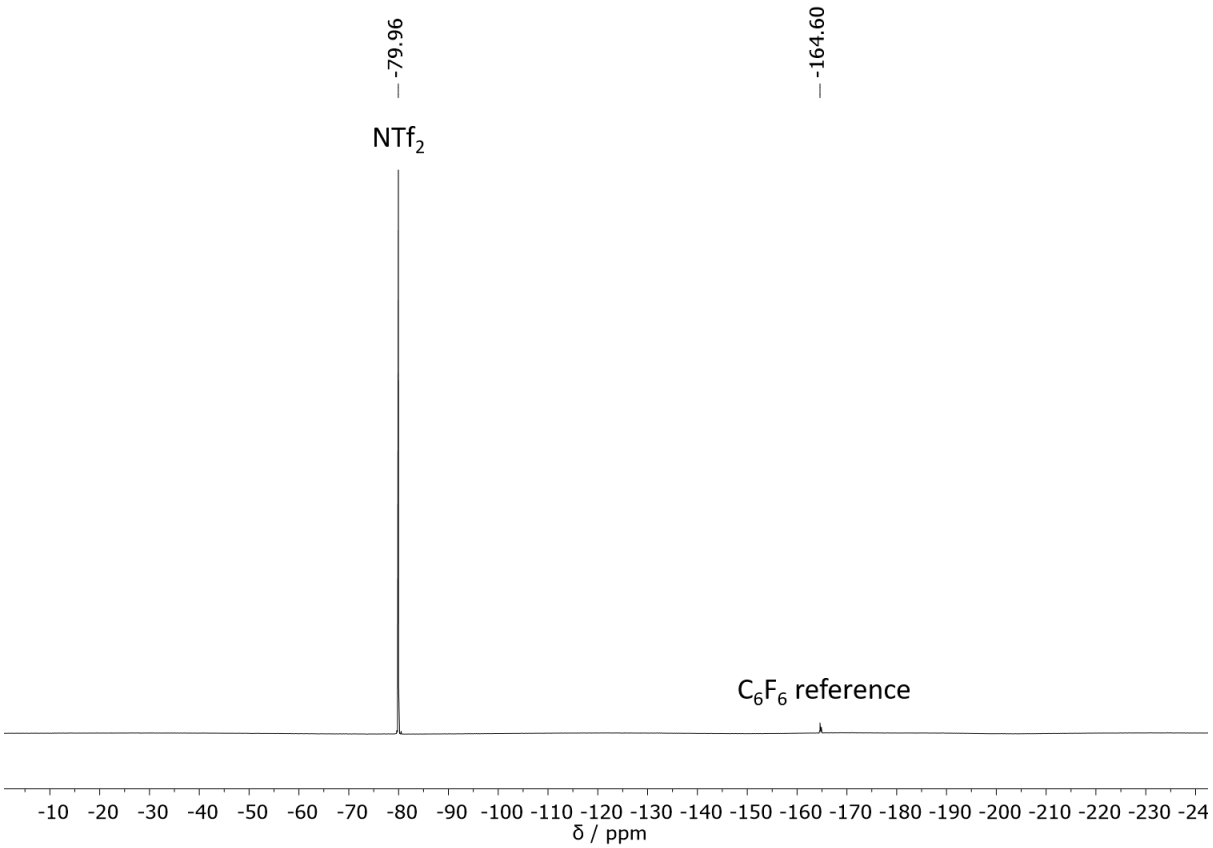

Figure 6.15: ^{19}F NMR (377 MHz, CD_3CN) spectrum of cage **6.2**.

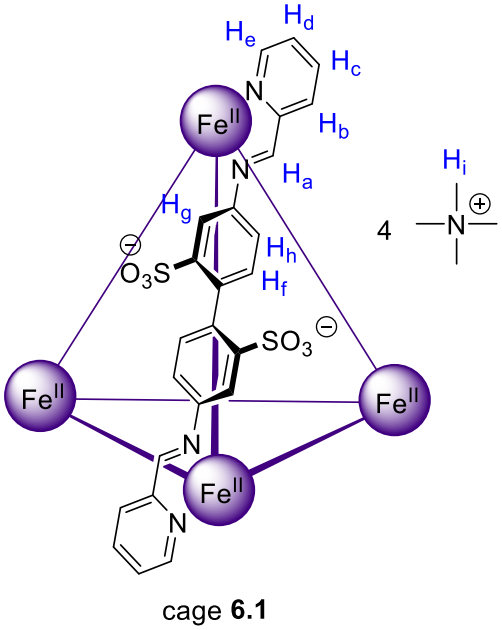

cage **6.1**

Cage **6.3**:

This cage was assembled *via* a previously published procedure.[3] The NMR data was consistent with previous reports.

^{1}H NMR (400 MHz, 298 K, CD_3CN): δ = 9.31 (s, 1H, H_a), 8.69 (d, J = 7.7 Hz, 1H, H_b), 8.40 (t, J = 7.7 Hz, 1H, H_c), 7.76 (t, J = 6.6 Hz, 1H, H_d), 7.53 (d, J = 5.6 Hz, 1H, H_e), 7.14 (s, 1H, H_f), 6.44 (s, 1Hm H_g), 5.83 (s, 1H, H_h), 3.19 (s, 4H, H_i).

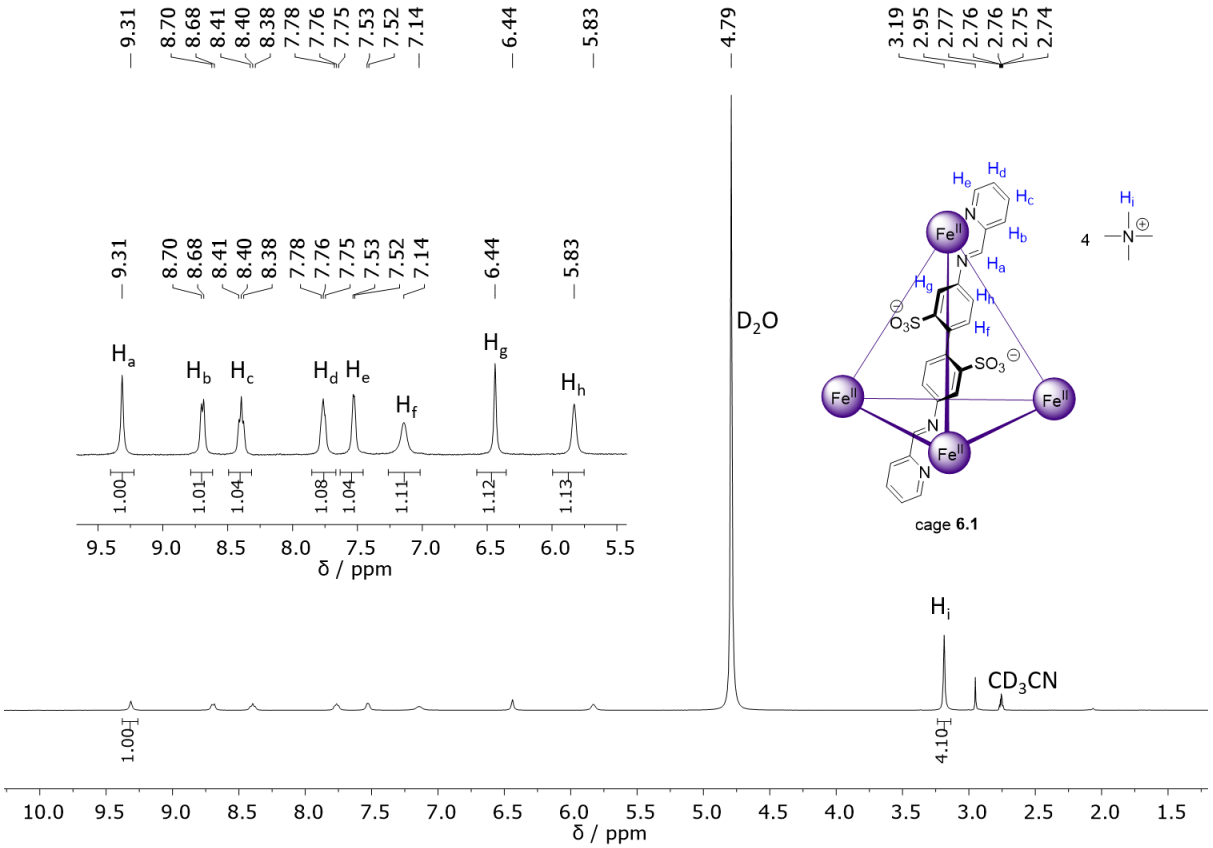

Figure 6.16: ^{1}H NMR (400 MHz, D_2O) spectrum of cage **6.3**.

6.6.2 Synthesis of hetero-cage samples

Cage **6.3** (14.88 mg, 4.08 µmol, 1.00 equiv.) was added to a H_2O solution of cage **6.1** (81.00 mg, 4.08 µmol, 1.00 equiv., 2 mL). The sealed test tube was then gently inverted five times to mix the cages. Ethyl acetate (2 mL) was added and the test tube was gently inverted three times before being cooled in an ice water bath. The organic layer was removed and this process was repeated 20 times. The aqueous layer was dried under vacuum to yield **HC-1:1**, a viscous blue-purple liquid (82.32 mg, 92% yield).

This synthesis was repeated with 44.64 mg of cage **6.3** (12.25 µmol, 3.00 equiv.) to yield **HC-1:3**. A scaled-down version of the procedure was used to synthesise **HC-1:5** with 44.51 mg of cage **6.1** (2.24 µmol, 1.00 equiv.) and 40.88 mg of cage **6.3** (11.22 µmol, 5.00 equiv.).

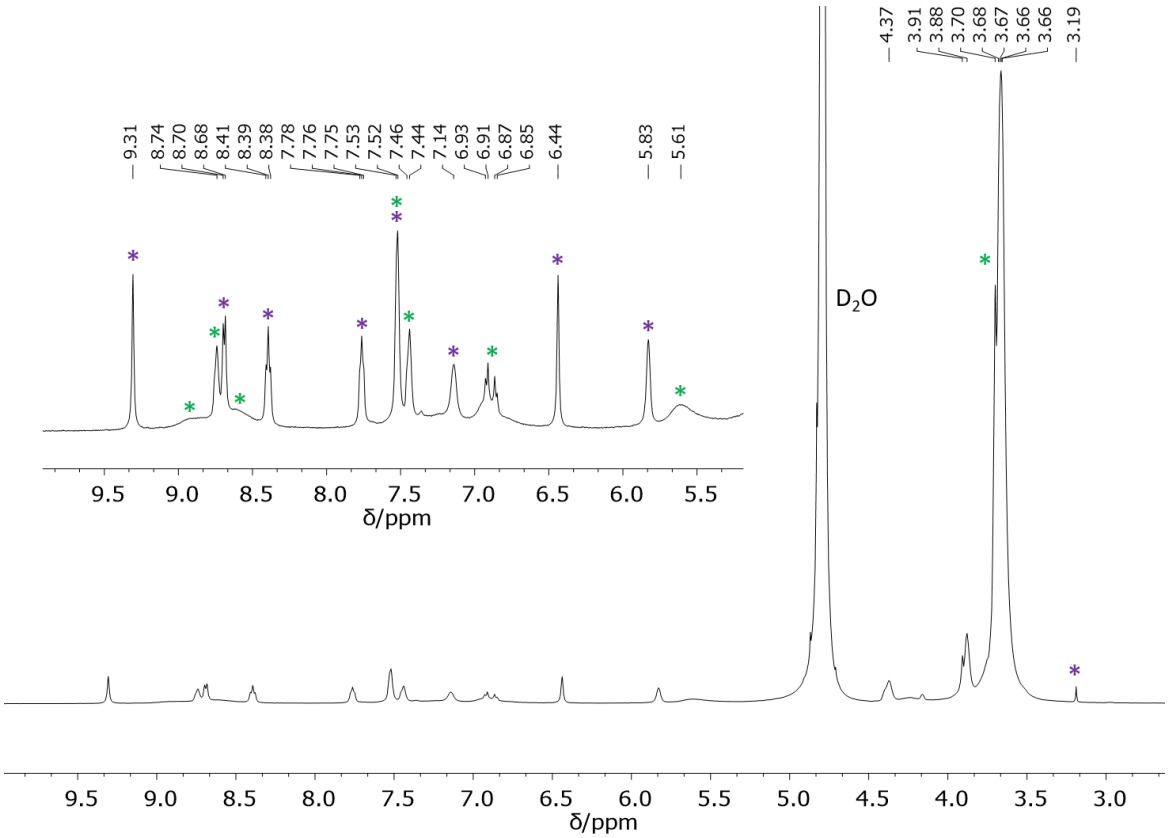

Figure 6.17: ^{1}H NMR (400 MHz, D_2O) spectrum of **HC-1:1**. Peaks from cages **6.1** (*)and **6.3** (*) are labelled with green and purple asterisks, respectively.

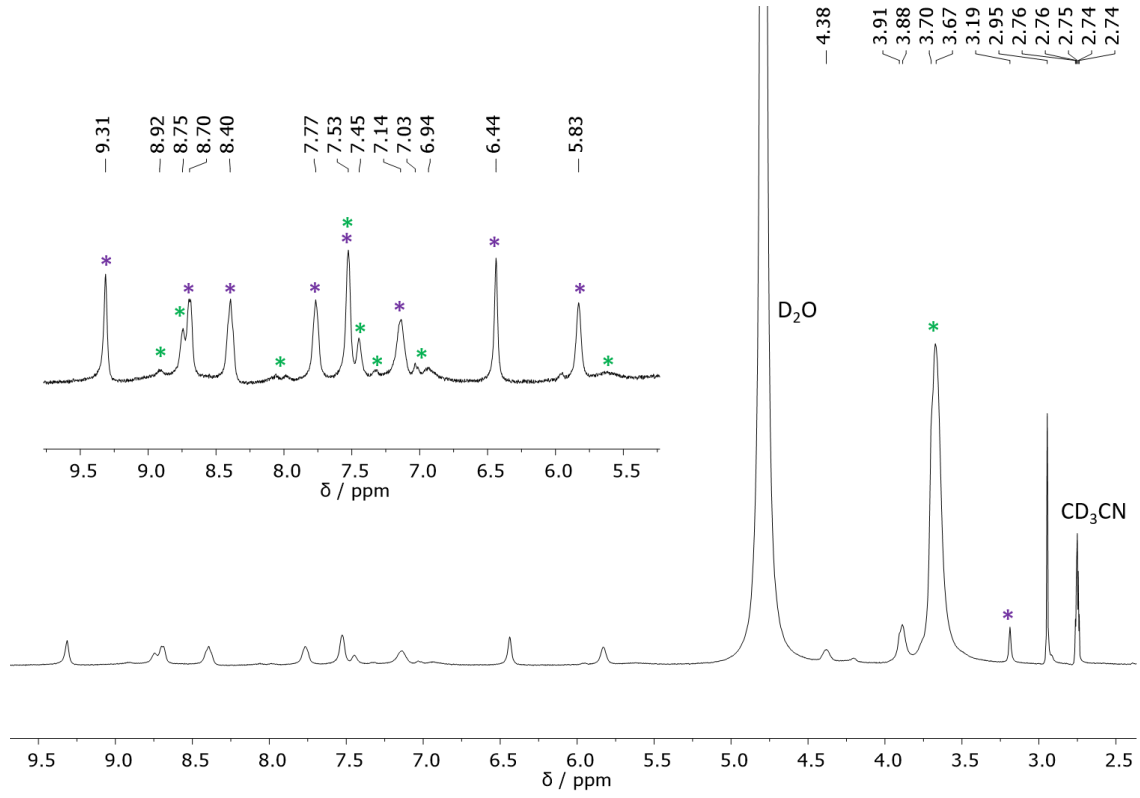

Figure 6.18: ^{1}H NMR (400 MHz, D_2O) spectrum of **HC-1:3**. Peaks from cages **6.1** (*)and **6.3** (*) are labelled with green and purple asterisks, respectively.

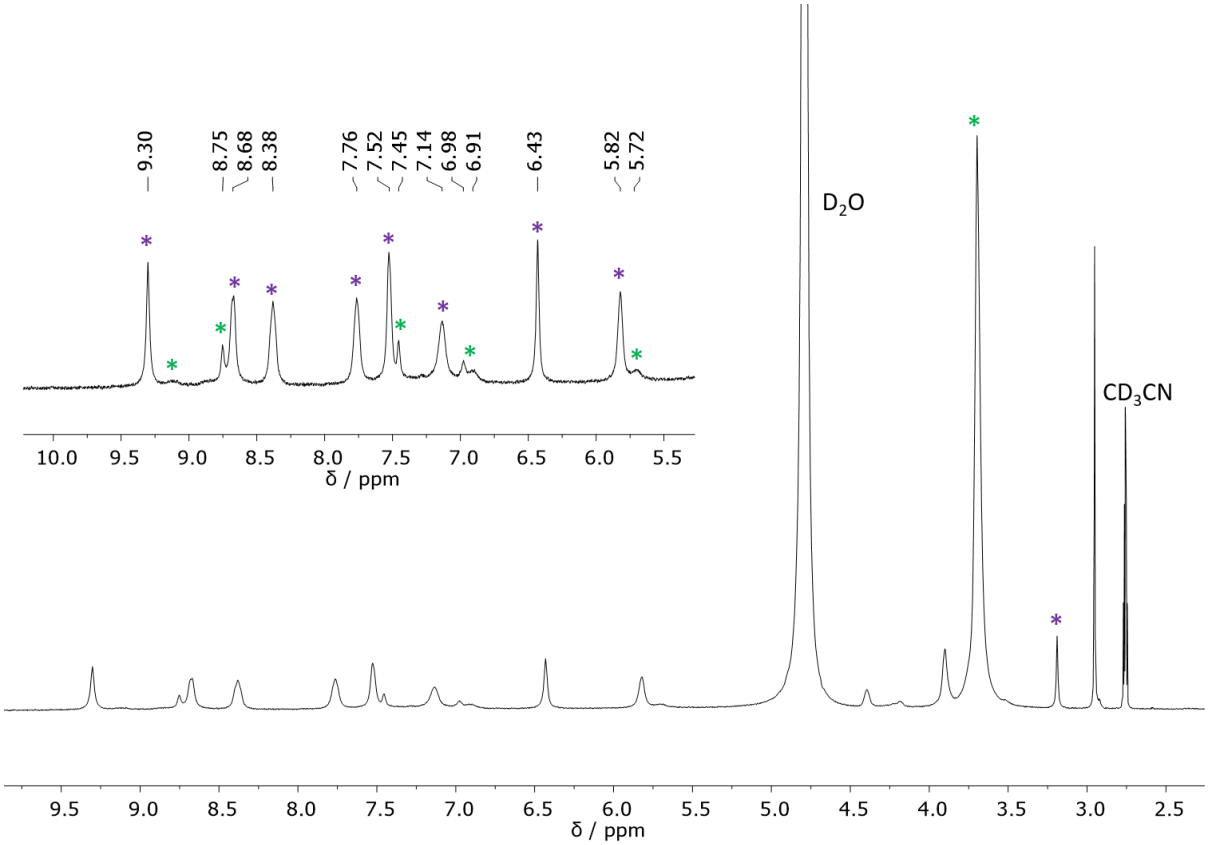

Figure 6.19: ^{1}H NMR (400 MHz, D_2O) spectrum of **HC-1:5**. Peaks from cages **6.1** (*)and **6.3** (*) are labelled with green and purple asterisks, respectively.

6.6.3 Full DSC curves

Full DSC and TGA curves of cage **6.1**, **HC-1:1**, **HC-1:3**, **H-C1:5** and cage **6.3** are included below. All DSC experiments were run with the same method as follows: the sample was prepared under ambient conditions but the run was conducted under argon. The sample was cooled at 10 °C/min to -90 °C, at which the temperature was equilibrated. The sample was then heated at 10 °C/min to 200 °C.

The DSC curve of cage **6.1** showed a broad reversible T_g at -36.9 ± 1.2 °C and -41.7 ± 0.7 °C. An artefact appeared at approximately -90 °C which was attributed to the fact that this temperature was the lowest limit of the instrument. At higher temperatures, some artefacts appeared between 100-150 °C as well as at 190-200 °C. The former feature is attributed to intermittent closing of the pan lid due to foaming of the sample; the latter feature is a result of the pan lid bursting. We do not believe the dislodgment of the lid affected the DSC results because the sample was analyzed under an inert atmosphere. The TGA curve showed a small amount of solvent (H_2O or CH_3CN) evaporating in this temperature range, and we therefore hypothesized that the increase of vapor pressure in the pan was due to residual solvents.

The DSC curve of cage **6.3** contained a single feature consistent with a T_m at 170.8 °C. Additionally, two artefacts were present in this curve. The dislocation of the pan lid manifested as feature between 148.9-154.5 °C. Also, the melting feature was not a single peak but a loop. This looping artefact is observed during a sudden and intense enthalpic response of the sample;[8] the artefact can be prevented by decreasing the sample weight in future runs.

The DSC curve of **HC-1:1** showed no features other than the reversible T_g of cage **6.1** at -36.3 ± 0.8 °C °C and -43.2 ± 0.3 °C °C and a broad T_m consistent with cage **6.3** at 142.9 °C. The broadness of the melting feature was attributed to the mixture of anions, a phenomenon previously observed in ionic liquid mixtures.[9] The DSC curve of **HC-1:3** was similar to that of **HC-1:1**. The reversible T_g consistent with cage **6.1** was still present at -36.3 ± 1.1 °C and -43.8 ± 1.1 °C. The T_m consistent with cage **6.3** was also still observable at 157.1 °C; the feature appeared less broad than its equivalent in the sample of **HC-1:1**. An artefact was present at 152.4 °C, which was again attributed to the pan lid dislocating due to an increase of vapor pressure from the evaporation of residual solvents present in the sample.

In contrast to the previous hetero-cage samples, the main feature present in **HC-1:5** was the T_m of cage **6.3** at 177.6 °C. A broad glass transition, similar to the T_g present in cage **6.1**, was also observed but the onset of the phase change was not calculated due to the broadness of the feature. The reduced intensity of the T_g signal is consistent with the decreased ratio of cage **6.1** to **6.3** in **HC-1:5**. Both artefacts present in the DSC curve of cage **6.3** were also observable in this sample.

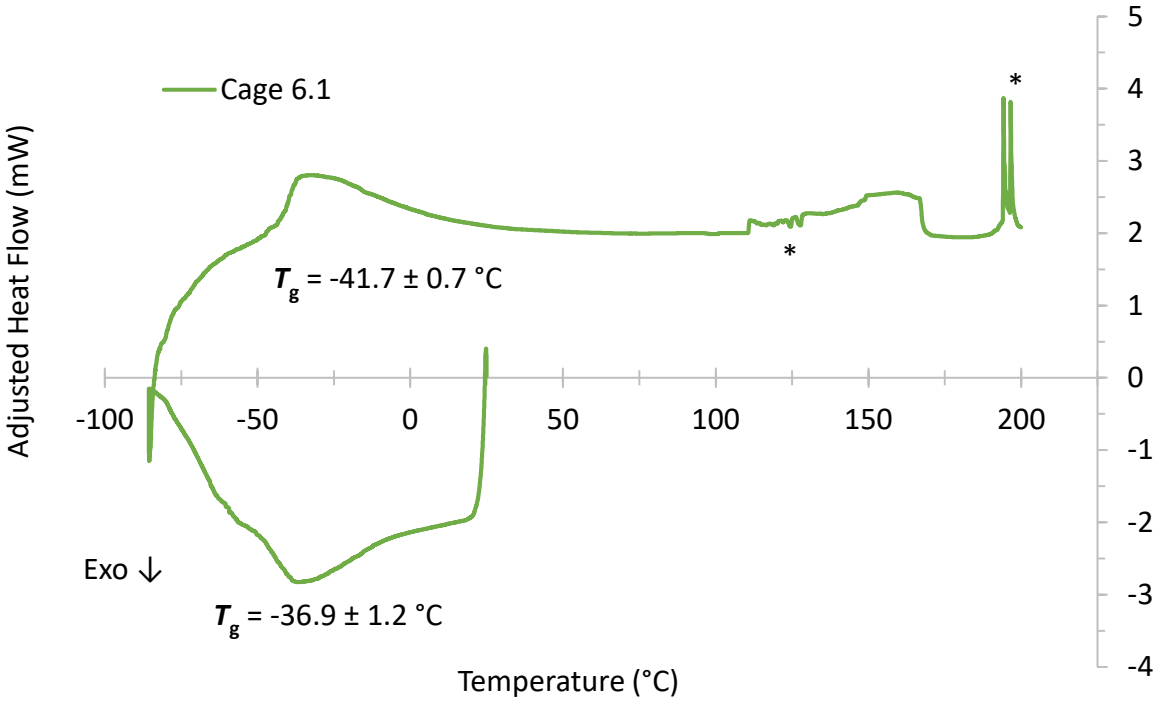

Figure 6.20: DSC curve of cage **6.1** (8.35 mg). A broad reversible T_g was observed at -36.9 ± 1.2 °C and -41.7 ± 0.7 °C °C. Artefacts are marked with asterisks.

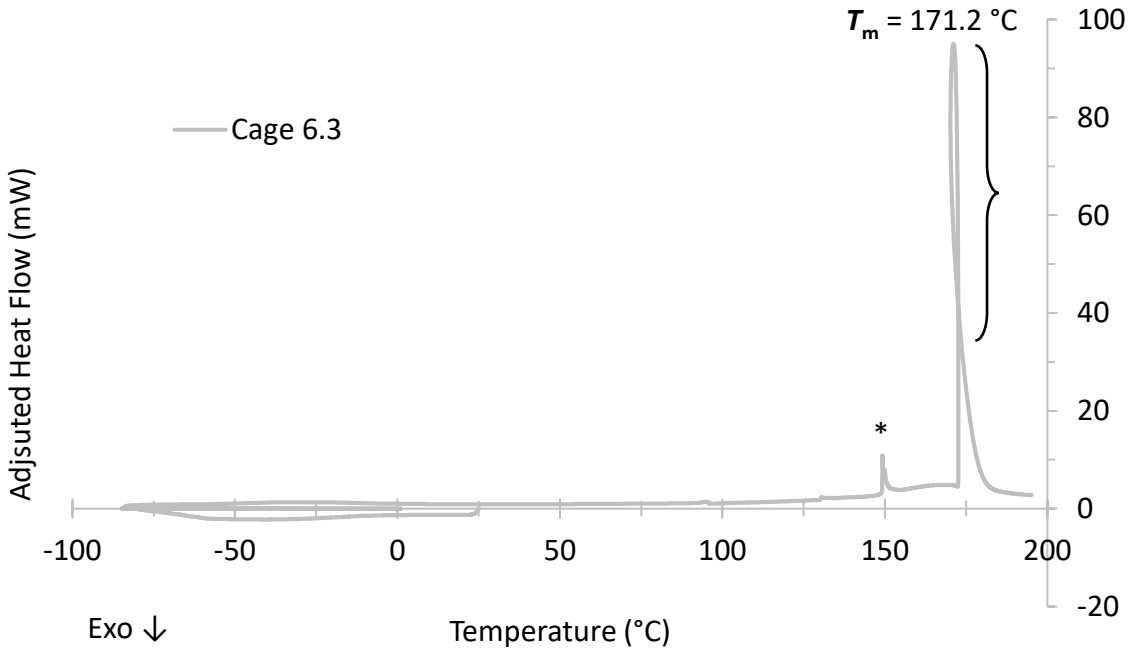

Figure 6.21: DSC curve of cage **6.3** (5.69 mg). A T_m was observed at 171.2 °C. Artefacts are marked with asterisks.

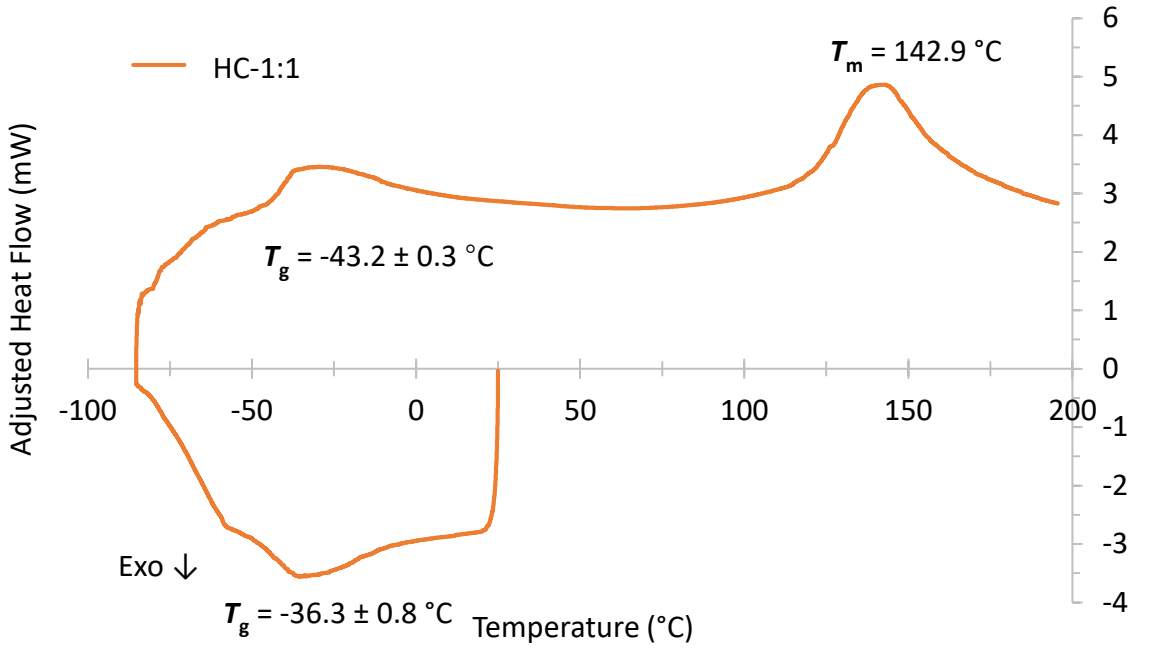

Figure 6.22: DSC curve of **HC-1:1** (8.60 mg). A reversible T_g was observed at -36.3 ± 0.8 °C and -43.2 ± 0.3 °C. A broad T_m consistent with cage **6.3** was observed at 142.9 °C.

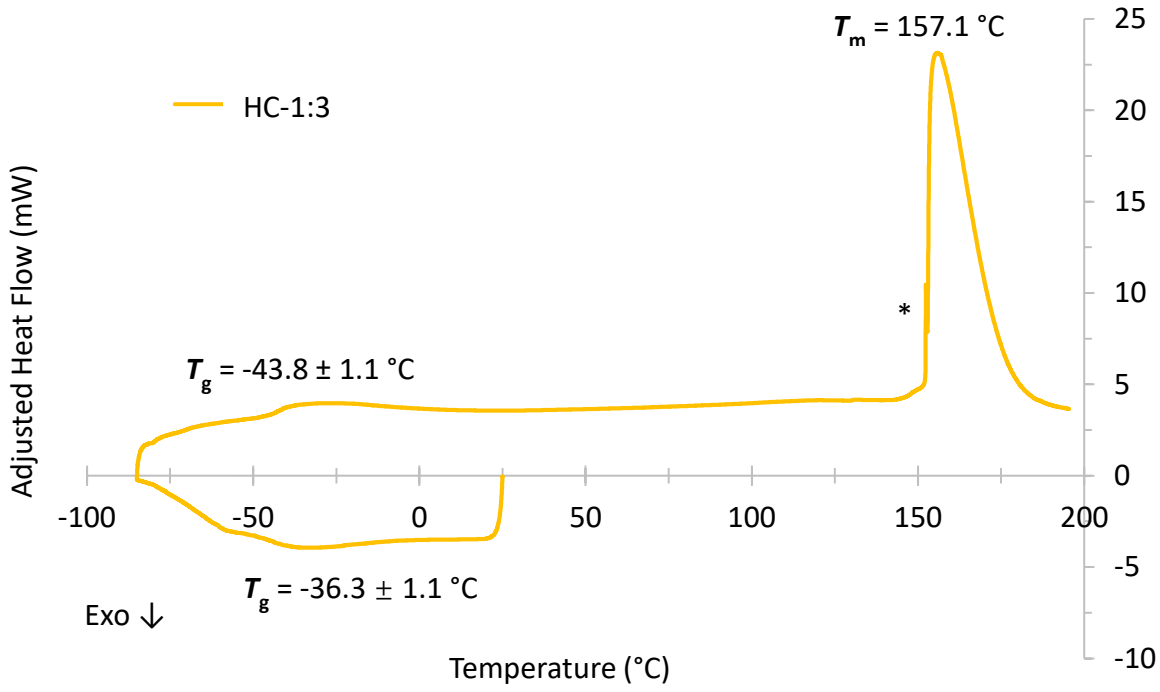

Figure 6.23: DSC curve of **HC-1:3** (10.74 mg). A reversible T_g was observed at -36.3 ± 1.1 °C and -43.8 ± 1.1 °C. A broad T_m was observed at 157.1 °C. The artefact present is marked with an asterisk.

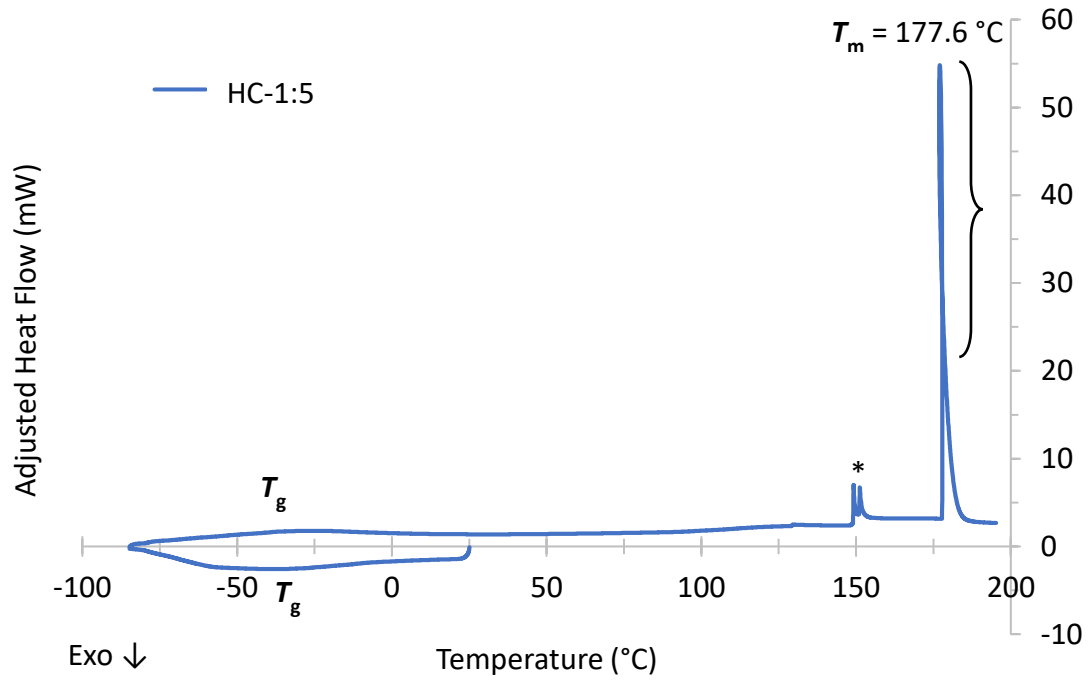

Figure 6.24: DSC curve of **HC-1:5** (4.79 mg). A T_m was observed at 177.6 °C. Broad T_g was observed below 0 °C. Artefacts are marked with asterisks.

6.6.4 Full TGA curves

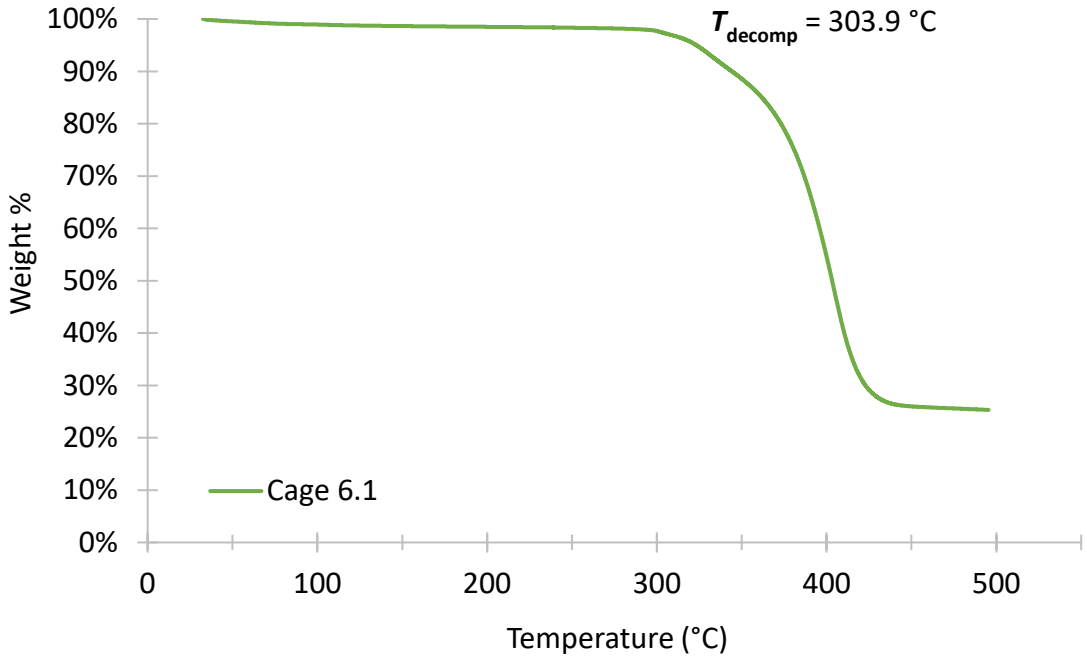

Figure 6.25: TGA curve for cage **6.1** (6.97 mg). T_{decomp} was observed at 303.9 °C.

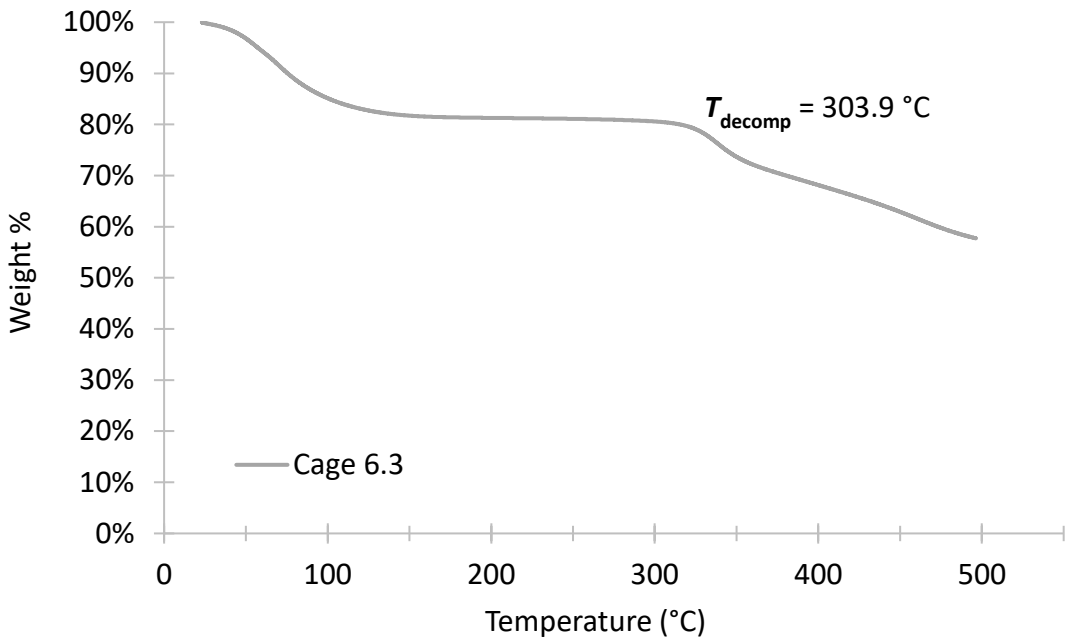

Figure 6.26: TGA curve for cage **6.3** (6.32 mg). T_{decomp} was observed at 329.7 °C.

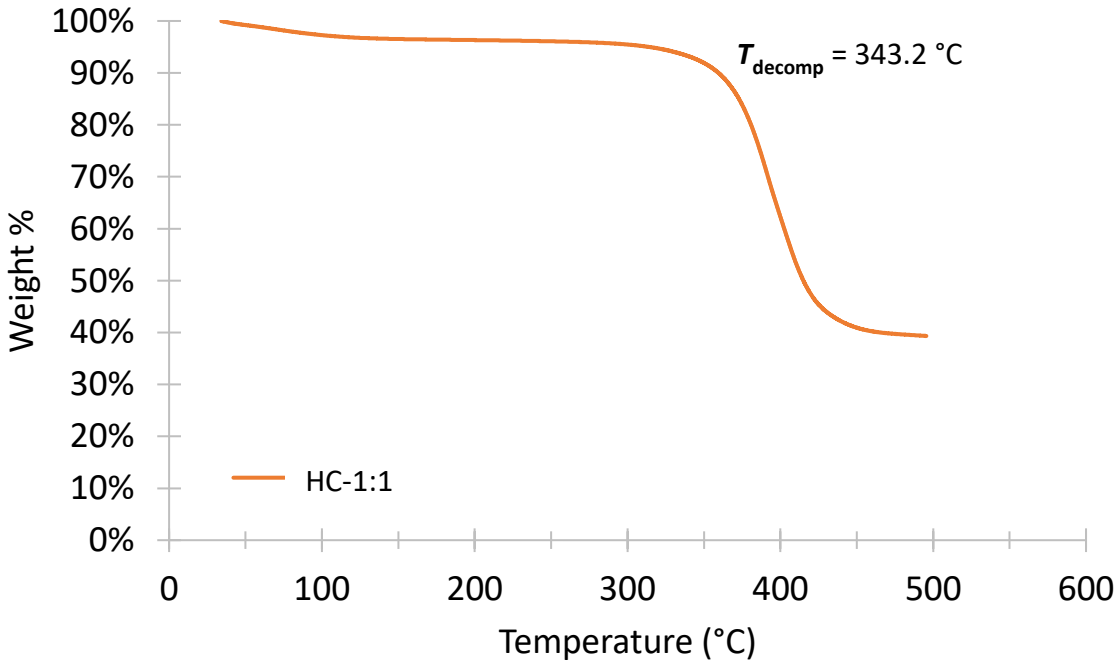

Figure 6.27: TGA curve for **HC-1:1**. T_{decomp} was observed at 343.2 °C.

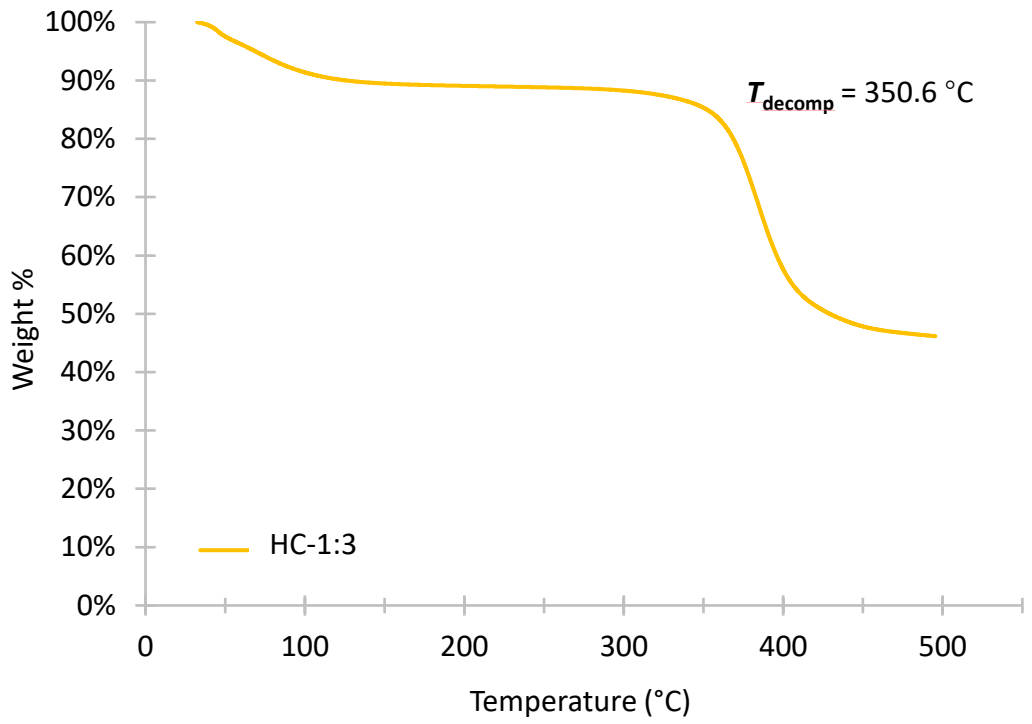

Figure 6.28: TGA curve for **HC-1:3** (13.03 mg). T_{decomp} was observed at 350.6 °C.

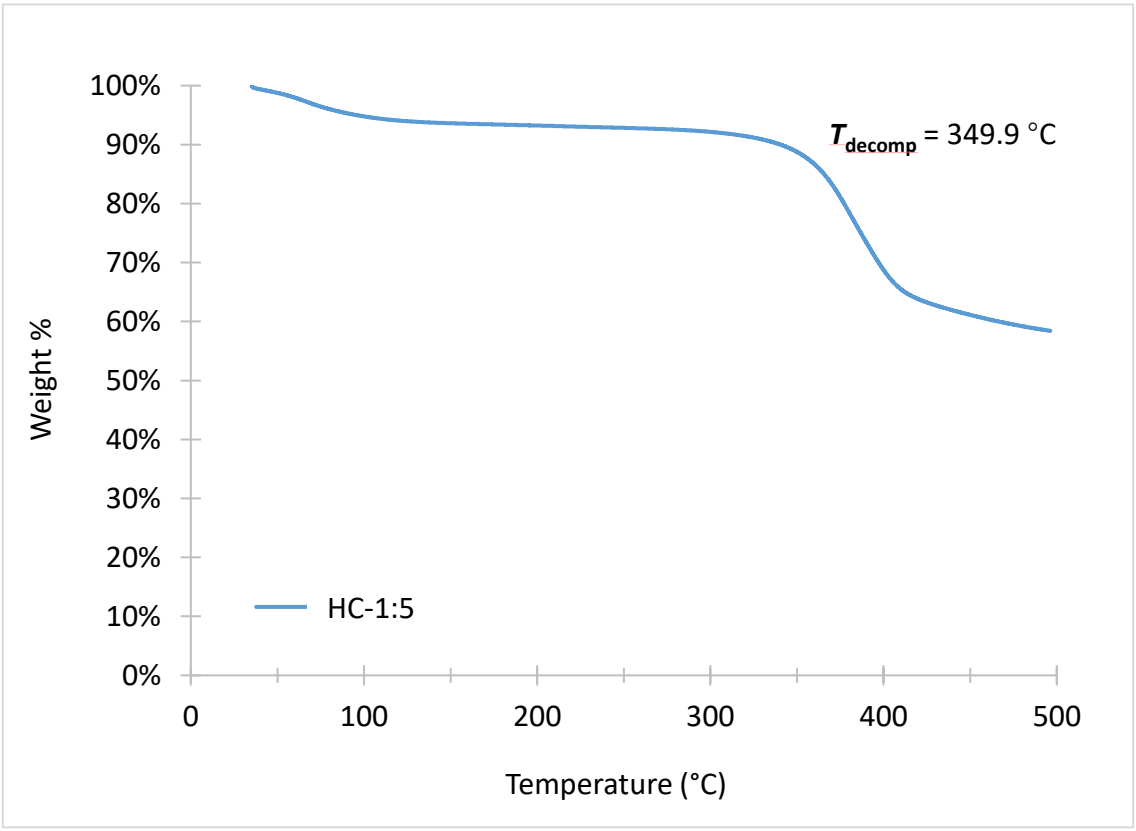

Figure 6.29: TGA curve for **HC-1:5** (6.64 mg). T_{decomp} was observed at 349.9 °C.

6.7 References

(1) Grommet, A. B.; Bolliger, J. L.; Browne, C.; Nitschke, J. R. *Angew. Chemie - Int. Ed.* **2015**, *54* (50), 15100–15104.

(2) Longley, L.; Collins, S. M.; Zhou, C.; Smales, G. J.; Norman, S. E.; Brownbill, N. J.; Ashling, C. W.; Chater, P. A.; Tovey, R.; Schönlieb, C. B.; et al. *Nat. Commun.* **2018**, *9* (1).

(3) Mal, P.; Schultz, D.; Beyeh, K.; Rissanen, K.; Nitschke, J. R. *Angew. Chemie - Int. Ed.* **2008**, *47* (43), 8297–8301.

(4) Castilla, A. M.; Miller, M. A.; Nitschke, J. R.; Smulders, M. M. J. *Angew. Chemie - Int. Ed.* **2016**, *55* (36), 10616–10620.

(5) Yao, W.; Wang, H.; Cui, G.; Li, Z.; Zhu, A.; Zhang, S.; Wang, J. *Angew. Chemie - Int. Ed.* **2016**, *55* (28), 7934–7938.

(6) Gemmei-Ide, M.; Miyashita, T.; Kagaya, S.; Kitano, H. *Langmuir* **2015**, *31* (39), 10881–10887.

(7) Nguyen, N.; Tron, A.; Georges, M. *Unpublished*.

(8) Yang, P.; Mather, Patrick T. "Thermal Analysis to Determine Various Forms of Water Present in Hydrogels", *TAInstruments* **2014**.

(9) Kunze, M.; Jeong, S.; Paillard, E.; Winter, M.; Passerini, S. *J. Phys. Chem. C* **2010**, *114* (28), 12364–12369.